Leader-Assisted Localization Approach for a Heterogeneous Multi-robot System

by

©Thumeera R. Wanasinghe

A Thesis submitted to the School of Graduate Studies in partial fulfillment of the requirements for the degree of

Doctor of Philosophy

Faculty of Engineering and Applied Science

Memorial University of Newfoundland

May 2017

St. John's   Newfoundland

Abstract

This thesis presents the design, implementation, and validation of a novel leader-assisted localization framework for a heterogeneous multi-robot system (MRS) with sensing and communication range constraints. It is assumed that the given heterogeneous MRS has a more powerful robot (or group of robots) with accurate self-localization capabilities (leader robots) while the rest of the team (child robots), i.e. less powerful robots, is localized with the assistance of leader robots and inter-robot observation between teammates. This will eventually pose a condition that the child robots should be operated within the sensing and communication range of leader robots. The bounded navigation space therefore may require added algorithms to avoid inter-robot collisions and limit robots' maneuverability. To address this limitation, first, the thesis introduces a novel distributed graph search and global pose composition algorithm to virtually enhance the leader robots' sensing and communication range while avoiding possible double counting of common information. This allows child robots to navigate beyond the sensing and communication range of the leader robot, yet receive localization services from the leader robots. A time-delayed measurement update algorithm and a memory optimization approach are then integrated into the proposed localization framework. This eventually improves the robustness of the algorithm against the unknown processing and communication time-delays associated with the inter-robot data exchange network. Finally, a novel hierarchical

sensor fusion architecture is introduced so that the proposed localization scheme can be implemented using inter-robot relative range and bearing measurements.

The performance of the proposed localization framework is evaluated through a series of indoor experiments, a publicly available multi-robot localization and mapping data-set and a set of numerical simulations. The results illustrate that the proposed leader-assisted localization framework is capable of establishing accurate and non-overconfident localization for the child robots even when the child robots operate beyond the sensing and communication boundaries of the leader robots.

Table of Contents

List of Tables

List of Figures

xiv

xvi

List of Abbreviations

C-SLAM Cooperative simultaneous localization and mapping

CCL Centralized Cooperative Localization

CI Covariance intersection

CKF Cubature Kalman filter

CPS Cooperative positioning system

DCL Decentralized cooperative localization

DGPS Differential global positioning system

DOF Degrees of freedom

DOO Degrees of observation

EKF Extended Kalman filter

FIFO First-in-first-out

GPS Global positioning system

IRMCG Inter-robot measurement and communication graph

IRRM Inter-robot relative measurements

LOS Line of sight

MAV Micro-aerial vehicle

MRS Multi-robotics system

MUGV Micro unmanned ground vehicle

NEES Normalized estimation error squared

NIS Normalized innovation squared

OOSM Out-of-sequence-measurement

RL Relative localization

RMSE Root-mean-squared error

RPMG Relative pose measurement graph

SLAM Simultaneous localization and mapping

SOI-KF Sign-of-innovation Kalman filter

Split-CI Split covariance intersection

UKF Unscented Kalman filter

Chapter 1

Introduction

Autonomous mobile robots are becoming one of the commonly available industrial tools for a variety of applications ranging from floor cleaning [1] to planetary exploration [2]. Traditional autonomous mobile robot-based implementations relied on a single robot equipped with various perceptive sensors [3]. In the past few decades, multi-robotic systems (MRSs) have been preferred over single robot-based systems. Some of the advantages of MRSs compared with single robot systems are the robustness to an individual failures, the shorter time for the completion of set missions, the improved productivity by enabling parallel tasks, the better coverage of an environment and the utilization of resources; and the enhanced flexibility to achieve a high quality of service [4, 5]. Available MRSs can be categorized into two groups: homogeneous MRSs and heterogeneous MRSs. The studies related to homogeneous MRSs focus on the MRSs with the agents of identical characteristics [6, 7]. In contrast, the studies related to the latter focus on the robots unifying from different domains of operation such as the ground and air, different perception and processing capabilities, and a variety of sizes in a single framework [8–10]. The complementary unique characteristics of agents in a heterogeneous MRS can be integrated to enhance their

relative capabilities and to overcome limitations of stand-alone systems [8].

Accurate estimation of position and orientation (pose)[1] is a key requirement for successful implementation of any mission using autonomous MRSs. Self-localization of a given robot can be empowered with either basic localization algorithms, such as dead-reckoning or with complex localization approaches, such as simultaneous localization and mapping (SLAM). Dead-reckoning-based self-localization approaches generally demonstrate unbounded drifting of pose estimations, limiting their applicability to a short-period of time. In contrast, SLAM is capable of generating more accurate pose estimation for agents in MRSs, when they navigate in a feature rich environment. Successful implementation of SLAM entails high sensor payload, fast computational resources and larger memory space. These requirements limit its applicability for resource constrained robotic systems such as micro aerial vehicles (MAVs) and micro unmanned ground vehicles (MUGVs).

In general, agents in a heterogeneous MRS host different proprioceptive and exteroceptive sensory systems. This results in a significant variation in the self-localization capability of teammates. Inter-robot observations and flow of information between teammates can establish a sensor sharing technique so that the localization accuracy of each member improves over the localization approaches that solely depend on the robot's onboard sensors. These techniques are termed *collaborative localization* [9, 11–13]. When each robot can sense and communicate with its teammates at all times, then every member of the MRS has less uncertainty about its pose than the robot with the best result of localization with self-localization [12]. There are various methods that have been studied to implement multi-robot collaborative localization for MRSs: centralized/multi-centralized cooperative localization approaches [11, 14–19], distributed cooperative localization approaches [12, 20], decentralized cooperative lo-

---

[1]Note that, in this thesis, the terms *pose* and *robot's state vector* are used interchangeably to represent robot position and orientation.

calization approaches [13, 21–24], relative localization approaches [9, 25] and leader-assisted localization [9, 25, 26].

In order to implement a leader-assisted navigation technique, the MRS should have a minimum of one robot with higher sensor payload, higher processing power, and larger memory capacity. This robot can then execute complex localization algorithms such as SLAM and can host advanced localization sensors such as laser scanners, cameras, global positioning system/differential global positioning system (GPS/DGPS) units, compass and accurate wheel odometers leading to more accurate self-localization. Robots with these capabilities are termed **leader robots**. The rest of the agents in the MRS are termed **child robots**. As the leader robots have the means of accurate localization, the objective of the leader-assisted localization is to establish localization for the child robots using the pose estimations of the leader robots and the inter-robot observations among the teammates [25, 26]. This thesis proposes novel sensor fusion architectures for leader-assisted localization in which child robots are allowed to navigate beyond the sensing and the communication range of leader robots yet guarantee the bounded estimation error for the child robots. Additionally, a novel distributed cooperative localization framework is also presented in this thesis.

1.1 Multi-Robot Localization Strategies

The initial formulation of multi-robot collaborative localization was inspired by SLAM where mobile agents are used as dynamic portable landmarks in an environment to assist navigation of multiple robots [11]. This initial implementation splits the mobile robots in MRS into two groups. When one group navigates, the other group remains stationary. The agents in the stationary group act as static landmarks to assist the localization and navigation of the agents in the moving group. After a few time steps,

the two groups exchange their roles and this process continues until all agents have approached the goal location. This "*leap-frogging*" motion pattern-based framework was later improved by several other researchers [14, 15, 17]. The key limitation of leap-frogging motion-based cooperative localization strategies is that only one robot or a portion of the MRS is allowed to navigate at a given time step, resulting in longer mission completion time. There are numerous multi-robot collaborative localization frameworks which have been developed since the work of Kurazume *et al.* in 1994. These implementations can be categorized into six main groups: (1) centralized cooperative localization, (2) multi-centralized cooperative localization, (3) distributed cooperative localization, (4) decentralized cooperative localization, (5) relative localization, and (6) leader-assisted localization. Figure 1.1 graphically illustrates these multi-robot localization configurations.

Centralized cooperative localization approaches have a central processing unit to perform the sensor fusion task [11, 14–19]. Each robot in the MRS acquires its ego-motion sensory data (odometry), and relative range/bearing measurements for its neighbours and transmit them to a central processing unit (Figure 1.1 (a)). This central processing unit can be either a server computer or one of the agents in the MRS. The central processing unit augments each robot's pose into a single state vector and maintains the joint-state and the associated dense covariance matrix in order to accurately represent the correlation with the teammates' pose estimations. Therefore, these approaches are known to generate an optimum solution for the cooperative localization problem at the expense of high computational complexity, i.e. $\mathcal{O}(N^4)$ where N is the number of robots in the team. Besides the high computational complexity, centralized cooperative localization approaches generally require a communication network to have high data bandwidth to accommodate the high-frequency ego-centric
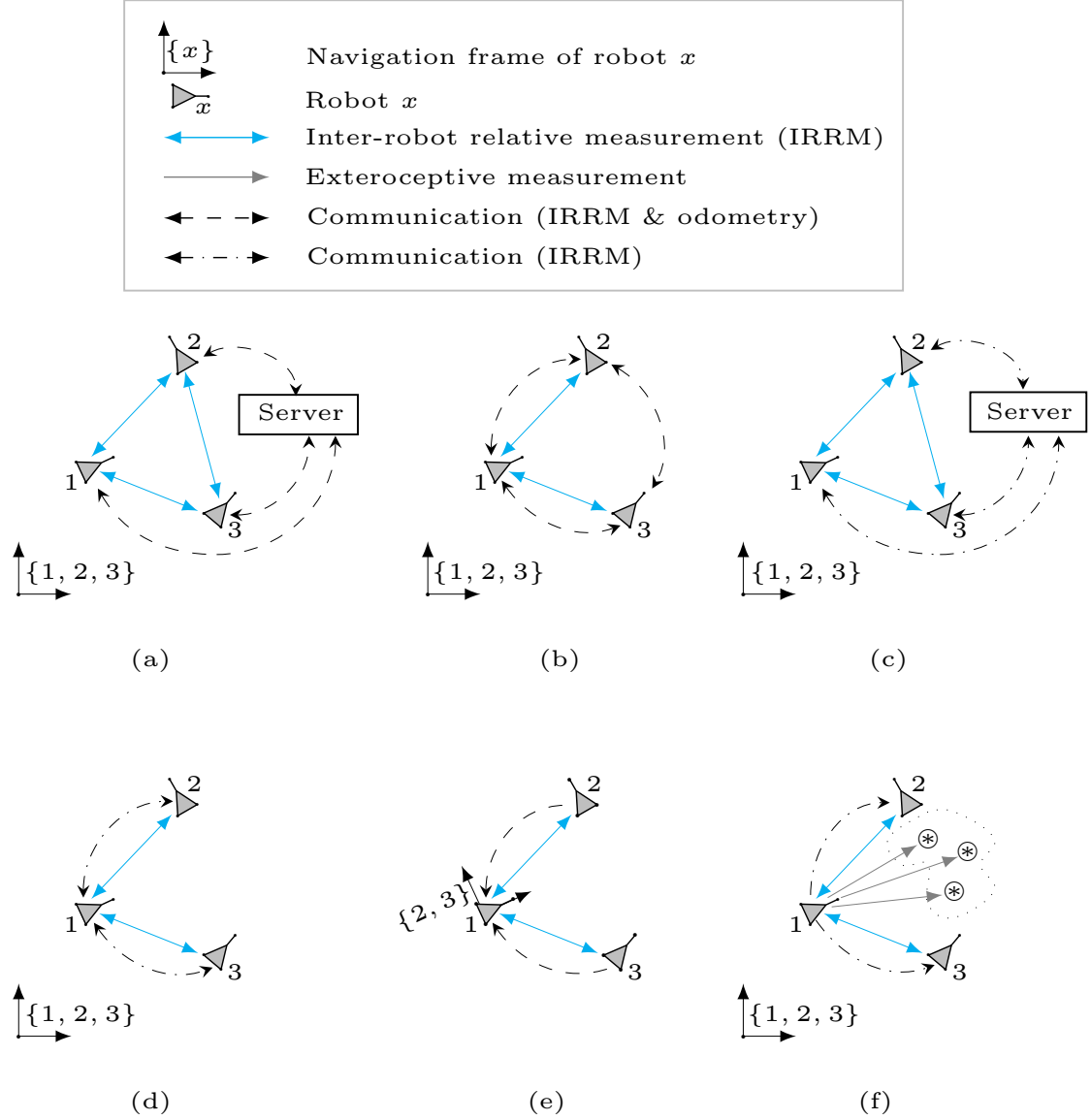
Figure 1.1: Overview of multi-robot localization strategies. (a) Centralized cooperative localization, (b) Multi-centralized cooperative localization, (c) Distributed cooperative localization, (d) Decentralized cooperative localization, (e) Relative localization, (f) Leader-assisted localization. Note that the communication links with two arrowheads represent bidirectional communications and the communication links with single arrowhead represent unidirectional communications.

measurements to the central processing unit.

Multi-Centralized cooperative localization approaches have been introduced to

improve the robustness of the traditional centralized cooperative localization methods against the single point of failure. In these multi-centralized methods, the team state estimation task is duplicated for each member of the team [19, 27]. Therefore, each robot exchanges its local sensor reading with every other member of the team as shown in Figure 1.1(b). Since now each robot has an independent team state estimate, these approaches are robust against the single point of failure. However, the per measurement communication cost of multi-centralized cooperative localization approaches is relatively higher, i.e. $\mathcal{O}(N)$, as compared to $\mathcal{O}(1)$ in centralized approaches.

Distributed cooperative localization schemes have been proposed to address the communication bandwidth limitations associated with the centralized and multi-centralized cooperative localization strategies. In the distributed cooperative localization approaches, each robot runs a local filter to fuse odometer data while inter-robot observations are fused at a central processor [12, 20]. As a result, high-frequency ego-centric measurements are no longer required to be transmitted either to a central processing unit or among teammates. This reduces the communication bandwidth demand considerably. However, the measurement update step is still performed in a centralized manner. Therefore, each robot communicates its local estimates and inter-robot relative measurement (IRRM) data to the central processor at each IRRM event[2]. The central processing unit performs the sensor fusion and the updated decomposed state estimations are sent back to each robot to ensure the continuity of the accurate time propagation. Figure 1.1 (c) shows the overview of this localization strategy.

---

[2]Each robot hosts a sensory system to measure relative pose, range, or bearing to neighbouring robots. These sensors are synchronized and acquire measurements periodically. The process of each robot synchronously acquires relative measurements for neighbours is defined as IRRM event.

Decentralized cooperative localization algorithms are proposed to address the computational and communication limitations associated with centralized, multi-centralized and distributed architectures. In decentralized cooperative localization, each robot maintains a local estimator, such as an extended Kalman filter (EKF) or a particle filter, to estimate its own pose in a pre-defined coordinate frame. Each robot exchanges information only with the robots that operate within its sensing range (Figure 1.1 (d)) reducing the bandwidth requirement for data exchange. Since there is no state augmentation at the state propagation or at the measurement update step, the per IRRM computational complexity becomes independent of the number of robots in the network, i.e. $\mathcal{O}(1)$. Overall computational cost increases linearly with the number of robots, $\mathcal{O}(N)$. Decentralized cooperative localization approaches generally do not track the possible interdependencies among robots' local pose estimates, leaving the same information to propagate forward and backward within the communication network. This may results in generating overconfident state estimations[3] for agents in the MRS [21, 22, 28, 29].

Relative localization algorithms are inspired by the target tracking applications. The key objective of relative localization is to detect and track one or a set of moving agents on the body-fixed coordinate frame of another moving agent(s) in the team [30, 31]. Most of the relative localization implementations assume that the mobile agents which run tracking filters, have ego-motion sensory information of neighbouring robots. Therefore, robots are required to exchange high-frequency ego-centric data with the tracking robot (Figure 1.1 (e)) causing the bandwidth requirement of the communication link to increase. It is possible

---

[3]If the estimated uncertainty is lesser than the estimation error, the estimation is said to be overconfident.

to implement relative localization without exchanging ego-motion data. Then, it is required for tracking filter to estimate velocities of the target. This entails relatively longer time for tracking filter to converge compared the relative localization implemented with known ego-motion data of target robot.

Leader-assisted localization is introduced to establish the localization for child robots (less capable robots) with the help of leader robots (more capable robots) while using the inter-robots' observation among teammates. These localization algorithms assume that the leader robots in the team implement an advanced localization approach, such as SLAM, and are capable of acquiring relative pose measurements for child robots. The acquired relative pose measurements are then converted into a reference coordinate frame and sent to child robots. Child robots fuse these global pose measurements with their local estimations and improve the accuracy of their localization. The overview of this localization strategy is shown in Figure 1.1 (f).

1.1.1 Issues Associated with Multi-Robot Localization

Each multi-robot localization approach outlined in the previous section has its own strengths and weaknesses. Some of the demerits are common across multiple multi-robot localization strategies. A brief insight into these weaknesses is summarized below:

Scalability : Scalability of a given multi-robot collaborative localization approach is governed by two parameters: computational complexity of the algorithm and communicative complexity of the communication network. Centralized, multi-centralized and distributed cooperative localization algorithms are scaled in $\mathcal{O}(N^4)$ where N is the number of robots in the network. Therefore, these

algorithms scale poorly in terms of the number of members in the team. The computational complexity of the decentralized cooperative localization, leader-assisted localization and relative localization schemes increase linearly with the number of robots in the team, and is considerably lower than other three multi-robot localization approaches; thus, these algorithms are scalable in terms of the number of robots in the team. Centralized cooperative localization, multi-centralized cooperative localization approaches and general relative localization algorithms require teammates to exchange high-frequency ego-centric data with one another or with central processing systems. A higher number of robots in the team entails a greater bandwidth requirement imposing an upper bound for the size of the robot team. Distributed and decentralized cooperative localization and leader-assisted localization techniques do not require teammates to exchange high-frequency ego-motion data, resulting in reduced communicative complexity.

Communication range limitations : To generate a pose estimation with bounded estimation error, centralized cooperative localization, multi-centralized cooperative localization, leader-assisted localization and relative localization approaches imposes the condition that teammates navigate within communication boundaries of each other or within the communication boundaries of the central processing unit. This constraint limits the teammates' maneuvering room, reduces the area covered by the robots, and demands a complex algorithm to avoid inter-robot collisions.

Sensing range limitation : In general, measurement uncertainty of any IRRM system increases when the distance between the IRRM sensor and the target is increased. Therefore, the accuracy of the relative measurement may degener-

ate with the increase of the distance between observer and target. Once the distance between two robots exceeds a certain threshold value, the acquired measurement may become more erroneous. This upper threshold is known as the sensing range for the particular IRRM system. For the localization approaches that rely on direct observation between robots (i.e. leader-assisted localization and relative localization), the pose estimations tend to diverge if the observed robots (child robots or target robots) navigate beyond the sensing range of the observing robot (leader robot or tracking robot). In order to have a bounded estimation error, the observed robots are required to navigate within the sensing range boundaries of the observing robot. This constraint also limits the teammates' maneuverability, reduces the area covered by the robots, and demands a complex algorithm to avoid inter-robot collisions.

Over-confident state estimations : This limitation mainly exists with the decentralized cooperative localization approaches. General decentralized cooperative localization approaches neglect the possible interactions among teammates' local pose estimations, and each pose measurement sent by the neighbours is considered as independent information. This drawback would allow the same information to propagate back and forth in the communication network causing overconfident state estimations.

Dynamic lag measurement update : Relative observations between teammates and flow of information among the teammates are the two key elements that form multi-robot collaborative localization. Pre-processing the acquired raw sensory data and exchange of these measurements between robots introduce unknown dynamic time lags between the actual observation and information available at the observed robot. The majority of available implementations

neglect this time delay and assume that the information is available for the observed robot instantly.

Out-of-sequence-measurement (OOSM) update : The behaviour of the communication networks is complex and may be effected by several environmental factors. Further, propagation time between two robots varies with the propagation path length between robots. Additionally, the processing time for a given estimation problem may vary depending on the types of processor used in the robot computer. Due to these three factors, the observations made by any observing robot may arrive at the observed robot or central processing center with some random time delays. As a result, the received information may not be in the same sequence as the measurements are taken. The majority of the available implementations assume the availability of a fully connected reliable network for data communication between robots and assume that the measurements are received in the same order as they are sent. In regards to practical implementation, these assumptions are not realistic.

Sensor fusion and system nonlinearity: Robots' motion models and IRRM are often nonlinear with respect to system states. In the paradigm of Bayesian filtering with Gaussian approximation, the EKF remains the popular sub-optimal nonlinear filtering approach for sensor fusion. However, hard linearization steps associated with the EKF potentially introduce bias and lead to an inconsistent representation of estimation uncertainty [10, 32]. This causes filter estimation to diverge. In other words, an EKF does not guarantee convergence [33]. In contrast to the EKF, an unscented Kalman filter (UKF) [34, 35] demonstrates better performance in terms of estimation accuracy and estimation uncertainty representation. Additionally, it preserves the second-order information of the

linearized system (motion or measurement) while the EKF preserves only the first-order information. However, a UKF-computed covariance matrix is not always guaranteed to be positive definite [36]. This eventually causes the filter to halt its operation. Heuristic solutions, such as fudging the covariance matrix artificially and the use of scaled unscented transformation have been proposed to overcome the non-positive definiteness of the covariance matrix [37–39]. The Cubature Kalman filter (CKF) is a recently developed sub-optimal nonlinear filter which uses the spherical-radial cubature rule to solve the multi-dimensional integral that is associated with the Bayesian filter under the Gaussian approximation [36]. CKF is a Jacobian-free approach that guarantees a positive definite covariance matrix and demonstrates superior performance compared with the celebrated EKF and the UKF [40–42].

Stability : Stability of the estimator is defined as the ability of an estimator to generate an estimation with a bounded uncertainty. Under certain conditions, each estimator (filter) could produce stable estimations. As an example, for the EKF, the estimation error remains bounded in a mean square if the system satisfies the nonlinear observability rank condition, the initial estimation error as well as the disturbing noise terms are small and the nonlinearities are not discontinuous. It is important to identify these conditions and select the appropriate filtering approach for sensor fusion in order to avoid the possible divergence (instability).

Data correspondence : When an observing robot acquires IRRM for multiple observed robots it is essential to accurately register each IRRM with the associated observed robot. Several approaches have been applied to solve the data correspondence problem (sensor registration problem) such as the nearest neighbour approach [43], maximum likelihood-based approach [44], joint compatibil-

ity branch and bounce approach [45], iterative closest point method [46], multiple hypothesis tracking approach [47] and joint probability data association method [48]. Each method has its own strength and weaknesses. Physical tagging is the commonly applied sensor registration method in cooperative localization in which colour or bar-codes are used to distinguish robots from one another [49].

1.2   Problem Statement
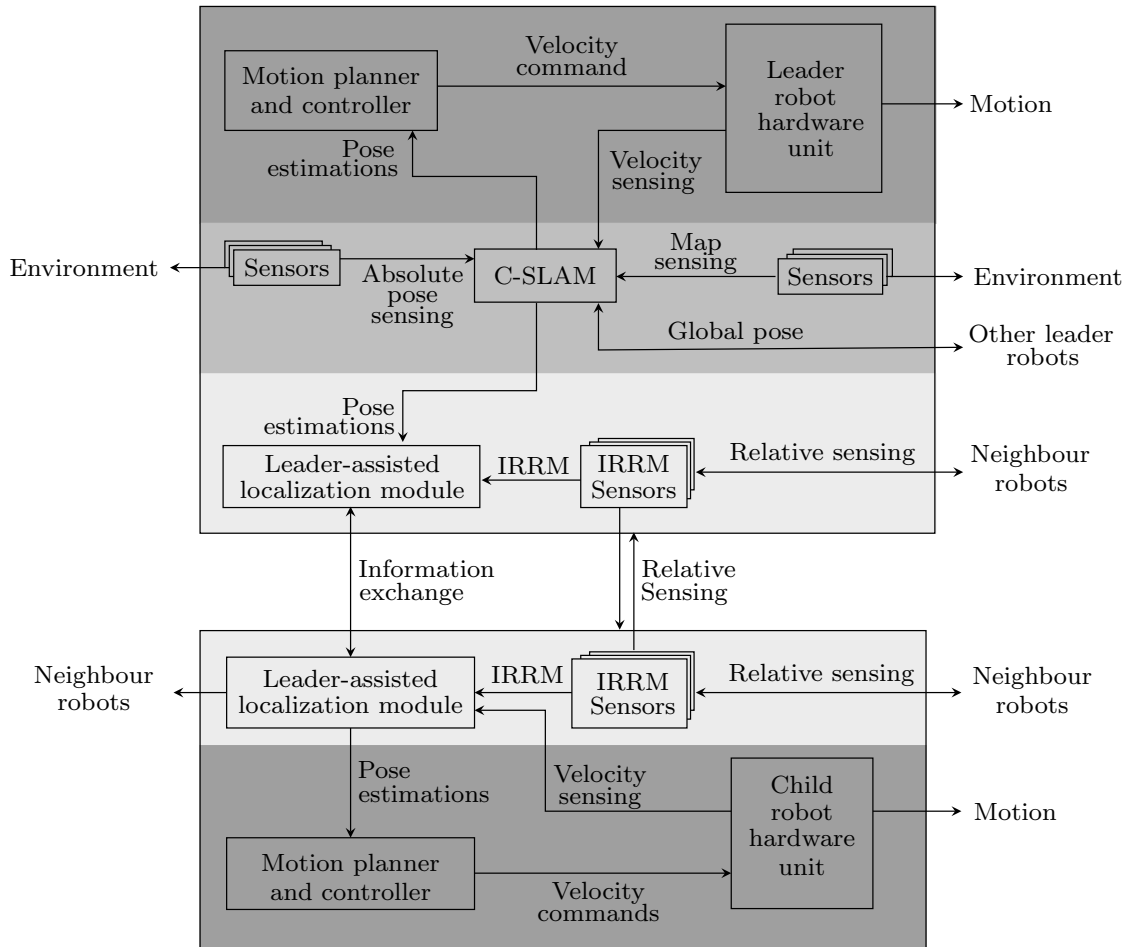
Figure 1.2: The localization and control architecture of the proposed heterogeneous MRS

This research study proposes an innovative leader-assisted localization framework in order to address the multi-robot collaborative localization problem of a heterogeneous MRS. Figure 1.2 shows the localization and control architecture for a leader-assisted localization based heterogeneous MRS. This MRS consists of a minimum of one leader robot and one or multiple child robots. Cooperative SLAM (C-SLAM) integrated with advanced localization sensors can be implemented for leader robots to provide better (more accurate) localization. Key modules of this architecture are the "Leader-assisted localization module", "IRRM sensors" and "C-SLAM" module. Research presented in this thesis mainly focuses on the "Leader-assisted localization" module and addresses a number of key limitations as discussed below.

1.2.1 Problem I: Finite-Range Sensing

Availability of relative pose measurements from leader to child is essential for the successful implementation of leader-assisted localization techniques. It is known that the uncertainty of the relative measurements obtained from the majority of the IRRMs degenerates when the gap between the sensor and the target is increased [50]. Therefore, the majority of available IRRM systems are incapable of generating relative measurements when the separation between the two robots exceeds a certain threshold value, imposing a sensing range limitation on the measurement system. Therefore, global pose measurements for child robots are not practical when the child robots operate beyond the sensing range of the leaders. The simple solution for this problem is to restrict the child robot's navigation to be within the sensing range of the leader robots. However, this constraint may limit the maneuverability of the MRS and may reduce the area covered by the robots. Additionally, this constraint requires higher processing power to execute a robust inter-robot collision avoidance algorithm specially when the team is contains relatively a large number of child robots as robots operate so

closely to one another. This additional processing power requirement can be eliminated by reducing the number of child robots in the MRS which indirectly adds a scalability issue to the leader-assisted localization framework. Therefore, developing a localization scheme for a heterogeneous MRS, allowing child robots to operate beyond the sensing range of the leader robot while ensuring bounded estimation error, has been identified as a requirement for implementing a leader-assisted localization-based collaborative mission.

This thesis investigates the feasibility of virtually expanding the leader robots' sensing range by enabling relative pose sensing capabilities in child robots . The initial study considers an MRS with single leader robot, which is later extended to more general scenarios where the MRSs can be formed with more than one leader robot. Priority is given to obtain non-overconfident pose estimations with bounded estimation error for each child robot by incorporating a graph search algorithm to avoid the problem of *double-counting*[4].

1.2.2   Problem II: Finite-Range Communication

Ability to communicate the calculated global pose measurement from the leader robot to a child robot is a key requirement for a heterogeneous MRS that relies on leader-assisted localization. The majority of the robots' onboard communication modules have a communication range limit constraint. The default communication range can be slightly enhanced by allocating more power for the transmitter unit causing the onboard power source to drain faster than at its usual rate. Then the heterogeneous MRS-based mission has to pause until batteries are re-charged, causing frequent in-

---

[4]This is also known as a *data incest* problem, a problem of *mutual information*, a *circular update* problem or a *cyclic update* problem. The double-counting problem arises when common information is shared by the local state estimate and state observation. Additionally, this can occur when the same measurement is used for a measurement update more than once.

terruptions to the mission. An alternative solution for this problem is to restrict the child robots' navigation within the communication boundaries of the leader robots. This constraint limits the maneuverability of the MRS, reduces the area covered by the robots, adds a scalability issue to the MRS, and may demand higher processing power to execute the state-of-the-art collision avoidance algorithm to avoid inter-robot collisions when the team is empowered with a large number of child robots. Some implementations assume that a robot can exchange information with the robots outside its communication range by instantaneously relaying information through another robot [51, ch. 2]. An instantaneous information relay through other robots is practically challenging and may not be possible. Therefore, development of an information exchange strategy that accounts for the time delay of information exchange between two robots is identified as a requirement to enable child robots' navigation beyond the communication range of the leader robot.

This thesis initially evaluates the instantaneous communication model in the context of leader-assisted localization incorporating a novel distributed graph search algorithm to avoid the double-counting problem. Priority is then given to extending the instantaneous communication model to a time-delayed communication model and developing algorithms to optimize memory usage and detect the best time step to apply the Markov property.

1.2.3   Problem III: IRRM Sensors

Available IRRM systems for multi-robot collaborative localization can be categorized into four major groups: relative range only [52, 53], relative bearing only [54–58], relative range and bearing (or relative position) [9, 10] and relative range and mutual bearing (or relative pose) [12, 59]. Most of these relative measurement approaches are applicable to the traditional leader-assisted framework wherein the leader robot pro-

vides localization information only for the child robots operating within the sensing and communication range of the leader. As the intention of my study is to develop a localization framework allowing child robots to navigate beyond the sensing and communication boundaries of the leaders while maintaining a bounded estimation error and a bounded estimation uncertainty, IRRM sensors with full relative pose sensing capability become a system requirement. Therefore, development of an algorithm in order to partially or fully eliminate this IRRM sensor type constraint is identified as a requirement to enhance the applicability of the proposed leader-assisted localization framework.

This thesis evaluates the applicability of a target tracking method in order to realize the proposed leader-assisted localization scheme using a relative range and bearing measurement system. To this end, the thesis implements a hierarchical filtering approach in which each robot runs local tracking filters to estimate the relative pose of neighbours using a general range-and-bearing based relative observation system. It is assumed that this sensory system is also has the sensing range constraint. These tracks (relative pose estimations) then pass through the leader-assisted localization module implementing the proposed localization scheme.

1.2.4 Problem IV: Scalability and Consistency of Cooperative Localization

When the robots in the MRS have long rage sensing and communication capabilities so that child robots are always connected to a measurement and communication network which has a minimum of one leader robot, then cooperative localization approaches become more viable compared with leader-assisted localization approaches. As outlined in previous sections, both centralized and multi-centralized cooperative localization approaches have the computational complexity of $\mathcal{O}(N^4)$ with respect

to the number of robots in the team (N). The computational complexity of the distributed cooperative localization approaches which use optimal fusion algorithms varies from $\mathcal{O}(N^4)$ to $\mathcal{O}(N^2)$ [59]. Thus, the centralized cooperative localization approaches, multi-centralized cooperative localization approaches and distributed cooperative localization approaches limit the scalability of the team. Additionally, these three architectures demand high communication bandwidth, and eventually limiting the number of robots in the MRS. Alternatively, decentralized cooperative localization approaches demonstrate linear computational cost with respect to the number of robots in the team. Moreover, the communication bandwidth requirement is also considerably lower as only neighbouring robots need to exchange information with one another. Further, decentralized cooperative localization approaches are robust against the single point of failure. However, most of the decentralized localization strategies neglect possible interdependencies between robots' predictive poses; thus, leading to the problem of double-counting. As a result, estimated poses using decentralized cooperative localization approaches are generally inconsistent with the true statistics of the estimation error. Therefore, developing a scalable and consistent cooperative localization strategy is identified as another key requirement for implementing a leader-assisted localization based heterogeneous MRS.

This thesis investigates a scalable cooperative localization approach which is capable of accurately representing the interaction between teammates' local pose estimations resulting in non-overconfident state estimations for each robot in the team.

1.3 Objectives and Expected Contributions

In order to achieve the proposed research goals, the following key objectives have been identified.

Objective 1 To develop a novel algorithm to virtually enhance leader robots' sensing range.

- Contribution 1: An algorithm to generate a centralized equivalent observation for each leader robot in an MRS.

- Contribution 2: A method to synthesize missing IRRMs between leader robots and child robots that operate beyond the sensing range of the leaders.

- Contribution 3: An algorithm to avoid the possible double counting of common information.

Objective 2 To extend the proposed distributed leader-assisted localization algorithm to address the finite-range communication problem.

- Contribution 4: An algorithm to virtually enhance leader robots' communication range.

- Contribution 5: A distributed global pose composition and graph search algorithm to synthesise the missing global pose measurements between the leader robots and the child robots while avoiding the problem of double-counting.

- Contribution 6: An algorithm to support time delayed state updates.

- Contribution 7: Theoretical analysis and a decentralized algorithm to define the length of a local Markov chain, and to define the optimal time step to marginalize the local Markov chain as well as discard the history of the measurements and state estimations.

Objective 3 To enable the implementation of the proposed distributed leader-assisted localization framework using general relative range and bearing measurement

systems.

- Contribution 8: Evaluation of the fast convergence filtering approach to estimate the relative pose of neighbouring robots using inter-robot range and bearing measurements.

- Contribution 9: Observability analysis for pseudo-linear measurement-based relative localization framework.

- Contribution 10: A hierarchical filtering approach implementing the proposed leader-assisted localization framework using inter-robot range and bearing measurements.

Objective 4 To design a scalable cooperative localization algorithm.

- Contribution 11: A decentralized cooperative localization approach that is capable of accurately representing independencies and interdependencies of each robot's local pose estimations.

1.4   Organization of the Thesis

Chapter 1 - Introduction : This chapter presents an overview of the research area, highlights the research statement, and outlines the objectives and the associated contributions of this study.

Chapter 2 - Background : This chapter presents the literature review in the area of multi-robot collaborative localization.

Chapter 3 - **Distributed leader-assisting localization with sensing range constraint :** This chapter relates to objective 1 of the thesis. The chapter

presents the mathematical formulation of the proposed decentralized leader-assisted localization framework addressing the limited-range sensing problem. Simulations and experimental results will be presented to validate the proposed localization architecture.

Chapter 4 - Distributed leader-assisting localization with sensing and communication range constraint : This chapter relates to objective 2 of the thesis. The chapter extends the work presented in Chapter 3 by incorporating the mathematical formulation to address the limited range communication problem. It concludes with presenting a series of simulation and experimental results to validate the proposed sensor fusion architecture.

Chapter 5 - Distributed leader-assisting localization with relative range and bearing measurements : This chapter relates to objective 3 of the thesis. The chapter integrates a hierarchical filtering architecture with the proposed decentralized leader-assisted localization framework enabling its usability over the inter-robot relative range and bearing measurement systems. The performance of the proposed hierarchical filtering approach is evaluated in a series of simulations and experiments.

Chapter 6 - Decentralized cooperative localization for a heterogeneous MRS : This chapter relates to objective 4 of the thesis. The chapter extends the general CKF to a split-covariance intersection (Split-CI)-based multi-sensor data fusion paradigm in order to develop a scalable, consistent decentralized cooperative localization framework. Simulation and experimental results will be presented to validate the proposed localization architecture.

Chapter 7 - Summary and Future Research : This chapter concludes the thesis

presenting the applicability of the proposed localization framework, its limitations and future directions for this research work.

Chapter 2

Background

2.1 Multi-robots Collaborative Localization

2.1.1 Leap-frogging Motion Pattern

The initial formulation of the multi-robot collaborative localization framework is reported in the works of Kurazume *et al.* [11]. In this initial formulation, an MRS is divided into two groups: *landmark group* and *moving group*. The localization of robots in the moving group is established through the pose information of the robots in the landmark group and relative observation between agents in the two groups. To this end, the robots in the landmark group remain stationary and act as portable landmarks while the robots in the moving group navigate. After a few iterations, the roles of the two groups are exchanged and this process continues until all agents have approached the goal location. This localization algorithm produces a "*leap-frogging*" motion pattern and is also known as the "*dance algorithm*" and was later adapted by several other researchers [14, 15]. The key limitation of the initial version of the cooperative positioning system, (CPS-I), [11], apart from the leap-frogging motion strategy, was that it neglects the measurement noise associated with the exteroceptive

sensory system. The second version of the cooperative positioning system, CPS-II, was introduced in 1996, and accounts for the noise associated with the exteroceptive sensory system [16, 60]. The final version of the cooperative positioning system was proposed in 1998 and is known as the CPS-III [61, 62]. This work studied the optimal motion strategies that teammates can follow so that pose estimation uncertainty can be minimized. The performance of the CPS-III was evaluated experimentally with UGVs that navigate in large open terrains and terrains which are cluttered with large numbers of obstacles. Several other researchers [17, 18] also searched for the optimal motion strategy and showed that there are multiple optimal trajectories that exist for reducing the estimation uncertainty, compared to the equilateral triangle formulation proposed by [61]. Recently, the cooperative positioning system has employed laser-based geometrical modeling of large-scale architectural structures [63, 64]. In this implementation, the cooperative positioning system was integrated with multi-robot SLAM and an interactive closest point algorithm to generate an accurate model of large-scale architectural structures. The key limitations of the leap-frogging-based cooperative localization strategies are:(a) at a given time step, only one robot or a portion of an MRS is allowed to navigate, increasing total mission completion time; (b) members in a moving team must maintain the line-of-sight (LOS) for a minimum of three stationary robots at all times; and (c) all implementations are essentially centralized systems where all the processing is done with a single processing system. Numerous multi-robot collaborative localization frameworks have been developed since 1994. These implementations can be categorized into six main groups: (1) Centralized cooperative localization, (2) Multi-centralized cooperative localization, (3) Distributed cooperative localization, (4) Decentralized cooperative localization, (5) Relative localization and (6) Leader-assisted localization.

2.1.2 Centralized Cooperative Localization

All centralized cooperative localization algorithms augment each robot's pose into a single state vector and perform the state estimation (group localization) task at a single processor which is referred to as the relative pose measurements for all robots in the team, then a maximum of $\mathcal{O}(N^2)$, relative pose measurements will be acquired at an IRRM event. As the computational complexity for processing a single relative pose measurement equals $\mathcal{O}(N^2)$, all centralized cooperative localization schemes have the overall computational complexity of $\mathcal{O}(N^4)$, per time step. Besides the high computational complexity, each robot needs to send both the proprioceptive and exteroceptive sensor readings to the central processor, demanding high data bandwidth for communication channels. These two limitations eventually introduce a scalability constraint for the MRS in terms of number of robots in the team. The requirement of an uninterrupted communication channel between the central processor and each agent in the team poses another condition where each robot should be operated within the communication range of the central processing unit. The bounded navigation space therefore may require added algorithms to avoid inter-robot collisions and may limit robots' maneuverability. In addition to these key limitations, all centralized cooperative localization algorithms are susceptible to the single point of failure. The recent advancement of centralized cooperative localization demonstrated that localization and moving object tracking are mutually beneficial [65]. This implementation augments the robots' pose, position of static landmarks, and position of the moving objects into a single state vector in order to maintain pairwise cross-correlation between robots and moving objects.

2.1.3 Multi-centralized Cooperative Localization

Multi-centralized approaches are proposed to improve the robustness of the general centralized cooperative localization approach against the single point of failure wherein the group state estimation process is duplicated on a few or all of the robots in the team [19, 27]. Although such duplication can improve the robustness against the single point of failure, these algorithms entail increased communicative complexity as compared to general centralized cooperative localization schemes. In general, the communicative complexity of the multi-centralized cooperative localization approach increases linearly with the number of robots (or processors). Hence, it demands even more bandwidth for data communication channels, unlike the general centralized cooperative localization approaches. Besides the increased communicative complexity, each robot is required to operate within the communication range of the others. The bounded navigation space therefore may require added algorithms to avoid inter-robot collisions and the limiting of robots' maneuverability. Work presented in [66] addressed the finite-range communication problem and proposed an innovative cooperative localization scheme for a sparsely-communicating robot network. The proposed architecture enables each robot to produce a delayed estimation of the team poses at a higher demand of communication bandwidth and memory usage. Although the proposed method is robust against the single point of failure and can perform the group localization task with an asynchronous communication network, practical applicability of this architecture is still questionable due to the large amount of data that need to be relayed within the network.

2.1.4 Distributed Cooperative Localization Approaches

The distributed cooperative localization algorithm is introduced to reduce the high bandwidth requirement associated with centralized and multi-centralized cooperative localization schemes. To this end, in the distributed cooperative localization algorithm, each robot runs a local filter to fuse ego-centric data while inter-robot observations are fused at a central processor. Therefore, high frequency ego-centric measurements are not required to communicate with the central processing unit which reduces the bandwidth requirement for the communication network. However, computational complexity shall remains at $\mathcal{O}(N^4)$ because the measurement update still performs in a centralized manner. The work presented in [12, 20] develops mathematical formulations to factorize the dense covariance matrix and then it propagates this factorized matrix using local sensory data of each robot. The key challenge of this implementation is that the failure of a single robot leads to the failure of the entire team pose estimation task. This initial formulation assumed the availability of relative pose measurements among teammates which is later relaxed by extending the algorithm for exteroceptive sensory systems that measure relative bearing, relative distance and relative orientation among robots [67]. A maximum a posteriori estimator-based distributed cooperative localization algorithm is presented in [68] which improves the robustness of the distributed localization algorithm against the single point of failure while reducing the computational cost to $\mathcal{O}(N^2)$. However, this implementation also demands a fully connected synchronous network throughout the mission. An extended information filter-based optimal decentralized cooperative localization algorithm is reported in [69, 70]. This algorithm maintains the history of the IRRM in order to produce consistent state estimations. As a result, the algorithm possesses an increased computational cost with every new inter-robot observation.

2.1.5 Decentralized Cooperative Localization Approaches

The key objective of decentralized cooperative localization approaches is to reduce the computational complexity associated with the three multi-robot collaborative localization schemes outlined in the previous sections. Using decentralized cooperative localization, each robot locally runs an estimator (filter), such as an EKF or particle filter, to estimate its own pose. Each robot hosts an exteroceptive sensory system to acquire the IRRM of its neighbours. At an inter-robot measurement event, a robot taking inter-robot relative measurements for an arbitrary robot is termed the *observing robot* and the robot that came into the sensing range of the observing robot is called the *observed robot*. Robots exchange their current pose estimation and IRRMs with neighbours in order to perform the measurement update steps independently. Although this approach is computationally less complex and demands less memory space, it neglects the possible correlation between the pose estimates between teammates. This simplification allows common past information to flow backwards-and-forwards within the team, generating overconfident pose estimations for teammates. The first Monte-Carlo decentralized cooperative localization algorithm was introduced in 2000 by Fox *et al.* [21]. This was later adapted by several other researchers [28]. This algorithm demands larger particle sets in order to avoid the depletion of particles. Prorok *et al.* [22] introduced a novel sampling algorithm, named a *reciprocal sampling algorithm*, in order to reduce the size of the particle set. In this method, the observed robots re-sample particles from two probability distributions; (a) from their own belief with the probability of $(1-\alpha)$, and (b) from reciprocal robot observation with a probability of α; where α is defined as reciprocal proportion. The overall complexity of the reciprocal sampling algorithm is further reduced using a particle clustering algorithm [29]. All these algorithms neglect cross-correlation between each team member's local pose estimation, leading to an overconfident state update.

Several works have been reported to improve the consistency of the decentralized cooperative localization algorithms. A hierarchical filtering approach is presented in [71] in which the MRS is divided into several subgroups. Each group has a leader robot which produces a pose estimation for members in the corresponding subgroup. Leader robots themselves form a subgroup. However, this algorithm also neglected possible interactions between subgroups, causing inconsistent state updates. The state exchange approach is presented in [72,73], wherein only the independent information is allowed to be exchanged between teammates after an inter-robot observation. Since only the independent information is exchanged, this implementation does not suffer from the overconfident state generation problem. However, it has two other limitations, i.e., a vehicle cannot benefit from the vehicles beyond its sensing range and needs to maintain a bank of estimators similar to [74], leading to higher memory and processing requirements. Work presented in [75] uses a *dependency-tree* to track the recent interaction of robots. However, this approach maintains only the recent interdependencies of the robot pose estimate; it tends to be overconfident. An interlaced EKF-based sub-optimal filtering approach is presented in [23, 74] to avoid the possibility of generating an overconfident state estimation. This approach requires each robot in the MRS to maintain a bank of EKFs representing the interaction among teammates. Although it produces a non-overconfident state estimation, this book-keeping approach is unscalable, as the number of EKF runs on a single robot increases exponentially with the number of robots in the MRS. A sub-optimal filtering approach called *channel filtering* is presented in [76] which requires a communication network without loops as the algorithm does not include a mechanism to identify double counting of common information. However, a communication network without loops is an unrealistic assumption for practical implementation of cooperative localization. Covariance-intersection (CI)-based approaches are also reported

for decentralized cooperative localization [59]. However, the general CI algorithm neglects possible independencies between local estimates. This may lead to a more conservative state estimation and may produce an estimation error covariance which is larger than that of the best unfused estimate [77]. A common past-invariant ensemble Kalman filter-based optimal decentralized cooperative localization algorithm is proposed in [78]. This implementation uses 10,000 ensembles to represent robot pose estimation and develop mathematical formulas for generating optimal state estimation without maintaining cross-correlation information for the vehicles' predictive densities. However, larger number of ensembles are undesirable for robotic systems as they have limited processing power and memory space.

2.1.6 Relative Localization and Leader-Assisted Localization

Relative localization attempts to detect and track one or more robots in another moving robot body-fixed coordinate frame [30, 31]. The estimation of relative positions within an MRS is important for many collective operations, such as inter-robot collision avoidance [79], pattern generation [80, 81], self-configuration [82], flocking [83] and chain formation [84]. In the absence of a common global reference frame and associated inter-robot pose estimates, an MRS encounters difficulty in performing effective coordination and executing a collaborative mission. When the robots' self-localization becomes erroneous, the sharing of sensory and other information between robots becomes less valuable.

Relative localization has been developed as a viable solution for effective and accurate execution of multi-robot collaborative missions [85, 86]. Moreover, relative localization has been identified as a feasible localization solution for a heterogeneous MRS wherein the localization of child robots is established with the help of leader robots [9, 87]. Available literature widely studied about various filtering approaches [9, 88–90],

IRRM systems [9, 50, 91], and algorithms to handle measurement anonymity [92–95] for implementing relative localization for multi-agent systems. Candidate indoor positioning systems are also reported for the purpose of relative localization in ground aerial robot teams. Some of these implementations could not achieve the acceptable level of accuracy [96] while the others are laboratory level implementations [97, 98] which may not directly applicable for real-world applications.

Leader-assisted localization is mainly implemented to assist the navigation of less capable robots (child robots) using inter robot observation between the less capable robots and more capable robots (leader robots) [25]. Although relative localization approaches also attempt to establish accurate localization for child robots with the help of leader robots [9, 87], these algorithms estimate the pose of the child robots on the body-fixed coordinate system of the leader robots. In contrast, leader-assisted localization attempts to establish the accurate localization for child robots in a reference coordinate frame. Apart from this key difference, both the localization algorithms are based on the same principle, that the system has a leader robot(s) and child robots wherein the child robots' navigation is assisted by the leader robots. This will eventually imposes a condition that the child robots should be operated within the sensing and communication range of leader robots. The bounded navigation space therefore may require added algorithms to avoid inter-robot collisions and may limit the robots' maneuverability. However, if this constraint can be relaxed it will allow the robots to operate within a larger space, giving MRS a larger volume of coverage. Any algorithm that attempts to relax this constraint should address the finite-range sensing and communication problem associated with leader-assisted localization.

2.2 Communication Bandwidth Constraints in Multi-robot Collaborative Localization

Communication bandwidth constraints associated with general cooperative localization algorithms have drawn some attention from the robotic research community. An optimal sensor scheduling method for a resource-constrained MRS is presented in [99]. The method limits the number of measurements processed at each time step so that the available bandwidth is sufficient to transmit the selected measurement set. The proposed method is sub-optimal as only the subset of available data is processed for state estimation. Additionally, the method is not scalable as the IRRM frequency inevitably decreases with an increase in team size. The limited range communication problem is addressed by Leung *et al.* [66]. Although this implementation is capable of generating a centralized equivalent form of cooperative localization, it demands considerably larger communication bandwidth. Nerurkar *et al.* [68] extended the work presented in [66] and attempted to solve the bandwidth requirement problem associated with decentralized cooperative localization. This study proposed two information-transformation schemes, where each robot communicates: (i) only the measurements acquired by its local sensors, but from the beginning of the mission, and (ii) all available measurements, which include local sensory data as well as measurement data collected from teammates, for past q time steps. The problem of multi-centralized cooperative localization under server communication constraints is studied in [100]. This study adopted the sign-of-innovation Kalman filter (SOI-KF) for sensor fusion and considered server communication constraints where each robot can communicate only a single bit per time step. The general formulation of the SOI-KF does not allow the use of the quantized version of the egocentric reading for state estimation. Work presented in [100] addressed this limitation and proposed a hybrid

estimation framework that allows both local sensory data as well as information sent from neighbours to be fused together in order to compute the posterior density of the robot's state. This work was later extended to allow robots to communicate more than a single bit per time [101]. The major limitation of all the approaches that studied communication constraints is that they are essentially multi-centralized approaches which have a computational cost of $\mathcal{O}(N^4)$. Thus, all these algorithms are poorly scalable with the number of robots in the team.

2.3 Performance Evaluation of Multi-robot Collaborative Localization

Apart from the numerous implementations and sensor fusion architectures, the analytical evaluation of the performance of multi-robot collaborative localization has received limited attention from the robotics community. Work presented in [102] evaluated the effect of various relative measurement approaches on the accuracy of cooperative localization. Additionally, it evaluated how the accuracy of the localization is affected by the number of robots in the team. This study revealed that the full relative-pose measurement always[1] generates a more accurate estimation compared with range-only, bearing-only, and range-and-bearing measurement systems. The lowest estimation accuracy was found with the bearing-only measurement system. Additionally, it was found that increasing the number of robots in an MRS has a positive impact on the estimation accuracy. Later it was discovered that there is a diminishing advantage in regards to uncertainty reduction as the size of the team increases [103]. The study presented in [104] demonstrated that the most important

---

[1]Under the assumption that each robot operate one another sensing and communication boundaries.

factors for estimation accuracy are not the number of robots in the team or number of IRRMs between teammates but the availability of an accurate proprioceptive sensory system and the means of accurate orientation estimates.

2.4 Out-of-Sequence Measurement Update

The observation produced by an observing robot or multiple observing robots may reach the corresponding observed robot with an unknown time delay due to the delays in communication channels and pre-processing delay. The challenge is how to utilize the *older* measurement to update the *current* pose estimation. This problem has received minor attention from the robotics community. Work presented in [66] and [70] are the known cooperative localization implementations that can handle an out-of-sequence-measurement (OOSM) update problem. These implementations maintain a history of IRRM as well as temporarily storing the ego-motion sensor reading. Thus, these algorithms can use *older* measurements to update a current pose estimation.

The OOSM update is a widely discussed topic in multi-sensor target tracking applications. A number of optimal algorithms [105–109] as well as suboptimal algorithms [105, 110, 111] have been proposed to perform one-lag [105] as well as multi-lag [106, 107, 110, 111] OOSM updates. Both the optimal and suboptimal one-lag OOSM update algorithms demand a nonsingular state transition matrix. The optimal multi-lag OOSM update algorithms generally use augmented state smoothing approaches [106, 107]. The studies presented in [105, 110] suggested that the only way to incorporate OOSM to produce an optimal solution for a given state estimation problem is to sequentially reprocess all available measurements. Work presented in [112, 113] combines the data association problem and OOSM update problem to implement a multi-sensor multi-target tracking application.

Chapter 3

Distributed Leader-Assisted Localization with Sensing Range Constraints

This chapter, introduces the study of distributed leader-assisted localization with sensing range constraints by assuming an unbounded communication range for each robot in a heterogeneous-MRS[1]. This assumption allows a focus on developing a mathematical framework in order to virtually expand the sensing range of each leader robot in the heterogeneous-MRS.

3.1   Mathematical Preliminaries

To facilitate the mathematical formulation, superscript or subscript 'l' is used to represent variables or parameters that are related to leader robots, while the super-

---

[1]The work in this chapter is published in IEEE transaction on automation science and engineering * T. R. Wanasinghe, G. K. I. Mann and R. G. Gosine, "Distributed Leader-Assistive Localization Method for a Heterogeneous Multi-robotic System," in IEEE Transactions on Automation Science and Engineering, vol. 12, no. 3, pp. 795-809, July 2015.

script or subscript 'c' is used to represent variables or parameters that are related to child robots. For an MRS, let $\mathcal{C}$ represent the set that contains the unique identification indices of all the child robots. The cardinality of the set $\mathcal{C}$, i.e. $|\mathcal{C}|$, gives the total number of child robots in the MRS. These child robots are represented by $\{\mathcal{R}_{c_1},\ \mathcal{R}_{c_2},\ \cdots,\ \mathcal{R}_{c_{|\mathcal{C}|}}\}$. Similarly, let $\mathcal{L}$ represent the set that contains the unique identification indices of all leader robots. The cardinality of the set $\mathcal{L}$, i.e. $|\mathcal{L}|$, gives the total number of leader robots in the MRS. The leader robots in the MRS are represented by $\{\mathcal{R}_{l_1},\ \mathcal{R}_{l_2},\ \cdots,\ \mathcal{R}_{l_{|\mathcal{L}|}}\}$. Let $\mathcal{S}$ represent the set that contains the unique identification indices of all robots in the MRS; i.e., $\mathcal{S}$ is the union of set $\mathcal{C}$ and set $\mathcal{L}$. This study assumes that each robot navigates on flat terrain and is equipped with a communication device in order to exchange information with leader robots. Two sensory systems are hosted by each robot in the MRS: (a) a wheel encoder to obtain odometry, and (b) a light-weight exteroceptive sensory system to measure the relative pose of neighbours. It is assumed that the exteroceptive sensory system is capable of uniquely identifying neighbours. In other words, it is assumed that the data association problem has been solved by the exteroceptive sensory system. This sensory system acquires relative pose measurements periodically. Besides these two sensory systems, leader robots host additional sensors, such as the DGPS and compass, resulting in higher pose estimation accuracy compared to the child robots.

3.1.1 Robots' Motion Model

Robots' navigation in a 2D space is modelled by the general three degrees of freedom (3-DOF) discrete-time kinematic model for the ground robots in the MRS

$$\mathbf{x}_{q,k} = \mathbf{g}(\mathbf{x}_{q,k-1}, \bar{\mathbf{u}}_{q,k-1}) \quad \forall q \in \mathcal{S}$$

$$\begin{bmatrix} x \\ y \\ \phi \end{bmatrix}_{q,k} = \begin{bmatrix} x \\ y \\ \phi \end{bmatrix}_{q,k-1} + \delta t \begin{bmatrix} \bar{v}_x \cos(\phi) - \bar{v}_y \sin(\phi) \\ \bar{v}_x \sin(\phi) + \bar{v}_y \cos(\phi) \\ \bar{\omega}_z \end{bmatrix}_{q,k-1} \tag{3.1}$$

where, $\mathbf{x}_{q,k} \in \mathbb{R}^3$ is the robot's pose at discrete time k and $\mathbf{g}(\cdot)$ represents the nonlinear state propagation function. δt is the sampling time interval. $\bar{\mathbf{u}}_{q,k} \in \mathbb{R}^3$ is the system input and $\bar{\mathbf{u}}_{q,k} = \mathbf{u}_{q,k} + \boldsymbol{\nu}_{q,k}$; where, $\mathbf{u}_{q,k} = [v_x \ v_y \ \omega_z]$. v_x and v_y are nominal linear velocities in x-, and y-directions, respectively. ω_z is the nominal angular velocity. $\boldsymbol{\nu}_{q,k}$ represents the additive white Gaussian noise term with covariance $\mathbf{Q} \in \mathbb{R}^{3\times3}$. For nonholonomic robotic systems, terms associated with linear velocities in y-direction, i.e. $\bar{v}_y \sin(\phi)$ and $\bar{v}_y \cos(\phi)$, are set to zero.

3.1.2 Inter-Robot Relative Measurement Model

Relative pose measurement capability is assumed for each member in the MRS. Consider a scenario where robot $\mathcal{R}_q$ measures the relative pose of robot $\mathcal{R}_r$. This relative pose measurement can be modeled as

$$\mathbf{y}_{q,k}^{r,q} = \mathbf{h}(\mathbf{x}_{q,k}, \mathbf{x}_{r,k}) + \mathbf{n}_{q,k}^{r,q} \quad \forall q \in \mathcal{S},$$

$$\forall r \in \mathcal{S}_{q,k}, \ d_{q,k}^{r,q} \leq d_m$$

$$\begin{bmatrix} \delta x \\ \delta y \\ \delta \phi \end{bmatrix}_{q,k}^{r,q} = \boldsymbol{\Gamma}_{\mathbf{x}_{q,k}}^T (\mathbf{x}_{r,k} - \mathbf{x}_{q,k}) + \mathbf{n}_{q,k}^{r,q} \tag{3.2}$$

with

$$\mathbf{\Gamma}_{\mathbf{x}_{q,k}} = \begin{bmatrix} \mathbf{C}(\phi_{q,k}) & \mathbf{0}_{2\times 1} \\ \mathbf{0}_{1\times 2} & 1 \end{bmatrix}$$

$$\mathbf{C}(\phi_{q,k}) = \begin{bmatrix} \cos(\phi_{q,k}) & -\sin(\phi_{q,k}) \\ \sin(\phi_{q,k}) & \cos(\phi_{q,k}) \end{bmatrix}$$

where $\mathbf{y}_{q,k}^{r,q} \in \mathbb{R}^3$ is the relative pose of robot $\mathcal{R}_r$ as measured by $\mathcal{R}_q$; i.e. $\mathbf{y}_{q,k}^{r,q} = \begin{bmatrix} \delta x_{q,k}^{r,q} & \delta y_{q,k}^{r,q} & \delta\phi_{q,k}^{r,q} \end{bmatrix}^T$ where δx, δy and $\delta\phi$ are x-position, y-position and the orientation of robot $\mathcal{R}_r$ with respect to local coordinate frame of robot $\mathcal{R}_q$. This pose measurement is on the body-fixed coordinate system of robot $\mathcal{R}_q$. The nonlinear measurement function is represented by $\mathbf{h}(\cdot)$. The measurement noise covariance, $\mathbf{n}_{q,k}^{r,q}$, is assumed to be an additive white Gaussian noise with covariance $\mathbf{R}_{q,k}^{r,q} \in \mathbb{R}^{3\times 3}$. Parameters $d_{q,k}^{r,q}$ and d_m represent the distance between two robots and the sensing range of robot $\mathcal{R}_q$, respectively. $\mathcal{S}_{q,k}$ represents the set that contains unique identification indices of robots that are within the sensing range of robot R_q at the discrete time k. The matrix transpose operation is represented by T.

For a given inter-robot relative measurement event, a given robot in the MRS may acquire relative pose measurements for multiple neighbours. Let

$$\mathcal{Y}_{q,k} = \{p(\mathbf{z}_{q,k}^{r,q}) | r \in \mathcal{S}_{q,k}, \ d_{q,k}^{r,q} \leq d_m\} \tag{3.3}$$

represent all relative pose measurements acquired by robot R_q at time step k; where $p(\mathbf{z}_{q,k}^{r,q}) = \mathcal{N}(\mathbf{y}_{q,k}^{r,q}, \mathbf{R}_{q,k}^{r,q})$. A subset of the measurement set $\mathcal{Y}_{q,k}$ contains relative measurements for neighbouring child robots. This subset is represented by

$$\mathcal{Y}_{q,k}^{c,q} = \{p(\mathbf{z}_{q,k}^{r,q}) | r \in \mathcal{S}_{q,k}^c, \ d_{q,k}^{r,q} \leq d_m\}. \tag{3.4}$$

where $\mathcal{S}_{q,k}^c$ represents the set that contains unique identification indices of child robots that are within the sensing range of robot $\mathcal{R}_q$ at the discrete time k.

3.1.3 Child Robots' Pose Measurement

The leader robot's pose estimation density (belief) is defined as $p(\mathbf{x}_{l,k}) = \mathcal{N}(\hat{\mathbf{x}}_{l,k}, \hat{\mathbf{P}}_{l,k})$, where $\mathcal{N}(\hat{\mathbf{x}}_{l,k}, \hat{\mathbf{P}}_{l,k})$ represents that the pose estimation follows a Gaussian distribution with mean pose estimation of $\hat{\mathbf{x}}_{l,k}$ and covariance of $\hat{\mathbf{P}}_{l,k}$. According to equation (3.4), $\mathcal{Y}_{l,k}^{c,l}$ contains relative pose measurement densities for child robots that operate within the sensing range of the leader robot. The leader robot combines its current pose estimation $p(\mathbf{x}_{l,k})$ with the measurement densities in $\mathcal{Y}_{l,k}^{c,l}$, to generate global pose measurements for child robots. Let

$$\mathcal{Y}_{l,k}^{c,*} = \{p(\mathbf{y}_{l,k}^{c,*}) | l \in \mathcal{L}, c \in \mathcal{S}_{l,k}\} \tag{3.5}$$

represent the set of global pose measurement densities for child robots that are generated by a given leader robot at time k; where $p(\mathbf{z}_{l,k}^{c,*}) = \mathcal{N}(\mathbf{y}_{l,k}^{c,*}, \mathbf{R}_{l,k}^{c,*})$ represents the pose measurement density of a child robot as computed by a leader robot and $p(\mathbf{y}_{l,k}^{c_i,*}) = p(\mathbf{x}_{l,k}) \oplus p(\mathbf{z}_{l,k}^{c_i,l}); \ \forall c_i \in \mathcal{S}_{l,k}^c$. Operator $\oplus$ is the pose composition operator [13, 114, 115]. This pose composition is analogous to Cartesian-to-Cartesian coordinate conversion[2]. A superscript asterisk (*) indicates that the parameter (vector or matrix) associated with the asterisk mark is in the reference (global) coordinate frame.

---

[2]Cartesian-to-Cartesian coordinate conversion will be discussed in detail in Section 6.3.2

3.2 Relative Pose Measurement in an MRS

In the proposed localization algorithm, it is important for the leader robots to have complete knowledge of the instantaneous relative pose measurement data and the relative pose measurement topology in order to ensure that: (a) all the child robots that are connected with the measurement network receive localization data from the leader robots even when the child robots operate beyond the sensing range of the leader robots; and (b) the problem of double-counting does not occur.

3.2.1 Relative Pose Measurement Graph (RPMG)

A relative pose measurement graph (RPMG) is a directed graph $\mathbf{G}_{\mathcal{S}} \triangleq \{\zeta, \vartheta\}$, where ζ is the node set that represents robots in the MRS and $\vartheta \subset \{\zeta \times \zeta\} = p(\mathbf{z}_{j,k}^{i,j})$, $i \in \mathcal{S}$, $j \in \mathcal{S}$ and $i \neq j$ is the edges set representing the available relative pose measurements between robots. The RPMG for a given MRS can be presented in two perspectives: a global perspective and a local perspective. In the global perspective, the available relative pose measurements between robots are examined from the perspective of an outside observer. This contains all robots (nodes) in the MRS and all the available measurements between robots (edges) in a single graph. From the perspective of a given robot, it awares of the robots operating within its sensing range. This is known as the local perspective of the RPMG. A sample robot configuration and the associated RPMGs are illustrated in Fig. 3.1 and Fig. 3.2, respectively.

3.2.2 Hierarchical-RPMG

A hierarchical-RPMG is a directed graph $\mathbf{G}_{\mathcal{L}} \triangleq \{\bar{\zeta}, \bar{\vartheta}\}$, where $\bar{\zeta} \subseteq \zeta$ and $\bar{\vartheta} \subseteq \vartheta$, without symmetric pairs of directed edges and without loops between two nodes. The root-node of the hierarchical-RPMG represents a given leader robot and all other

nodes (head-nodes) represent child robots. The hierarchical-RPMG that corresponds to the sparse robot configuration given in Fig. 3.1 is illustrated in Fig. 3.3.
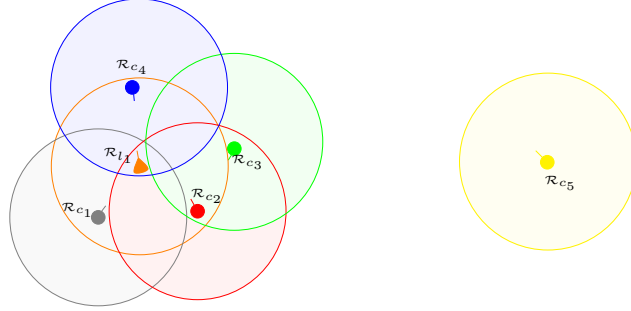
Figure 3.1: Sparse configuration of a robot team. A shaded area with a solid outline represents an individual robot's sensing range.

(a) Global perspective

(b) Local perspective of robot $\mathcal{R}_{c_2}$
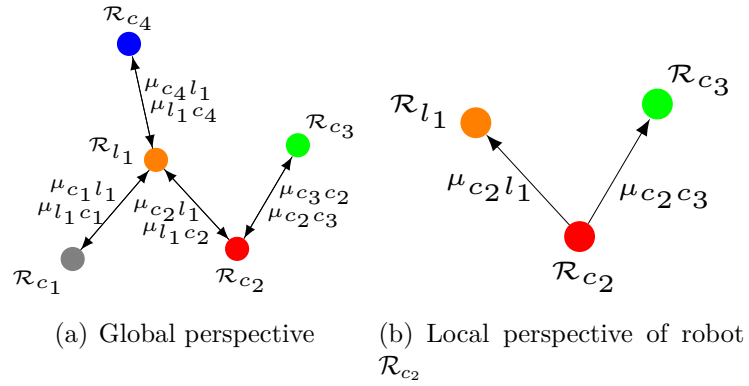
Figure 3.2: Relative pose measurement graph (RPMG). The nodes represent a robot's pose and the edge represents pose measurements. $\mu_{ij} = p(\mathbf{z}_{i,k}^{j,i})$
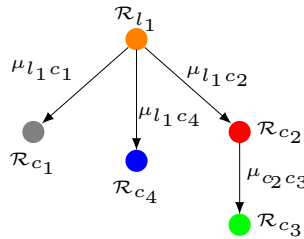
Figure 3.3: Hierarchical relative pose measurement graph for the sparse robot configuration given in Fig. 3.1. $\mu_{ij} = p(\mathbf{z}_{i,k}^{j,i})$

41

3.3 MRS with a Single Leader Robot and Multiple Child Robots

At each relative pose measurement event, each robot communicates unique identification indices of robots within its sensing range along with the corresponding relative pose measurements, i.e., set $\mathcal{S}_{q,k}$ and set $\mathcal{Y}_{q,k}$, to the leader robot. When the leader robot has received this information its knowledge set becomes the union of its own information set and the information sent by the teammates:

$$
\mathcal{S}_{l,k}^{+} = \mathcal{S}_{l,k} \bigcup_{\forall q \in \mathcal{S}} \mathcal{S}_{q,k} = \mathcal{S} \tag{3.6}
$$

$$
\mathcal{Y}_{l,k}^{+} = \mathcal{Y}_{l,k} \bigcup_{\forall q \in \mathcal{S}} \mathcal{Y}_{q,k} = \mathcal{Y}_k \tag{3.7}
$$

where

$$
\mathcal{Y}_k = \{p(\mathbf{z}_{q,k}^{r,q}) | p(\mathbf{z}_{q,k}^{r,q}) \in \bigcup_{\forall q \in \mathcal{S}} \mathcal{Y}_{q,k}\}
$$

represents the set of relative pose measurement densities that corresponds to the relative pose measurements acquired by all the members of the MRS at time step k. The leader can then construct the RPMG in the global perspective. Let $v_l \xrightarrow{\exists(\text{path})_b^a} v_{c_j}$ represent a path between leader node (v_l) and an arbitrary child node (v_{c_j}), where a is the number of paths available between the v_l and v_{c_j}, and b is the number of edges in the shortest path. In the global perspective, child robots in the MRS can be classified into four groups:

- $\mathcal{G}_1 = \{c_j | v_l \xrightarrow{\exists(\text{path})_1^1} v_{c_j}\}$; where $v_l \xrightarrow{\exists(\text{path})_1^1} v_{c_j}$ represents that there exists only a single path from the leader robot to child robot $\mathcal{R}_{c_j}$. Furthermore, this path consists of a single edge.

- $\mathcal{G}_2 = \{c_j | v_l \xrightarrow{\exists(\text{path})^1_{>1}} v_{c_j}\}$; where $v_l \xrightarrow{\exists(\text{path})^1_{>1}} v_{c_j}$ represents that there exists a single path from the leader to child robot $\mathcal{R}_{c_j}$. However, the number of edges in this path is greater than one.

- $\mathcal{G}_3 = \{c_j | v_l \xrightarrow{\exists(\text{path})^{\geq 1}_{\geq 1}} v_{c_j}\}$; where $v_l \xrightarrow{\exists(\text{path})^{\geq 1}_{\geq 1}} v_{c_j}$ represents that there exist multiple paths from leader robot to child robot $\mathcal{R}_{c_j}$. The number of edges in the shortest path can be greater than or equal to one.

- $\mathcal{G}_4 = \{c_j | v_l \xrightarrow{\nexists(\text{path})} v_{c_j}\}$; where $v_l \xrightarrow{\nexists(\text{path})} v_{c_j}$ represents that no path exists from the leader robot to child robot $\mathcal{R}_{c_j}$.

3.3.1 Search for the Best Path to a Child Robot

Child robots in the group $\mathcal{G}_3$ have multiple paths from the leader robot. If the leader robot composes and provides global pose measurements for a single child robot through all available paths then the pose estimation of the child robot tends to be overconfident. This can be attributed to the double-counting of the leader robot's pose information through multiple paths. In order to overcome this issue, it is essential to select a single path based on some optimization criteria. To this end, this study uses a breadth-first graph search algorithm to obtain the shortest path while discarding all other paths between the leader robot and a given child robot, constructing the hierarchical-RPMG for the current relative pose measurement event. As the hierarchical-RPMG does not include symmetric pairs of directed edges and loops between two nodes, child robots in an MRS can be classified into three groups with respect to the associated hierarchical-RPMG:

- $\mathcal{G}_{h1} = \{c_j | v_l \xrightarrow{\exists(\text{path})^1_1} v_{c_j}\}$;

- $\mathcal{G}_{h2} = \{c_j | v_l \xrightarrow{\exists(\text{path})^1_{>1}} v_{c_j}\}$; and

- $\mathcal{G}_{h3} = \{c_j | v_l \xrightarrow{\nexists(\text{path})} v_{c_j}\}.$

Equation (3.5) can be instantly exploited to construct the global pose measurement for child robots in the group $\mathcal{G}_{h1}$. Although a given robot in the group $\mathcal{G}_{h2}$ has a path from the leader robot, no direct relative pose measurement from the leader robot to the child robot exists. Therefore, pre-processing is required in order to construct the missing relative pose measurement between the leader robot and the child robots. This will be discussed in the next section (Section 3.3.2). Since there is no path available between the leader robot and the child robots in the group $\mathcal{G}_{h3}$, no measurement update will occur on any robot in $\mathcal{G}_{h3}$.

3.3.2   Enhancing Local Perspective of the Leader Robot

Consider a sample branch of a hierarchical-RPMG shown in Fig. 3.4.
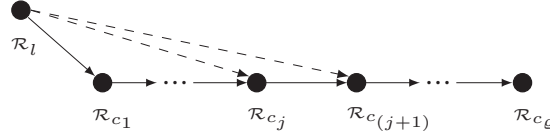
Figure 3.4: A sample branch of a hierarchical-RPMG

The leftmost node, $\mathcal{R}_l$, is the root-node (or top-node) of this hierarchical-RPMG while the rightmost node, $\mathcal{R}_{c_\varrho}$, is the end-node (or bottom-node) of this branch. Assume that the relative pose measurement for the child robot $\mathcal{R}_{c_j}$ is available in the measurement space of the leader robot, i.e. $\mathbf{y}_{l,k}^{c_j,l} \in \mathcal{Y}_{l,k}^{c,l}$. Additionally, the relative pose measurement from child robot $\mathcal{R}_{c_j}$ to child robot $\mathcal{R}_{c_{(j+1)}}$ is also available with the leader robot, i.e. $\mathbf{y}_{c_j,k}^{c_{(j+1)},c_j} \in \mathcal{Y}_{l,k}^{+}$. Then the following pose composition gives the relative pose measurement for child robot $\mathcal{R}_{c_{(j+1)}}$ as measured by the leader robot, where $\mathbf{g}_r(\cdot)$ is the nonlinear relative coordinate frame transformation function.

$$\mathbf{y}_{l,k}^{c_{(j+1)},l} = \mathbf{g}_r(\mathbf{y}_{l,k}^{c_j,l}, \mathbf{y}_{c_j,k}^{c_{(j+1)},c_j}) = \mathbf{y}_{l,k}^{c_j,l} \oplus \mathbf{y}_{c_j,k}^{c_{(j+1)},c_j}, \tag{3.8}$$

Once this operation is performed, the relative pose measurement and the associated measurement covariance for child robot $\mathcal{R}_{c_{j+1}}$ become available in the leader robot's measurement space. This implies that set $\mathcal{S}_{l,k}^c$ and set $\mathcal{Y}_{l,k}^c$ are updated as (3.9) and (3.10), respectively.

$$
\begin{align}
\mathcal{S}_{l,k}^c &= \mathcal{S}_{l,k}^c \cup \{c_{j+1}\} \tag{3.9} \\
\mathcal{Y}_{l,k}^c &= \mathcal{Y}_{l,k}^c \cup \{(\mathbf{y}_{l,k}^{c_{(j+1)},l}, \mathbf{R}_{l,k}^{c_{(j+1)},l})\} \tag{3.10}
\end{align}
$$

The leader robot sequentially performs this coordinate transformation until it reaches all the end nodes of the hierarchical-RPMG. This operation virtually enhances the sensing range of the leader robot.

Lemma 3.3.1. *For an MRS with a single leader robot and one or more child robots, $p(\mathbf{z}_{l_1,k}^{c_j,*})$ exists if and only if a path exists from the leader robot to the child robot on $\mathbf{G}_\mathcal{S}$, $(c_j \in \mathcal{C})$.*

Proof. First, assume that the $p(\mathbf{z}_{l_1,k}^{c_j,*})$ exists. From equation (3.5), the relative pose measurement for the child robot $\mathcal{R}_{c_j}$, $p(\mathbf{z}_{l_1,k}^{c_j,l_1})$ must exist in order to construct the child robot's pose measurement density $p(\mathbf{z}_{l_1,k}^{c_j,*})$. $p(\mathbf{z}_{l_1,k}^{c_j,l_1})$ exists only if there exists a path from the leader robot to the child robot $\mathcal{R}_{c_j}$, $(c_j \in \mathcal{C})$.

Now assume that at least one path exists from the leader robot to child robot $\mathcal{R}_{c_j}$ on $\mathbf{G}_\mathcal{S}$, $(c_j \in \mathcal{C})$. This implies that the child robot $\mathcal{R}_{c_j}$ is a node on $\mathbf{G}_\mathcal{L}$ and a member of either group $\mathcal{G}_{h1}$ or $\mathcal{G}_{h2}$. When there exists a path from the leader robot to child robot $\mathcal{R}_{c_j}$ on $\mathbf{G}_\mathcal{L}$, then relative pose measurement and associated measurement error covariance for the child robot exists, i.e. $p(\mathbf{z}_{l_1,k}^{c_j,l_1})$ exists. If $p(\mathbf{z}_{l_1,k}^{c_j,l_1})$ exists, from

equation (3.5) $p(\mathbf{z}_{l_1,k}^{c_j,*})$ also exists. □

Theorem 3.3.1. *For an MRS with a single leader robot and one or more child robots, the given child robot's (say $\mathcal{R}_{c_j}$) pose is corrected at a relative pose measurement event if and only if a path exists from the leader robot to the child robot on $\mathbf{G}_{\mathcal{S}}$, ($c_j \in \mathcal{C}$).*

Proof. First assume that the child robot's pose is corrected at the relative pose measurement event. This implies that $p(\mathbf{z}_{l_1,k}^{c_j,*})$ exists in the child robot's measurement space. The child robot receives $p(\mathbf{z}_{l_1,k}^{c_j,*})$ from the leader robot. This implies that $p(\mathbf{z}_{l_1,k}^{c_j,*})$ exists in the leader robot's measurement space. If $p(\mathbf{z}_{l_1,k}^{c_j,*})$ exists, from **Lemma 3.3.1** there exists a path from the leader robot to child robot $\mathcal{R}_{c_j}$, ($c_j \in \mathcal{C}$).

Now assume that a path from the leader robot to child robot $\mathcal{R}_{c_j}$, ($c_j \in \mathcal{C}$), exists. From **Lemma 3.3.1**, there exists $p(\mathbf{z}_{l_1,k}^{c_j,*})$ in the measurement space of the leader robot. Under the assumption of availability of a reliable communication channel, the child robot's pose measurement density $p(\mathbf{z}_{l_1,k}^{c_j,*})$ becomes available in the child robot's measurement space as soon as it is computed by the leader robot. Once $p(\mathbf{z}_{l_1,k}^{c_j,*})$ is available in the child robot's measurement space, the child robot can fuse it with its current belief in order to correct its pose estimation. □

3.4 MRS with Multiple Leader Robots and Multiple Child Robots

For an MRS with multiple leader robots, a multi-centralized graph search algorithm is proposed to ensure that: (a) a given leader robot generates only a single pose measurement, $p(\mathbf{z}_{l_1,k}^{c_j,*})$, for a given child robot, $\mathcal{R}_{c_j}$, at a given time step k; (b) two or more leader robots do not use the same relative measurement[3] to synthesize the

---

[3]Use of the same relative pose measurement by multiple leader robots leads to an overconfident state estimation.

missing relative pose measurements between the leaders and the child robots; and (c) the mathematical formulation that handles the double-counting problem will meet the requirement for practical (realtime) implementation.

The proposed graph search algorithm is termed *multi-root breadth-first search algorithm* and is summarized in **Algorithm 3.1**[4].

Algorithm 3.1 : Graph-based search algorithm for multi-leader system

---
1: Create an empty set $\mathbf{E}$
2: **for** $i = 1 : 1 : |\mathcal{L}|$ **do**
3:     Create an empty queue $\mathcal{Q}_i$
4:     Create an empty queue $\bar{\mathcal{Q}}_i$
5:     Create an empty vector $\mathbf{V}_i$
6:     Add l_i to $\mathbf{V}_i$
7:     Enqueue l_i onto $\bar{\mathcal{Q}}_i$
8:     Create an empty hierarchical-RPMG $\mathbf{G}_{l_i}$
9: **end for**
10: **while** all $\bar{\mathcal{Q}}_i$ are not empty **do**
11:     **for** $i = 1 : 1 : |\mathcal{L}|$ **do**
12:         **if** $\bar{\mathcal{Q}}_i$ is not empty **then**
13:             Copy the queue $\bar{\mathcal{Q}}_i$ to the $\mathcal{Q}_i$
14:             Dequeue all elements of the queue $\bar{\mathcal{Q}}_i$
15:             **while** $\mathcal{Q}_i$ is not empty **do**
16:                 $t \leftarrow \mathcal{Q}_i.dequeue()$
17:                 **while** all x $\{x|x \in \mathcal{S}_{t,k}^c\}$ are considered **do**
18:                     **if** $x \notin \mathbf{V}_i$ and $(t,x) \notin \mathbf{E}$ **then**
19:                         Add x to $\mathbf{V}_i$
20:                         Enqueue x onto $\bar{\mathcal{Q}}_i$
21:                         Add (t,x) to $\mathbf{E}$
22:                         Add $\{t, (t,x)\}$ to $\mathbf{G}_{l_i}$
23:                     **end if**
24:                 **end while**
25:             **end while**
26:         **end if**
27:     **end for**
28: **end while**

It is essential for leader robots to possess the global perspective of the current rela-

---

tive pose measurement topology. This can be enabled through information exchange among robots. Initialization of the proposed multi-root breadth-first search algorithm has two parts:

1. First, the algorithm creates an empty set ($\mathbf{E}$) to hold relative pose measurements that are already considered by any of the leader robots in the MRS. [line 1]

2. Second, for each leader robot, the algorithm creates two first-in-first-out (FIFO) queues ($\mathcal{Q}_i$ and $\bar{\mathcal{Q}}_i$), an empty vector ($\mathbf{V}_i$), and an empty hierarchical-RPMG ($\mathbf{G}_{l_i}$). Vector $\mathbf{V}_i$ stores the unique indices of the child robots that are members of ith leader robot's ($\mathcal{R}_{l_i}$) hierarchical-RPMG. The initial value for queue $\bar{\mathcal{Q}}_i$ is the unique identification index of the leader robot, i.e. l_i. [lines 2-9]

Subsequent operations of **Algorithm 3.1** consists of 6 additional steps:

3. Dequeue all elements from $\bar{\mathcal{Q}}_i$ and enqueue these elements onto queue $\mathcal{Q}_i$ [lines 13-14];

4. Dequeue an element from queue $\mathcal{Q}_i$ [line 16];

5. Examine the successor of the dequeued element, if it has not been considered by this leader robot and the relative measurement from the dequeued element and its successor is not considered by any leader robot [line 18]:

   - Add the successor to vector ($\mathbf{V}_i$) [line 19];

   - Enqueue the successor onto queue $\bar{\mathcal{Q}}_i$ [line 20];

   - Relative measurement between the dequeued robot and the successor robot as measured by the dequeued robot is added to the set $\mathbf{E}$ [line 21];

   - Update hierarchical-RPMG with the newly added successor and associated relative pose measurement [line 22];

6. Repeat step 5 until all child successors of the dequeued element have been considered [line 17];

7. Repeat steps 4, 5 and 6 until queue $\mathcal{Q}_i$ is empty [line 15];

8. Repeat steps 3, 4, 5, 6 and 7 until each $\bar{\mathcal{Q}}_i$ is empty [line 10-12].

This algorithm constructs a hierarchical-RPMG for each leader robot. When hierarchical-RPMGs are constructed, each leader robot can exploit the approach discussed in Section 3.3.2 in order to virtually enhance its local perspective.

Lemma 3.4.1. *For an MRS with multiple leaders and one or more child robots, $p(\mathbf{z}_{l_i,k}^{c_j,*})$ exists if and only if an independent path[5] exists from leader robot $\mathcal{R}_{l_i}$ to child robot $\mathcal{R}_{c_j}$ on $\mathbf{G}_\mathcal{S}$; $(c_j \in \mathcal{C})$ and $(l_i \in \mathcal{L})$.*

Proof. First, assume that $p(\mathbf{z}_{l_i,k}^{c_j,*})$ exists. This implies that child robot $\mathcal{R}_{c_j}$ receives a pose measurement from the leader robot $\mathcal{R}_{l_i}$ at time step k. Therefore, $p(\mathbf{z}_{l_i,k}^{c_j,*})$ exists in the leader robot's measurement space. The measurement $p(\mathbf{z}_{l_i,k}^{c_j,*})$ is constructed by composing $p(\mathbf{z}_{l_i,k}^{c_j,l_i})$ and $p(\mathbf{z}_{l_i,k})$ as given in (3.5). This implies that $p(\mathbf{z}_{l_i,k}^{c_j,l_i})$ is a member of $\mathcal{Y}_{l_i,k}^{c_j,l_i}$. Hence, c_j is a node of the hierarchical-RPMG of l_i, i.e., c_j is a node of $\mathbf{G}_{l_i}$. A child node in a hierarchical-RPMG possesses only a single path from the leader robot to the child robot. In accordance with **Algorithm 3.1**, hierarchical-RPMGs corresponding to multiple leaders are independent and do not share a common relative pose measurement (edge). Therefore, in order for $\mathcal{R}_{c_j}$ to become a member of the hierarchical-RPMG of $\mathcal{R}_{l_i}$ there must be an independent path from l_i to c_j on $\mathbf{G}_\mathcal{S}$. Now assume that there exists an independent path from l_i to c_j on $\mathbf{G}_\mathcal{S}$. In accordance with **Algorithm 3.1**, c_j then becomes a member of the hierarchical-RPMG of $\mathcal{R}_{l_i}$,

---

[5]An independent path is the shortest path between the leader and the child robot when none of the edges in this path are shared with other leader robots while calculating the hierarchical-RPMG of an individual leader robot.

i.e., c_j is a node of $\mathbf{G}_{l_i}$. This implies that child robot $\mathcal{R}_{c_j}$ is a member of either group $\mathcal{G}_{h1}$ or $\mathcal{G}_{h2}$ with respect to $\mathcal{R}_{l_i}$. Hence, the $p(\mathbf{z}_{l_i,k}^{c_j,l_i})$ is a member of set $\mathcal{Y}_{l_i,k}^c$. If $p(\mathbf{z}_{l_i,k}^{c_j,l_i})$ exists, from equation (3.5), $p(\mathbf{z}_{l_1,k}^{c_j,*})$ will also exist. $\qquad\square$

Theorem 3.4.1. *For a MRS, if* $|\mathcal{Y}_{c_j,k}^*| > 1$ *then the MRS has more than one leader robot; where* $(c_j \in \mathcal{C})$ *and* $\mathcal{Y}_{c_j,k}^* = \{p(\mathbf{z}_{l_i,k}^{c_j,*}) | i \subseteq (1,\cdots,|\mathcal{L}|)\}.$

Proof. Assume that the cardinality of the set $\mathcal{Y}_{c_j}^*$ at time k is greater than one, i.e., $|\mathcal{Y}_{c_j,k}^*| > 1$. This implies that child robot $\mathcal{R}_{c_j}$ receives more than one pose measurement at time step k. In other words, $|\mathcal{Y}_{c_j,k}^*| > 1$ implies that there exists more than one $p(\mathbf{z}_{l_i,k}^{c_j,*})$; where, $l_i \in \mathcal{L}$. From **Lemma 3.4.1**, $p(\mathbf{z}_{l_i,k}^{c_j,*})$ exists if and only if an independent path from $\mathcal{R}_{l_i}$ to $\mathcal{R}_{c_j}$ exists. To have multiple measurements, there should be multiple independent measurement paths. Each independent measurement path originates from a leader robot. This implies that the system has more than one leader robot. Therefore, the inequality $|\mathcal{Y}_{c_j,k}^*| > 1$ is possible if the MRS has multiple leader robots. $\qquad\square$

Theorem 3.4.2. *For an MRS with multiple leader robots and one or more child robots, if* $|\mathcal{Y}_{c_j,k}^*| = m$ *then the* $|\mathcal{L}| \geq m$; *where* $(c_j \in \mathcal{C})$ *and* $\mathcal{Y}_{c_j,k}^* = \{p(\mathbf{z}_{l_i,k}^{c_j,*}) | i \subseteq (1,\cdots,|\mathcal{L}|)\}.$

Proof. For child robot $\mathcal{R}_{c_j}$, assume that $|\mathcal{Y}_{c_j,k}^*| = m$. This implies that $\mathcal{R}_{c_j}$ receives m pose measurements at time step k. In order to have m pose measurements, there should be m independent relative pose measurement paths; hence, m leader robots (see **Theorem 3.4.1** for further details). In accordance with **Algorithm 3.1**, when the shortest paths from two or more leader robots to a given child robot share a common relative pose measurement (common edges on $\mathbf{G}_{\mathcal{S}}$) only one leader robot is allowed to use this information. The remaining leader robots will not then provide pose measurements for the child robot. As a result, the number of leaders can be

greater than m. Therefore, when the cardinality of the set $\mathcal{Y}^*_{c_j,k}$ is equivalent to m, then the MRS has a minimum of m leader robots, i.e., $|\mathcal{L}| \geq m$. $\qquad\square$

Theorem 3.4.3. *For an MRS with multiple leader robots and one or more child robots, if a subset of nodes can be disjoint from the global RPMG by breaking an edge between two nodes while maintaining the following properties:*

- *disjointed subset contains only the nodes representing set of child robots, or*

- *disjointed subset contains a single leader node and multiple child nodes such that the leader node is the interface where the disjoint is made,*

then the child robots in this subset receive the pose measurement from only one leader robot.

Proof. Consider the global RPMG shown in Fig. 3.5. Node $\mathcal{R}_1$ can either be a leader robot or a child robot. Similarly, node $\mathcal{R}_2$ can either be a leader robot or a child robot. The left hand side network may consist of one or more child robots as well as one or more leader robots. However, the right hand side network contains only the child robots.
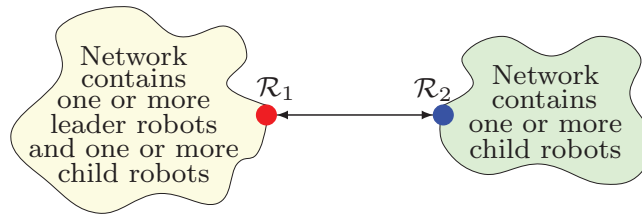
Figure 3.5: Divide global RPMG into two sub graphs by disjointing edges between two nodes.

First consider that $\mathcal{R}_2$ is a child robot. All leaders in the left hand side network then have relative pose measurement paths to all child robots in the right hand side network through the edge between $\mathcal{R}_1$ and $\mathcal{R}_2$. After applying **Algorithm 3.1**, only

one leader has an opportunity to use this edge to reach child robots in the right hand side network. Thus, child robots in the right hand side network receive pose measurements from only one leader robot in the left hand side network.

Now consider $\mathcal{R}_2$ as a leader robot. After applying **Algorithm 3.1**, none of the leaders in the left hand side network has an independent measurement path to the child robots in the right hand side network, as the interface to right hand side is a leader robot. Only $\mathcal{R}_2$ provides pose measurements to the child robots in the right hand side network.

Therefore, if a subset of nodes can be disjointed from the global RPMG by breaking an edge between two nodes while holding the two properties mentioned in this theorem, then the child robots in this subset receive pose measurements from only one leader robot. □

3.4.1   Leader Robot Competition

Consider a relative pose measurement event at time step k where independent paths from n leader robots ($n \leq |\mathcal{L}|$) to a given child robot (say $\mathcal{R}_{c_j}$) have an equal number of edges. Additionally, assume that the child robot $\mathcal{R}_{c_{j+1}}$ operates within the sensing range of the child robot $\mathcal{R}_{c_j}$ as illustrated in Fig. 3.6.
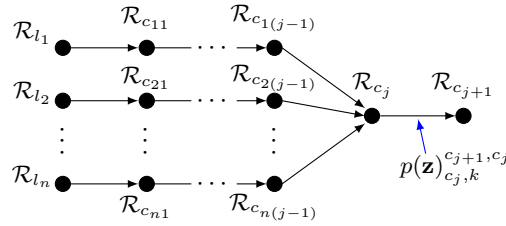
Figure 3.6: Global-RPMG that potentially leads to a competition between leader robots for a single relative pose measurement.

In accordance with **Algorithm 3.1**, only one leader can use $p(\mathbf{z}_{c_j,k}^{c_{j+1},c_j})$. Therefore,

a competition between leader robots arises to use this relative pose measurement. In order to resolve this competition, the priorities can be assigned to each leader robot. To account for the dynamic nature of the robot network, this study examines the uncertainty distribution of each leader robot's pose estimation. The leader robot with the lowest pose estimation uncertainty gets the highest priority in the network. This can be evaluated by computing either the trace or the determinant of the leader robots' pose estimation covariance matrices. The leader robot with the lowest trace (determinant) receives the highest priority for the current time step.

3.5 Distributed Leader-Assisted Localization Algorithm

It was assumed that each robot initially knows its pose with respect to a given reference coordinate frame. In the proposed algorithm, each agent in the heterogeneous-MRS locally runs a CKF[6] for sensor fusion. Fig. 3.7 graphically illustrates the proposed localization algorithm which incorporates two independent algorithms where one algorithm establishes the localization for the leader robots and the second algorithm establishes localization for the child robots.

3.5.1 Leader Robot's Localization

Algorithm 3.2 outlines the recursive state estimation steps for leader robot localization. This algorithm is implemented on each leader robot and iterates at each discrete time step. The leader robot reads its ego-motion sensor at each time step and predicts its current pose using prior state estimation densities and acquired odometry measurements (lines 3-4). Different sensory systems, such as laser range finders and

---

[6]Please refer to [36, 90] and their references for more details on CKF.
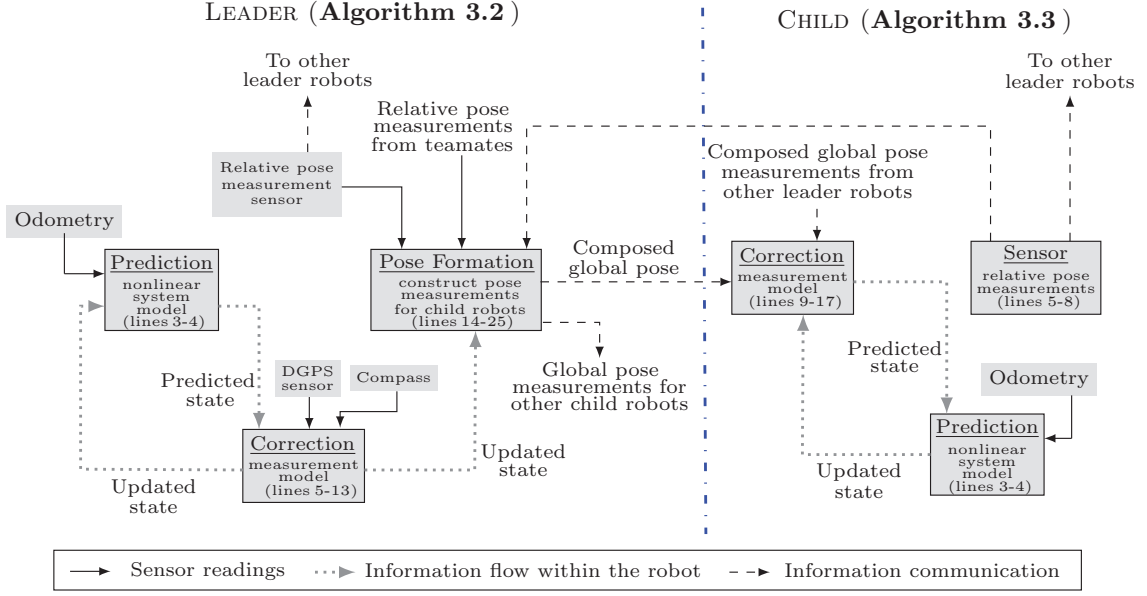
Figure 3.7: Sensor fusion architecture of the proposed distributed leader-assisted cooperative localization scheme

cameras, and different localization algorithms, such as SLAM and cooperative localization, can be exploited to establish the localization of leader robots. For simplicity, the current study assumed the availability of a DGPS sensor and a compass for each leader robot. When the DGPS/compass measurements are available, then the measurements are validated through an ellipsoidal measurement gate [116] (lines 5-6). If the measurements satisfy the measurement gating condition, the leader robot fuses these measurements with its current state estimation in order to improve its localization (line 7). Otherwise the predictive density is directly assigned to the posterior density of the state estimation (lines 8-9). In this way, any outlier can be identified and dismissed. When there is no DGPS/compass measurement, then the predictive density is directly assigned to the posterior density of the state estimation (lines 11-12). At a relative pose measurement event, the leader robot measures the relative pose of its neighbours (line 15) and communicates these measurements to other leader robots in the MRS (line 16). Simultaneously it collects relative pose measure-

ments from all teammates through the communication network (line 17). All available relative pose measurements are then examined in **Algorithm 3.1** which constructs the hierarchical-RPMG (line 21). Prior to constructing the hierarchical-RPMG it is important to have the knowledge of the leaders' priority in the dynamic network.

Algorithm 3.2 : Distributed leader-assisted localization - Leader's perspective

1: Initialize with $\mathbf{X}_{l_q,\circ}$ and $\mathbf{P}_{l_q,\circ}$
2: **for** $k \in (1, \cdots, \infty)$ **do**
3:     Read ego-motion sensor: $\bar{\mathbf{u}}_{l_q,k}$
4:     Estimate predictive density $p(\mathbf{x}_{l_q,k|k-1})$ using prior density $p(\mathbf{x}_{l_q,k-1})$ and odometry reading $\bar{\mathbf{u}}_{l_q,k-1}$
5:     **if** DGPS/Compass measurement is available **then**
6:         **if** measurement gate validated **then**
7:             Compute posterior density $p(\mathbf{x}_{l_q,k})$ using predictive density $p(\mathbf{x}_{l_q,k|k-1})$, DGPS measurement $p(\mathbf{z}_k^{DGPS})$, and/or Compass measurement $p(\mathbf{z}_k^{Comp})$
8:         **else**
9:             $p(\mathbf{x}_{l_q,k}) \leftarrow p(\mathbf{x}_{l_q,k|k-1})$
10:        **end if**
11:    **else**
12:        $p(\mathbf{x}_{l_q,k}) \leftarrow p(\mathbf{x}_{l_q,k|k-1})$
13:    **end if**
14:    **if** relative pose measurement event **then**
15:        Read relative pose measurement sensor: $\mathcal{Y}_{l_q,k}$
16:        Communicate $\mathcal{S}_{l_q,k}$ and $\mathcal{Y}_{l_q,k}$
17:        Collect relative pose measurement from other leaders and child robots:
           $\mathcal{Y}_{l_q,k}^+ = \mathcal{Y}_{l_q,k} \bigcup_{\forall i \in (1,\cdots,|\mathcal{L}|), i \neq q} \mathcal{Y}_{l_i,k} \bigcup_{\forall j \in (1,\cdots,|\mathcal{C}|)} \mathcal{Y}_{c_j,k};$
           $\mathcal{S}_{l_q,k}^+ = \mathcal{S}_{l_q,k} \bigcup_{\forall i \in (1,\cdots,|\mathcal{L}|), i \neq q} \mathcal{S}_{l_i,k} \bigcup_{\forall j \in (1,\cdots,|\mathcal{C}|)} \mathcal{S}_{l_j,k}$
18:        Calculate trace of self-localization covariance matrix: $t_{l_q,k} \leftarrow \text{trace}(\mathbf{P}_{l_q,k})$
19:        Collect trace values of other leaders:
           $Tr = t_{l_q,k} \bigcup_{\forall i \in (1,\cdots,|\mathcal{L}|), i \neq q} t_{l_i,k}$
20:        Construct leader priority (Section 3.4.1)
21:        Construct hierarchical-RPMG: (**Algorithm 1**)
22:        Update $\mathcal{S}_{l_q,k}^c$ and $\mathcal{Y}_{l_q,k}^c$: (eqs. (3.9) and (3.10) in Section 3.3.2)
23:        Update $\mathcal{Y}_{l_q,k}^*$: (eq. (3.5))
24:        Communicate $p(\mathbf{z}_{l_q,k}^{c_j,*}) \; \forall c_j \in \mathcal{S}_{l_q,k}^c$
25:    **end if**
26: **end for**

To accomplish this requirement, each leader robot calculates the trace of its pose estimation covariance matrix (line 18) and collects the trace of the pose estimation covariance matrixes of other leader robots (line 19). Each leader robot then constructs the priorities of the leaders based on the trace values (line 20). Construction of the hierarchical-RPMG is followed by synthesizing missing relative pose measurements between the leader robot and the child robots that operate beyond the sensing range of the leader robot (line 22). Finally, the leader robot generates pose measurements for child robots and communicates these measurements to the corresponding child robots (lines 23-24).

3.5.2   Child Robot's Localization

Algorithm 3.3 : Distributed leader-assisted localization - Child's perspective

---

1: Initialize with $\mathbf{X}_{c_r,\circ}$ and $\mathbf{P}_{c_r,\circ}$
2: **for** $k \in (1, \cdots, \infty)$ **do**
3:     Read ego-motion sensor: $\bar{\mathbf{u}}_{c_r,k}$
4:     Estimate predictive density $p(\mathbf{x}_{c_r,k|k-1})$ using prior density $p(\mathbf{x}_{c_r,k-1})$ and odometry reading $\bar{\mathbf{u}}_{c_r,k-1}$
5:     **if** relative pose measurement event **then**
6:         Read relative pose measurement sensor: $\mathcal{Y}_{c_r,k}$
7:         Communicate $\mathcal{S}_{c_r,k}$ and $\mathcal{Y}_{c_r,k}$
8:     **end if**
9:     **if** pose measurement available from leaders **then**
10:         **if** measurement gate validated **then**
11:             Compute posterior density $p(\mathbf{x}_{c_r,k})$ using predictive density $p(\mathbf{x}_{c_r,k|k-1})$ and received pose measurement $\mathcal{Y}_{l_i,k}^{c_r,*}$, $i \subseteq (1, \cdots, |\mathcal{L}|)$
12:         **else**
13:             $p(\mathbf{x}_{c_r,k}) \leftarrow p(\mathbf{x}_{c_r,k|k-1})$
14:         **end if**
15:     **else**
16:         $p(\mathbf{x}_{c_r,k}) \leftarrow p(\mathbf{x}_{c_r,k|k-1})$
17:     **end if**
18: **end for**

Algorithm 3.3 outlines the recursive state estimation steps of child robot localiza-

tion. This algorithm is implemented on each child robot and iterates at each discrete time step. Each child robot reads its ego-motion sensor at each time step and predicts its current pose using prior state estimation densities and acquired odometry measurements (lines 3-4). At a relative pose measurement event, each child robot acquires the relative pose measurements of neighbours and transmits these measurements to leader robots (lines 5-8). Upon an arrival of pose measurements from leader robots, measurements are first evaluated through an ellipsoidal validating gate in order to remove outliers (lines 9-10). If the measurements satisfy the measurement gating condition, the child robot fuses these measurements with its current state estimation in order to improve its localization accuracy (line 11). Otherwise, the predictive density is directly assigned to the posterior density of the state estimation (line 13). When no pose measurements are received from leaders, the child robot assigns its predictive density to the posterior density (line 16).

3.6 Evaluations

The proposed leader-assisted localization algorithm was evaluated in a series of numerical simulations. Two simulation configurations were considered.

1. Heterogeneous-MRS with a single leader robot

2. Heterogeneous-MRS with multiple leader robots

3.6.1 Heterogeneous-MRS with a single leader robot

3.6.1.1 Setup

Simulations were performed for a group of communicating robots navigating in a 2D arena[7]. Known data correspondence was assumed for relative pose measurements. Simulation parameters and the characteristics of each sensory systems are summarized in Table 3.1 and Table 3.2, respectively. It was assumed that the DGPS and compass sensors are available only for the leader robots.

Table 3.1: Simulation parameters

Symbol	Parameter Description	Value
$|\mathcal{L}|$	Number of leader robots	1
$|\mathcal{C}|$	Number of child robots	4
simt	Number of simulation time steps	90000
dt	Width of a single time step	0.01 sec
d_m	Sensing range limits	10 m
$W \times L$	Size of the simulation arena	20 m $\times$ 25 m
N_{MC}	Number of Monte-Carlo runs	20

Table 3.2: Characteristics of odometry, absolute positioning and heading sensors

Sensor type	Measure	Frequency	Noise σ
Odometry	Linear velocity	100 Hz	$5\%v$
	Angular velocity	100 Hz	5 deg/sec
Relative pose	x-position	10 Hz	0.05 m
	y-position	10 Hz	0.05 m
	Relative orientation	10 Hz	1 deg
DGPS	x-position	10 Hz	0.1 m
	y-position	10 Hz	0.1 m
Compass	Orientation (heading)	10 Hz	0.5 deg

Linear and angular velocities of the leader robot were set to zero. The trajectories of

---

[7]Video: https://youtu.be/Ixoa34k2G1c

child robots were then set so that:

- the first child robot ($\mathcal{R}_{c_1}$) always operated within the sensing range of the leader robot; thus, it always had the first degree observation[8];

- the second and the third child robots ($\mathcal{R}_{c_2}$ and $\mathcal{R}_{c_3}$) intermittently appeared within the sensing range of the leader robot; thus, they had the first-, the second- and the third-degree observations intermittently;

- the fourth child robot ($\mathcal{R}_{c_4}$) never appeared within the sensing range of the leader robot; thus, it always had the second- or higher-degree observation.

3.6.1.2 Results

The average state estimation error and associated 3-σ error boundaries of the child robot $\mathcal{R}_{c_4}$ are shown in Fig. 3.8. It can be seen that the average estimation error of x- and y-position estimations and ϕ-orientation estimation always stay inside the associated 3-σ error boundaries. This implies that the proposed localization scheme is capable of generating a consistent state estimation for child robots even when the child robots operate beyond the sensing range of the leader robot.

When the proposed algorithm is not applied, child robot $\mathcal{R}_{c_4}$ does not receive pose measurements from the leader robot and relies only on the odometry reading. Therefore, without the proposed algorithm $\mathcal{R}_{c_4}$ performs dead reckoning-based localization. Fig. 3.9 compares the root-mean-squared-error (RMSE) of child robot, $\mathcal{R}_{c_4}$ pose estimation, with and without the proposed localization algorithm. These results verified that the proposed algorithm is capable of establishing the localization for child robots with high accuracy even when the child robots navigate beyond the sensing range of

---

[8]For a given hierarchical-RPMG, the number of edges between the leader robot node (root-node) to a child robot node is termed the degree of observation of the child robot with respect to the leader robot.
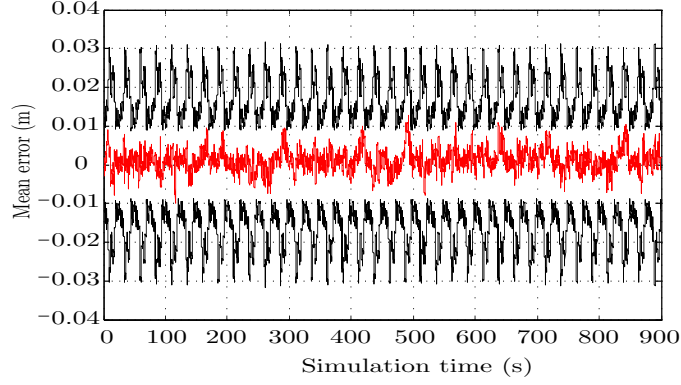
(a) x-position
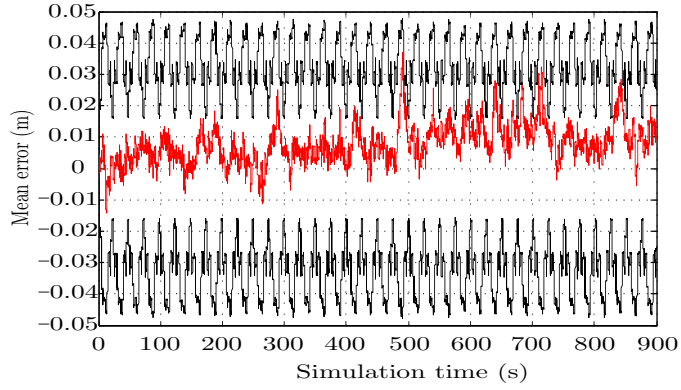
(b) y-position
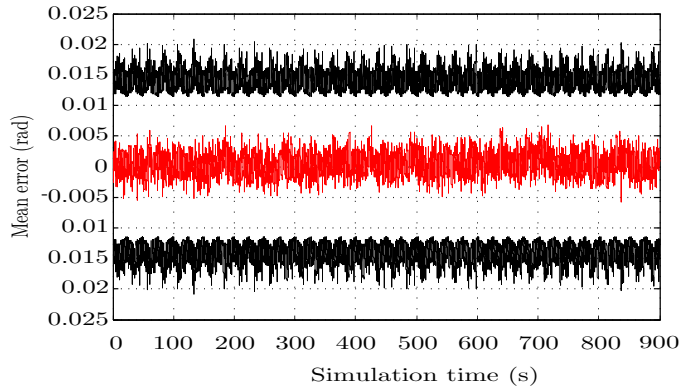
(c) ϕ-orientation

Figure 3.8: Mean estimation error of child robot $\mathcal{R}_{c_4}$ for 20 Monte-Carlo simulations. Red solid line indicates a mean estimation error while the black solid lines indicate double-sided 3-σ error boundaries

the leader robots. Statistical comparison of the child robots' pose estimation, with and without the proposed localization algorithm, is illustrated in Fig. 3.10. In both the cases (with and without the proposed algorithm), the mean and the standard deviation of the RMSE of child robot $\mathcal{R}_{c_1}$'s pose estimation are identical to one another as shown in Fig. 3.10(a). This is the expected result, as child robot $\mathcal{R}_{c_1}$ has operated within the sensing range of the leader robot. Child robots $\mathcal{R}_{c_2}$ and $\mathcal{R}_{c_3}$ appeared in the sensing range of the leader robot intermittently. As a result, these robots recovered their localization to some extent even without the proposed localization algorithm (Fig. 3.10(b) and Fig. 3.10(c)). However, it could be seen that the proposed algorithm slightly improved the localization accuracy of child robots $\mathcal{R}_{c_2}$ and $\mathcal{R}_{c_3}$ compared with a generic leader-assisted localization approach. A noticeable improvement of localization was achieved for child robot $\mathcal{R}_{c_4}$ by using the proposed algorithm (Fig. 3.10(d)). Since child robot $\mathcal{R}_{c_4}$ never appeared within the sensing range of the leader robot, the general leader-assisted localization algorithm was incapable of establishing localization.

3.6.1.3   Estimation accuracy vs. characteristic of relative pose measurement sensory system

To evaluate the impact of noise level and update rate of the relative pose measurement sensory system on the estimation accuracy, two noise configurations and update rates were considered. These noise levels and update rates are summarized in Table 3.3. Table 3.4 presents a comparison of the mean of the RMSE and the corresponding standard deviation values of the child robot $\mathcal{R}_{c_4}$ pose estimation. These results suggest that the estimation error for child robots increases with the increase of the uncertainty of the relative pose measurement sensory system. Further, estimation error increases with a decrease in the update rate of the relative pose measurement sensory system.
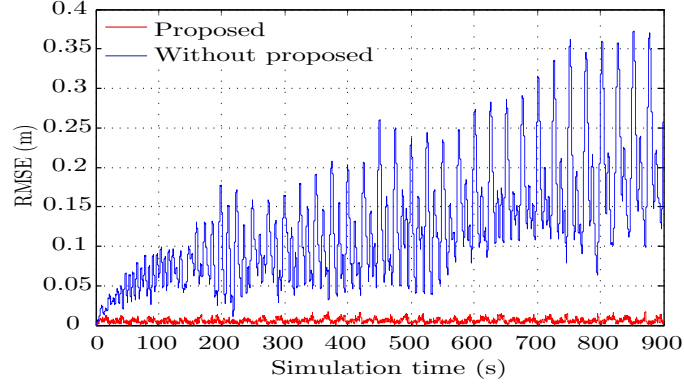
(a) x-position
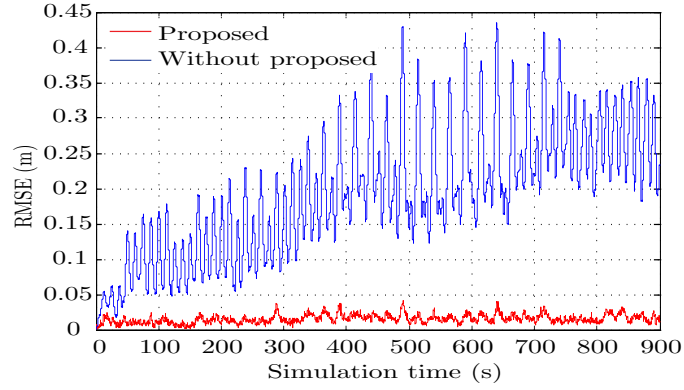
(b) y-position
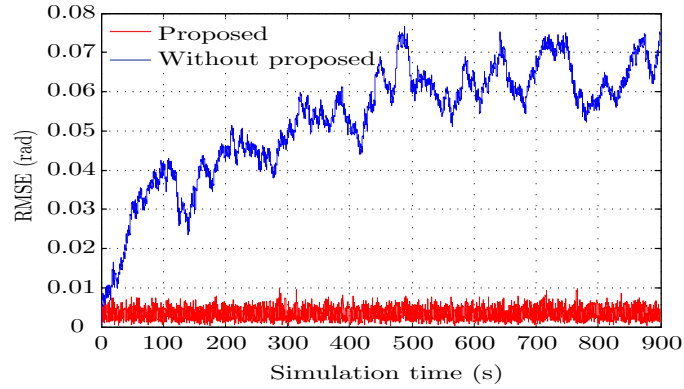
(c) ϕ-orientation

Figure 3.9: Comparison of the estimation error of child robot $\mathcal{R}_{c_4}$ for 20 Monte-Carlo simulations. Without the proposed method, child robot $\mathcal{R}_{c_4}$ relies only on the odometry reading as it operates beyond the sensing range of the leader robot

(a) Child robot $\mathcal{R}_{c_1}$

(b) Child robot $\mathcal{R}_{c_2}$

(c) Child robot $\mathcal{R}_{c_3}$
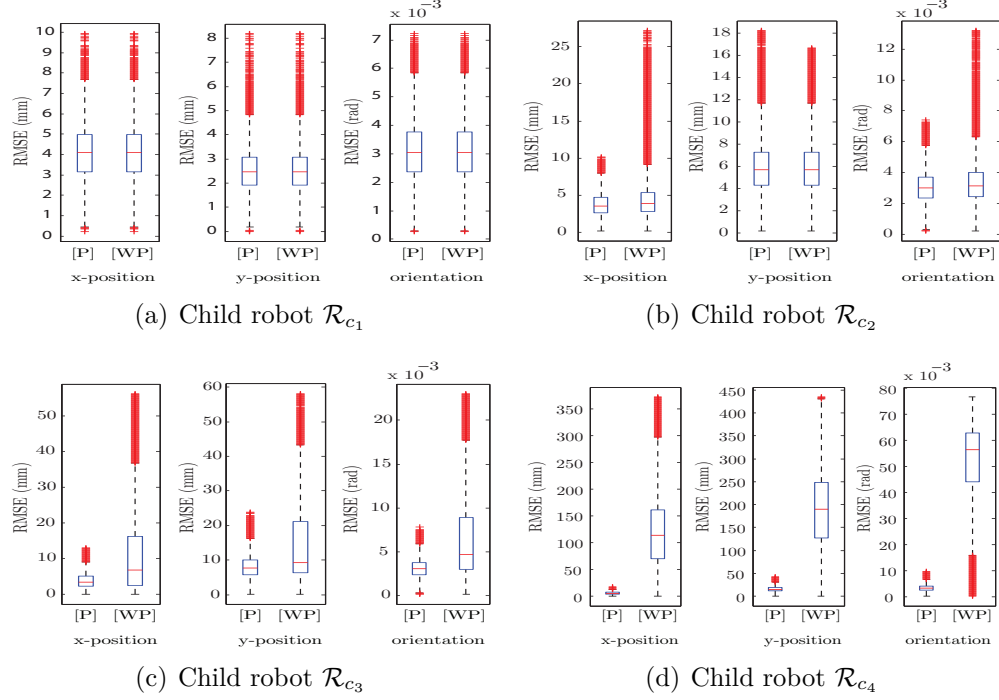
(d) Child robot $\mathcal{R}_{c_4}$

Figure 3.10: RMSE of pose estimation of each child robot. Box plots show median values (red solid horizontal line inside the box), 25th percentile value and 75th percentile value (box outline), $\pm 2.7\sigma$ values (whiskers), and outlier values (horizontal red lines). [P]: proposed localization algorithm, [WP]: without the proposed localization algorithm (i.e. general leader-assisted localization algorithm)

Table 3.3: Characteristics of relative pose measurement sensor

	Noise $[\sigma_x,\ \sigma_y,\ \sigma_\phi]$	Frequency
Case (1)	[0.05 m, 0.05 m, 1 deg]	10 Hz
Case (2)	[0.05 m, 0.05 m, 1 deg]	1 Hz
Case (3)	[0.15 m, 0.15 m, 3 deg]	10 Hz
Case (4)	[0.15 m, 0.15 m, 3 deg]	1 Hz

From these results, it is possible to conclude that the noise level of an exteroceptive sensory system is the most critical factor that governs the accuracy of the estimation.

Table 3.4: Comparison of the pose estimation error of child robot $\mathcal{R}_{c_4}$. The format of the listed estimation errors is (mean±standard deviation)

Case	x-position estimation (cm)	y-position estimation (cm)	ϕ-orientation estimation (rad)
Case (1)	0.54±0.34	1.66±0.86	0.0032±0.0017
Case (2)	3.41±1.89	5.45±2.90	0.0107±0.0058
Case (3)	6.61±3.77	11.44±6.56	0.0195±0.0116
Case (4)	8.19±4.70	19.86±9.44	0.0336±0.0160

3.6.2 Heterogeneous-MRS with multiple leader robots

3.6.2.1 Setup

A publicly available multi-robot localization and mapping data-set [49] was used to evaluate the proposed localization algorithm for a multiple leader scenario [9]. This robot team consists of five mobile robots. Two of them are assumed to be leader robots ($\bar{\mathcal{R}}_{l_1}$, $\bar{\mathcal{R}}_{l_2}$) and the remaining three robots are assumed to be child robots ($\bar{\mathcal{R}}_{c_1}$, $\bar{\mathcal{R}}_{c_2}$, $\bar{\mathcal{R}}_{c_3}$). This simulation study used only the odometry measurements and ground truth measurements from the data-set. Relative pose measurements between robots, compass measurements and DGPS measurements for the leader robots were generated using the ground truth data. Additionally, the maximum sensing range was set to 4 m. The noise level and the update rate of the relative pose measurement sensors were set to $\begin{bmatrix} \sigma_x = 0.05\text{m} & \sigma_y = 0.05\text{m} & \sigma_\phi = 1\text{deg} \end{bmatrix}$ and 5Hz, respectively. Two measurement noise configurations and two update rates were assumed for the absolute pose measurement sensor and are summarized in Table 3.5.

3.6.2.2 Results

Fig. 3.11 illustrates the mean estimation error along with the associated 3-σ double sided error boundaries for child robot $\bar{\mathcal{R}}_{c_1}$. These results correspond to the noise

---

[9]Video: https://youtu.be/6HAR0w7bvjA
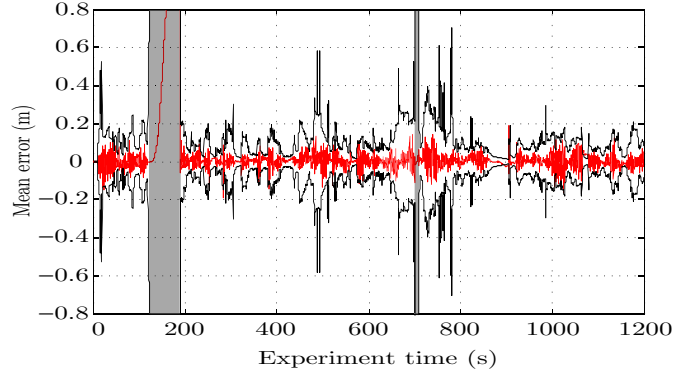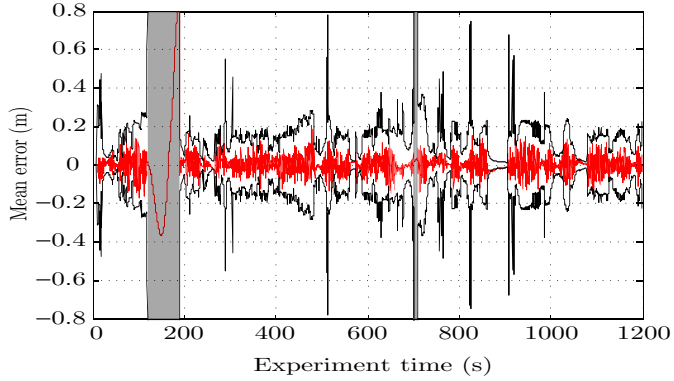
(a) x-position

(b) y-position
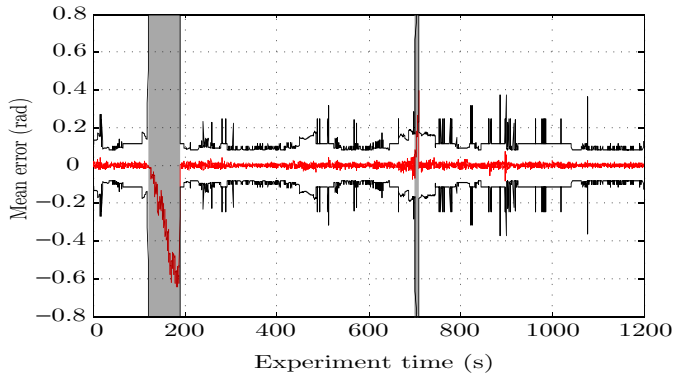
(c) ϕ-orientation

Figure 3.11: Mean estimation error of child robot $\bar{\mathcal{R}}_{c_1}$. Red solid line indicates mean estimation error while the black solid lines indicate double-sided 3-σ error boundaries. Shaded regions represent time windows with no measurement updates

Table 3.5: Characteristics of absolute pose measurement sensor

	Noise-DGPS $[\bar{\sigma}_x,\ \bar{\sigma}_y]$	Noise-Compass $[\bar{\sigma}_\phi]$	Frequency
Case (5)	[0.1 m, 0.1 m]	[0.5 deg]	5 Hz
Case (6)	[0.1 m, 0.1 m]	[0.5 deg]	1 Hz
Case (7)	[0.3 m, 0.3 m]	[1.5 deg]	5 Hz
Case (8)	[0.3 m, 0.3 m]	[1.5 deg]	1 Hz

level and the update rate of absolute pose measurement sensors given in Case (5). It can be seen that the estimation errors always stay inside the associated 3-σ error boundaries. This implies that the proposed leader-assisted localization algorithm is consistent. During the time windows 118.8s - 187.8s and 701.8s - 709.6s child robot $\bar{\mathcal{R}}_{c_1}$ did not receive pose measurements from either leader robot (shaded regions in Fig. 3.11). During these time windows child robot $\bar{\mathcal{R}}_{c_1}$ was disconnected from the measurement network. In other words, during these two time windows robot $\bar{\mathcal{R}}_{c_1}$ was not within the sensing range of any of the teammates. This implies that the robot is a member of group $\mathcal{G}_{h3}$ with respect to the both leader robots. Since the robot does not receive pose measurements from the leaders during these time windows, its pose estimation diverges from its true pose.

Table 3.6 summarizes the time averaged RMSE and the associated standard deviation of $\mathcal{R}_{c_1}$ pose estimation for different characteristics of the absolute positioning sensor as listed in Table 3.5. Two sets of statistics have been presented for each case: (a) the time averaged RMSE and the associated standard deviation values of $\mathcal{R}_{c_1}$ pose estimation neglecting the time windows 118.8s - 187.8s and 701.8s - 709.6s; (b) the time averaged RMSE and the associated standard deviation values of $\mathcal{R}_{c_1}$ pose estimation for the entire experiment period.

The results show that the estimation error increases with the increase of noise level of the absolute positioning sensor system. Further, estimation error increases with

Table 3.6: Comparison of the pose estimation error of child robot $\mathcal{R}_{c_1}$ for cases 5-8. The format of the listed estimation errors is mean±standard deviation

		x position estimation (cm)	y-position estimation (cm)	ϕ-orientation estimation (rad)
Case (5)	(a)	4.11±3.42	5.36±3.88	0.0207±0.0306
	(b)	7.36±17.15	6.88±8.76	0.0363±0.0826
Case (6)	(a)	5.29±4.03	6.27±4.34	0.0334±0.0420
	(b)	8.85±18.07	7.75±9.14	0.0483±0.0862
Case (7)	(a)	8.31±6.67	10.62±7.54	0.0301±0.0341
	(b)	11.89±19.11	12.21±10.54	0.0450±0.0795
Case (8)	(a)	11.92±8.65	15.34±9.64	0.0452±0.0456
	(b)	15.38±19.69	16.15±11.70	0.0583±0.0817

a decrease in the update rate of the absolute positioning sensor system. Additionally, it can be seen that higher accuracy can be achieved by ensuring the continuous connectivity with the measurement network. However, disconnecting from the measurement network for a short period of time (< 1 minute) will not greatly diverge the child robots' pose estimation. In addition, a rapid convergence could be achieved soon after the reconnecting with the measurement network. This result demonstrates the applicability of the proposed method for a real-world application where temporal occlusion by an obstacle is present.

3.7 Consistency and Complexity

When stochastic filters are exploited for sensor fusion, these filters estimate two information namely state vector and state estimation uncertainty (covariance matrix). It is important to evaluate whether estimated uncertainty accurately represent the estimation error. If the estimated uncertainty is too smaller than the estimation error, the estimator is said to be overconfident, and if the estimated uncertainty is too bigger than the estimation error, the estimator is said to be conservative. Otherwise,

estimator is said to be consistent. There are several approaches to evaluate the consistency of an estimator. In this research work, I used normalized estimation error squared (NEES) test and normalized innovation squared (NIS) test to evaluate the consistency of the proposed sensor fusion architecture and the proposed global pose composition algorithm.

3.7.1 Normalized Estimation Error Squared (NEES)

To examine the consistency of the proposed distributed leader-assisted cooperative localization scheme, NEES values of the child robots' pose estimations for a multi-leader scenario were computed using

$$\epsilon_{c_i,k} = \boldsymbol{\xi}_{c_i,k}{}^T \mathbf{P}_{c_i,k}^{-1} \boldsymbol{\xi}_{c_i,k} \quad i \in (1,2,3) \tag{3.11}$$

where, ϵ is the computed NEES and is a scalar. $\boldsymbol{\xi}$ is the pose estimation error at time step k and $\mathbf{P}$ represents the estimated error covariance matrix. For a single run, estimation is consistent if the computed NEES is such that the following inequality holds:

$$\epsilon_{c_i,k} \leq \chi^2_{n_x,\delta} \tag{3.12}$$

where $\chi^2_{n_x,\delta}$ represents the Chi-square distribution with n_x DOF and δ is the significance level [117]. The upper-bound of the 95% acceptance region for the 3-DOF stochastic process is given by $\chi^2_{3,0.95}$ and is equal to 7.8147. For the noise characteristics given in Table 3.3 Case (1) and Table 3.5 Case (5), the NEES of the pose estimation of the child robot $\bar{\mathcal{R}}_{c_1}$ is shown in Fig. 3.12(a). The percentage of the NEES values falling outside the 95% acceptance region are summarized in Table 3.7. It can be seen that fewer than 10% of values fall outside the 95% region, which is acceptable [23].
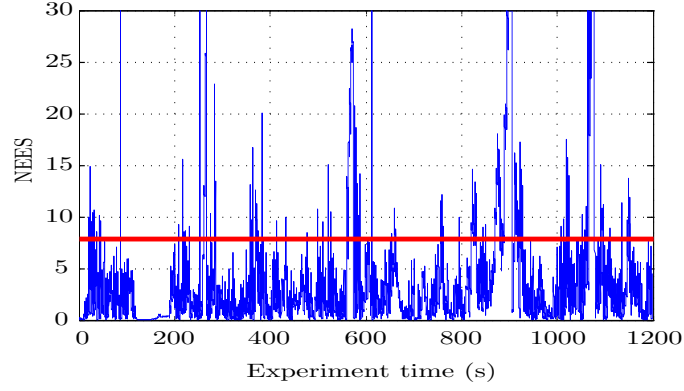
(a) NEES
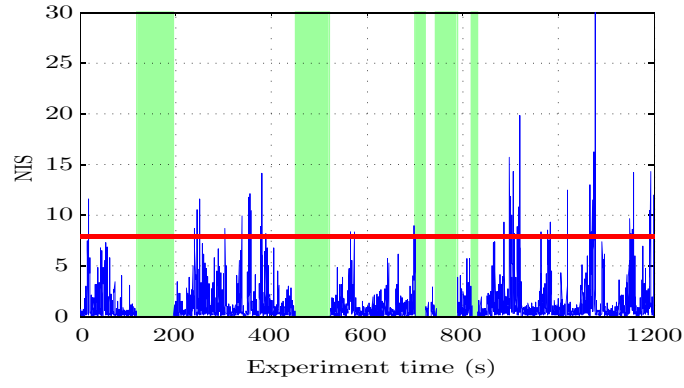
(b) NIS with respect to leader $\bar{\mathcal{R}}_{l_1}$
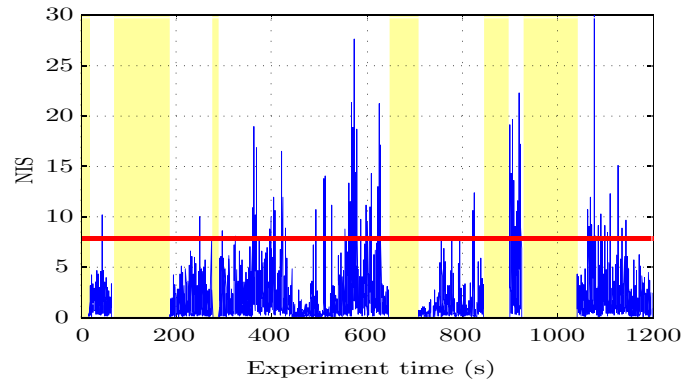
(c) NIS with respect to leader $\bar{\mathcal{R}}_{l_2}$

Figure 3.12: Consistency analysis results for child robot $\bar{\mathcal{R}}_{c_1}$. Blue solid lines represent (a) NEES, (b) NIS, and (c) NIS values while the horizontal red solid lines represent the Chi-square upper bounds

69

3.7.2 Normalized Innovation Squared (NIS)

To examine the consistency between the measurements and predicted observations, NIS values of the child robot pose estimation for the multi-leader scenario are computed using

$$\varepsilon_{c_i,k} = {\boldsymbol{\eta}_{c_i,k}}^T \mathbf{S}_{c_i,k}^{-1} \boldsymbol{\eta}_{c_i,k} \quad i \in (1,2,3) \tag{3.13}$$

where ε is the computed NIS value and is a scalar. $\boldsymbol{\eta}$ is the difference between the pose measurement sent from a leader robot and the predicted pose measurement. $\mathbf{S}$ is the innovation covariance matrix. This also follows the Chi-square distribution with n_z DOF [117]. When a child robot receives multiple pose measurements at a single time step these measurements are independent from one another. As a result, a sequential update can be performed at the filter update resulting in reduced computational complexity for child robots [118]. For the noise characteristics given in Table 3.6 Case (5), NIS values corresponding to two leader robots can be computed independently and are shown in Fig. 3.12(b) and Fig. 3.12(c). During the highlighted time windows (Fig. 3.12(b) and Fig. 3.12(c)) child robot $\bar{\mathcal{R}}_{c_1}$ did not receive pose measurements from the corresponding leader robot. This is due to one of the following reasons: (a) child robot $\bar{\mathcal{R}}_{c_1}$ has disconnected from the relative pose measurement network; (b) the leader robot has disconnected from the relative pose measurement network; or (c) it was possible to disconnect child robot $\bar{\mathcal{R}}_{c_1}$ from the relative pose measurement network by disjoining a single edge on the global-RPMG (see **Theorem 3.4.3** for more information). There is no NIS value associated with these time windows. The pose measurement sent by a leader robot consists of x- and y-positions and ϕ-orientation. This measurement has 3-DOF leading to the Chi-square upper bound of $\chi^2_{3,0.95}$ and is equal to 7.8147. The percentage of the NIS values falling outside the 95% acceptance region are summarized in Table 3.7. It can be seen that fewer than 10% of values fall

outside the 95% region, which is acceptable [119].

Table 3.7: Percentage of NEES and NIS values that fall outside the Chi-square upper-bound

Robot	NEES	NIS (leader 1)	NIS (leader 2)
$\bar{\mathcal{R}}_{c_1}$	8.03%	1.35%	2.56%
$\bar{\mathcal{R}}_{c_2}$	3.81%	1.61%	2.67%
$\bar{\mathcal{R}}_{c_3}$	9.82%	1.42%	2.03%

3.7.3 Complexity

3.7.3.1 Computational and Time Complexity

As the pose estimation task is decentralized and pose measurements sent by different leaders are independent from one another, for a given child robot, the per-measurement computational complexity remains constant $\mathcal{O}(1)$. The computational complexity of the leader robot pose estimation depends on the sensory system and localization algorithm that the leader robots execute. In this study, an absolute position measuring capabilities and availability of a compass for the leader robot's localization are assumed. Thus, this algorithm also has constant computational complexity per measurement $\mathcal{O}(1)$. However, if the leader robots execute a complex SLAM algorithm in order to establish their localization, the computational complexity will increase. The breadth-first search algorithm has the worst case time complexity of $\mathcal{O}(|\zeta|+|\vartheta|)$ (Please refer to Section 3.2.1 for notations.). This time complexity linearly increases with the number of leader robots in the MRS.

3.7.3.2 Communication Complexity

None of the robots are required to communicate their high-frequency ego-centric measurements with one another or with the leader robots. This decreases the bandwidth requirement of the data network. Each robot needs to communicate its relative pose measurement to the leader robots. Thus, the communication cost per relative pose measurement increases linearly with the number of leader robots in the MRS, i.e., the per relative pose measurement communication cost is in the order of $\mathcal{O}(|\mathcal{L}|)$.

3.8 Summary

This chapter presented a novel localization framework addressing the finite-range sensing problem of leader-assisted localization. This framework consists of (1) a method to virtually enhance the leader robots' sensing range allowing child robots to navigate beyond the sensing range of leader robots while maintaining bounded error and uncertainty, and (2) a novel graph search algorithm to address the double counting problem. The performance of the proposed framework is evaluated in a series of numerical simulations and a publicly available multi-robot localization and mapping data-set. The results confirmed that the proposed distributed leader-assisted localization framework is capable of establishing consistent localization for the child robots with bounded uncertainty even when they operate beyond the sensing range of the leader robots. From the perspective of child robots, per-measurement communication cost of the proposed method is constant $\mathcal{O}(1)$ while the per-measurement communication cost linearly increases with the increases of the number of the leader robots in the MRS, i.e., per-measurement communication cost is $\mathcal{O}(|\mathcal{L}|)$ per-relative pose measurement, where $|\mathcal{L}|$ represents the number of leader robots in the MRS. Overall communication cost if the system, potential maximum value, is $\mathcal{O}(|\mathcal{C}^2||\mathcal{L}|)$.

Chapter 4

Distributed Leader-Assisted Localization with Sensing and Communication Range Constraints

In the previous chapter, the solution that is presented for the sensing range constraint is formulated with the assumption of an unbounded communication range. However, this assumption may not valid for practical applications, because most of the available wireless communication infrastructures have a bounded communication range. Therefore, in this chapter, this study is extended in order to address both the sensing and the communication range constraints and these boundaries are virtually expanded[1].

In general, the communication range limit, d_{com}, of a wireless communication network is greater than the sensing range limit, d_m, of any exteroceptive sensory system attached to the robots. Robots that operate beyond the leader robots' communication boundaries can send and receive information to/from a leader robot through one or

---

[1]The work in this chapter is to be submitted for Journal of Autonomous Robots.
* T. R. Wanasinghe, G. K. I. Mann and R. G. Gosine, "Leader-Assistive Localization Framework for Multi-robot Systems with Communication and Sensing Range Constraints," submitted for Journal of Autonomous Robots (Under review)

a set of intermediate robots. This eventually leads to a high bandwidth requirement for the communication channel between leader robot and the child robots that are within the leader robot's communication range. Therefore, this chapter formulates a hierarchical communication architecture that does not require child robots to communicate their local measurements to the leaders. In the proposed method, the exchange of information occurs between the robots, that can measure the relative pose of each other. Therefore, it is reasonable to assume $d_{com} = d_m$.

4.1 Inter-robot Measurements and Communications in an MRS

4.1.1 Inter-Robot Measurement and Communication Graph (IRMCG)

An inter-robot measurement and communication graph (IRMCG) is a directed graph $\mathbf{G}_{\mathcal{S}} \triangleq \{\zeta, \vartheta\}$, where ζ is the node-set representing the agents in the MRS and $\vartheta \in \{\zeta \times \zeta\}$ is the edge set that represents the availability of a communication link and relative pose measurements from agent $\mathcal{R}_i$ to agent $\mathcal{R}_j$. In the global perspective, available relative pose measurements between robots are viewed as external observers, whereas in the local perspective, each robot can measure the relative pose of robots that operate within its sensing range. Fig. 4.1 gives a sample robot configuration and the associated global-IRMCG and local-IRMCG are illustrated in Fig. 4.2(a) and Fig. 4.2(b).
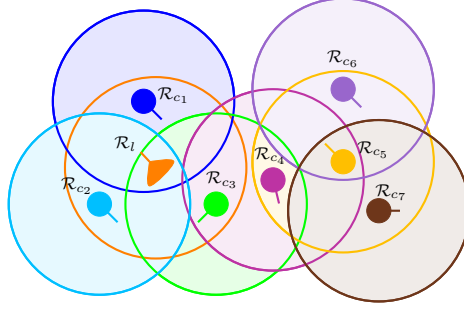
Figure 4.1: Sample heterogeneous MRS. Each shaded area with a solid outline represents the communication and sensing range of corresponding robot.

(a) Global perspective

(b) Local perspective of robot $\mathcal{R}_{c_5}$
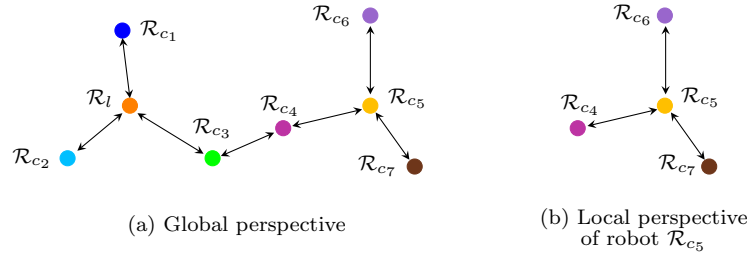
Figure 4.2: Inter-robot measurement and communication graph (IRMCG). Nodes represent robots and edges represent availability of communication link and relative pose measurement between two robots. Bi-directional arrow indicates that robots can measure relative pose of each other and send and receive data to/from their neighbours

4.1.2 Hierarchical-IRMCG

A Hierarchical-IRMCG is a directed graph $\mathbf{G}_{\mathcal{L}} \triangleq \{\bar{\zeta}, \bar{\vartheta}\}$, where $\bar{\zeta} \subseteq \zeta$ and $\bar{\vartheta} \subseteq \vartheta$, without a symmetrical pair of directed edges and without a loop between two nodes. This graph has a single leader robot and one or multiple child robots. The leader robot is the root-node and the child robots are the head-nodes. Fig. 4.3(a) illustrates the hierarchical-IRMCG that corresponds to the robot configuration given in Fig. 4.1.

4.1.3 Local-Hierarchical-IRMCG

A local-hierarchical-IRMCG is a directed graph $\mathbf{G}_{\mathcal{C}} \triangleq \{\underline{\zeta}, \underline{\vartheta}\}$, where $\underline{\zeta} \subseteq \bar{\zeta}$ and $\underline{\vartheta} \subseteq \bar{\vartheta}$. This is defined with respect to a child robot. For a given child robot, the local-

hierarchical-IRMCG gives the shortest communication and measurement path to the child robot from a given leader robot. Further, this graph includes immediate successors of the child robots. Fig. 4.3(b) illustrates the local-hierarchical-IRMCG with respect to robot $\mathcal{R}_{c1}$ for the robot configuration illustrated in Fig. 4.1.

(a) Hierarchical-IRMCG for the robot configuration given in Fig 1

(b) Local-Hierarchical-IRMCG with respect to robot $\mathcal{R}_{c_4}$
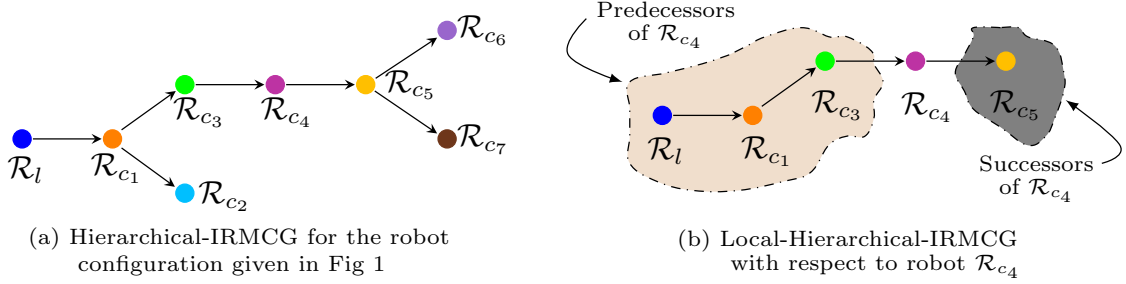
Figure 4.3: Hierarchical inter-robot communication graph (Hierarchical-IRMCG). The hierarchy goes from left to right. The leader robot is the root-node and child robots are the head nodes. Arrow direction indicates the information flow direction.

4.1.4 Communication Modes

Two types of communication modes are assumed: an instantaneous communication mode and a time-delayed communication mode. An instantaneous communication mode assumes that the information originating from a member of the MRS can communicate with any member of the global-IRMCG within the current sample time step. In contrast, a time-delayed communication mode assumes that a single time step is required for information hopping between two robots. Therefore, if a path of a hierarchical-IRMCG has n edges from the leader robot to a child robot, then the child robot will receive information originating from the leader robot with a delayed $(n-1)$ sample time step.

4.2 MRS with an Instantaneous Communication Mode

4.2.1 Single Leader Robot Scenario

When the MRS has only one leader robot, each child robot connected to a global IRMCG should use a single global measurement from the leader at each inter-robot observation event. As child robots in group $\mathcal{G}_{l_i,3}$ (refer to section 3.3 for notation) receive the same information originating from the leader through multiple neighbours, they use the first valid measurement for sensor fusion and discard all the subsequent global measurements that are associated with the current inter-robot observation event.

4.2.2 Multiple Leader Robots Scenario

For an MRS with multiple leader robots, a technique is required to ensure that: (a) a child robot will receive only a single global pose measurement from a given leader robot, and (b) a relative pose measurement will not be used more than once[2] to synthesize the global pose measurements for child robots. If all the available measurements can be collected in a central processing system, then the breadth-first graph search algorithm would be the best option to avoid double counting; i.e., find the shortest measurement and communication path from the leader robot to an arbitrary child robot. The proposed localization scheme is a distributed algorithm and there is no central processor available. Therefore, a novel distributed graph search algorithm is proposed to detect and discard the double counting of information.

Leader robots are the head nodes for any hierarchical-IRMCG. At each relative ob-

---

[2]Use of a given relative pose measurement more than once may lead to an overconfident state estimation.

Algorithm 4.1 Distributed graph search and global pose composition: Leader robots' perspective

---

1: Create an empty local-hierarchical-IRMCG $\mathbf{G}_{l_i}^{l_i}$
2: **for** each member of $\mathcal{S}_{l_i}^c$ **do**
3:     Compute $p(\mathbf{z}_{l_i,k}^{c_q;*})$ where $c_q \in \mathcal{S}_{l_i}^c$: $p(y_{l_i,k}^{c_q;*})$
4:     Initialize a graph for sending to child successor:
        $\mathbf{G}_{l_i,c_q}^{l_i} = \{(l_i,c_q),(l_i-c_q)\}$
5:     Send $\{p(\mathbf{z}_{l_i,k}^{c_q;*}),\mathbf{G}_{l_i,c_q}^{l_i}\}$ to $\mathcal{R}_{c_q}$
6:     Update: $G_{l_i}^{l_i} \leftarrow G_{l_i}^{l_i} \cup \{c_q,(l_i-c_q)\}$
7: **end for**

---

servation event, each leader robot computes global pose measurement, the associated noise covariance matrix, and initial entries of the hierarchical-IRMCG of each child robot operating within the leader robot's sensing and communication range. This information is then communicated to the corresponding child robot. Simultaneously, each leader robot constructs its local-hierarchical-IRMCG. These steps are summarized in **Algorithm 4.1**.

As the leader robots are the root node for each hierarchical-IRMCG they only need to send data (measurements/graph) to child successors. However, an arbitrary child robot may receive data from a leader or child predecessors and send data to child successors. Therefore, the distributed graph search algorithm that runs on the child robots' local processors differs from the algorithm that runs on the leader robots. **Algorithm 4.2** outlines the distributed graph search and global pose composition approach with the perspective of child robots.

Step 1 - Initialization (lines 1-4)

When an inter-robot relative measurement event occurs, each child robot creates an empty local-hierarchical-IRMCG per leader robots in the MRS. Additionally, an empty set i.e., set M, is created to hold the identification indices of the neighbouring child robots that have already received global pose measurements from the child robot

Algorithm 4.2 Distributed graph search and global pose composition: Child robots' perspective

---

1: Create an empty set $\mathbf{M}$
2: **for** $i = 1 : 1 : |\mathcal{L}|$ **do**
3:     Create an empty local-hierarchical-IRMCG $\mathbf{G}_{c_q}^{l_i}$
4: **end for**
5: **while** current sample time step elapsed **do**
6:     Listening
7:     **if** data $\{\mathcal{Y}_{l_i,k}^{c_q,*}, \mathbf{G}_{p,c_q}^{l_i}\}$ received from $\mathcal{R}_p$, $\mathcal{R}_p \in \mathcal{S}$ **then**
8:         **if** $\mathbf{G}_{c_q}^{l_i} \neq \varnothing$ **then**
9:             Send $Ack = 0$ to $\mathcal{R}_p$
10:        **else**
11:            Send $Ack = 1$ to $\mathcal{R}_p$
12:            Assign: $\mathbf{G}_{c_q}^{l_i} \leftarrow \mathbf{G}_{p,c_q}^{l_i}$
13:            Update: $\mathcal{Y}_{l,k}^{c_q,*} \leftarrow \mathcal{Y}_{l,k}^{c_q,*} \cup \mathcal{Y}_{l_i,k}^{c_q,*}$
14:            **if** $|\mathbf{M}| < |\mathcal{S}_{c_q}^c|$ **then**
15:               Find potential successors:
$$\mathbf{D} = \left(\left(\mathcal{S}_{c_q}^c \cap \{p\} \right)' \cap \mathbf{M} \right)'$$
16:               **for** each member of $\mathbf{D}$ **do**
17:                  Compute global pose for $\mathcal{R}_{c_r}$: $\mathcal{Y}_{l_i,k}^{c_r,*}$
18:                  Compute graph to communicate:
$$\mathbf{G}_{c_q,c_r}^{l_i} = \mathbf{G}_{p,c_q}^{l_i} \cup \{c_r, (c_q - c_r)\}$$
19:                  Send $\{\mathcal{Y}_{l_i,k}^{c_r,*}, \mathbf{G}_{c_q,c_r}^{l_i}\}$ to $\mathcal{R}_{c_r}$
20:                  **if** received $Ack = 1$ **then**
21:                     Update: $\mathbf{M} \leftarrow \mathbf{M} \cup \{c_r\}$
22:                     Update: $G_{c_q}^{l_i} \leftarrow G_{c_q}^{l_i} \cup \{c_r, (c_q - c_r)\}$
23:                  **end if**
24:               **end for**
25:            **end if**
26:        **end if**
27:     **end if**
28: **end while**

---

which runs the algorithm.

Step 2 - Check the applicability of the received global pose measurements (lines 7-11)

When a child robot receives a global pose measurement from a neighbouring robot, the child robot analyzes the received information in order to detect and discard the

information originating from the same leader robot. If the received information is not an independent measurement, the child robot notifies the predecessor that the measurement has been discarded. This acknowledgement is important, since it allows the predecessor to re-use the relative observation between these two robots in subsequent steps of the graph search algorithm.

Step 3 - Update local knowledge set and find potential immediate successors (lines 12-15)

If the received measurement is an independent measurement then the local measurement set and the sensing and the corresponding local-hierarchical-IRMCG of the child robot are updated. The received independent global pose measurement can then be integrated with the relative pose measurements for neighbouring robots (immediate successors) to generate global pose measurements for them. To avoid the use of a single relative-pose measurement more than once, the algorithm selects the neighbouring child robot with following characteristics as the potential immediate successor: (i) it operates within the sensing and communication range of the current child node, (ii) it is not the predecessor of the current global pose measurement, and (iii) it has not received a pose measurement from the current child node for the current inter-robot relative pose measurement event.

Step 4 - Compute and communicate global pose measurements and associated graph for potential immediate successors (lines 16-22)

For each potential immediate successor, a child robot computes the global pose measurement, the associated noise covariance matrix and local-hierarchical-IRMCG. The computed information is then communicated to the corresponding child robot. However, the neighbouring child robot may have already received global pose information

originating from the same leader robot through another sensing and communication path. Therefore, set M and local-hierarchical-IRMCG of the current child robot is updated only if the neighbouring robot acknowledges that the measurement has been selected as an independent measurement.
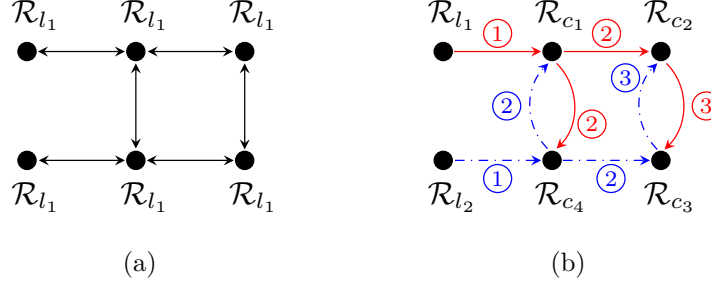
Figure 4.4: Sample multi leader scenario. (a) Multi leader global IRMCG, (b) Information propagation on the global IRMCG where solid arrows (or red arrows) indicate the information propagation steps of leader $\mathcal{R}_{l_1}$, dot-dashed arrows (or blue arrows) indicates the information propagation steps of leader $\mathcal{R}_{l_2}$, and the circled numbers on the lines indicate the order of the communication steps

For the global IRMCG presented in Fig. 4.4(a), the data (measurements and graph) propagation sequence that was obtained from the proposed distributed graph search algorithm is shown in Fig. 4.4(b). In the first communication step, leader $\mathcal{R}_{l_1}$ sends data to child $\mathcal{R}_{c_1}$ and leader $\mathcal{R}_{l_2}$ sends data to child $\mathcal{R}_{c_4}$. When $\mathcal{R}_{c_1}$ receives data from its predecessor, the received data is combined with onboard measurements and generates global pose measurements and associated communication graphs for $\mathcal{R}_{c_2}$ and $\mathcal{R}_{c_4}$. These constructed data is communicated to $\mathcal{R}_{c_2}$ and $\mathcal{R}_{c_4}$ at the second communication step. Similarly, $\mathcal{R}_{c_4}$ extends the information received from $\mathcal{R}_{l_2}$ and sends data to $\mathcal{R}_{c_1}$ and $\mathcal{R}_{c_3}$ during the second communication step. As $\mathcal{R}_{c_1}$ and $\mathcal{R}_{c_4}$ have already used all available relative pose measurements for neighbouring child robots, no information can be hopped through these robots in subsequent communication steps. At the third communication step, $\mathcal{R}_{c_2}$ extends and relays data initialized from

$\mathcal{R}_{l_1}$ to $\mathcal{R}_{c_3}$ while $\mathcal{R}_{c_3}$ extends and relays data initialized from $\mathcal{R}_{l_2}$ to $\mathcal{R}_{c_2}$. This will be the last communication step as there is no room to extend available data without double counting any information. Table 4.1 summarizes the communications steps and Table 4.2 summarizes local-hierarchical IRMCGs that have been constructed on individual child robot local processors.

Table 4.1: The communication steps and associated data for the robot configuration given in Fig. 4.4(a)

Step	From	To	Data (measurement and graph)	Re:
1	$\mathcal{R}_{l_1}$	$\mathcal{R}_{c_1}$	$p(\mathbf{z}_{l_1,k}^{c_1,*})$; $\mathbf{G}_{l_1,c_1}^{l_1} : l_1 \to c_1$	E
	$\mathcal{R}_{l_2}$	$\mathcal{R}_{c_4}$	$p(\mathbf{z}_{l_2,k}^{c_4,*})$; $\mathbf{G}_{l_2,c_4}^{l_2} : l_2 \to c_4$	E
2	$\mathcal{R}_{c_1}$	$\mathcal{R}_{c_2}$	$p(\mathbf{z}_{l_1,k}^{c_2,*})$; $\mathbf{G}_{c_1,c_2}^{l_1} : l_1 \to c_1 \to c_2$	E
	$\mathcal{R}_{c_1}$	$\mathcal{R}_{c_4}$	$p(\mathbf{z}_{l_1,k}^{c_4,*})$; $\mathbf{G}_{c_1,c_4}^{l_1} : l_1 \to c_1 \to c_4$	T
	$\mathcal{R}_{c_4}$	$\mathcal{R}_{c_1}$	$p(\mathbf{z}_{l_2,k}^{c_1,*})$; $\mathbf{G}_{c_4,c_1}^{l_2} : l_2 \to c_4 \to c_1$	T
	$\mathcal{R}_{c_4}$	$\mathcal{R}_{c_3}$	$p(\mathbf{z}_{l_2,k}^{c_3,*})$; $\mathbf{G}_{c_4,c_3}^{l_2} : l_2 \to c_4 \to c_3$	E
3	$\mathcal{R}_{c_2}$	$\mathcal{R}_{c_3}$	$p(\mathbf{z}_{l_1,k}^{c_3,*})$; $\mathbf{G}_{c_2,c_3}^{l_1} : l_1 \to c_1 \to c_2 \to c_3$	T
	$\mathcal{R}_{c_3}$	$\mathcal{R}_{c_2}$	$p(\mathbf{z}_{l_2,k}^{c_2,*})$; $\mathbf{G}_{c_3,c_2}^{l_2} : l_2 \to c_4 \to c_3 \to c_2$	T

Re:remarks, E:extendable, T:terminate

Table 4.2: Local hierarchical-IRMCG for communication steps shown in Fig. 4.4(b) and Table 4.1

4.3 MRS with a Delayed Communication Mode

When a child robot receives global pose measurements from a leader robot, the child robot needs to examine the potential child successors, compose global pose measurements and associated noise covariance for the potential child successors and extend the received communication graph by adding new nodes and edge. Data cannot be communicated to the immediate child successors until these processing steps are completed. This adds some time delay to the communication network. Additionally, there exists a propagation path delay in each information exchange. Because of these delays, an instantaneous communication mode assumption may become invalid for some MRSs. Therefore, this section extends the mathematical formulation of the proposed leader-assisting localization scheme for a time-delayed communication network. The time-delayed communication mode presented in this study assumes that a single sample time step is required for hopping information between two robots. Consider the path from $\mathcal{R}_{l_1}$ to $\mathcal{R}_{c_4}$ in the hierarchical IRMCG presented in Fig. 4.3 (a). The corresponding information flows in the time-delayed communication network are shown in Fig. 4.5.

In this inter-robot relative pose measurement event, the measurements are taken at time $t_\circ$. In the initial time step, the leader robot computes the global pose measurement and the communication graph for $\mathcal{R}_{c_1}$ and sends them to $\mathcal{R}_{c_1}$. Once $\mathcal{R}_{c_1}$ receives a global pose measurement from the leader, the robot combines the received pose measurement with the relative pose measurement for $\mathcal{R}_{c_3}$. This global pose measurement and the associated communication graph are communicated to $\mathcal{R}_{c_3}$ at time $(t_\circ + T)$. This implies that $\mathcal{R}_{c_3}$ receives information with a single time step delay. However, this measurement should be used to update the pose estimation at time $t_\circ$ instead of time $(t_\circ + T)$. This can be achieved if the pose prediction at time $t_\circ$ is available. Therefore, this study keeps the history of state prediction and odometry
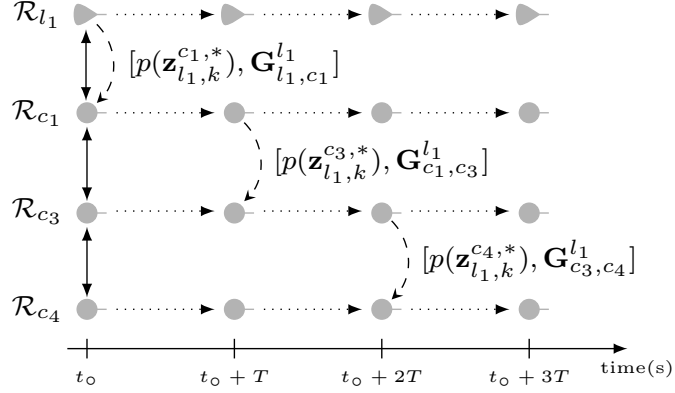
Figure 4.5: Sample information hopping for delayed communication network. The dotted-line arrows represent time propagation, dashed-line arrows indicate the information flow in the network, bi-directional solid arrows represent inter-robot observations (relative pose measurements)

measurements from the inter-robot relative pose measurement event to global pose receiving event. Once the global pose is received, the robot first updates its pose at time $t_\circ$ using the received measurement. This measurement update is followed by a series of time updates using the saved odometry measurements. In addition to the pose update, $\mathcal{R}_{c_3}$ composes a global pose for $\mathcal{R}_{c_4}$ by combining the received global pose measurement with the relative pose measurement for $\mathcal{R}_{c_4}$ which is acquired at time $t_\circ$. This global pose measurement and the associated communication graph are sent to $\mathcal{R}_{c_4}$ at time $(t_\circ + 2T)$. This implies that $\mathcal{R}_{c_3}$ needs to keep its inter-robot relative pose measurement until time $t_\circ + 2T$ and may discard it (clear memory) once the measurements have been used. Robot $\mathcal{R}_{c_4}$ receives a global pose measurement at time $(t_\circ + 2T)$. This measurement corresponds to time $t_\circ$ and is used to update the pose estimation at time $t_\circ$. This update is followed by the update of state propagation from $t_\circ$ to $(t_\circ + 2T)$ using the stored odometry measurements. Note that the leader robot initialize the communication and uses all its available data at time step $t_\circ$. Therefor the leader does not require to maintain history and apply Markov rule at each time step without any delay.

The key challenge of this implementation is that a robot cannot exploit the Markov property at each time step as the previous state estimations and measurements are being used for sensor fusion at future time steps. This implies that each child robot has to keep old measurements and state estimations for future usage, causing the onboard memory space requirement to increase. To reduce the information storage requirement, the Markov property need to be applied so that each child robot that connects to the global IRMCG receives its optimum number of global pose measurements. For this purpose, a *liberate-point* is defined as follows:

Definition 4.3.1. *A liberate-point, $\mathfrak{L}_j(k_m, k_{lp})$, is an event that occurs at liberate-point time k_{lp}, in which child robot $\mathcal{R}_{c_j}$ receives a maximum number of possible delayed global pose measurements from leaders. These global pose measurements correspond to the inter-robot relative pose measurement event that occurred at time k_m ($\leq k_{lp}$). At the liberate-point, the corresponding child robot:*

1. *updates its pose at time step k_m using the received global pose measurements;*

2. *re-evaluates state propagation from k_m to k_n and computes new predictive density for the time step k_{n+1}; and*

3. *clears memory $\mathbf{u}(k_m : k_n)$, $\mathbf{x}(k_m : k_n)$, $\mathbf{P}(k_m : k_n)$.*

In the next time step, the child robot:

1. *transmits newly calculated global pose measurements for corresponding child successors; and*

2. *clears memory $\mathbf{z}(k_m : k_n)$.*

Consider Fig. 4.5 as an example, when an inter-robot relative pose measurement has occurred at time $t_\circ$. For this measurement event, for each child robot k_m equals $t_\circ$.

As the first child robot receives global pose measurements instantly it does not need to store odometry or previous pose estimations. Therefore, its liberate-point time is $t_\circ$. In other words, the liberate-point of the child $\mathcal{R}_{c_1}$ is $\mathfrak{L}_{c_1}(t_\circ, t_\circ)$. This child robot will clear the stored inter-robot relative pose measurements at time $(t_\circ + T)$, i.e. a single time step after the liberate-point time. The liberate-point for $\mathcal{R}_{c_3}$ and $\mathcal{R}_{c_4}$ are $\mathfrak{L}_{c_3}(t_\circ, t_\circ + T)$ and $\mathfrak{L}_{c_4}(t_\circ, t_\circ + 2T)$, respectively.

Lemma 4.3.1. *If a given child robot is an edge robot of the global-IRMCG it will receive maximally one global pose measurement per an inter-robot relative pose measurement event, i.e. if $|\mathcal{Y}_{q,k}| = 1$ then $|\mathcal{Y}^{c_q,*}_{l_i,k}| = 1$, $l_i \in \mathcal{L}$.*

Proof. The edge robot has only one neighbour (leader or child). **Algorithm 4.2** ensures that the single inter-robot relative pose measurement can be used only once for a global pose measurement computing task. Since a single relative pose measurement can be used only once, the edge robot can receive maximally one global pose measurement for time step k. □

Theorem 4.3.1. *If a given child robot is an edge robot of the global IRMCG, liberate-point time k_{lp} is the time that the robot receives the first global pose measurement for the inter-robot relative pose measurement event that occurred at time k_m.*

Proof. According to **Lemma 4.3.1**, an edge robot receives only one global pose measurements for a given inter-robot relative pose measurement event. This implies that the maximum number of global pose measurements for this child robot equals one. According to **definition 4.3.1**, the liberate-point occurred at the time where the child robot has received its maximum number of delayed global pose measurements from leaders. As the edge robot can receive only one global pose measurement, the liberate-point time k_{lp} for any edge robot is the time that the robot receives the first global pose measurement for the current inter-robot relative pose measurement event. □

Lemma 4.3.2. *For a given child node, if there exists no robot within the sensing and communication range of the child robot at an inter-robot measurement event, then the child robot will not receive any global pose measurement for this measurement event, i.e., if $\mathcal{Y}_{q,k} = \emptyset,\ q \in \mathcal{C}$ then $|\mathcal{Y}_{l_i,k}^{c_q,*}| = 0,\ l_i \in \mathcal{L}$.*

Proof. If $\mathcal{Y}_{q,k} = \emptyset$ then the child robot $\mathcal{R}_{c_q}$ belongs to group $\mathcal{G}_{l_i,4},\ \forall i \in \mathcal{L}$. This implies that there is no path existing from any leader robot to child robot $\mathcal{R}_{c_q}$ in the global-IRMCG. Therefore, global pose compositions initiated at any leader robot cannot be propagated to child robot $\mathcal{R}_{c_q}$. Hence, no global pose measurement will be available for this child robot, i.e., $|\mathcal{Y}_{l_i,k}^{c_q,*}| = 0,\ l_i \in \mathcal{L}$. $\qquad\square$

Lemma 4.3.3. *If a given child robot has n neighbours, i.e., $|\mathcal{Y}_{q,k}| = n$, and a team has N leader robots, i.e., $|\mathcal{L}| = N$, then the maximum number of global pose measurements that the child robot may receive is:*

$$|\mathcal{Y}_{l,k}^{c_q,*}|_{max} = \begin{cases} n, & if\ n \leq N \\ N, & otherwise \end{cases}$$

Proof. According to **Algorithm 4.2**, each leader robot can provide a single global pose measurement for a given child robot at an inter-robot relative pose measurement event. Therefore, if an MRS has N leader robots, i.e. $|\mathcal{L}| = N$, the maximum number of independent global pose measurements for each child robot equals N.

On the other hand, **Algorithm 4.2** does not allow the use of a single edge (single inter-robot relative pose measurement) more than once for the process of global pose composition. This implies that the neighbours of a given child robot can provide only one global pose measurement for the child robot. Hence, the child robot can receive maximally n independent global pose measurements as $|\mathcal{Y}_{q,k}| = n,\ q \in \mathcal{C}$.

Integrating these two conditions, it is clear that $|\mathcal{Y}_{l,k}^{c_q,*}|_{\max} = \min(n, N)$. $\qquad\square$

Theorem 4.3.2. *If a given child robot has n neighbours, i.e., $|\mathcal{Y}_{q,k}| = n$, and a team has N leader robots, i.e. $|\mathcal{L}| = N$, the liberate-point time k_{lp} for this child robot is the time that the robot receives $\bar{n}$ independent global pose measurements, where $\bar{n} = min(n, N)$, for the inter-robot relative pose measurement event that occurred at time k_m.*

Proof. According to **Lemma 4.3.1**, when a child robot has n neighbours and the MRS has N leader robots, the maximum number of independent global pose measurements that the child robot may receive is equal to $\min(n, N)$, i.e., $|\mathcal{Y}_{l,k}^{c_q,*}|_{\max} = \min(n, N)$. **Definition 4.3.1** states that the liberate-point occurs at the time when the child robot has received its maximum number of delayed global pose measurements from the leaders. Therefore, when $|\mathcal{Y}_{q,k}| = n$ and $|\mathcal{L}| = N$, the liberate-point time k_{lp} is the time that the robot receives $\bar{n}$ independent global pose measurements where $\bar{n} = \min(n, N)$. $\qquad\qquad\square$

There can be an IRMCG configuration such that the algorithm used for avoiding double counting causes one or more child robot to receive fewer global pose measurements than the expected maximum number of measurements as given by **Lemma 4.3.3**. For example, consider the global IRMCG shown in Fig. 4.6.
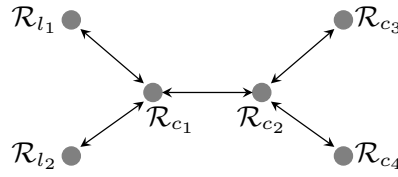
Figure 4.6: Sample robot configuration that causes a child robot to receive fewer global pose measurements than its expected maximum number of measurements

In this example, $\mathcal{R}_{c_2}$ has three neighbours and the MRS has two leader robots. Therefore, $|\mathcal{Y}_{c_2,k}| = 3$ and $|\mathcal{L}| = 2$. From Lemma 4.3.3, $\mathcal{R}_{c_2}$ is able to receive maximally

two independent global pose measurements, i.e., $\bar{n} = \min(n, N) = \min(2, 3) = 2$. However, **Algorithm 4.2** allows only one leader robot to exploit relative pose measurements from $\mathcal{R}_{c_1}$ to $\mathcal{R}_{c_2}$ for computation of a global pose measurement. Therefore, the second leader robot will not provide a global pose measurement for $\mathcal{R}_{c_2}$ causing $\mathcal{R}_{c_2}$ receives only one global pose measurement for this IRRM event. This is less than its expected maximum number of independent measurements. It is important to identify such conditions and apply the Markov property to optimize the memory usage. For this purpose, a *max-delay point* is defined as follows:

Definition 4.3.2. *A max-delay point, $\mathcal{M}_j(k_m, k_{md})$, is an event that occurs at max-delay point time k_{md}, in which child robot $\mathcal{R}_{c_j}$ exceeds maximum waiting time to receive delayed global pose measurements from leader robots. This global pose measurement(s) corresponds to the inter-robot relative pose measurement event that occurs at time k_m. At the max-delay point, the corresponding child robot clears the history of the measurements and estimations $\mathbf{u}(k_m : k_n)$, $\mathbf{x}(k_m : k_n)$, $\mathbf{P}(k_m : k_n)$, and $\mathcal{Y}_{c_j, k_m}$.*

Lemma 4.3.4. *For an MRS with $|\mathcal{L}|$ leader robots and $|\mathcal{C}|$ child robots, if the child robot within the leader robot's communication range receives a global pose measurement instantly and subsequent information hopping needs one time step per information hop between two robots, then the maximum time delay is equal to $(|\mathcal{C}| - 1)T$, where T is the sample time.*

Proof. For an MRS with $|\mathcal{L}|$ leader robots and $|\mathcal{C}|$ child robots, the maximum delay network configuration occurs when one child robot operates within the sensing and communication range of a leader robot (or group of leader robots) while others connect so that the hierarchical-IRMCG has a single branch, i.e., inter robot observation and communication of child robots form a chain-like formation as shown in Fig. 4.7. The first child robot of the chain receives the global pose measurement instantly, i.e. at $t_\circ$. The second child robot receives the measurements with a single time step
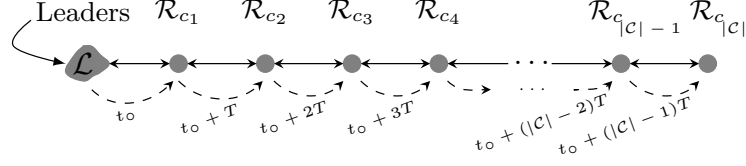
Figure 4.7: Chain-like IRMCG

delayed, i.e. at $t_{\circ} + T$. The third child robot receives a measurement with two time steps delay, i.e. at $t_{\circ} + 2T$. The fourth child robot receives a measurement with three time steps delayed, i.e. at $t_{\circ} + 3T$. This patten suggests that the child robots in a chain-like formation receive measurements with one time step less than its order (position) in the network. Therefore, $(|\mathcal{C}| - 1)^{\text{th}}$ child robot and $|\mathcal{C}|^{\text{th}}$ child robot receive pose measurements with $(|\mathcal{C}| - 2)$ and $(|\mathcal{C}| - 1)$ time steps delayed, i.e. at $t_{\circ} + (|\mathcal{C}| - 2)T$ and $t_{\circ} + (|\mathcal{C}| - 1)T$, respectively. $\mathcal{R}_{c_{|\mathcal{C}|}}$ is the last node (edge robot) of the network. This robot receives measurements with $(|\mathcal{C}| - 1)$ time step delayed. Therefore, the maximum time delay for this network is equal to $(|\mathcal{C}| - 1)T$, where T is the sample time step. □

Theorem 4.3.3. *Consider an MRS with $|\mathcal{L}|$ leader robots and $|\mathcal{C}|$ child robots. If a given child robot of the MRS has n child neighbours then the maximum time delay for this child robot equals $(|\mathcal{C}| - n)T$, where T is the sample time.*

Proof. According to **Lemma 4.3.4**, the maximum delay for the MRS with $|\mathcal{L}|$ leaders and $|\mathcal{C}|$ child is $(|\mathcal{C}| - 1)T$. In other words, maximum delay is equal to the (number of child robots in the chain formation-1)T. If a given child robot has n child neighbours, and the IRMCG has a chain-like formation, then $(n - 1)$ child robot will not be predecessors for this child robot (refer Fig. 4.8). Therefore, the maximum delay is reduced by $(n - 1)T$. This implies that the maximum delay for the child robot with n child neighbours equals $(|\mathcal{C}| - 1)T - (n - 1)T = (|\mathcal{C}| - n)T$.

□
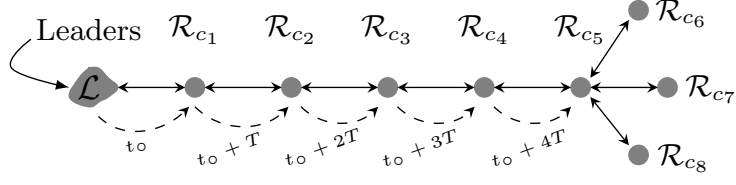
Figure 4.8: Sample robot configuration for **Lemma 4.3.3**. In this configuration $|\mathcal{C}| = 8$. Consider $\mathcal{R}_{c_5}$. It has 4 neighbouring child robots, i.e. $\{\mathcal{R}_{c_4}, \mathcal{R}_{c_6}, \mathcal{R}_{c_7}, \mathcal{R}_{c_8}\}$. Therefore $n = 4$ and maximum delay for $\mathcal{R}_{c_5}$ is $(|\mathcal{C}| - n)T = (8 - 4)T = 4T$, i.e., information is delayed by four sample time steps.

Theorem 4.3.4. *Consider a child robot, $\mathcal{R}_{c_i}$, in an MRS. If the neighbouring child robots of $\mathcal{R}_{c_i}$ have applied the Markov rule, i.e., the robot clears the history of state estimation, odometry data, and inter-robot relative measurements at time t_k, then $\mathcal{R}_{c_i}$ can apply the Markov rule at time step t_{k+1}.*

Proof. If all neighbours have applied the Markov rule at time t_k, the child robot $\mathcal{R}_{c_i}$ will not receive global pose measurements for current inter-robot observations in subsequent time steps. As a result, child robot $\mathcal{R}_{c_i}$ will not update its past estimation and will not generate any global pose measurement for its neighbours after time step t_k. Therefore, holding the past information such as previous state estimations, odometry data and inter-robot relative pose measurements becomes redundant. Clearing redundant information improves the memory utilization. Hence, the child robot $\mathcal{R}_{c_i}$ can apply the Markov rule at time step t_{k+1}. $\qquad\square$

4.4 Distributed Leader-Assisting Localization Algorithm

This study assumes that each robot in the MRS knows its initial pose with respect to a given reference coordinate system and exploits the CKF for sensor fusion. Sensor fusion architecture can be divided into two parts: (i) leader robot localization, and

(ii) child robot localization.

4.4.1   Leader Robot Localization

Fig. 4.9 illustrates the sensor fusion architecture for leader robots. The recursive state estimation steps of this sensor fusion architecture are summarized in **Algorithm 4.3**. This algorithm is implemented on each leader robot and iterates at each sample time step. The algorithm is initialized with known initial conditions and performs three main tasks: state prediction, state correction, and pose formation.
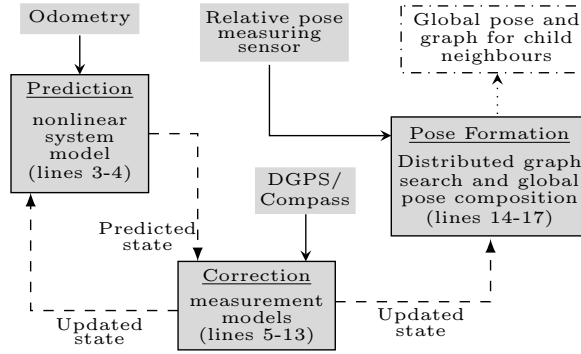
Figure 4.9: Sensor fusion architecture for leader robots. Arrows with solid-line represent measurement acquisition from sensors, arrows with dashed-line represent internal information flow of the robot, and arrow with dotted-line represents information communication with neighbours

Step 1 - State prediction (lines 2-4)

At each time step, the leader robot reads its odometry and predicts the current pose using the acquired velocity measurements and prior state estimation.

Step 2 - State correction (lines 5-13)

To establish an accurate localization for leader robots, this study assumes the availability of a DGPS sensor and compass for each leader robot. Prior to using the

---

Algorithm 4.3 : Distributed leader-assisted localization - Leader's perspective

---

1: Initialize with $\mathbf{X}_{l_q,\circ}$ and $\mathbf{P}_{l_q,\circ}$
2: **for** $k \in (1, \cdots, \infty)$ **do**
3:     Read ego-motion sensor: $\mathbf{u}_{l_q,k}$
4:     Estimate predictive density $p(\mathbf{x}_{l_q,k|k-1})$ using prior density $p(\mathbf{x}_{l_q,k-1})$ and odometry reading $\mathbf{u}_{l_q,k-1}$
5:     **if** DGPS/Compass measurement is available **then**
6:         **if** measurement gate validated **then**
7:             Compute posterior density $p(\mathbf{x}_{l_q,k})$ using predictive density $p(\mathbf{x}_{l_q,k|k-1})$, DGPS measurement $p(\mathbf{z}_{l_q,k}^{DGPS})$, and/or Compass measurement $p(\mathbf{z}_{l_q,k}^{Comp})$
8:         **else**
9:             $p(\mathbf{x}_{l_q,k}) \leftarrow p(\mathbf{x}_{l_q,k|k-1})$
10:        **end if**
11:    **else**
12:        $p(\mathbf{x}_{l_q,k}) \leftarrow p(\mathbf{x}_{l_q,k|k-1})$
13:    **end if**
14:    **if** relative pose measurement event **then**
15:        Read relative pose measurement sensor: $\mathcal{Y}_{l_q,k}$
16:        Distributed graph search and global pose composition: **Algorithm** 4.1
17:    **end if**
18: **end for**

---

available DGPS/compass measurements for sensor fusion, it is important to identify and discard outliers. Therefore, measured DGPS/compass measurements are evaluated through an ellipsoidal measurement validation gate [116]. Any measurement that violates the validation gate condition is considered an outlier and will not be used for the state estimation process. If the valid DGPS/compass measurement is acquired it will be fused with the predictive state estimate. When the available DGPS/compass measurement is an outlier or there is no DGPS/compass measurement, then the predictive density is directly assigned to the posterior density of the state estimation.

Step 3 - Pose formation (lines 14-17)

When an inter-robot relative pose measurement event occurs, each leader robot acquires the relative pose of its neighbouring robot and evaluates these measurements in **Algorithm 4.1** in order to compose a global pose, the associated noise covariance matrix and the local-hierarchical-IRMCG for neighbouring child robots.

4.4.2 Child Robot Localization

The sensor fusion architecture for child robots' localization is twofold:

I) sensor fusion architecture for instantaneous communication mode, and

II) sensor fusion architecture for delayed communication mode

I) Sensor Fusion Architecture for Instantaneous Communication Mode:
When the MRS has instantaneous communication capabilities, the recursive state estimation steps for a child robot are outlined in **Algorithm 4.4** and graphically illustrated in Fig. 4.10. This algorithm is implemented on each child robot and iterates at each sample time step. The algorithm is initialized with known initial conditions and performs three main tasks: state prediction, pose formation and measurement update.

Step 1 - State prediction (lines 3-5)

Each child robot reads its ego-motion sensor at each sample time step and predicts its current pose using prior state estimation densities and acquired odometry measurements. To enable recursive filtering, the predicted density is directly assigned to the posterior density.

94

Figure 4.10: Sensor fusion architecture for child robots for instantaneous communication mode. Arrows with solid-line represent measurement acquisition from sensors, arrows with dashed-line represent internal information flow of the robot and arrows with dotted-line represent information communication

---

Algorithm 4.4 : Distributed leader-assisted localization with instantaneous communication mode - Child's perspective

---

1: Initialize with $\mathbf{X}_{c_r,\circ}$ and $\mathbf{P}_{c_r,\circ}$
2: **for** $k \in (1, \cdots , \infty)$ **do**
3:   Read ego-motion sensor: $\bar{\mathbf{u}}_{c_r,k}$
4:   Estimate predictive density $p(\mathbf{x}_{c_r,k|k-1})$ using prior density $p(\mathbf{x}_{c_r,k-1})$ and odometry reading $\bar{\mathbf{u}}_{c_r,k-1}$
5:   Set $p(\mathbf{x}_{c_r,k}) \leftarrow p(\mathbf{x}_{c_r,k|k-1})$
6:   **if** relative pose measurement event **then**
7:    Read relative pose measurement sensor: $\mathcal{Y}_{c_r,k}$
8:    Run distributed graph search and global pose composition algorithm: **Algorithm 4.2**
9:    **if** $\mathcal{Y}_{l,k}^{c_r,*} \neq \emptyset$ **then**
10:     **for** $\forall p(\mathbf{z}_{l,k}^{c_r,*}) \in \mathcal{Y}_{l,k}^{c_r,*}$ **do**
11:      **if** measurement gate validated **then**
12:       Update the posterior density $p(\mathbf{x}_{c_r,k})$ using the current posterior density $p(\mathbf{x}_{c_r,k})$ and the global pose measurements in $\mathcal{Y}_{l,k}^{c_r,*}$
13:      **end if**
14:     **end for**
15:    **end if**
16:   **end if**
17: **end for**

Step 2 - Pose formation (lines 6-8)

When an inter-robot relative pose measurement event occurs, each child robot measures the relative pose of neighbours. This measurement acquisition is followed by

95

the evaluation of the distributed graph search and global pose composition algorithm (**Algorithm** 4.2) to compute and communicate global pose measurements and associated sensing and measurement graphs for neighbours.

Step 3 - Measurement update (lines 9-15)

When a child robot receives an independent measurement, it is fused with the child robot's local estimate. Prior to performing this sensor fusion, each child robot evaluates each received global pose measurement on an ellipsoidal measurement validation gate to detect and discard outliers.

II) Sensor Fusion Architecture for Delayed Communication Mode:

Fig. 4.11 illustrates the sensor fusion architecture for child robots for a delayed communication mode. The recursive state estimation steps of this sensor fusion architecture are summarized in **Algorithm** 4.5. This algorithm is implemented on each child robot and iterates at each discrete time step. The algorithm is initialized with known initial conditions and performs four main tasks: state prediction, pose formation initialization, pose composition, history maintenance and measurement update.

Step 1 - State prediction (lines 5-7)

Each child robot reads its ego-motion sensor at each sample time step and predicts its current pose using prior state estimation densities and acquired odometry measurements. To enable recursive filtering, the predicted density is directly assigned to the posterior density.

Algorithm 4.5 : Distributed leader-assisted localization with time-delayed communication mode - Child's perspective

---

1: Initialize with $\mathbf{X}_{c_r,\circ}$ and $\mathbf{P}_{c_r,\circ}$
2: Create empty set $\mathcal{U}_{c_r}$ to store odometry data
3: Create empty set $\mathcal{Y}_{c_r}$ to store relative pose measurement densities
4: **for** $k \in (1, \cdots, \infty)$ **do**
5:      Read ego-motion sensor: $\bar{\mathbf{u}}_{c_r,k}$
6:      Estimate predictive density $p(\mathbf{x}_{c_r,k|k-1})$ using prior density $p(\mathbf{x}_{c_r,k-1})$ and odometry reading $\bar{\mathbf{u}}_{c_r,k-1}$
7:      $p(\mathbf{x}_{c_r,k}) \leftarrow p(\mathbf{x}_{c_r,k|k-1})$
8:      **if** relative pose measurement event **then**
9:          Read relative pose measurement sensor: $\mathcal{Y}_{c_r,k}$
10:          Set delay time cont to zero: $t_{dc} = 0$
11:          Save current odometry reading: $\mathcal{U}_{c_r} = \mathcal{U}_{c_r} \cup \mathbf{u}_{c_r,k}$
12:          Save relative pose measurements for child neighbours: $\mathcal{Y}_{c_r} = \mathcal{Y}_{c_r,k}^{c,c_r}$
13:          Initialize the distributed graph search and global pose composition algorithm: Lines 1-4 of **Algorithm 4.2**
14:          Compute the max-delay point time t_{md}
15:          Set liberate-point time t_{lp} equal to max-delay point time: $t_{lp} = t_{md}$
16:          Compute maximum number of the possible independent global pose measurements, $|\mathcal{Y}_{c_r}|_{max}$
17:      **else**
18:          **if** $\mathcal{U}_{c_r} \neq \emptyset$ **then**
19:              Save current odometry reading:
$$\mathcal{U}_{c_r} = \mathcal{U}_{c_r} \cup \mathbf{u}_{c_r,k}$$
20:          **end if**
21:      **end if**
22:      **if** $(k \times T) \leq (t_{lp} + T)$ **and** $(k \times T) \leq (t_{md})$ **then**
23:          **if** $|\mathcal{Y}_{c_r}| == |\mathcal{Y}_{c_r}|_{max}$ **then**
24:              Set $t_{lp} = (k \times T)$
25:          **end if**
26:          Perform distributed graph search and global pose composition for neighbours: Line 5-28 of **Algorithm 4.2**
27:          Increment the delay count by one time step: $t_{dc} = t_{dc} + 1$
28:      **else**
29:          **if** $\mathcal{Y}_{l,k-t_{dc}}^{c_r,*} \neq \emptyset$ **then**
30:              **for** $\forall p(\mathbf{z}_{l,k-t_{dc}}^{c_r,*}) \in \mathcal{Y}_{l,k-t_{dc}}^{c_r,*}$ **do**
31:                  **if** measurement gate validated **then**
32:                      Compute new posterior density $p(\mathbf{x}_{c_r,k-t_{dc}})$ using current posterior density $p(\mathbf{x}_{c_r,k-t_{dc}})$ and the global pose measurements in $\mathcal{Y}_{l,k-t_{dc}}^{c_r,*}$
33:                  **end if**
34:              **end for**
35:              Update time propagation from sample time $(k - t_{dc})$ to k using posterior density $p(\mathbf{x}_{c_r,k-t_{dc}})$ and odometry measurements $\mathbf{u}_{c_r,k-t_{dc}:k}$

```
36:        else
37:            $p(\mathbf{x}_{c_r,k}) \leftarrow p(\mathbf{x}_{c_r,k|k-1})$
38:        end if
39:        Apply Markov property
40:     end if
41: end for
```
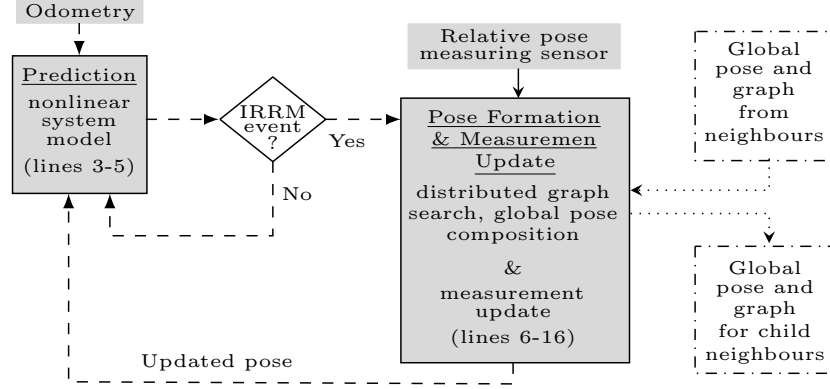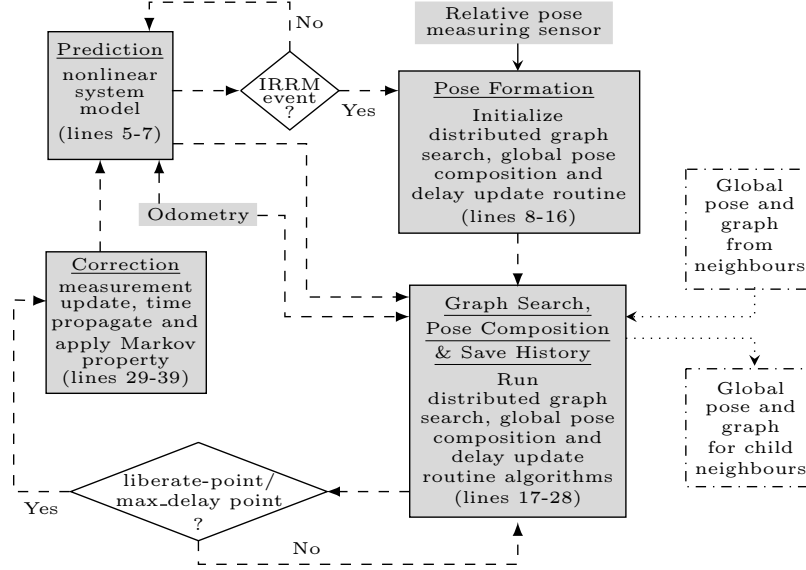

Figure 4.11: Sensor fusion architecture for child robots for delayed communication mode. Arrows with solid-line represent measurement acquisition from sensors, arrows with dashed-line represent internal information flow of the robot, and arrow with dotted-line represents information communication

Step 2 - Pose formation initialization (lines 8-16)

When an inter-robot relative pose measurement event occurs, each child robot measures the relative pose of neighbours. These relative pose measurements and odometry readings may be used in a future time step as the communication mode is assumed to be time delayed. Therefore, both relative pose measurements and odometry measurements are temporarily stored. Then a set of parameters, such as max-delay point time (t_{md}), liberate-point time (t_{lp}), delay time count (t_{dc}), and maximum number of potential independent measurements ($|\mathcal{Y}_{c_r}|_{max}$), need to be calculated and set to

appropriate values in order to facilitate the time delayed measurement update. However, t_{lp} cannot be calculated directly, because the liberation point occurs when a child robot receives the maximum number of independent global measurements for the current inter-robot observation event. It is known that $t_{lp} \leq t_{md}$. Using this property, the initial value for t_{lp} is set to t_{md}. When $|\mathcal{Y}_{c_r}| = |\mathcal{Y}_{c_r}|_{max}$, the value of t_{lp} is reset to the current sample time. Once all the parameters are computed, each child robot initiates the distributed graph search and global pose composition algorithm (**Algorithm 4.2**).

Step 3 - Pose composition and history maintenance (lines 17-28)

When the delay routine is running, each child robot keeps storing its local odometry data and evaluating lines 5-28 of the distributed graph search and global pose composition algorithm (**Algorithm 4.2**) while incrementing the delay count by a sample time step at each iteration. During this waiting time, if the number of the received independent global pose measurements becomes equal to the expected maximum value, then the child robot resets its liberate point time.

Step 4 - Measurement update (lines 29-39)

Once the child robot has received its maximum number of independent global pose measurements or the delay count exceeds the maximum waiting time, the child robot proceeds to the measurement update phase. Each available global pose measurement is independently fused with the state estimation at sample time step $(k - t_{dc})$. Prior to performing this sensor fusion, each child robot evaluates each received global pose measurement on an ellipsoidal measurement validation gate to detect and discard outliers. This measurement update is followed by the re-evaluation of the time propagation from sample time step $(k - t_{dc})$ to k using the updated pose at sample time

step $(k - t_{dc})$ and the odometry measurements are saved in the local memory. Finally, the Markov property is applied and the robot clears the saved odometry and relative pose measurements in order to optimize the memory usage.

4.5 Evaluation

Two simulation configurations were used to evaluate the proposed decentralized leader-assisted localization approach, i.e., heterogeneous-MRS with a single leader robot and heterogeneous-MRS with multiple leader robots.

4.5.1 Heterogeneous-MRS with a Single Leader Robot

4.5.1.1 Setup

Monte-Carlo simulation is performed for a heterogeneous MRS with a single leader robot and four child robots. The leader robot remained stationary. The first child robot, i.e., $\mathcal{R}_{c_1}$, always operated within the sensing and communication boundaries of the leader robot while the fourth child robot, i.e., $\mathcal{R}_{c_4}$, always operated beyond the sensing and communication boundaries of the leader robots. The remaining two child robots, i.e., $\mathcal{R}_{c_2}$ and $\mathcal{R}_{c_3}$, intermittently appeared within the sensing and communicating range of the leader robot. Simulation parameters and the characteristics of each sensory system are summarized in Table 3.1 and Table 3.2, respectively. It was assumed that the DGPS and compass sensors are available only for the leader robots.

4.5.1.2 Results

Average state estimation errors and the associated 3σ error boundaries of child robot $\mathcal{R}_{c_4}$ for the proposed leader-assisted navigation are shown in Fig. 4.12 and Fig. 4.13, respectively. The former is related to the instantaneous communication mode while

the latter is related to the delayed communication mode. These results demonstrate that the estimation error of child robot $\mathcal{R}_{c_4}$ always stays within the associated 3σ error boundaries. This observation implies that the proposed localization algorithm is capable of generating non-overconfident state estimations for child robots. This achievement can be attributed to the graph search and global pose composition algorithms, i.e., **Algorithm 4.1** and **Algorithm 4.2**, that are implemented to detect and discard all possible double counting of the same information when it propagates through the communication network.

Fig. 4.14 shows the comparison of the pose estimation error of child robot $\mathcal{R}_{c_4}$ using three different sensor fusion architectures: (1) the proposed leader-assisted localization technique with instantaneous communication mode, (2) the proposed leader-assisted localization technique with delayed communication mode, and (3) the leader-assisted localization without incorporating the proposed sensor fusion techniques. It can be seen that the localization error of the proposed leader-assisted localization algorithm is bounded even when the child robots navigate beyond the sensing and communication range of the leader robots. Additionally, these results illustrate that without the proposed sensor fusion architectures, localization of the child robots that operate beyond the sensing and communication range of the leader robots tends to diverge. In the traditional leader-assisted localization, dead reckoning is the key localization method available for child robots which operate beyond the sensing and communication range of leader robots. Dead-reckoning is known to be divergent. Hence, the traditional leader-assisted localization method is incapable of establishing an accurate localization for child robots that operate beyond the sensing and communication range of the leader robots (see Fig. 4.14).
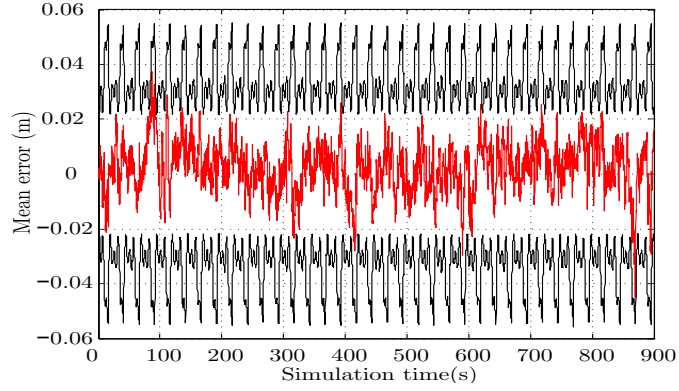
(a) x-position
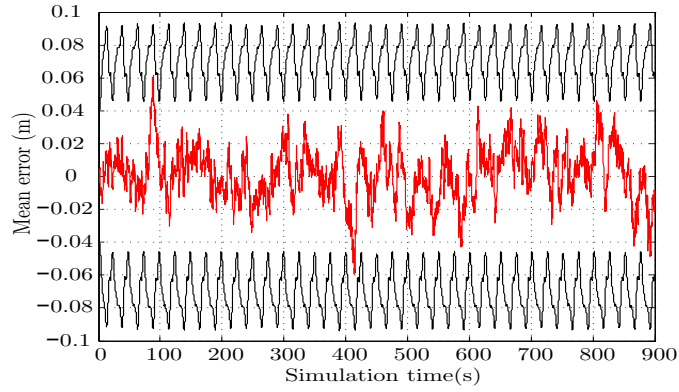
(b) y-position
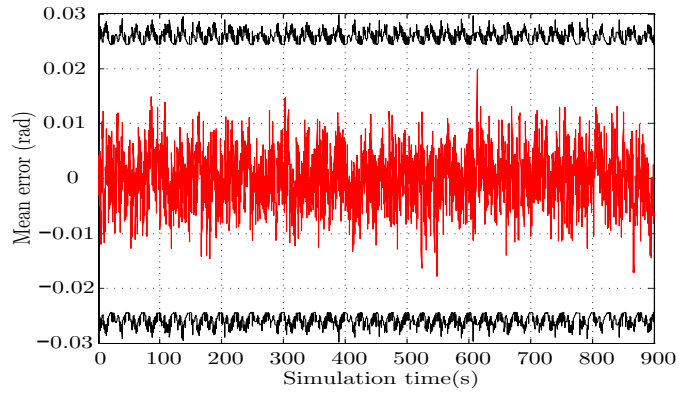
(c) ϕ-orientation

Figure 4.12: Mean estimation error of child robot $\mathcal{R}_{c_4}$ for 20 Monte-Carlo simulations with instantaneous communication mode. Red solid line indicates mean estimation error while the black solid lines indicate double-sided 3-σ error boundaries

102
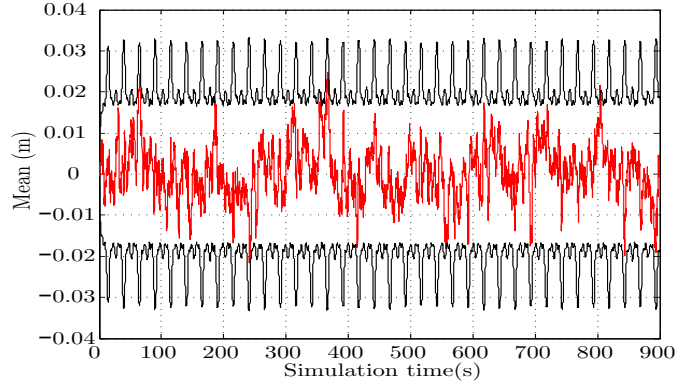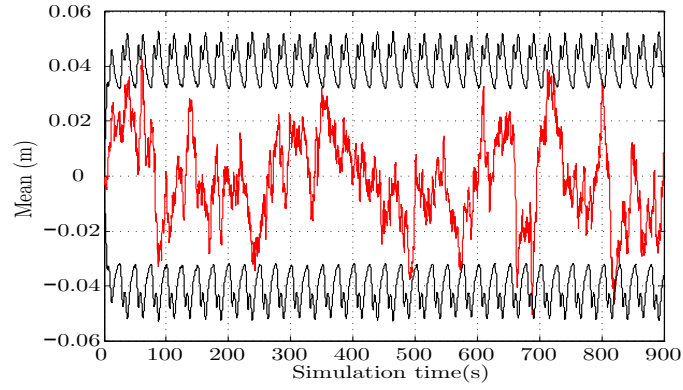
(a) x-position

(b) y-position
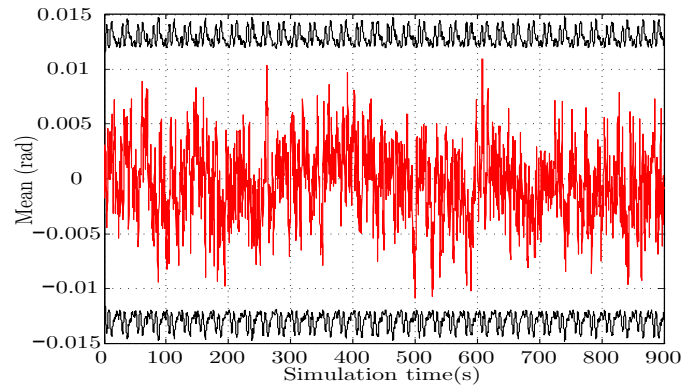
(c) ϕ-orientation

Figure 4.13: Mean estimation error of child robot $\mathcal{R}_{c_4}$ for 20 Monte-Carlo simulations with time-delayed communication mode. Red solid line indicates mean estimation error while the black solid lines indicate double-sided 3-σ error boundaries

103
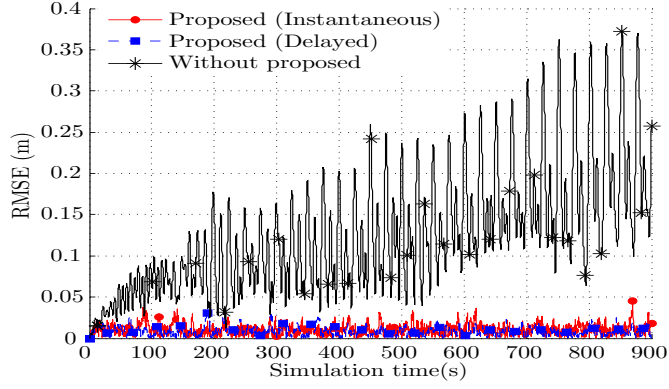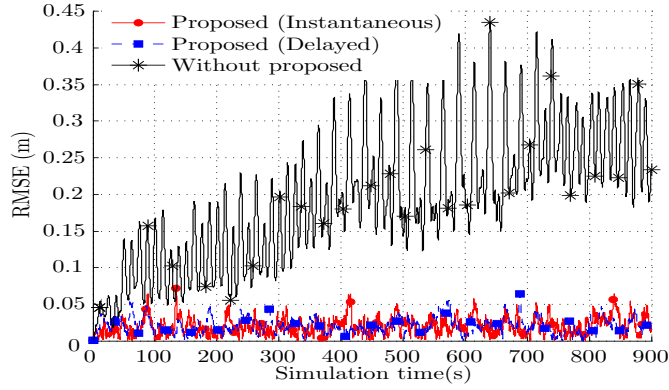
(a) x-position

(b) y-position
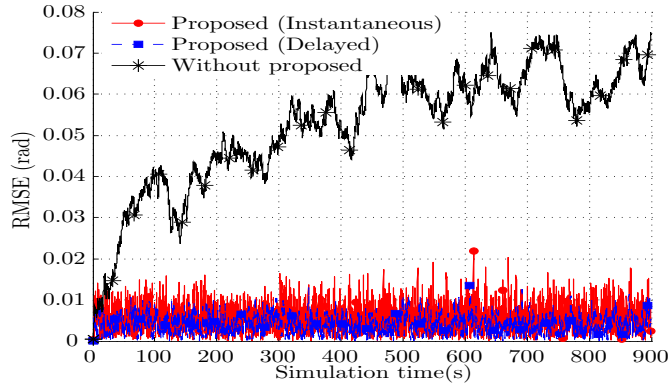
(c) ϕ-orientation

Figure 4.14: Comparison of the estimation error of child robot $\mathcal{R}_{c_4}$ for 20 Monte-Carlo simulations. Without the proposed method, child robot $\mathcal{R}_{c_4}$ relies only on the odometry reading as it operates beyond the sensing range of the leader robot

104

4.5.2 Heterogeneous-MRS with Multiple Leader Robots

4.5.2.1 Setup

The performance of the proposed leader-assisted localization scheme for a multi-leader scenario was evaluated using a publicly available multi-robot localization and mapping data-set [49]. The data-set consists of odometry data, inter-robot range and bearing measurements, and ground truth measurements for a team of five robots navigating in an indoor environment (2D arena). For the evaluation purpose, it was assumed that two of the robots are leader robots ($\bar{\mathcal{R}}_{l_1}$, $\bar{\mathcal{R}}_{l_2}$) and the remaining three robots are child robots ($\bar{\mathcal{R}}_{c_1}$, $\bar{\mathcal{R}}_{c_2}$, $\bar{\mathcal{R}}_{c_3}$). This study exploited only the odometry data and ground truth measurements from the data-set while the relative pose measurements, DGPS measurements and compass measurements were synthesized using the ground truth measurements. The noise levels for the relative pose measurement sensor, DGPS sensor and compass were kept at the same values given in Table 3.2 while their update rates were set to 5 Hz. In addition to this modification, the sensing and communication ranges of the teammates were set to 4 m.

4.5.2.2 Results

Fig. 4.15 shows how the network connectivity of child robot $\mathcal{R}_{c_1}$ varies throughout the experimental time period. It can be seen that the degrees of observation (DOO)[3] of child robot $\mathcal{R}_{c_1}$ with respect to either leader robot vary from zero to three. The zero degree observations (shaded regions in Fig. 4.15) are related to the time period where child robot $\mathcal{R}_{c_1}$ is a member of group $\mathcal{G}_{l_i,4}$, where $i = \{1, 2\}$. From these results, it is found that $\mathcal{R}_{c_1}$ has a zero degree observation with respect to both the leader robots during the time intervals $118.5s - 188.2s$, $701.2s - 709.9s$, and $1415.2s - 1457.3s$.

---

[3]For a given hierarchical-IRMCG, number of edges between the leader robot node (root-node) to a child robot node is termed as the degree of observation of the child robot with respect to the leader robot.
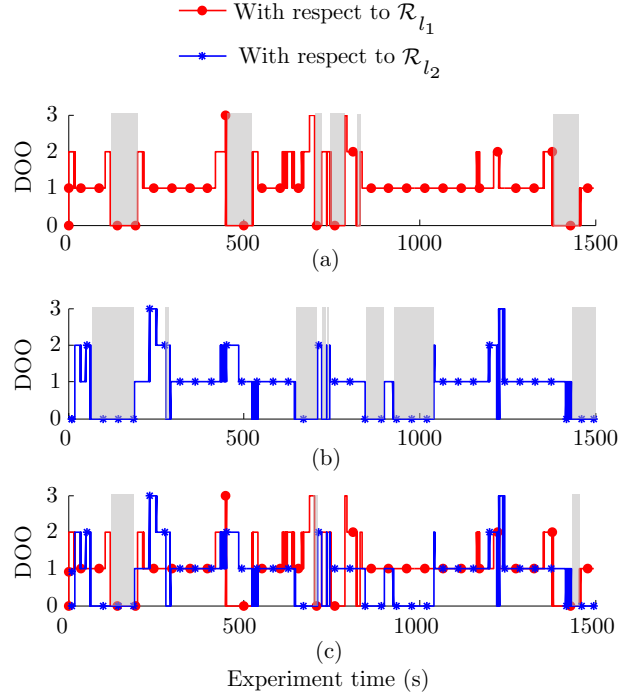
Figure 4.15: Order of network connectivity for child robot $\mathcal{R}_{c_1}$. Zero DOO implies that the robot is disconnected from the network, first order observation implies that the child robot is within the corresponding leader robot's sensing and communication boundaries. The higher order observations represent that the child robot is beyond the sensing and communication range of the corresponding leader but a member of the network with second or third order connectivity

During these time intervals, the child robot may not operate within the sensing and communication range of any teammates, or leader robots are disconnected from the sensing and communication network. As a result, $\mathcal{R}_{c_1}$ did not receive a global pose measurement from any of the leaders during these time windows and solely depended on its ego-motion sensor reading for localization.

Fig. 4.16 and Fig. 4.17 show the mean estimation error and the associated 3σ error boundaries for child robot $\mathcal{R}_{c_1}$. The former is related to the instantaneous communication mode and the latter is associated with the delayed communication mode. For both the communication modes, mean estimation error always stayed inside the associated 3σ error boundaries. This implies that the proposed leader-assisted

localization method is capable of establishing non-overconfident state estimations for child robots, i.e. the $3 - \sigma$ value of the estimated uncertainty always larger than the estimation error. During the time windows where no global pose measurements were received, the mean estimation error was gradually increased as the robot's localization solely depended on its odometry measurement. However, a rapid convergence was achieved soon after reconnection with the measurement network.

4.5.3   Memory Optimization

To evaluate the performance of the memory optimization approach that incorporates the proposed time delayed sensor fusion architecture, a simulation study was performed on an MRS with 15 robots. Two of the teammates were considered leader robots while the rest of the team was considered child robots. Each robot navigation was set so that the formation shown in the Fig. 4.18 was always maintained.

Table 4.3 summarizes the results of the memory optimization study. It was assumed that each member knows the number of leader robots and child robots in the MRS. At an inter robot observation event, each robot acquires global pose measurements for neighbours. Based on the number of unique relative pose measurements, each child robot becomes aware of how many neighbours it has. It can be seen that $\mathcal{R}_{c_{13}}$ has no neighbours. This implies that $\mathcal{R}_{c_{13}}$ is a member of group $\mathcal{G}_{l_i,4}$, where $i = \{1, 2\}$, with respect to each leader robot. When a given child robot has no neighbours then the information cannot be propagated from leader robots to that particular robot. Hence, there is no necessity of maintaining the history of measurements. Child robot $\mathcal{R}_{c_7}$ and $\mathcal{R}_{c_{11}}$ have one neighbour. Accordingly, these robots can be edge robots for the global IRMCG. For a given inter robot observation event, edge robots can receive only one global pose measurement (**Lemma 4.3.1**). Therefore, soon after these robots receive the first global pose measurement for the current measurement event, they can apply
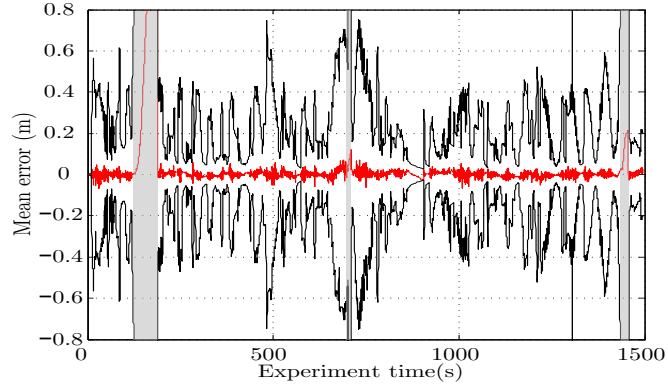
(a) x-position
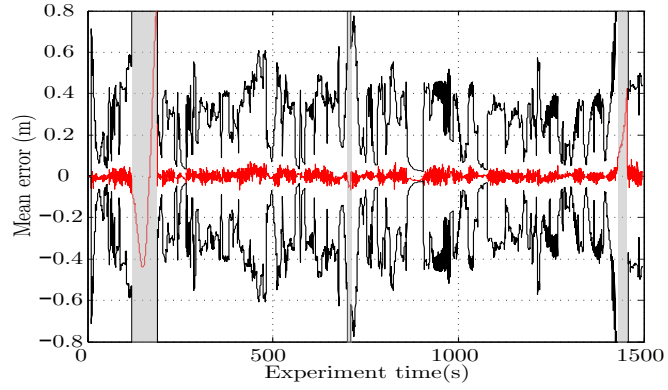
(b) y-position
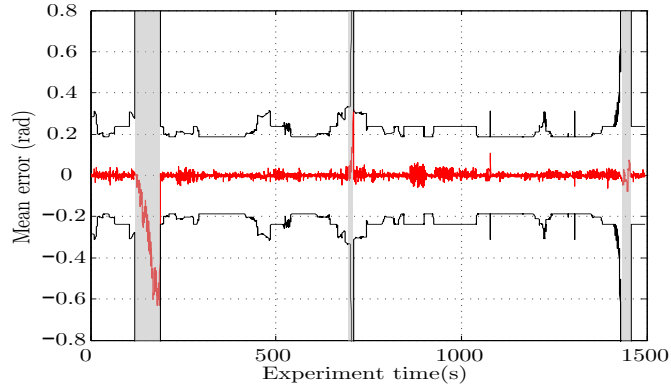
(c) ϕ-orientation

Figure 4.16: Mean estimation error of child robot $\bar{\mathcal{R}}_{c_1}$ with the instantaneous communication mode. Red solid line indicates mean estimation error while the black solid lines indicate double-sided 3-σ error boundaries. Shaded regions represent time windows with no measurement updates
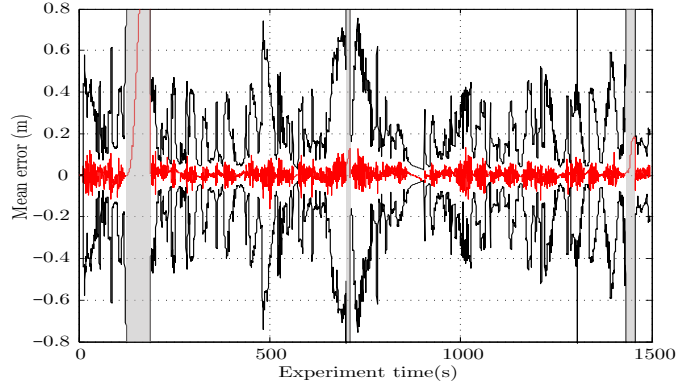
(a) x-position
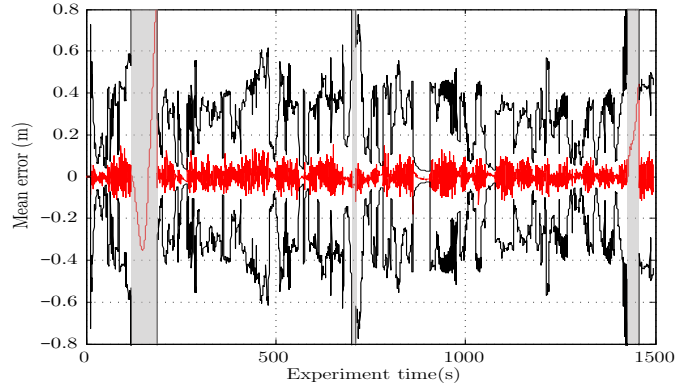
(b) y-position
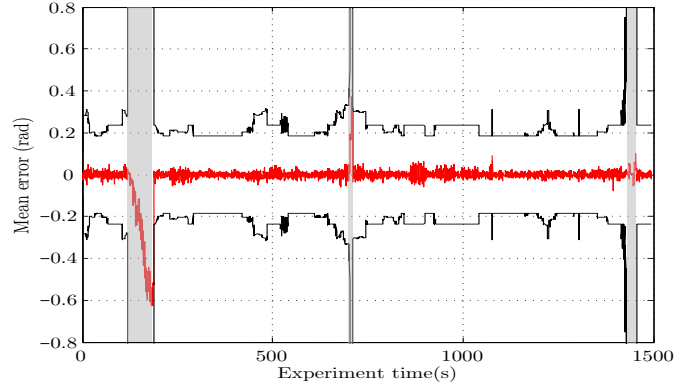
(c) ϕ-orientation

Figure 4.17: Mean estimation error of child robot $\bar{\mathcal{R}}_{c_1}$ with the time-delayed communication mode. Red solid line indicates mean estimation error while the black solid lines indicate double-sided 3-σ error boundaries. Shaded regions represent time windows with no measurement updates

109
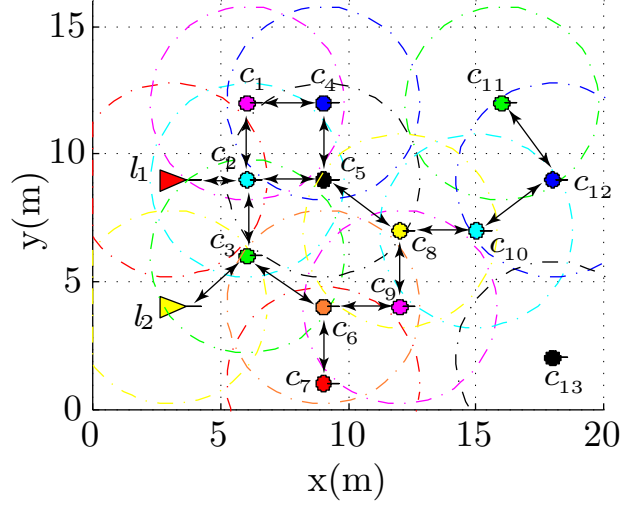
Figure 4.18: Sample robot formation for memory optimization study

the Markov property and clear the history. $\mathcal{R}_{c_7}$ has the third DOO with respect to $\mathcal{R}_{l_2}$; thus, this child robot receives global pose measurement from leader $\mathcal{R}_{l_2}$ and applies the Markov property three time steps after the inter robot observation event. $\mathcal{R}_{c_{11}}$ has the sixth DOO with respect to $\mathcal{R}_{l_1}$; thus, this child robot receives a global pose measurement from leader $\mathcal{R}_{l_1}$ and applies the Markov property six time steps after the inter robot observation event. Child robots $\mathcal{R}_{c_i}$, where $i = \{1, 2, 3, 4, 5, 6, 8, 9, 11, 12\}$, have two or more neighbours. The team has two leader robots. Therefore, the maximum number of global pose measurements that these robots may receive is equal to two (**Lemma 4.3.3**). Simulation results illustrated that child robots $\mathcal{R}_{c_j}$, where $j = \{1, 2, 3, 4, 5, 6, 8, 9\}$, received two measurements while $\mathcal{R}_{c_{10}}$ and $\mathcal{R}_{c_{12}}$ received only one global pose measurement. When the number of received measurements is equal to the expected maximum number of measurements, the Markov property applies at n_1 time steps delayed; where $n_1 = max(DOO\ from\ \mathcal{R}_{l_i})$, $\forall l_i \in \mathcal{L}$. Note that this delay is less than the expected maximum delay. When the number of received measurements is fewer than the expected maximum number of measurements, the Markov property applies at n_2 time steps delayed; where n_2 equals *Expected maximum delay*.

4.6 Summary

This chapter presented an innovative multi-robot localization framework addressing the finite-range sensing and communication problems of leader-assisted localization. This framework consists of (1) a method to virtually enhance the leader robots' sensing and communication ranges allowing child robots to navigate beyond the sensing and communication range of leader robots while maintaining bounded error and uncertainty, (2) a novel distributed graph search algorithm to effectively avoid the double counting problem, (3) a state estimation algorithm to enable the time-delayed measurement update for child robots, and (4) a memory optimization algorithm to detect the best time for applying the Markov property. The performance of the proposed framework is evaluated on the series of numerical simulations and on a publicly available multi-robot localization and mapping data-set. The results confirm that the proposed distributed leader-assisted localization framework is capable of establishing consistent localization for the child robots with bounded uncertainty even when they operate beyond the sensing and communication range of the leader robots.

Table 4.3: Results of the memory optimization study

	Description	$\mathcal{R}_{c_1}$	$\mathcal{R}_{c_2}$	$\mathcal{R}_{c_3}$	$\mathcal{R}_{c_4}$	$\mathcal{R}_{c_5}$	$\mathcal{R}_{c_6}$	$\mathcal{R}_{c_7}$	$\mathcal{R}_{c_8}$	$\mathcal{R}_{c_9}$	$\mathcal{R}_{c_{10}}$	$\mathcal{R}_{c_{11}}$	$\mathcal{R}_{c_{12}}$	$\mathcal{R}_{c_{13}}$
Extracted data from measurements and theories	Number of neighbours	2	4	3	2	3	3	1	3	3	2	1	2	0
	Number of child neighbours	2	3	2	2	3	3	1	3	3	2	1	2	0
	Edge-robot	✗	✗	✗	✗	✗	✗	✓	✗	✗	✗	✓	✗	✗
	Expected maximum delay (sample time steps)	11	10	11	11	10	10	12	10	11	11	12	11	0
	Expected maximum global pose measurements	2	2	2	2	2	2	1	2	2	2	1	2	0
Results	Number of global pose measurements received	2	2	2	2	2	2	1	2	2	1	1	1	0
	Memory cleared after (time steps)	7	2	2	6	5	5	3	4	4	11	6	11	0
	DOO from $\mathcal{R}_{l_1}$	2	1	2	3	2	5	0	3	4	4	6	5	0
	DOO from $\mathcal{R}_{l_2}$	7	2	1	6	5	2	3	4	3	0	0	0	0

Chapter 5

Distributed Leader-Assisted Localization with Relative Range and Bearing Measurements

The distributed leader-assisted localization scheme developed in the previous chapters assumed the availability of an IRRM system which is capable of measuring the relative pose of neighbouring robots. However, range and bearing between a pair of robots is the widely available relative sensory system for the MRS. Therefore, it is important to relax the assumption on the IRRM sensor so that the proposed leader-assisted localization scheme can be implemented using inter-robot range and bearing measurements. To this end, this chapter[1] develops a hierarchical filtering approach where each robot runs local tracking filters to estimate the relative pose of neighbours

---

[1]The work in this chapter was presented at International Conference on Advanced Robotics and Journal of Intelligent & Robotic Systems

* T. R. Wanasinghe, G. K. I. Mann and R. G. Gosine, "Pseudo-linear measurement approach for heterogeneous multi-robot relative localization", in International Conference on Advanced Robotics (ICAR), 2013.

* T. R. Wanasinghe, G. K. I. Mann and R. G. Gosine, "Relative localization approach for combined aerial and ground robotic system", Journal of Intelligent & Robotic Systems, 2016, vol. 77, no. 1, pp. 113-133, Jan 2015.

using a general range and bearing measurement based relative observation system. The updated localization and control architecture of a leader and a child implementing a hierarchical leader-assisted localization based heterogeneous MRS is illustrated in Figure 5.1. Note that the updated localization and control architecture has a new module named "Tracking filter" inserted between the "IRRM sensor" and "Leader-assisted localization module".
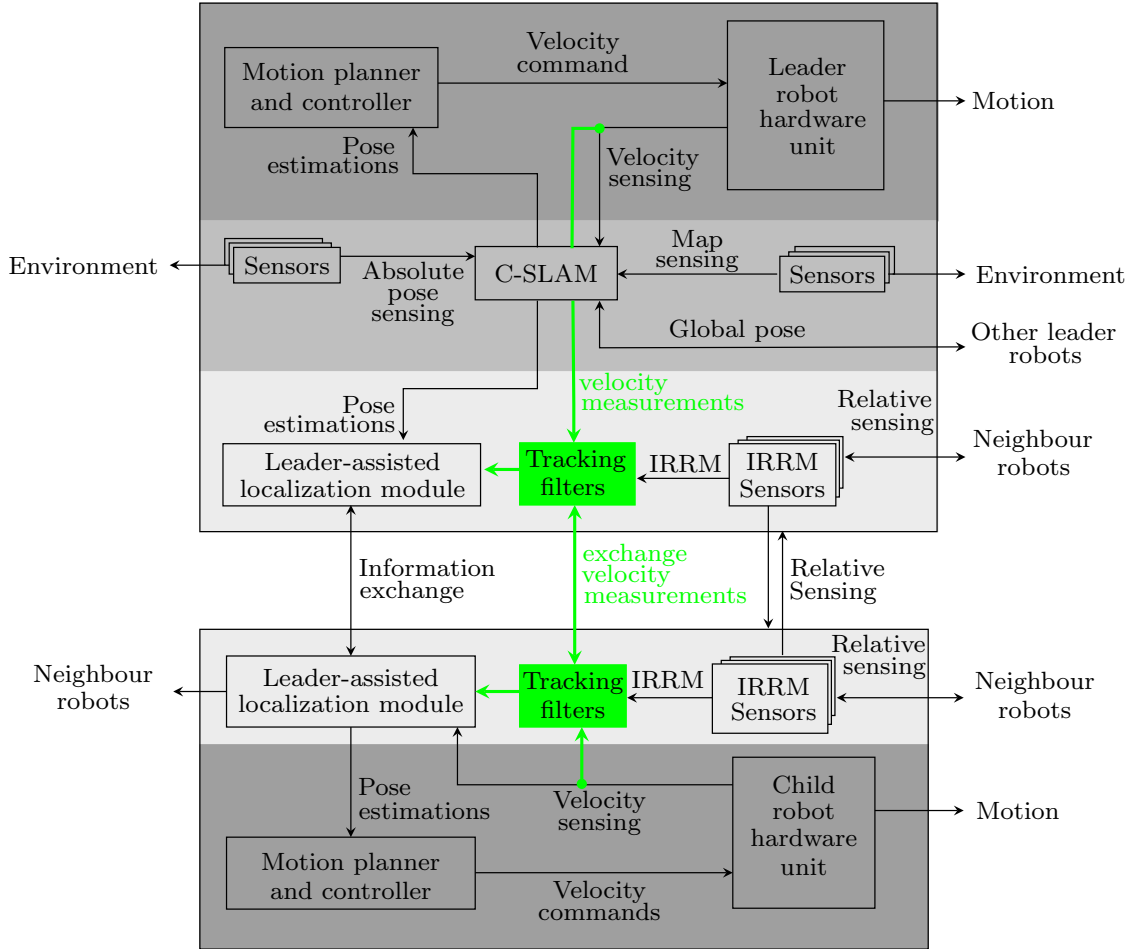
Figure 5.1: The localization and control architecture of the proposed heterogeneous MRS with range and bearing measuring system

The extended Kalman filter (EKF) has been the widely applied sub-optimal nonlinear estimator for implementing tracking filters [9, 67, 120]. The poor initialization of EKF

generally causes instability [9], leading to failure in the gating validation, and causing singularity in the innovation covariances. Additionally, unknown initialization causes a wider settling time[2] for estimating relative pose of neighbours. These limitations may result in erroneous interpretation of one robot's observation in another robot's body-fixed coordinate frame. This erroneous interpretation can lead to unpredictable behaviour and failure in collaborative missions. In order to overcome these issues, in the majority of past work, it is either assumed that there is a known transformation between any two robots at the initial encounter [121], or it is assumed that reliable range and bearing measurements are present in order to realize accurate initial transformation between robots. In this chapter, a pseudo-linear measurement-based relative localization scheme is proposed, which can be initialized with an arbitrary initial pose and which demonstrates faster convergence than the traditional EKF-based relative localization schemes.

5.1 Problem Formulation

Relative localization approaches are widely used in a heterogeneous MRS with both aerial and ground robots [9, 122]. Although this thesis mainly focuses on an MRS of ground robots, for the relative localization problem, MRSs with both aerial and ground robots was considered, so that the research outcomes of this chapter can be directly exploited for general relative localization applications. Consider a heterogeneous MRS with both aerial and ground robots. It is assumed that the ground robots navigate on flat surfaces and that the aerial robots obey the hovering conditions. A hovering condition is a valid assumption for MAVs as they possess a sufficiently accurate low-level controller loop to stabilize the pitch and roll angles during low velocity

---

[2]Time taken to reach acceptable error level is termed settling time.

maneuvers [9]. Each member of the team is capable of measuring its linear and angular velocities and measuring range and bearing to its neighbours. These measurements are exploited to detect and track neighbours' relative poses.

5.1.1 Relative State Propagation Model

A robot navigating in three-dimensional space is generally described in a 6-DOF kinematic model [123]. However, when ground robots navigate on a flat surface and aerial robots obey hovering conditions, the standard 6-DOF kinematic model can be simplified to a 4-DOF kinematic model which consists of position x, y, z, and orientation[3] ϕ. Then the relative pose of robot $\mathcal{R}_i$ as estimated by robot $\mathcal{R}_j$ is given by $\mathbf{x}_{j,k}^{i,j}$ where $\mathbf{x} = [x \; y \; z \; \phi]^T$. As the general relative localization problem is presented, hereafter, superscripts and subscripts of the relative pose vector will be omitted from the system equation. This will simplify the notation and improve the clarity of the presentation.

The relative state propagation can then be modelled by

$$\dot{\mathbf{x}} = \mathbf{f}(\mathbf{x}, \mathbf{u}_j, \mathbf{u}_i) + \nu_{\mathbf{x}}$$

$$\begin{bmatrix} \dot{x} \\ \dot{y} \\ \dot{z} \\ \dot{\phi} \end{bmatrix} = \begin{bmatrix} u_{x,i} \cos\phi - u_{y,i} \sin\phi - u_{x,j} + y\omega_{z,j} \\ u_{y,i} \cos\phi + u_{x,i} \sin\phi - u_{y,j} - x\omega_{z,j} \\ u_{z,i} - u_{z,j} \\ \omega_{z,i} - \omega_{z,j} \end{bmatrix} + \nu_{\mathbf{x}} \tag{5.1}$$

where $\mathbf{x} \in \mathbb{R}^n$ is the relative state vector; $\mathbf{u}_j \in \mathbb{R}^{nj}$ is the control input vector of the observing robot R_j, i.e. $\mathbf{u}_j = \begin{bmatrix} u_{x,j} & u_{y,j} & u_{z,j} & \omega_{z,j} \end{bmatrix}^T$ where, $u_{x,j}$, $u_{y,j}$, $u_{z,j}$ and $\omega_{z,j}$ represent linear and angular body-fixed velocities of robot R_j; $\mathbf{u}_i \in \mathbb{R}^{ni}$ is the control

---

[3]This is the yaw angle of the robot as the pitch and roll angles are assumed to be fixed for low velocity maneuvers

input vector of the observed robot R_i, i.e. $\mathbf{u}_i = \begin{bmatrix} u_{x,i} & u_{y,i} & u_{z,i} & \omega_{z,i} \end{bmatrix}^T$ where $u_{x,i}$, $u_{y,i}$, $u_{z,i}$ and $\omega_{z,i}$ represent linear and angular body-fixed velocities of an observed robot R_i; and $\nu_{\mathbf{x}}$ is a zero mean, additive white Gaussian noise term that accounts unmodelled system dynamics and system modeling inaccuracies. For the modified relative state propagation model, dimensional variables n, nj and ni are equal to four (i.e. $n = nj = ni = 4$).

5.1.2   Inter-Robot Observation Model

Each robot in the MRS is equipped with an exteroceptive sensory system to measure 3D ranging and bearing for the neighbours. It is assumed that the local coordinate frame of this sensor coincides with the robot's body-fixed coordinate frame. The inter-robot observation model is then given by

$$\mathbf{y}_{pco} = \mathbf{g}(\mathbf{x}) + \nu_{pco}$$

$$\begin{bmatrix} r \\ \theta \\ \alpha \end{bmatrix} = \begin{bmatrix} \sqrt{x^2 + y^2 + z^2} \\ \arctan\left(\dfrac{y}{x}\right) \\ \arctan\left(\dfrac{z}{\sqrt{x^2 + y^2}}\right) \end{bmatrix} + \begin{bmatrix} \nu_r \\ \nu_\theta \\ \nu_\alpha \end{bmatrix} \tag{5.2}$$

where r, θ and α are relative range, relative azimuth angle, and relative elevation angle, respectively. x, y and z are relative positions of an observed robot. Parameters ν_r, ν_θ and ν_α are zero mean, additive white Gaussian noise terms for measurements and are defined as follows:

$$\nu_r \sim \mathcal{N}(0, \sigma_r^2) \qquad \nu_\theta \sim \mathcal{N}(0, \sigma_\theta^2) \qquad \nu_\alpha \sim \mathcal{N}(0, \sigma_\alpha^2).$$

Traditional EKF approaches directly linearize this nonlinear measurements model,

and the linearized measurement model are then applied for sensor fusion. Explicit linearization of measurement introduces a bias problem and loss of information [124,125]. To overcome these issues, in this study, nonlinear observations are algebraically transformed and a new series of relative measurements, called pseudo-linear measurements [126], is constructed. The inter-robot observation model is then given by

$$\mathbf{y}_{pmo} = \bar{\mathbf{g}}(\mathbf{x}) = \mathbf{H}_{pmo}\mathbf{x} + \nu_{pm}(\mathbf{x}, \nu_{\mathbf{x}})$$

$$\begin{bmatrix} y_1 \\ y_2 \\ y_3 \end{bmatrix} \triangleq \begin{bmatrix} r \\ 0 \\ 0 \end{bmatrix} = \begin{bmatrix} c\theta c\alpha & s\theta c\alpha & s\alpha & 0 \\ -s\theta & c\theta & 0 & 0 \\ -c\theta s\alpha & -s\theta s\alpha & c\alpha & 0 \end{bmatrix} \mathbf{x} + \nu_{pm}(\mathbf{x}, \nu_{\mathbf{x}}) \tag{5.3}$$

where $c\theta = \cos\theta$, $c\alpha = \cos\alpha$, $s\theta = \sin\theta$, $s\alpha = \sin\alpha$. Note that the first pseudo-linear measurement y_1, is equivalent to the noisy relative range measurement r while the second and the third pseudo-linear measurements y_2 and y_3 are equivalent to zero. Therefore, $[r\ 0\ 0]^T$ is used as the measured parameters while the corresponding predicted measurement values are obtained from (5.3). The resulting pseudo-linear measurements (y_1, y_2, y_3) are linear with respect to system states. On the other hand, their measurement coefficient matrix, $\mathbf{H}_{pmo}$, becomes a nonlinear function of true measurements (r, θ, α). The noise covariance matrix of the pseudo-linear measurement, i.e. $\mathbf{R}_{pmo}$, can be calculated as follows:

$$\mathbf{R}_{pmo} = \mathbf{J}^T \begin{bmatrix} \sigma_r^2 & 0 & 0 \\ 0 & \sigma_\theta^2 & 0 \\ 0 & 0 & \sigma_\alpha^2 \end{bmatrix} \mathbf{J} \tag{5.4}$$

$\mathbf{J}$ is the Jacobian of the pseudo-linear measurement in (5.3) with respect to range and bearing measurements, i.e.

$$\mathbf{J} = \left. \frac{\partial(\mathbf{y}_{pmo})}{\partial(r,\theta,\alpha)} \right|_{r=\bar{r}, \ \theta=\bar{\theta}, \ \alpha=\bar{\alpha}} \tag{5.5}$$

where $\bar{r}$, $\bar{\theta}$, and $\bar{\alpha}$ are noisy relative measurements. The state dependent pseudo-linear noise covariance matrix can be simplified to a temporally uncorrelated pseudo-linear measurement noise covariance matrix and is given in (5.6) [127].

$$\mathbf{R}_{pmo} = \begin{bmatrix} \sigma_r^2 & 0 & 0 \\ 0 & (x^2 + y^2)\sigma_\theta^2 & 0 \\ 0 & 0 & (x^2 + y^2 + z^2)\sigma_\alpha^2 \end{bmatrix} \tag{5.6}$$

Note that the true states are not available and estimated states are utilized to calculate the measurement covariance matrix.

5.1.3 Sensor Fusion

The EKF is employed for sensor fusion. The prediction and the correction structures of the EKF are summarized in (5.7) and (5.8), respectively. The proposed pseudo-linear measurements are used at the measurement update step of the sensor fusion instead of nonlinear range and bearing measurements.

Prediction

$$\dot{\hat{\mathbf{x}}}^- = \mathbf{f}(\hat{\mathbf{x}}, \mathbf{u}_l, \mathbf{u}_c)$$

$$\mathbf{F} = \left. \frac{\partial}{\partial \mathbf{x}} \mathbf{f}(\hat{\mathbf{x}}, \mathbf{u}_l, \mathbf{u}_c) \right|_{\mathbf{x}=\hat{\mathbf{x}}} \tag{5.7}$$

$$\mathbf{P}^- = \mathbf{F}\mathbf{P}\mathbf{F}^T + \mathbf{Q}$$

Correction

$$\hat{\mathbf{y}} = \bar{\mathbf{g}}(\hat{\mathbf{x}})$$

$$\mathbf{K} = \mathbf{P}\mathbf{H}_{\mathbf{pmo}}^{\mathbf{T}}(\mathbf{H}_{\mathbf{pmo}}\mathbf{P}\mathbf{H}_{\mathbf{pmo}}^{\mathbf{T}} + \mathbf{R}_{\mathbf{pmo}})^{-1}$$

$$\hat{\mathbf{x}}^{+} = \hat{\mathbf{x}}^{-} + \mathbf{K}(\mathbf{z} - \hat{\mathbf{y}})$$

$$\mathbf{P} = \mathbf{P}^{-} - \mathbf{K}\mathbf{H}_{\mathbf{pmo}}\mathbf{P}^{-}$$

$$(5.8)$$

$\hat{\mathbf{y}}$ represents the predicted pseudo-linear measurements using noisy bearing measurements as given in (5.3). Measurement matrix $\mathbf{H}_{pmo}$ is constructed as shown in (5.3), and the corresponding measurement covariance $\mathbf{R}_{pmo}$ is obtained from (5.6). $\mathbf{z}$ is the noisy pseudo-linear measurement vector and is given by $[r\ 0\ 0]^{T}$; where r is the noisy range measurement.

5.2 Observability Analysis

The conversion of the nonlinear inter-robot relative measurements into a pseudo-linear format may affect the system observability. Hence, it is essential to evaluate the system observability for pseudo-linear relative measurements. Although the inter-robot observation model given in (5.3) is linear with respect to the state variables, the 4-DOF relative motion model given in (5.1) is nonlinear with respect to the state variables. Therefore, the rank of Gramian matrix [128] or the Popov-Belevitch-Hautus test [129] are not applicable for evaluating the system observability as these methods are designed for linear time-invariant systems. Graph-based nonlinear observability analysis has been recently introduced and applied to evaluate the observability of the bearing only cooperative localization [54, 130]. The observability rank condition test based on the Lie derivatives [123, 131–133] is the well established and widely employed method for nonlinear observability analysis. Therefore, this study employs the observability rank condition based on the Lie derivatives to perform the observability analysis of

the proposed pseudo-linear measurement-based relative localization scheme.

5.2.1 Nonlinear Observability

For a nonlinear system, local observability is more sought as global observability is typically difficult to achieve [132]. For a given continuous-time nonlinear system as described in (5.9), the corresponding control affine form can be written as (5.10).

$$\begin{cases} \dot{\mathbf{x}} = \mathbf{f}(\mathbf{x}, \mathbf{u}) \\ \mathbf{y} = \mathbf{h}(\mathbf{x}) \end{cases} \quad (5.9) \qquad \begin{cases} \dot{\mathbf{x}} = \mathbf{f}_\circ(\mathbf{x}) + \sum_{\forall i = 1:q} \mathbf{f}_i(\mathbf{x}) u_i \\ \mathbf{y} = \mathbf{h}(\mathbf{x}) \end{cases} \quad (5.10)$$

where $\mathbf{x} \in \mathbb{R}^n$ is the state vector, $\mathbf{u} = [u_1 \cdots u_q]^T \in \mathbb{R}^q$ is the control input vector, $\mathbf{y} = [y_1 \cdots y_m]^T \in \mathbb{R}^m$ is the measurement vector and $\mathbf{f}_\circ(\mathbf{x})$ characterizes system dynamics at zero input conditions. $\mathbf{f}_i(\mathbf{x})$ characterizes system dynamics for the ith input, i.e. u_i, and can be given as $\mathbf{f}_i(\mathbf{x}) = [f_{i1}(\mathbf{x}) \quad f_{i2}(\mathbf{x}) \quad \cdots \quad f_{in}(\mathbf{x})]^T$. The observability matrix is then defined as the matrix of zero-order through $(n-1)$ order of Lie-derivatives. In other words, a matrix with rows as given in (5.11) is defined as the observability matrix.

$$\mathcal{O} \triangleq \{ \nabla \mathfrak{L}^q_{f_i \cdots f_j} h_p(\mathbf{x}) | i, j = 0, \cdots, q; p = 1, \cdots, m; q \in \mathbb{N} \} \quad (5.11)$$

where $\mathfrak{L}$ represents the Lie-derivative, q represents the order of the Lie-derivative and ∇ represents the gradient operator. The measurement model may consists of m number of measurements. An introduction to the Lie-derivatives can be found in [123, VII-A.]. **Definition 5.2.1** and **Theorem 5.2.1** which are adopted from [133, Th. 3.1] are employed to evaluate the observability of a nonlinear system.

Definition 5.2.1. *A nonlinear system satisfies the* observability rank condition *when the observability matrix defined in* (5.11) *is full rank.*

Theorem 5.2.1. *If a nonlinear system satisfies the observability rank condition then the nonlinear system is locally weakly observable. This is known as the sufficient condition for observability.*

5.2.2 Continuous-Time Relative Motion Model

The control affine form of the continuous-time relative state propagation model given in (5.1) can be written as

$$
\underbrace{\begin{bmatrix} \dot{\mathbf{p}} \\ \dot{\phi} \end{bmatrix}}_{\dot{\mathbf{x}}} = \underbrace{\begin{bmatrix} -\mathbf{I}_3 \\ \mathbf{0}_{1\times3} \end{bmatrix}}_{f_1} \mathbf{v}_j + \underbrace{\begin{bmatrix} \mathbf{C} \\ \mathbf{0}_{1\times3} \end{bmatrix}}_{f_2} \mathbf{v}_i + \underbrace{\begin{bmatrix} \lfloor \mathbf{p} \times [0\ 0\ 1]^T \rfloor \\ -1 \end{bmatrix}}_{f_3} \omega_{z,j}
$$
$$
+ \underbrace{\begin{bmatrix} \mathbf{0}_{3\times1} \\ 1 \end{bmatrix}}_{f_4} \omega_{z,i} \tag{5.12}
$$

where $\mathbf{I}_3$ is the 3×3 identity matrix, $\mathbf{C}$ is the rotational matrix around z-axis which is given in (5.13), $\mathbf{p}$ is the relative position vector, and $\mathbf{v}_j$ and $\mathbf{v}_i$ are the body-fixed linear velocities of the observing robot and observed robot, respectively, and $\omega_{z,j}$ and $\omega_{z,i}$ are the body-fixed yaw rates of the observing and observed robot, respectively.

$$
\mathbf{C} = \begin{bmatrix} \cos(\phi) & -\sin(\phi) & 0 \\ \sin(\phi) & \cos(\phi) & 0 \\ 0 & 0 & 1 \end{bmatrix} \tag{5.13}
$$

5.2.3 Observability of the Proposed Relative Localization Scheme

When an exteroceptive sensory system is capable of measuring the 3D range and bearing for an observed robot, then the corresponding pseudo-linear measurement

model is illustrated in (5.3). The pseudo-linear relative measurement function, $\mathbf{h}(\mathbf{x})$, can then be expressed as below:

$$\mathbf{h}(\mathbf{x}) = \begin{bmatrix} xc(\theta)c(\alpha) + ys(\theta)c(\alpha) + zs(\alpha) \\ -xs(\theta) + yc(\theta) \\ -xc(\theta)s(\alpha) - ys(\theta)s(\alpha) + zc(\alpha) \end{bmatrix} \tag{5.14}$$

- Zero-order Lie derivatives ($\mathfrak{L}°\mathbf{h}$)

  The function itself becomes the zero-order Lie derivative of a function [123].

$$\mathfrak{L}°\mathbf{h} = \mathbf{h}(\mathbf{x}) \tag{5.15}$$

  The gradient of the (5.15) is as follows:

$$\nabla\mathfrak{L}°\mathbf{h} = \begin{bmatrix} c(\theta)c(\alpha) & s(\theta)s(\alpha) & s(\alpha) & 0 \\ -s(\theta) & c(\theta) & 0 & 0 \\ -c(\theta)s(\alpha) & -s(\theta)s(\alpha) & c(\alpha) & 0 \end{bmatrix} = \begin{bmatrix} \mathbf{h}_{pmo} & 0_{3\times1} \end{bmatrix} \tag{5.16}$$

- First-order Lie derivatives ($\mathfrak{L}_{\mathbf{f}_2}^1\mathbf{h}$)

$$\begin{aligned} \mathfrak{L}_{\mathbf{f}_2}^1\mathbf{h} &= \nabla\mathfrak{L}°\mathbf{y}.f_2 \\ &= \begin{bmatrix} \mathbf{h}_{pmo} & 0_{3\times1} \end{bmatrix} \cdot \begin{bmatrix} \mathbf{C} \\ 0_{1\times3} \end{bmatrix} = \mathbf{h}_{pmo}.\mathbf{C} \end{aligned} \tag{5.17}$$

This contains only relative orientation components. Hence, take the gradient of $\mathfrak{L}_{\mathbf{f}_2}^1\mathbf{h}$ with respect to ϕ. Note that columns of (5.17) are stacked to form a 9×1 vector prior to computing the gradient of $\mathfrak{L}_{\mathbf{f}_2}^1\mathbf{h}$ with respect to ϕ.

123

$$\nabla_\phi \mathfrak{L}_{\mathbf{f_2}}^1 \mathbf{h} = \begin{bmatrix} c(\phi)s(\alpha)s(\theta) - s(\phi)c(\alpha)c(\theta) \\ c(\phi)c(\theta) + s(\phi)s(\theta) \\ s(\phi)s(\alpha)c(\theta) - c(\phi)s(\alpha)s(\theta) \\ -c(\phi)c(\alpha)c(\theta) - s(\phi)s(\alpha)s(\theta) \\ c(\phi)s(\theta) - s(\phi)c(\theta) \\ c(\phi)s(\alpha)c(\theta) + s(\phi)s(\alpha)s(\theta) \\ 0 \\ 0 \\ 0 \end{bmatrix} \tag{5.18}$$

Lemma 5.2.1. *: Given the 3D range and bearing measurements, a sufficient condition for the system given in* (5.12) *and* (5.14) *to be locally weakly observable is* $\mathbf{v}_i \neq 0$

Proof. : Given the 3D range and bearing measurements, the observability matrix for the system expressed in (5.12) and (5.14) can be constructed using (5.16) and (5.18) and is given as follows:

$$\mathcal{O}_1 = \begin{bmatrix} \nabla \mathfrak{L}^\circ \mathbf{h} \\ \nabla \mathfrak{L}_{\mathbf{f_2}}^1 \mathbf{h} \end{bmatrix} = \begin{bmatrix} \mathbf{h}_{pmo} & 0_{3\times 1} \\ 0_{9\times 3} & \nabla_\phi \mathfrak{L}_{\mathbf{f_2}}^1 \mathbf{h} \end{bmatrix} \tag{5.19}$$

It is sufficient to show that the $\mathbf{h}_{pmo}$ and $\nabla_\phi \mathfrak{L}_{\mathbf{f_2}}^1 \mathbf{h}$ are full rank in order to prove that the $\mathcal{O}_1$ retains full column rank condition.

$$\begin{aligned} \det(\mathbf{h}_{pmo}) &= c(\alpha)^2 c(\theta)^2 + c(\alpha)s(\alpha)s(\theta)^2 \\ &\quad + s(\alpha)^2 c(\theta)^2 + s(\alpha)^2 s(\theta^2) \neq 0 \end{aligned} \tag{5.20}$$

$$\det\left((\nabla_\phi \mathfrak{L}^1_{\mathbf{f}_2}\mathbf{h})^T(\nabla_\phi \mathfrak{L}^1_{\mathbf{f}_2}\mathbf{h})\right) = 2s(\alpha)^2 s(\theta)^2$$
$$-s(\theta)^2 + 2 \neq 0 \qquad (5.21)$$

According to (5.20) and (5.21), $\mathbf{h}_{pmo}$ and $\nabla_\phi \mathfrak{L}^1_{\mathbf{f}_2}\mathbf{h}$ are full rank. Hence, $\mathcal{O}_1$ has full column rank; thus, the observability rank condition is satisfied. Therefore, from Theorem 1, a system is locally weakly observable when $\mathbf{v}_i \neq 0$. In other words, the pseudo-linear measurement based relative localization scheme that is described in (5.12) and (5.14) is locally weakly observable when observed robot's linear velocities are not equal to zero. $\qquad\square$

To preserve the completeness of the observability study, the observability analysis for a bearing only measurement system and range only measurement system are presented in **Appendix B**.

5.3 Evaluation - Relative Localization Scheme

5.3.1 Simulation Results

The performance of the proposed relative localization scheme was evaluated in a series of numerical simulations. This simulation was set up with a single leader robot and four child robots as illustrated in Fig. 5.2. A 10 m $\times$ 20 m $\times$ 3 m 3D arena was selected as the robots' navigation space.

For all simulation schemes, robot modeling inaccuracies and unmodelled internal and external disturbances are encapsulated within the low acceleration variance. The noise variances for relative range and bearing measurements are adapted from [9] and set to 0.007 m and 0.0036 rad, respectively. The frequency of the inter-robot relative
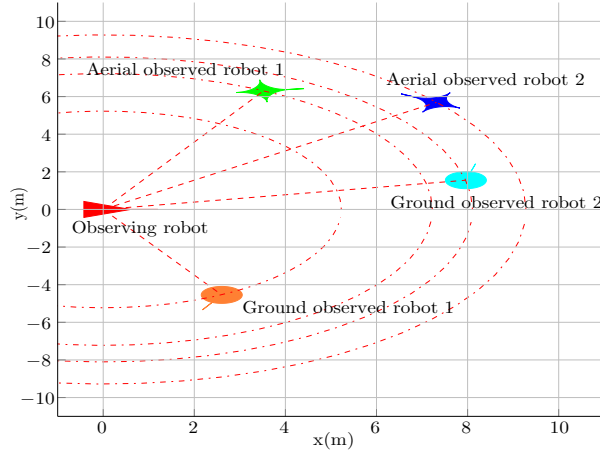
Figure 5.2: Simulation configuration

observations is set to 10 Hz and the kinematic model is set to operate at 100 Hz. Twenty Monte Carlo simulation were performed and the results indicate the average values of all the variables.

The initial simulation configuration assumed a team of mobile robots with the following characteristics: Total number of robots: 5, Number of observing robots: 1, Number of observed robots: 4. This simulation configuration is illustrated in Fig. 5.2. The navigation plane of the observing robot's sensor nodes is considered as the zero elevation level, and navigation planes for the first aerial, the second aerial, the first ground and the second ground observed robots were elevated to 2 m, 1.5 m, -0.1 m, and -0.2 m, respectively. Fig. 5.3 illustrates the estimation errors and 3σ error boundaries for the first aerial observed robot. It can be seen that error is always within the 3σ error boundaries indicating that no overconfident estimation occurs during the estimation process. This observation was identical for all other observed robots. Estimation errors for all four observed robots are depicted in Fig. 5.4 and demonstrate that the proposed relative localization (RL) scheme is capable of performing relative localization with 5~10 cm positional accuracy and 0.075~0.1 rad orientational accuracy.
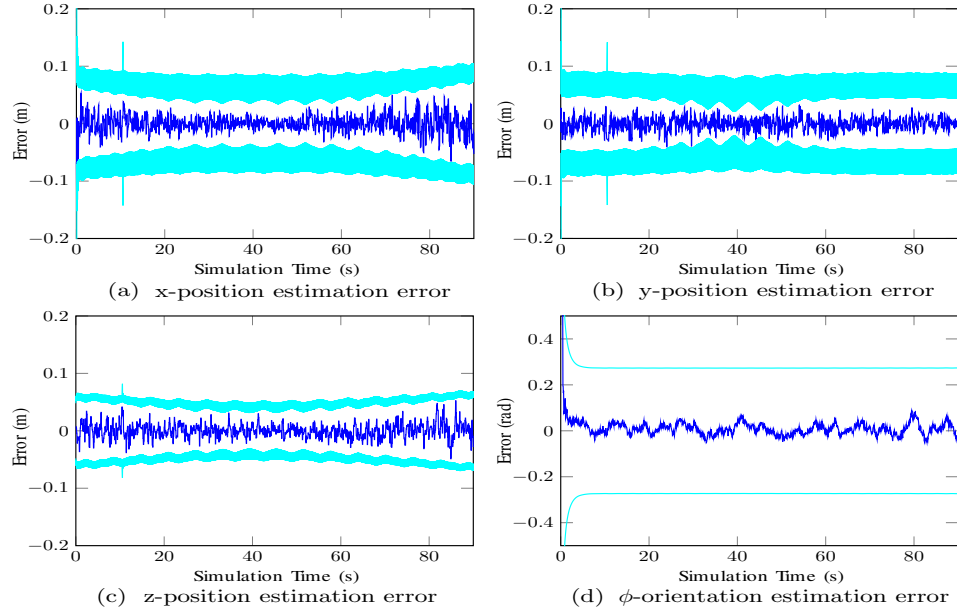
Figure 5.3: Average estimation error of aerial observed robot 1 for 20 Monte Carlo simulations. Blue solid line indicates error while cyan solid lines indicate double-sided 3σ error boundaries
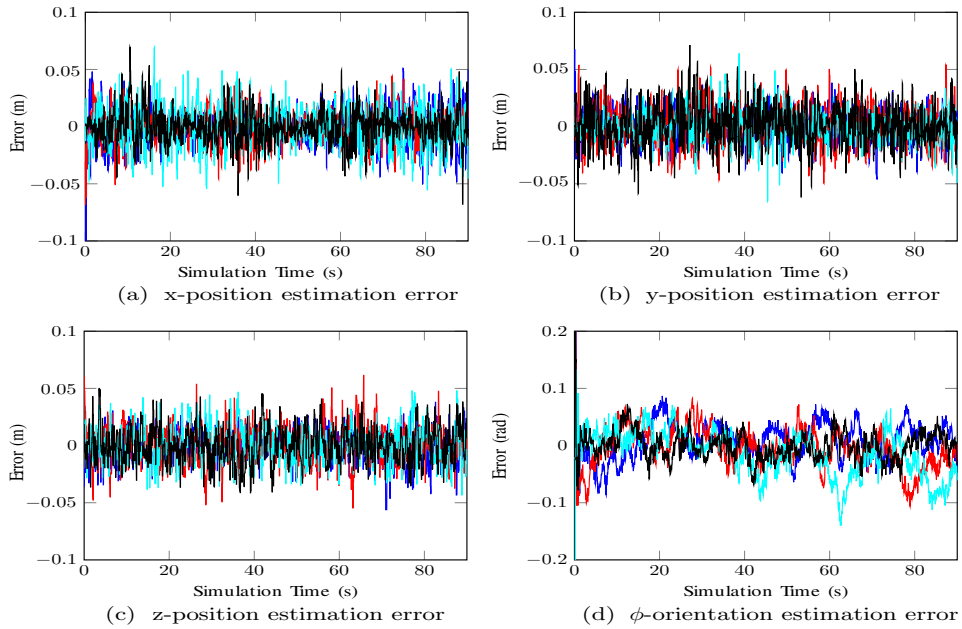
Figure 5.4: Average estimation error of all four observed robots for 20 Monte Carlo simulations. Solid blue line: aerial observed robot 1; solid red line: aerial observed robot 2; solid cyan line: ground observed robot 1; solid black line: ground observed robot 2

127

5.3.1.1 Performance Comparison Against Traditional EKF Approach

The performance of the proposed method over a traditional EKF approach for arbitrary initialization is evaluated in the second simulation setup. This simulation configuration comprises an observing robot and an aerial observed robot. The navigation plane of the observed robot is elevated at 2 m above that of the observing robot's sensor nodes. All the presented results are the average of 20 Monte Carlo simulations. Four main cases are studied:

Case 1: The initial relative pose of the observed robot is accurately known.

Case 2: Only the initial relative position of the observed robot is known and the orientation is completely unknown.

Case 3: The initial relative orientation of the observed robot is known and the initial relative position is set as random.

Case 4: The initial relative pose of the observed robot is completely unknown and set as random. In this case, 13 arbitrary initial poses have been simulated. These 13 arbitrary points are spatially distributed within the observing robot's field of view.

All the cases given above have been compared to the traditional EKF-based RL approach. For case 1, both the proposed method and traditional EKF approach exhibit a similar performance, as shown in Fig. 5.5.

Maximum RMSE for each state estimation when relative localization is performed with a known initial condition (i.e. maximum RMSE of case 1) is increased by 5%, as defined in (5.22), and used as an upper bound for performance evaluation for arbitrary filter initializations.
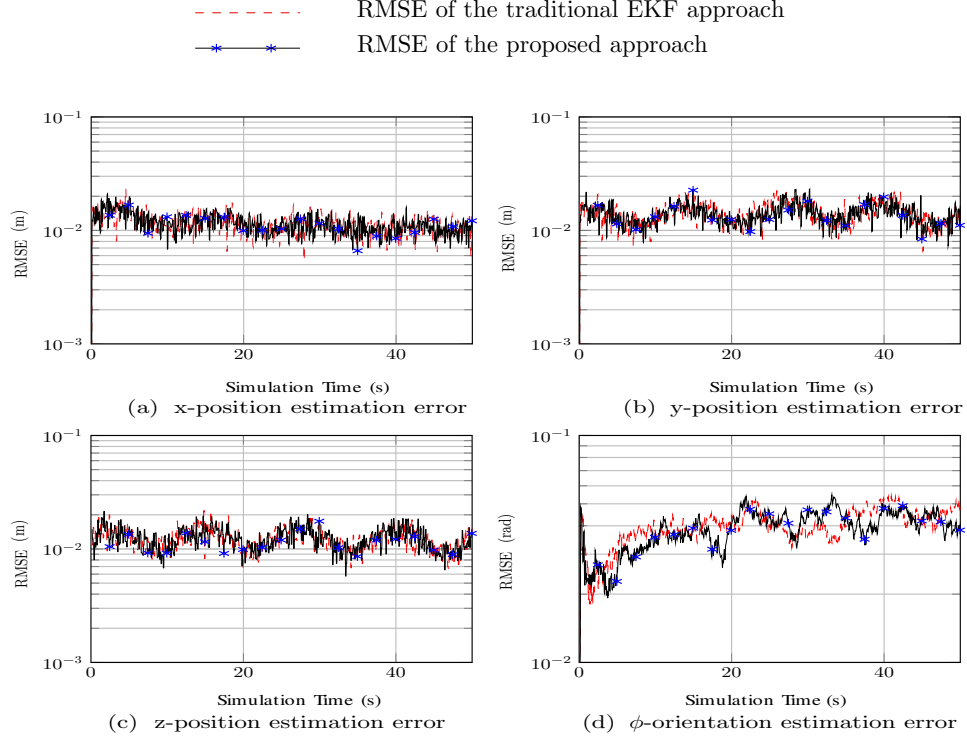
Figure 5.5: RMSE of relative pose measurement for case 1.

Table 5.1: Number of measurement updates required for RL to converge to an acceptable accuracy level for the cases of inaccurate filter initialization

Relative state	Case 2		Case 3		Case 4	
	PLKF	TEKF	PLKF	TEKF	PLKF	TEKF
x-position	1	2	1	34	1	37
y-position	1	1	1	5	1	31
z-position	1	1	1	5	1	6
ϕ-orientation	5	12	4	141	12	263

PLKF: proposed pseudo-linear Kalman filter based approach
TEKF: traditional EKF approach

$$x_{th} \triangleq \max(X_{RMSE_{known\ initial\ pose}}) \times 1.05$$

$$y_{th} \triangleq \max(Y_{RMSE_{known\ initial\ pose}}) \times 1.05$$

$$z_{th} \triangleq \max(Z_{RMSE_{known\ initial\ pose}}) \times 1.05 \tag{5.22}$$

$$\phi_{th} \triangleq \max(\phi_{RMSE_{known\ initial\ pose}}) \times 1.05$$

Fig. 5.6 illustrates sample simulation outcomes for an arbitrary filter initialization that were obtained in case 4. These results confirms that the proposed method has faster convergence capability than the traditional EKF-based approach. A significant improvement has been achieved in relative orientation tracking.

- - - - - - - RMSE of the traditional EKF approach
————*————*———— RMSE of the proposed approach
———————— The upper threshold, as defined in (5.22)

(a) x-position estimation error

(b) y-position estimation error

(c) z-position estimation error

(d) ϕ-orientation estimation error
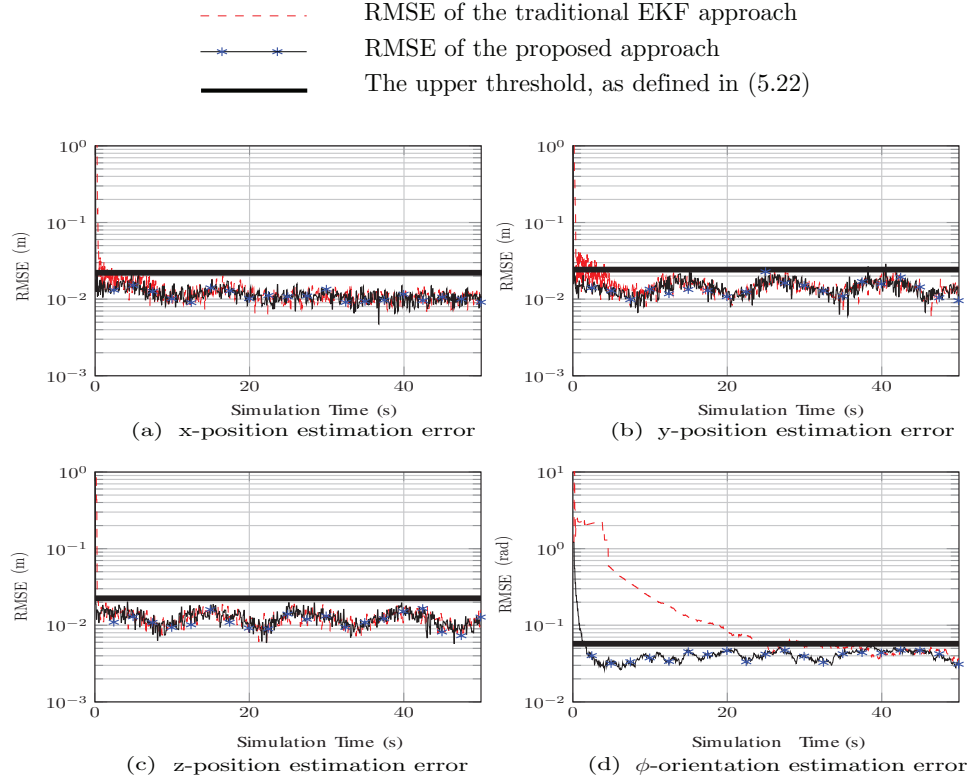
Figure 5.6: Comparison of the proposed method with the traditional EKF approach for arbitrary filter initialization.

Table 5.1 summarizes the number of measurement updates required for state estimation to converge to an acceptable accuracy level when the filter is initialized with an arbitrary pose. Results presented for case 4 are the average result of 13 arbitrary initializations.

These results demonstrate that when the tracking is performed with arbitrary initialization, the proposed method is able to achieve both positional and orientational

accuracy within 12 iterations, whereas the traditional methods require more than 250 iterations to achieve the same accuracy. As a result, settling time of the relative pose estimation is considerably smaller in the proposed method than with the traditional EKF-based approach.

5.3.2 Experimental Results

An experimental validation of the proposed method for an unknown filter initialization was performed using a team of two Pioneer P3AT robots, as shown in Fig. 5.7. One Pioneer robot was treated as an observing robot while the other was treated as an observed robot. Both robots were provided with a map of the environment where the experiment was performed. The robots obtained the range and the bearing for nearby static and dynamic objects using SICK LMS 200 laser scanners. Each robot performed state-of-the-art map-based localization; this localization data served as the ground truth data for the experiment's evaluations.
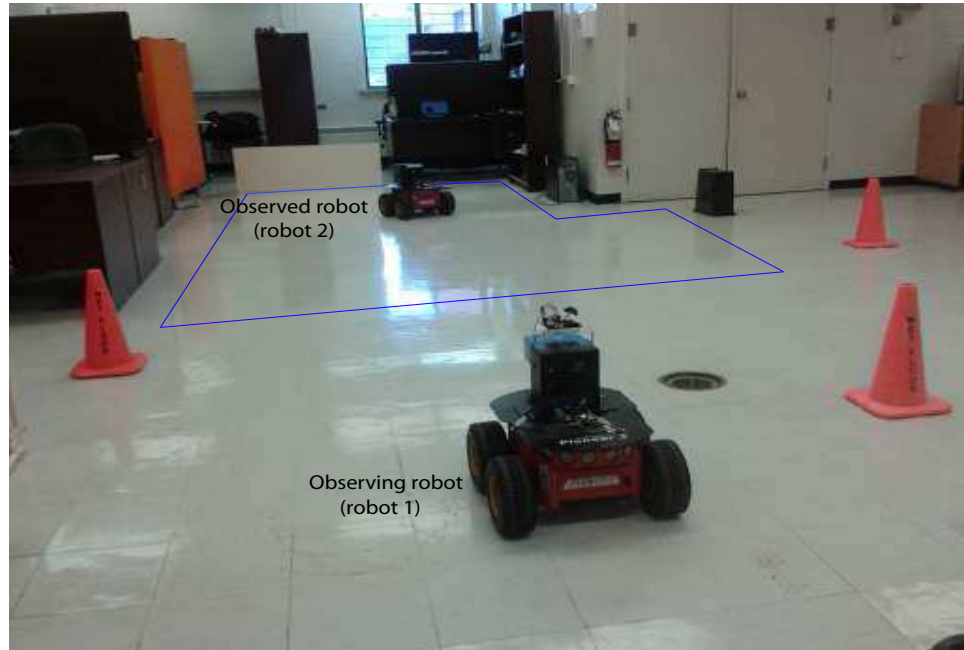
Figure 5.7: Experiment test bed which includes two pioneer P3AT robots
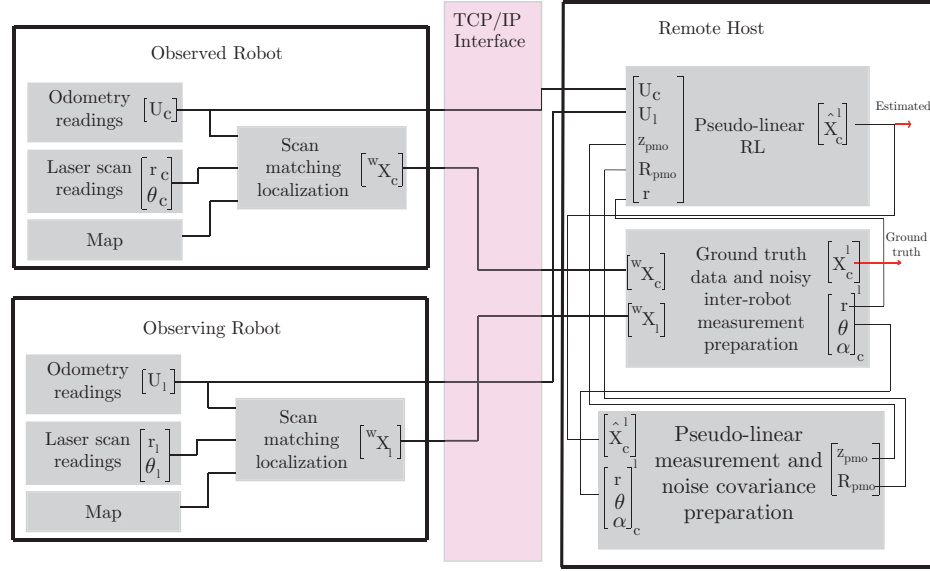
Figure 5.8: System architecture of the experiment setup to validate the proposed RL scheme

5.3.2.1 Inter Robot Relative Measurements

Instead of implementing an exteroceptive sensory system that directly measures range and bearing for neighbouring robots, as presented in [9], the behaviour of an exteroceptive sensory system was simulated by analytically computing the relative range and bearing data from the ground truth data via (5.2), as suggested in [134]. This provided the freedom to select the accuracy level of the exteroceptive sensory data and controlled its update rates. Such flexibility is required in order to evaluate the robustness of the proposed method for changing sensor noise levels and updating rates, as they are the parameters that potentially affect the estimation accuracy [12, 41]. Two measurement noise configurations and two update rates for exteroceptive sensory systems (as given in Table 5.2) were studied.

Table 5.2: Characteristics of exteroceptive sensory systems

Case	Noise levels for exteroceptive sensory system	Measurement update frequencies
Case (1)	σ_r=0.0068m[4], σ_θ=0.0036 rad[5] [9][6]	10 Hz
Case (2)	σ_r=0.1466m, σ_θ=0.1 rad [51]	10 Hz
Case (3)	σ_r=0.0068m, σ_θ=0.0036 rad [9]	1 Hz
Case (4)	σ_r=0.1466m, σ_θ=0.1 rad [51]	1 Hz

5.3.2.2   System Architecture

The system architecture of the experiment setup is illustrated in Fig. 5.8. Each robot acquired its egocentric (odometry) data and laser scan data. Scan matching-based localization is then performed by each robot. These localization data and odometry readings are then transmitted to a host computer through a TCP/IP interface. The ground truth data preparations, noisy relative range and bearing measurement construction, pseudo-linear measurement and corresponding measurement error variance matrix formation and observed robot tracking were performed at the host computer. The estimated relative pose of the observed robot was then compared with the ground truth data. Note that the experiment setup was limited to 2D space; hence it was assumed that the observed robot's navigation plane was two metres above its actual navigation plane.

5.3.2.3   Results

For the noise level and update rate given in Case (1), Fig. 5.9 illustrates the RMSE of the observed robot's pose estimation. It was assumed that the filter was initialized with a completely unknown initial pose. The results are congruent with the simulation

results, showing that the proposed method is capable of establishing the relative pose for the observed robots with 5∼10 cm positional accuracy and 0.075∼0.1 rad orientational accuracy. Additionally, the proposed method demonstrates a fast convergence property even though the filter is arbitrarily initialized.
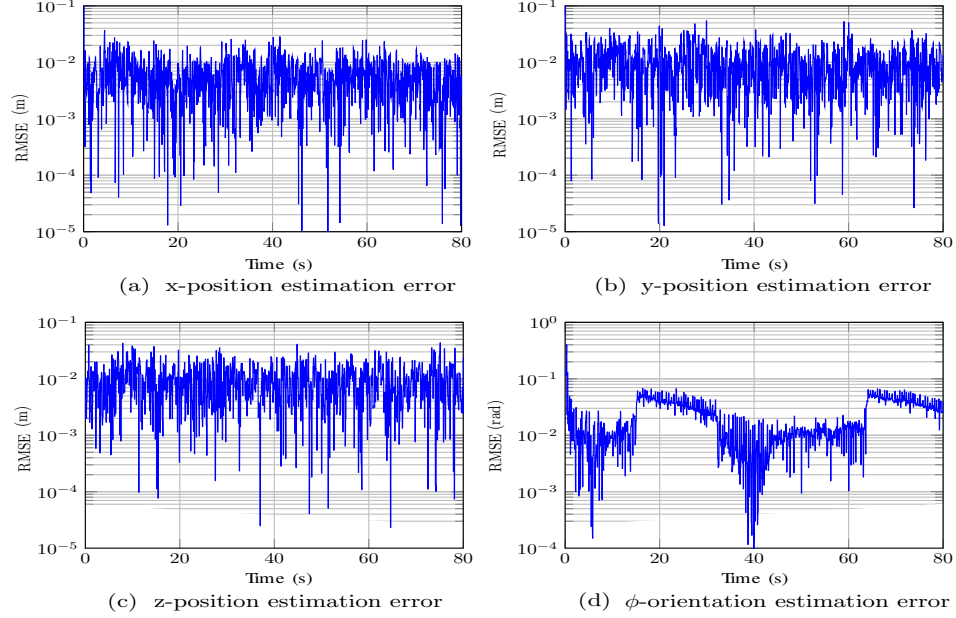
Figure 5.9: Relative localization accuracy of the proposed method for arbitrary filter initialization (Experiment results)

Table 5.3 presents the comparison of the mean of the steady state RMSE and corresponding standard deviations (Std-RMSE) of the proposed relative localization scheme for all four scenarios given in Table 5.2. These results can be summarized as follows:

- The mean of the RMSE and corresponding standard deviations increase with the increase of the uncertainty of the exteroceptive sensory system.

- The mean of the RMSE and corresponding standard deviations increase with the decrease of the update rate of the exteroceptive sensory system.

134

Case	ϕ (rad)	x (m)	y (m)	z (m)
Case (1)	0.0313±0.0341	0.0098±0.0028	0.0131±0.0038	0.0123±0.0032
Case (2)	0.0962±0.0447	0.0925±0.0210	0.1264±0.0304	0.0849±0.0201
Case (3)	0.0443±0.0820	0.0266±0.0227	0.0357±0.0463	0.0135±0.0042
Case (4)	0.1836±0.1431	0.1510±0.0380	0.2246±0.0629	0.1439±0.0353

Table 5.3: Comparison of relative pose estimation error for the observed robot at different IRRM update rates and different noise levels of exteroceptive sensory system

- When an observing robot is equipped with a highly accurate sensory system (e.g. [9]), then the proposed relative localization scheme is capable of establishing relative localization with 0∼8 cm positional accuracy and 0∼0.13 rad orientational accuracy for both 10 Hz and 1 Hz exteroceptive measurement update rates.

- When the exteroceptive sensory system has high measurement uncertainty, then the proposed relative localization scheme is capable of establishing relative localization with 0∼16 cm positional accuracy and 0∼0.15 rad orientational accuracy for the 10 Hz exteroceptive measurement update rate, and with 0∼27 cm positional accuracy and 0∼0.33 rad orientational accuracy for the 1 Hz exteroceptive measurement update rate.

5.3.3   Consistency Analysis

5.3.3.1   Normalized Estimation Error Squared (NEES) Test

To assess the consistency of the proposed RL scheme, the NEES is computed, as given in (3.11). A 95% acceptable region for 4-DOF (x, y, z, ϕ) is upper bounded by $\chi^2_{4,0.95}$, which is equal to 9.4877. Fig. 5.10 presents the NEES test results for Case (1) of Table 5.2.

Table 5.4 summarizes the results obtained from the NEES analysis.
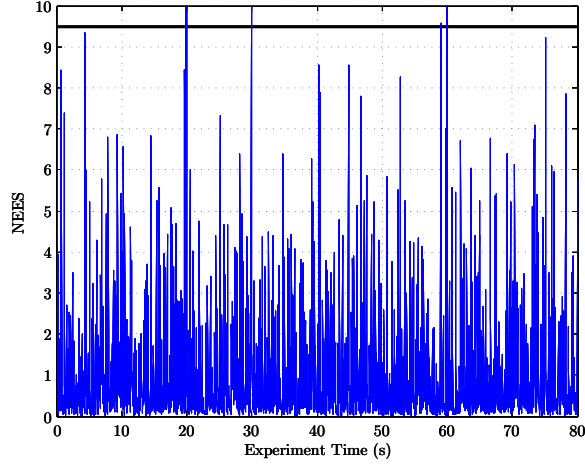
Figure 5.10: NEES values for the proposed method. Horizontal black line indicates the Chi-square upper bound

Case	% of NEES values beyond the upper boundary
Case (1)	0.0625%
Case (2)	2.9375%
Case (3)	4.6875%
Case (4)	9.25%

Table 5.4: Percentage of NEES values beyond the Chi-square upper bound

For the proposed method, fewer than 10% of the values fall outside of the 95% region, as listed in Table. 5.4, which is acceptable [23, 119].

5.3.3.2   Normalized Innovation Squared (NIS) Test

The consistency of predicted measurements compared to actual measurements is evaluated using NIS as defined in (3.13). A 95% acceptable region for 3-DOF (y_1, y_2, y_3 given in (5.3)) is upper bounded by $\chi^2_{3,0.95}$ which is equal to 7.8147. Fig. 5.11 presents the NIS test results for Case (1) of Table 5.2.

It can be seen that all the NIS values are within the acceptable region. This observation was identical for all other scenarios given in Table 5.2. Hence, pseudo-linear

136
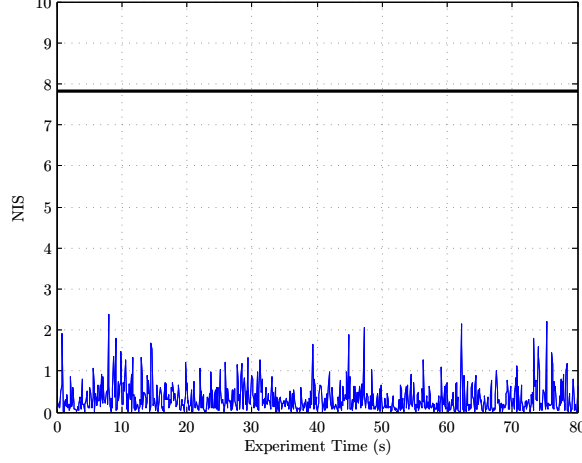
Figure 5.11: NIS values for the proposed method. Horizontal black line indicates the Chi-square upper bound

measurements are consistent.

5.3.3.3 Covariance Conditioning

As measurements are transformed into pseudo-linear format the corresponding measurement covariances become a function of the estimated states (ref. (5.6)). The error covariance $\mathbf{R}$ then becomes time dependent compared to the constant measurement covariance in traditional EKF approaches. This dynamic nature may lead to ill-conditioning of the matrix $\mathbf{R}$; and therefore, for matrix $\mathbf{S}$ and the matrix $\mathbf{P}$. A covariance conditioning test, as proposed in [117], has been performed to evaluate the ill-conditioning nature of each covariance matrix. The condition value $C_{\mathbf{x}}$ for the given matrix is defined as (5.23).

$$C_{\mathbf{x}} = \log_{10}\left(\frac{\lambda_{max}}{\lambda_{min}}\right) \tag{5.23}$$

where λ_{min} and λ_{max} are the minimum and the maximum eigenvalues of corresponding covariance matrices. The upper bound that represents good conditioning is set to 6, as given in [117]. Fig. 5.12 illustrates that the covariance conditioning values for

(a) Case (1)

(b) Case (2)

(c) Case (3)

(d) Case (4)
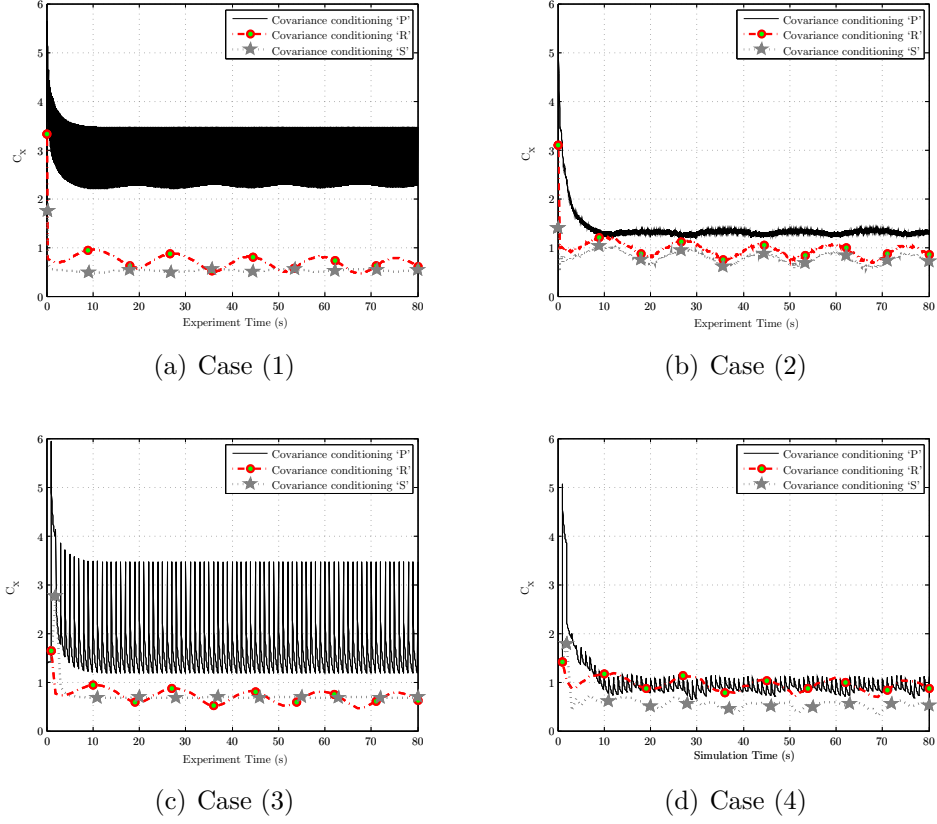
Figure 5.12: Covariance conditioning values for four test scenarios given in Table 5.2

P, **R**, and **S** for all four test scenarios are below the conditioning bound ($C_\mathbf{x} = 6$), indicating that the simplified, zero-mean temporally uncorrelated pseudo-measurement covariance matrix does not lead to ill-conditioning of any of the estimated covariances.

5.4   Evaluation - Leader-Assisted Localization Scheme

5.4.1   Sensor Fusion Algorithms

The localization and control architecture illustrated in Figure 5.1 includes a new module, named "Tracking filter", added to the original localization architecture presented

in Figure 1.2. This modification eventually introduces a set of new processing steps into the sensor fusion algorithms presented in Chapter 4, i.e. **Algorithms 4.3, 4.4,** and **4.5**. To perform relative state propagation as given in (5.1), the observing robot must possess the odometry data of both the observing and the observed robot. This can be achieved by enabling the odometry information exchange between the neighbouring robots. The newly introduced "Tracking filter" performs five main tasks:

1. Acquires relative measurements: Each robot acquires relative range and bearing measurements for neighbours.

2. Initializes tracks: Each robot maintains a single tracking filter for each neighbour. For each new robot appearing within the sensing and communication boundaries of the observing robot, a new track needs to be initialized.

3. Maintains tracks: Acquired relative range and bearing measurements are fused with the local tracks in order to improve the estimation accuracy and reduce the uncertainty of the existing tracks.

4. Deletes tracks: When a neighbour (or a set of neighbours) navigates beyond the sensing and communication boundaries, then maintaining the tracks related to these robots become redundant, because, without the measurements and communication between the pair of robots, the associated tracks diverge.

5. Extracts relative pose of neighbours: In general, tracking filters are initialized with larger error and larger estimation uncertainty. It is important to wait until the tracking uncertainty reduces below a pre-defined threshold level prior to exploiting it for the leader-assisted localization. Each track that has less uncertainty than the pre-defined threshold is considered as a valid relative pose measurement and employed for implementing the proposed leader-assisted localization scheme.

To this end, **Algorithms** 4.3, 4.4, and 4.5 are modified by incorporating above five steps.

5.4.2 Setup

Consider an MRS with single leader robot, $\mathcal{R}_l$ and two child robots, $\mathcal{R}_{c_1}$ and $\mathcal{R}_{c_2}$. Navigation trajectories for two child robots were set so that $\mathcal{R}_{c_1}$ always operated within the sensing and communication boundaries of the leader robot, while $\mathcal{R}_{c_2}$ never appeared within the sensing and communication boundaries of the leader robot. The hierarchical sensor fusion architecture that integrates the pseudo-linear measurement-based tracking filter and the leader-assisted localization filters are then exploited to establish localization for the child robots in the team.

5.4.3 Results

For 20 Monte Carlo simulations, the mean state estimation error and the associated 3σ error boundaries of child robot $\mathcal{R}_{c_2}$ are shown in Figure 5.13. It can be seen that the mean state estimation error of child robot $\mathcal{R}_{c_2}$ is bounded although it operates beyond the sensing and communication boundaries of the leader robot. Additionally, it can be seen that the mean state estimation error is always within the estimated 3σ error boundaries. These two observations imply that the proposed hierarchical sensor fusion framework is capable of establishing accurate localization for child robots using a general range and bearing measurements-based exteroceptive sensory system.

5.5 Summary

This chapter presented a novel sensor fusion architecture addressing the exteroceptive sensor type limitation associated with leader-assisted localization. This framework
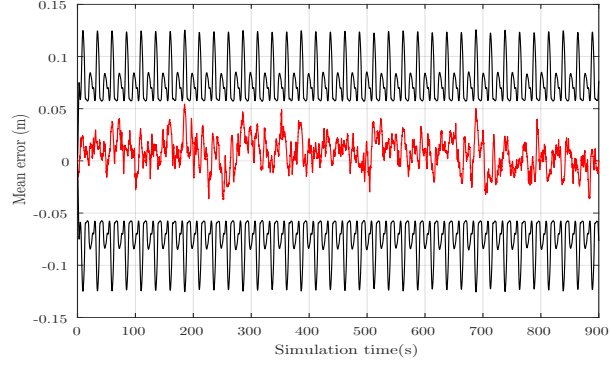
(a) x-position
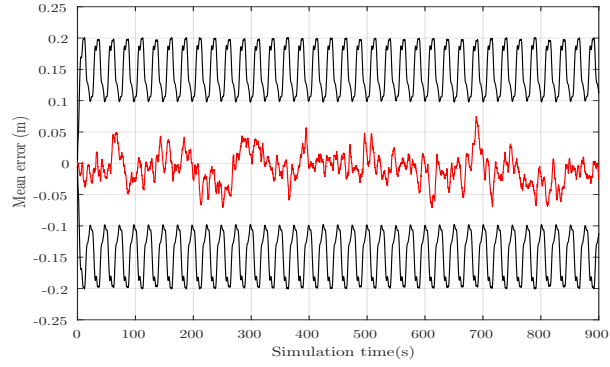
(b) y-position
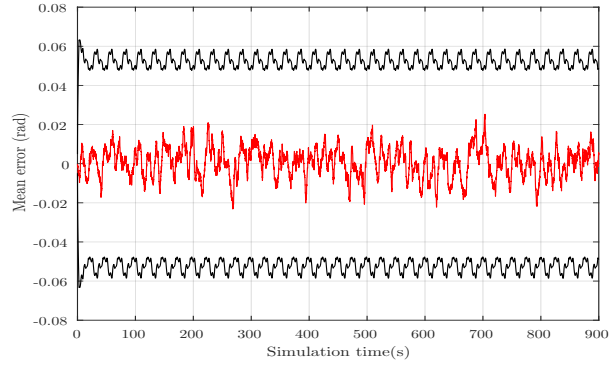
(c) ϕ-orientation

Figure 5.13: Mean estimation error of child robot R_{c_2} for 20 Monte Carlo simulations. Red solid line indicates mean estimation error while the black solid lines indicate double-sided $3 - \sigma$ error boundaries

consists of (1) a fast converging relative localization approach that generates relative pose estimations for neighbouring robots through relative range and bearing measurements between the teammates and (2) a hierarchical sensor fusion architecture that integrates the pseudo-linear measurement-based relative localization scheme with the proposed leader-assisted localization. The proposed pseudo-linear measurement-based relative localization approach is more robust against unknown filter initialization and shows faster convergence for an arbitrary filter initialization than the traditional EKF-based relative localization scheme. The observability analysis confirmed that the state vector of the pseudo-linear measurement-based relative localization scheme is fully observable as long as the observed robots have non-zero linear velocity.

Chapter 6

Decentralized Cooperative Localization for a Heterogeneous MRS

The previous chapters presented a framework for establishing localization for child robots even when they operate beyond the sensing and communication range of the leader robots. If it is possible to ensure that the child robots are **always** connected with a measurement network which has a minimum of one leader robot, then a decentralized cooperative localization approach can be exploited to establish the localization for child robotss in a heterogeneous MRS. The majority of the available decentralized cooperative localization approaches are known to generate inconsistent (overconfident) pose estimations for agents in the team. This chapter[1] presents a scal-

---

[1]The work in this chapter was presented at Canadian Conference on Computer and Robot Vision 2014 and in the Journal of Robotics, Hindawi Publishing Corporation

* T. R. Wanasinghe, G. K. I. Mann and R. G. Gosine, "Decentralized Cooperative Localization for Heterogeneous Multi-robot System Using Split Covariance Intersection Filter", in Canadian Conference on Computer and Robot Vision (CRV), 2014, pp. 167-174.

* T. R. Wanasinghe, G. K. I. Mann and R. G. Gosine, "Decentralized Cooperative Localization Approach for Autonomous Multi-Robot Systems", Journal of Robotics, Hindawi Publishing Corporation, 2016, 18 pages

able decentralized cooperative localization (DCL) approach for heterogeneous MRSs which guarantees a non-overconfident pose estimate with the bounded estimation error. The proposed DCL approach incorporates a split covariance intersection (Split-CI) algorithm proposed by Julier *et al.* [135] to accurately track independencies and interdependencies among teammates' local pose estimates.

6.1 Split Covariance Intersection Algorithm

Consider the pair of state estimates $\{\hat{\mathbf{x}}_j, \mathbf{P}_j\}$, where $j = \{1, 2\}$, $\hat{\mathbf{x}}_j \in \mathbb{R}^n$ represents estimated state vector, $\mathbf{P}_j \in \mathbb{R}^{n \times n}$ is the associate error covariance matrix, and n is the dimension of the state vector, i.e., degrees of freedom of the system model. If these two estimates are consistent and independent, then the general Kalman filter-based information fusion which is given in (6.1) will result in consistent state updates.

$$
\begin{aligned}
\mathbf{P} &= \left(\mathbf{P}_1^{-1} + \mathbf{P}_2^{-1}\right)^{-1} \\
\hat{\mathbf{x}} &= \mathbf{P}\left(\mathbf{P}_1^{-1}\hat{\mathbf{x}}_1 + \mathbf{P}_2^{-1}\hat{\mathbf{x}}_2\right)
\end{aligned}
\tag{6.1}
$$

where $\hat{\mathbf{x}}$ and $\mathbf{P}$ are the resulting state and associate error covariance matrix of the fusion, respectively. However, this traditional Kalman filter-based information fusion tends to generate overconfident state estimations when there exists an unknown correlation between two input state estimates. *Julier et al.*, [136], proposes the CI algorithm in order to fuse two correlated pieces information. The algorithm uses the convex combination of the mean and covariance of the input estimates, as given in (6.2), in order to avoid possible double counting of common information.

$$
\begin{aligned}
\mathbf{P} &= \left[\omega\mathbf{P}_1^{-1} + (1 - \omega)\mathbf{P}_2^{-1}\right]^{-1} \\
\hat{\mathbf{x}} &= \mathbf{P}\left[\omega\mathbf{P}_1^{-1}\hat{\mathbf{x}}_1 + (1 - \omega)\mathbf{P}_2^{-1}\hat{\mathbf{x}}_2\right]
\end{aligned}
\tag{6.2}
$$

where coefficient ω belongs to the interval $[0,1]$, and can be determined such that the trace or determinant of the resulting covariance matrix, i.e. $\mathbf{P}$, is minimized. However, the general CI algorithm neglects possible independencies between local estimates. This may lead to a more conservative state estimation and may produce an estimation error covariance which is larger than that of the best unfused estimate [77]. A Split-CI algorithm is later introduced to address the limitations associated with the general CI algorithm [135] wherein the independent and interdependent parts of the covariance matrix are separately calculated and maintained. A theoretical analysis and the simulation-based validation for the consistency of the split-CI-based information fusion is presented in [137].

Consider the pair of state estimates $\{\hat{\mathbf{x}}_j, \mathbf{P}_{ji} + \mathbf{P}_{jd}\}$, where $j = \{1,2\}$, $\hat{\mathbf{x}}_j \in \mathbb{R}^n$ represents the estimated state vector, and covariance components $\mathbf{P}_{jd} \in \mathbb{R}^{n \times n}$ and $\mathbf{P}_{ji} \in \mathbb{R}^{n \times n}$ represent possible correlated components of two estimations and possible independent components of two estimations, respectively. The posterior state estimation structure (steps) is then given by (6.3).

$$
\begin{aligned}
\mathbf{P}_1 &= \mathbf{P}_{1d}/\omega + \mathbf{P}_{1i} \\
\mathbf{P}_2 &= \mathbf{P}_{2d}/(1-\omega) + \mathbf{P}_{2i} \\
\mathbf{P} &= \left(\mathbf{P}_1^{-1} + \mathbf{P}_2^{-1}\right)^{-1} \\
\hat{\mathbf{x}} &= \mathbf{P}\left(\mathbf{P}_1^{-1}\hat{\mathbf{x}}_1 + \mathbf{P}_2^{-1}\hat{\mathbf{x}}_2\right) \\
\mathbf{P}_i &= \mathbf{P}\left(\mathbf{P}_1^{-1}\mathbf{P}_{1i}\mathbf{P}_1^{-1} + \mathbf{P}_2^{-1}\mathbf{P}_{2i}\mathbf{P}_2^{-1}\right)\mathbf{P} \\
\mathbf{P}_d &= \mathbf{P} - \mathbf{P}_i
\end{aligned}
\tag{6.3}
$$

6.2 Preliminaries

Robot motion in a 2D arena is modelled by the 3-DOF discreet-time kinematic model as outlined in Section 3.1.1. Additionally, it is assumed that each agent in the MRS

hosts an exteroceptive sensory system to measure the relative pose of neighbours. The mathematical model of this relative pose measurement system is presented in Section 3.1.2. For an MRS with $|\mathcal{S}|$ mobile robots, the maximum number of robots that can operate within an arbitrary robot's, i.e., $\mathcal{R}_q$, where $q \in \mathcal{S}$, sensing and communication boundaries is one robot less that the total number of robots in the MRS.

$$\Rightarrow 0 \leq |\mathcal{S}_{q,k}| \leq |\mathcal{S}| - 1 \;\; \Rightarrow \;\; 0 \leq |\mathcal{Y}^q_{q,k}| \leq |\mathcal{S}| - 1, \;\;\; \forall k = 1, 2, \cdots, \infty, \;\;\; q \in \mathrm{S}$$

6.3 Decentralized Cooperative Localization Algorithm

6.3.1 State Propagation

The objective of the state propagation step is to predict the current pose and associated estimation uncertainties of a given robot using both the robot's posterior state density and the odometry reading at the previous time step. In order to avoid cyclic update, each robot maintains two covariance matrices: total covariance and independent covariance. Once the total and independent covariances are known, dependent covariance can be calculated as

$$P_{q_{\mathbf{d}},k} = P_{q,k} - P_{q_{\mathbf{i}},k} \tag{6.4}$$

where $P_{q,k}$, $P_{q_{\mathbf{i}},k}$ and $P_{q_{\mathbf{d}},k}$ are total covariance, independent covariance and dependent covariance of R_q's pose estimation at time step k, respectively.

This study employs CKF for sensor fusion. In this study, robot pose and odometry vectors are augmented into a single state vector leading to $n = n_x + n_c$, where n_x is the size of the pose vector and n_c is the size of the odometry vector. Standard CKF

formulation computes only the total error covariance of the estimated parameters. However, in order to apply the split-CI-based sensor fusion, independent and inter-dependent covariance matrixes also need to be computed and maintained. Therefore, this study extends the standard CKF algorithm presented in [36] by incorporating independent and dependent covariance calculation and maintaining capabilities.

The proposed state propagation approach is summarized in **Algorithm 6.1**. This algorithm is implemented on each robot's local processor and iterates at each time step. The algorithm initializes with known prior density $p(\mathbf{x}_{q,k_+}) = \mathcal{N}(\hat{\mathbf{x}}_{q,k_+}, \mathbf{P}_{q,k_+})$, independent covariance matrix $\mathbf{P}_{q_i,k_+}$, and odometry reading $\bar{\mathbf{u}}_{q,k}$ at the previous time step (say, time step k). The algorithm predicts the robot pose for the next time step along with the associated total and independent covariances. First, the algorithm augments the estimated pose vector $\hat{\mathbf{x}}_{q,k_+}$ with the odometry vector at time k. The associated covariance matrix is then computed by block-diagonalization of the estimation and the process covariance matrices. In the CKF, a set of the cubature points is used to represent the current estimated pose and associated estimation uncertainties. To generate these cubature points, the square-root factor of the covariance matrix is required. Any matrix decomposition approach that preserves the equality given in (6.7) can be exploited to compute the square-root factor of the covariance matrix. The cubature points that represent current state and odometry measurements are evaluated with the nonlinear state propagation function, which generates the cuba-ture point distribution for a predicted state. The predicted pose (or state) of the robot is the average of the propagated cubature points. Total predictive covariance is then computed from (6.11). Once the total predictive covariance is calculated, a new block-diagonalized covariance matrix, i.e., $\mathbf{P}_{i,k_+}$, is generated using the independent covariance matrix of time k, i.e., $\mathbf{P}_{q_i,k_+}$, and process covariance matrix, i.e., $\mathbf{Q}$. After computing $\mathbf{P}_{i,k_+}$, its square-root factor is computed; then a set of cubature points is

Algorithm 6.1 State propagation

Data: Assume at time k posterior density function of robot's pose estimation $p(\mathbf{x}_{q,k_+}) = \mathcal{N}(\hat{\mathbf{x}}_{q,k_+}, \mathbf{P}_{q,k_+})$, independent covariance matrix $\mathbf{P}_{q_\mathbf{i},k_+}$, and odometry reading $\bar{\mathbf{u}}_{q,k}$ are known.

Result: Predictive density function of robot's pose estimation $p(\mathbf{x}_{q,(k+1)_-}) = \mathcal{N}(\hat{\mathbf{x}}_{q,(k+1)_-}, \mathbf{P}_{q,(k+1)_-})$ and associated independent covariance matrix $\mathbf{P}_{q_\mathbf{i},(k+1)_-}$.

1: Augment state end odometry reading into single vector:

$$\hat{\mathbf{x}}_{k_+} = \begin{bmatrix} \hat{\mathbf{x}}_{q,k_+}^T & \bar{\mathbf{u}}_{q,k}^T \end{bmatrix}^T \tag{6.5}$$

2: Compute the corresponding covariance matrix:

$$\mathbf{P}_{k_+} = \begin{bmatrix} \mathbf{P}_{q,k_+} & \mathbf{0}_{n_x \times n_c} \\ \mathbf{0}_{n_c \times n_x} & \mathbf{Q} \end{bmatrix} \tag{6.6}$$

3: Factorize:
$$\mathbf{P}_{k_-} = \mathbf{S}_{k_+} \mathbf{S}_{k_+}^T \tag{6.7}$$

4: Generate cubature points ($j = 1, 2, \cdots, m$):

$$\mathbf{X}_{j,k_+} = \mathbf{S}_{k_+} \xi_j + \hat{\mathbf{x}}_{k_+} \tag{6.8}$$

where $m = 2(n_x + n_c)$

5: Propagate each set of cubature points through nonlinear state propagation function given in (3.1) ($j = 1, 2, \cdots, m$):

$$\mathcal{X}_{j,(k+1)_-} = \mathbf{g}(\mathbf{X}_{j(1:n_x),k_+},\ \mathbf{X}_{j(n_x+1:n_x+n_c),k_+}) \tag{6.9}$$

6: Predict next state:
$$\hat{\mathbf{x}}_{q,(k+1)_-} = \frac{1}{m} \sum_{j=1}^{m} \mathcal{X}_{j,(k+1)_-} \tag{6.10}$$

7: Estimate the predictive error covariance:

$$\mathbf{P}_{q,(k+1)_-} = \frac{1}{m} \sum_{j=1}^{m} \mathcal{X}_{j,(k+1)_-} \mathcal{X}_{j,(k+1)_-}^T - \hat{\mathbf{x}}_{q,(k+1)_-} \hat{\mathbf{x}}_{q,(k+1)_-}^T \tag{6.11}$$

8: To calculate independent covariance, construct new block diagonalize covariance matrix as follows:

$$\mathbf{P}_{i,k_+} = \begin{bmatrix} \mathbf{P}_{q_\mathbf{i},k_+} & \mathbf{0}_{n_x \times n_c} \\ \mathbf{0}_{n_c \times n_x} & \mathbf{Q} \end{bmatrix} \tag{6.12}$$

9: Factorize $\mathbf{P}_{i,k_+}$, then generate a new set of cubature points, and propagate this new cubature point set through the nonlinear state propagation function (3.1) (refer to lines 3, 4, and 5 for equations)

10: Predict new state using independent covariance:

$$\hat{\mathbf{x}}_{q_{\mathbf{i}},(k+1)_-} = \frac{1}{m} \sum_{j=1}^{m} \mathcal{X}_{j,(k+1)_-} \tag{6.13}$$

11: Estimate the independent predictive error covariance:

$$\mathbf{P}_{q_{\mathbf{i}},(k+1)_-} = \frac{1}{m} \sum_{j=1}^{m} \mathcal{X}_{j,(k+1)_-} \mathcal{X}_{j,(k+1)_-}^{T} - \hat{\mathbf{x}}_{q_{\mathbf{i}},(k+1)_-} \hat{\mathbf{x}}_{q_{\mathbf{i}},(k+1)_-}^{T} \tag{6.14}$$

---

n_x: size of robot's pose vector,
n_c: size of robot's odometry vector,
$\mathbf{0}_{a \times b}$: matrix with a rows and b columns and all entries are zeros,
k_+: represents $k|k$, $(k+1)_-$: represents $(k+1)|k$.

---

generated using the new square-root factor; and finally, the newly generated cubature points are propagated through the nonlinear state propagation function. These steps are followed by the computation of prediction for an independent propagated state and the associated covariance matrix.

6.3.2   Compute Pose of Neighbours

The measured relative pose measurements are in the local coordinate system of the observing robot and are required to be transformed to the reference coordinate system prior to executing the sensor fusion at the neighbouring robot's local processor. Assume that, at time $(k+1)$, robot $\mathcal{R}_q$ measures the relative pose of robot $\mathcal{R}_r$. This nonlinear coordinate transformation can be modeled as

$$\begin{aligned}
\mathbf{y}_{q,k+1}^{r,*} &= \mathbf{f}(\hat{\mathbf{x}}_{q,(k+1)_-} \ , \ \mathbf{y}_{q,k+1}^{r,q}) \\
&= \hat{\mathbf{x}}_{q,(k+1)_-} \oplus \mathbf{y}_{q,k+1}^{r,k} \\
&= \hat{\mathbf{x}}_{q,(k+1)_-} + \mathbf{\Gamma}_{x_{q,(k+1)_-}} \mathbf{y}_{q,k+1}^{r,k}
\end{aligned} \tag{6.15}$$

where $\oplus$ is known as the pose composition operator and $\mathbf{y}_{q,k+1}^{r,*}$ is the global pose of $\mathcal{R}_r$ on the reference coordinate frame, as measured by $\mathcal{R}_q$. The superscript asterisk '$*$' is used to indicate that the measurement is on the reference coordinate system. Symbol $\boldsymbol{\Gamma}_{x_{q,(k+1)_-}}$ has the same meaning as in (3.1). Since this Cartesian-to-Cartesian transformation is nonlinear, a cubature point-based approach, as summarized in **Algorithm 6.2**, is employed to achieve consistent and unbiased coordinate transformation (see Appendix A).

The algorithm is initialized with a known predictive density of the pose estimation of the observing robot along with the predictive independent covariances. At an inter-robot-relative-pose measurement event, the observing robot augments its predictive pose and relative pose measurement into a single state vector (Line 1). The associated covariance matrix is obtained by block-diagonalization of the predictive total covariance ($\mathbf{P}_{q,k+1_-}$) and noise covariance of the relative pose measurement ($\mathbf{R}_q$) (Line 2). This block-diagonalized covariance matrix is then factorized and exploited for generating a set of cubature points to represent the state vector (Lines 3 and 4). The generated cubature points are evaluated on the nonlinear Cartesian-to-Cartesian coordinate transformation function, i.e. (6.15), in order to compute the coordinate transformed cubature points (Line 5). This step is followed by the computation of the observed robot pose in the reference coordinate system (Line 6) and associated total noise (error) covariance matrix (Line 7). Once the total noise covariance is calculated, the algorithm constructs a new block-diagonalized covariance matrix, $\bar{\mathbf{R}}_{i,k+1}$, using the predictive independent covariance matrix and the relative pose measurement noise covariance matrix (Line 8). After computing the $\bar{\mathbf{R}}_{i,k+1}$, its square-root factor is computed as in line 3; then a set of cubature points is generated using the new square-root factor (as in line 4); and finally, newly generated cubature points are transformed from the local coordinate system into the global coordinate system (as in line 5) (line

---

Algorithm 6.2 Relative-to-global conversion

Data: Assume at time k the predictive density function of a robot's (say $\mathcal{R}_q$) pose estimation $p(\mathbf{x}_{q,(k+1)_-}) = \mathcal{N}(\hat{\mathbf{x}}_{q,(k+1)_-}, \mathbf{P}_{q,(k+1)_-})$, independent covariance matrix $\mathbf{P}_{q_i,(k+1)_-}$, and relative pose measurement of a neighbour (say $\mathcal{R}_r$) are available.

Result: Global pose measurement of $\mathcal{R}_r$, i.e. $\mathbf{y}_{q,k+1}^{r,*}$, and associated independent and dependent measurement covariances, i.e., $\mathbf{R}_{q_\mathbf{i},k+1}^*$ and $\mathbf{R}_{q_\mathbf{d},k+1}^*$.

1: Augment the predictive state and relative pose into single vector:

$$\mathbf{y}_{k+1} = \begin{bmatrix} \mathbf{x}_{q,(k+1)}^T & (\mathbf{y}_{q,(k+1)}^{r,*})^T \end{bmatrix} \tag{6.16}$$

2: Construct corresponding covariance matrix:

$$\bar{\mathbf{R}}_{k+1} = \begin{bmatrix} \mathbf{P}_{q,(k+1)_-} & \mathbf{0}_{n_x \times n_x} \\ \mathbf{0}_{n_x \times n_x} & \mathbf{R}_q \end{bmatrix} \tag{6.17}$$

3: Factorize:

$$\bar{\mathbf{R}}_{k+1} = \bar{\mathbf{S}}_{k+1} \bar{\mathbf{S}}_{k+1}^T \tag{6.18}$$

4: Generate set of cubature points ($j = 1, 2, \cdots, m$):

$$\mathcal{Y}_{j,k+1}^{r,q} = \bar{\mathbf{S}}_{k+1} \boldsymbol{\xi}_j + \mathbf{y}_{k+1} \tag{6.19}$$

where $m = 2 * n_x$

5: Perform coordinate transform for each set of cubature points ($j = 1, 2, \cdots, m$):

$$\mathcal{Y}_{j,k+1}^{r,*} = \mathbf{f}(\mathcal{Y}_{j(1:n_x),k+1}^{r,q}, \mathcal{Y}_{j(n_x+1:2n_x),k+1}^{r,q}) \tag{6.20}$$

6: Compute global pose of neighbour:

$$\mathbf{y}_{q,k+1}^{r,*} = \frac{1}{m} \sum_{j=1}^{m} \mathcal{Y}_{j,k+1}^{r,*} \tag{6.21}$$

7: Compute total noise (error) covariance:

$$\mathbf{R}_{q,k+1}^{r,*} = \frac{1}{m} \sum_{j=1}^{m} \left(\mathcal{Y}_{j,k+1}^{r,*} \right) \left(\mathcal{Y}_{j,k+1}^{r,*} \right)^T - \left(\mathbf{y}_{q,k+1}^{r,*} \right) \left(\mathbf{y}_{q,k+1}^{r,*} \right)^T \tag{6.22}$$

8: Construct a block-diagonalized matrix using independent predictive covariance and measurement noise covariance:

$$\bar{\mathbf{R}}_{i,k+1} = \begin{bmatrix} \mathbf{P}_{q_\mathbf{i},(k+1)_-} & \mathbf{0}_{n_x \times n_x} \\ \mathbf{0}_{n_x \times n_x} & \mathbf{R}_q \end{bmatrix} \tag{6.23}$$

9: Factorize $\bar{\mathbf{R}}_{i,k+1}$, then generate a new set of cubature points followed by the coordination transformation for each cubature point (refer to lines 3, 4, and 5 for equations).

10: Compute coordinate transformed measurement using independent covariance:

$$\mathbf{y}_{q_{\mathbf{i}},k+1}^{r,*} = \frac{1}{m} \sum_{j=1}^{m} \mathcal{Y}_{j,k+1}^{r,*} \tag{6.24}$$

11: Estimate independent covariance for the pose measurement:

$$\mathbf{R}_{q_{\mathbf{i}},k+1}^{r,*} = \frac{1}{m} \sum_{j=1}^{m} \left(\mathcal{Y}_{j,k+1}^{r,*} \right) \left(\mathcal{Y}_{j,k+1}^{r,*} \right)^{T} - \left(\mathbf{y}_{q_{\mathbf{i}},k+1}^{r,*} \right) \left(\mathbf{y}_{q_{\mathbf{i}},k+1}^{r,*} \right)^{T} \tag{6.25}$$

12: Estimate dependent covariance for the pose measurement:

$$\mathbf{R}_{q_{\mathbf{d}},k+1}^{r,*} = \mathbf{R}_{q,k+1}^{r,*} - \mathbf{R}_{q_{\mathbf{i}},k+1}^{r,*} \tag{6.26}$$

9). These steps are followed by computing the coordinate transformed measurement and associated independent noise covariance matrix (lines 10 and 11). Finally, the dependent covariance of the coordinate transformed measurement is calculated as the difference between total and independent covariances (Line 12).

6.3.3 Update Local Pose Estimation Using the Pose Sent by Neighbours

In order to perform split-CI-based sensor fusion, both the independent and dependent covariance matrices of input state estimates must be available. However, the proposed state propagation algorithm (**Algorithm 6.1**) maintains only the total and independent error covariance of the estimated pose. Therefore, dependent error covariance of the estimated pose needs to be calculated prior to fusing the received measurement with the local estimation. Once the independent and dependant covariances of the local estimate and received measurements are known, the weighted predicted covariance and the weighted measurement covariance can be calculated as given in (6.28) and (6.29), respectively. Coefficient α belongs to the interval $[0, 1]$ and can be determined so that the trace or determinant of the updated total covariance is minimized. The

152

Algorithm 6.3 State update with the measurement sent by neighbours

---

Data: Assume predictive density of robot pose estimation $p(\mathbf{x}_{r,(k+1)_-} = \mathcal{N}(\hat{\mathbf{x}}_{r,(k+1)_-}, \mathbf{P}_{r,(k+1)_-}))$, the associated independent covariance matrix $\mathbf{P}_{q_{\mathbf{i}},(k+1)_-}$ and pose measurements from a neighbour $\mathbf{y}_{q,k+1}^{r,*}$ along with the associated independent and dependent covariances are available.

Result: Posterior density of time $k+1$, i.e $p(\mathbf{x}_{r,(k+1)_+}) = \mathcal{N}(\hat{\mathbf{x}}_{r,(k+1)_+}, \mathbf{P}_{r,(k+1)_+})$ and the associated independent covariance matrix $\mathbf{P}_{r_{\mathbf{i}},(k+1)_+}$

1: Calculate the predictive dependant covariance:

$$\mathbf{P}_{q_{\mathbf{d}},(k+1)_-} = \mathbf{P}_{q,(k+1)_-} - \mathbf{P}_{q_{\mathbf{i}},(k+1)_-} \tag{6.27}$$

2: Compute the weighted predictive covariance:

$$\mathbf{P}_1 = \frac{\mathbf{P}_{q_{\mathbf{d}},(k+1)_-}}{\alpha} + \mathbf{P}_{q_{\mathbf{i}},(k+1)_-} \tag{6.28}$$

3: Compute the weighted measurement covariance:

$$\mathbf{P}_2 = \frac{\mathbf{R}_{q_{\mathbf{d}},k+1}^{r,*}}{1-\alpha} + \mathbf{R}_{q_{\mathbf{i}},k+1}^{r,*} \tag{6.29}$$

4: **if** measurement gate validated **then**
5:      Compute Kalman gain:
$$\mathbf{K} = \mathbf{P}_1 \left(\mathbf{P}_1 + \mathbf{P}_2\right)^{-1} \tag{6.30}$$

6:      Update robot pose:

$$\hat{\mathbf{x}}_{r,(k+1)_+} = \hat{\mathbf{x}}_{r,(k+1)_-} + \mathbf{K}\left(\mathbf{y}_{q,k+1}^{r,*} - \hat{\mathbf{x}}_{r,(k+1)_-}\right) \tag{6.31}$$

7:      Update total covariance:

$$\mathbf{P}_{r,(k+1)_+} = (\mathbf{I}_{n_x} - \mathbf{K})\mathbf{P}_1 \tag{6.32}$$

8:      Update independent covariance:

$$\mathbf{P}_{r_i,(k+1)_+} = (\mathbf{I}_{n_x} - \mathbf{K})\mathbf{P}_{r_i,(k+1)_-}(\mathbf{I}_{n_x} - \mathbf{K})^T + \mathbf{K}\mathbf{R}_{q_{\mathbf{i}},k+1}^{r,*}\mathbf{K}^T \tag{6.33}$$

9: **else**
10:      Assign predictive state and covariances into posterior state and covariances:

$$\hat{\mathbf{x}}_{r,(k+1)_+} \leftarrow \hat{\mathbf{x}}_{r,(k+1)_-}$$
$$\mathbf{P}_{r,(k+1)_+} \leftarrow \mathbf{P}_{r,(k+1)_-} \tag{6.34}$$
$$\mathbf{P}_{r_i,(k+1)_+} \leftarrow \mathbf{P}_{r_i,(k+1)_-}$$

11: **end if**

$\mathbf{I}_{n_x}$: identity matrix of $(n_x \times n_x)$
α: weighting coefficient and belongs to the interval $[0,1]$

detection and elimination of outliers are important for preventing the divergence of the state estimation. This requirement can be fulfilled by employing an ellipsoidal measurement validating gate [116]. As the pose measurements from the neighbours are in the reference coordinate frame, the measurement model of this sensor fusion becomes linear. Therefore, the linear Kalman filter can be exploited for sensor fusion. In this measurement update, the measurement matrix $\mathbf{H}$ of the traditional Kalman filter becomes an identity matrix, $(\mathbf{I}_{n_x})$, of $n_x \times n_x$. Using the multiplicative property of the identity matrix (i.e. $\mathbf{I}_m \mathbf{A} = \mathbf{A} \mathbf{I}_n = \mathbf{A}$ where $\mathbf{A}$ is $m \times n$) the Kalman gains, the updated robot pose and the associated total and independent covariance matrices can be computed from (6.30), (6.31), (6.32), and (6.33), respectively. For outliers, measurements are discarded and the predictive pose and the associated total and independent covariance matrices are directly assigned to the corresponding posterior quantities so that the recursion of the algorithm is preserved. These measurement update steps are summarized in **Algorithm 6.3**.

6.3.4 Update Local Pose Estimation Using the Measurement Acquired by the Absolute Positioning System

It is assumed that some of the robots in the MRS host a DGPS sensor in order to measure global position information. This position measurement at time $k + 1$ is modeled as

$$\mathbf{y}_{q,k+1}^A = \mathbf{H}_{q,k+1}^A \mathbf{x}_{q,k+1} + \boldsymbol{\nu}_{K+1}^A, \tag{6.35}$$

where $\mathbf{H}_{q,k+1}^A = \begin{bmatrix} \mathbf{I}_2 & \mathbf{0}_{2\times1} \end{bmatrix}$ is the measurement matrix and $\boldsymbol{\nu}_{K+1}^A$ is the additive white Gaussian noise term with covariance $\mathbf{R}^A \in \mathbb{R}^{2\times2}$. This measurement is linear and independent from the robot's pose estimate. Thus, this measurement can be fused with the current state estimation using the general linear Kalman filter measurement

update steps followed by

$$\mathbf{P}_{q_\mathbf{i},(k+1)_+} = (\mathbf{I} - \mathbf{KH}_{q,k+1}^A)\mathbf{P}_{q_\mathbf{i},(k+1)_-}(\mathbf{I} - \mathbf{KH}_{q,k+1}^A)^T + \mathbf{KR}^A\mathbf{K}^T. \qquad (6.36)$$

This equation computes the updated independent covariance matrix at the event of the DGPS measurement update.

6.3.5 Sensor Fusion Architecture

This study assumes that each agent in the MRS initially knows its pose with respect to a given reference coordinate frame. The recursive state estimation framework of the proposed decentralized cooperative localization algorithm is outlined in **Algorithm 6.4** and is graphically illustrated in Figure 6.1.

The algorithm has four main steps:

Step 1: *Propagate state (lines 4-5)*

At each time step, the robot acquires its ego-motion sensor reading (odometry). This measurement is fused with the previous time step's posterior estimate in order to compute the predicted pose and the associated total and independent error covariance matrices as detailed in **Algorithm 6.1**.

Step 2: *Measure neighbours' pose (lines 6-12)*

At an inter-robot relative pose measurement event, first, the robot reads its exteroceptive sensors and collects the relative poses of its neighbours. Then, each relative pose measurement is transformed into the reference coordinate frame as outlined in **Algorithm 6.2**. Finally, the transformed global pose measurements and the associated independent and dependent covariance matrices are transmitted to the corresponding neighbouring robots.

Algorithm 6.4 Split-CI based cooperative localization algorithm

---

1: Initialize with known $\mathbf{x}_{q,\circ}$ and $\mathbf{P}_{q,\circ}$
2: Set initial independent covariance: $\mathbf{P}_{q_{\mathbf{i}},\circ} \leftarrow \mathbf{P}_\circ$
3: **for** $k \in (1, \cdots, \infty)$ **do**
4:     Read ego-motion sensor $\bar{\mathbf{u}}_{q,k}$
5:     Propagate state: **Algorithm 6.1**
6:     **if** $|\mathcal{Y}_{q,k+1}^q| > 0$ **then**
7:         **for** $\forall r \in \mathbf{N}_{q,k+1}$ **do**
8:             Read $\mathbf{y}_{q,k+1}^{r,q}$
9:             Transform relative pose measurement to reference coordinate frame: **Algorithm 6.2**
10:             Transmit $(\mathbf{y}_{q,k+1}^{r,*},\ \mathbf{R}_{q_{\mathbf{i}},k+1}^{r,*},\ \mathbf{R}_{q_{\mathbf{d}}}^{r,*})$
11:         **end for**
12:     **end if**
13:     **if** pose measurement is received from neighbours **then**
14:         **for** $\forall r \in \overline{\mathbf{N}}_{q,k+1}$ **do**
15:             Collect $(\mathbf{y}_{r,k+1}^{q,*},\ \mathbf{R}_{r_{\mathbf{i}},k+1}^{q,*},\ \mathbf{R}_{r_{\mathbf{d}}}^{q,*})$ from $\mathcal{R}_r$
16:             Perform Split-CI-based measurement update: **Algorithm 6.3**
17:             Enable recursive update

$$\begin{aligned} \hat{\mathbf{x}}_{q,(k+1)_-} &\leftarrow \hat{\mathbf{x}}_{q,(k+1)_+} \\ \mathbf{P}_{q,(k+1)_-} &\leftarrow \mathbf{P}_{q,(k+1)_+} \\ \mathbf{P}_{q_{\mathbf{i}},(k+1)_-} &\leftarrow \mathbf{P}_{q_{\mathbf{i}},(k+1)_+} \end{aligned} \qquad (6.37)$$

18:         **end for**
19:         Set independent covariance to zero:$\mathbf{P}_{q_{\mathbf{i}},(k+1)_-} \leftarrow [\mathbf{0}_{3\times3}]$
20:     **end if**
21:     **if** DGPS measurement available **then**
22:         Read $\mathbf{y}_{q,k+1}^A$
23:         **if** measurement gate validated **then**
24:             Compute $\hat{\mathbf{x}}_{q,(k+1)_+}$, $\mathbf{P}_{q,(k+1)_+}$, and $\mathbf{P}_{q_{\mathbf{i}},(k+1)_+}$ as detailed in section 6.3.4.
25:         **else**
26:             Assign predictive quantities to corresponding posterior quantities

$$\begin{aligned} \hat{\mathbf{x}}_{q,(k+1)_+} &\leftarrow \hat{\mathbf{x}}_{q,(k+1)_-} \\ \mathbf{P}_{q,(k+1)_+} &\leftarrow \mathbf{P}_{q,(k+1)_-} \\ \mathbf{P}_{q_{\mathbf{i}},(k+1)_+} &\leftarrow \mathbf{P}_{q_{\mathbf{i}},(k+1)_-} \end{aligned} \qquad (6.38)$$

27:         **end if**
28:     **else**
29:         Assign predictive quantities to corresponding posterior quantities: (6.38)
30:     **end if**
31: **end for**

$\overline{\mathbf{N}}_{q,k+1}$ is the set containing unique identification indices of robots that communicate global pose measurements to $\mathcal{R}_q$ at time $k+1$.

Step 3: *Update with pose measurements sent by neighbours (lines 13-20)*

At a given time step, a robot may receive pose measurements from one (or more) neighbour(s). First, the received pose measurement is fused with the local estimation using the Split-CI measurement update structure that is detailed in **Algorithm 6.3**. In order to enable the recursion for available pose measurements from multiple neighbours, the updated pose and associated total and independent covariances are assigned back to the corresponding predictive parameter (Line 17). The recursion is then continued until all the received pose measurements are considered. Work presented in [137] provides a complete theoretical analysis and simulation-based validation for the consistency of the Split-CI-based filtering. However, the simulation study presented in [138] demonstrated that the estimated states using the Split-CI based decentralized cooperative localization algorithm sometimes diverge. This may occur because the resulting pose estimation might be correlated partially or fully to subsequent pose measurements received from neighbours. To overcome this issue, the proposed algorithm directly assigns the known-independent covariance component to the correlated component (line 19). In other words, this study set the independent covariance component to zero after every inter-robot measurement update event, which is not included in the standard Split-CIF algorithm described in [135].

Step 4: *Update with absolute position measurement (lines 21-30)*

The final step of this algorithm is to update the robot's local pose with the position measurement acquired from an absolute positioning system. When a new position measurement is available, it is evaluated through an ellipsoidal validation gate to identify whether the acquired measurement is a valid measurement or an outlier (line 23). If it is a valid measurement then the measurement is

157

fused with the local estimation (Line 24). Otherwise, the predictive quantities are directly assigned to the corresponding posterior quantities (Line 26). For the time steps where no absolute position measurements are available, the predictive quantities are directly assigned to the corresponding posterior quantities (Line 29).
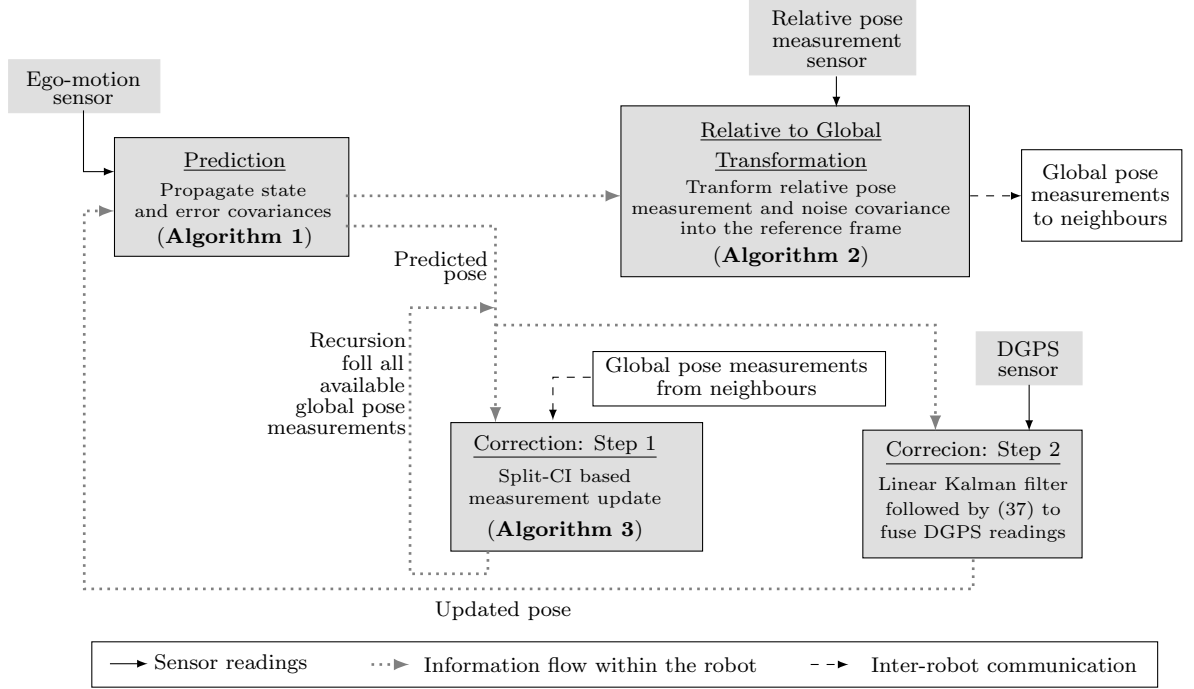
Figure 6.1: Sensor fusion architecture of the proposed decentralized multi-robot cooperative localization scheme

6.4 Simulation Results

6.4.1 Setup

The performance of the proposed decentralized cooperative localization algorithm was evaluated using a publicly available multi-robot localization and mapping data-set [49]. This 2D indoor data-set was generated from five robots (designated as

$\mathcal{R}_1$, $\mathcal{R}_2$, $\mathcal{R}_3$, $\mathcal{R}_4$, and $\mathcal{R}_5$) that navigated in a 15m × 8m indoor space. Although this data set consists of odometry readings, ground truth measurements and range and bearing measurements to neighbours and landmarks, only the odometry readings and ground truth measurements of each robot were used in order to evaluate the proposed decentralized cooperative localization algorithm. This simulation study assumed that all five robots would be equipped with light-weight sensory systems to uniquely identify and measure the relative poses of their neighbours. Further, it was assumed that only two members of the robot team (i.e., $\mathcal{R}_1$ and $\mathcal{R}_2$) were capable of acquiring DGPS measurements periodically. Inter-robot measurements and DGPS measurements were synthesized from the ground truth data. Simulation parameters and sensor characteristics related to this simulation setup are summarized in Table 6.1 and Table 6.2, respectively.

Table 6.1: Simulation parameters

Symbol	Parameter Description	Value
$|N|$	Number of robots in the team	5
t	Total time period of the data-set	1500 s
d_m	Maximum sensing range	10 m
$d \times l$	Size of the navigation arena	15 m × 8 m
MC	Number of Monte Carlo runs	20

6.4.2 Results

Figure 6.2 illustrates the mean estimation error and the associated $3 - \sigma$ error boundaries for $\mathcal{R}_1$, i.e. a robot with absolute position measuring capability, while Figure 6.3 illustrates the mean estimation error and the associated $3 - \sigma$ error boundaries for $\mathcal{R}_3$, i.e. a robot without absolute position measuring capability. All the results that are shown here is an average result of 20 Monte Carlo simulations. From these

Table 6.2: Sensor characteristics

Sensor type	Measure	Update rate	Noise σ
Odometry	Linear velocity	50Hz	$\sqrt{5.075}\bar{v}_{x_q,k}$
	Angular velocity	50Hz	$\sqrt{0.345}$ rads^{-1}
Relative pose	Relative x-position	10Hz	0.1 m
	Relative y-position	10Hz	0.1 m
	Relative orientation	10Hz	1 deg
DGPS	Global x-position	10Hz	0.1 m
	Global y-position	10Hz	0.1 m

Noise parameters for velocities were extracted from [51]

results, it can be seen that the estimation errors of the proposed decentralized cooperative localization algorithm are always inside the corresponding 3-σ error boundaries. This observation verifies that the proposed decentralized cooperative localization algorithm is capable of avoiding the cyclic update and generating non-overconfident state estimations. Additionally, it is clear that robots with absolute position measuring capabilities can achieve a more accurate pose estimation than robots without such capabilities (Note that the y axes of Figure 6.2 and Figure 6.3 are presented in two different scales.). Further, the results confirm that the estimation error of the proposed decentralized cooperative localization algorithm is bounded.

6.4.3 Comparison

The estimation accuracy of the proposed decentralized cooperative localization algorithm is compared with the estimation accuracies that were obtained from the following localization schemes:

1. *Single-Robot Localization (SL) Method*: Each robot continually integrates its odometry readings in a given coordinate frame in order to estimate its pose.
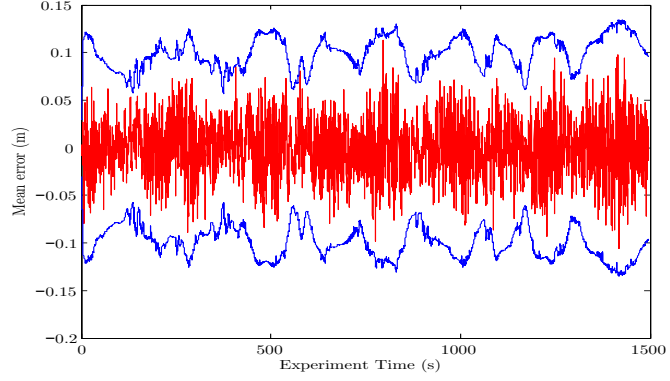
(a) x-position
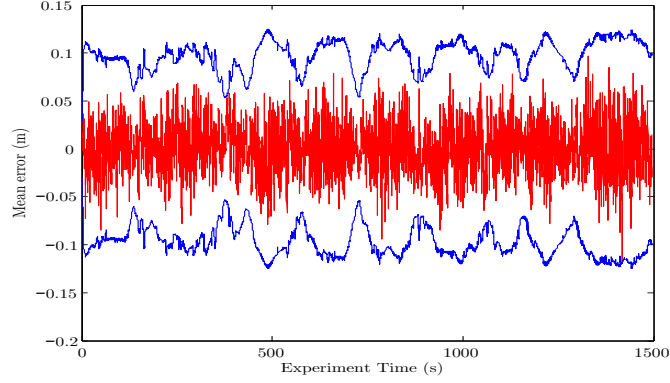
(b) y-position
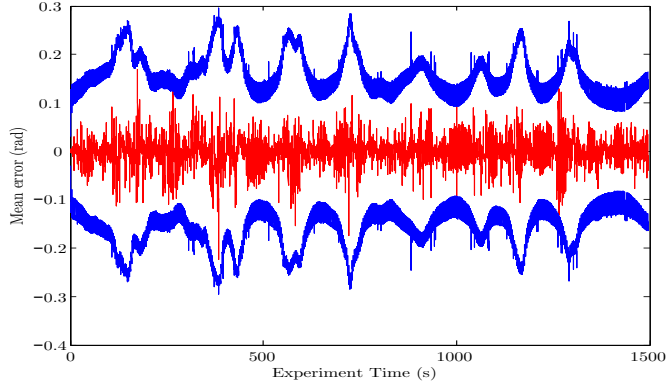
(c) ϕ-orientation

Figure 6.2: Mean estimation error of $\mathcal{R}_1$ for 20 Monte-Carlo simulations (a robot with absolute position measuring capabilities). In each graph, the solid red line indicates mean estimation error while the solid black lines indicate double-sided 3-σ error boundaries

161
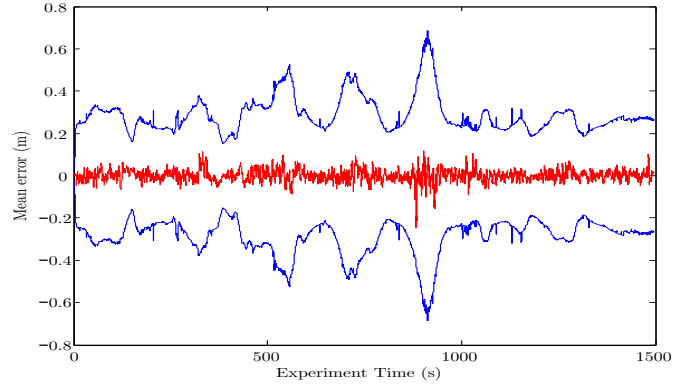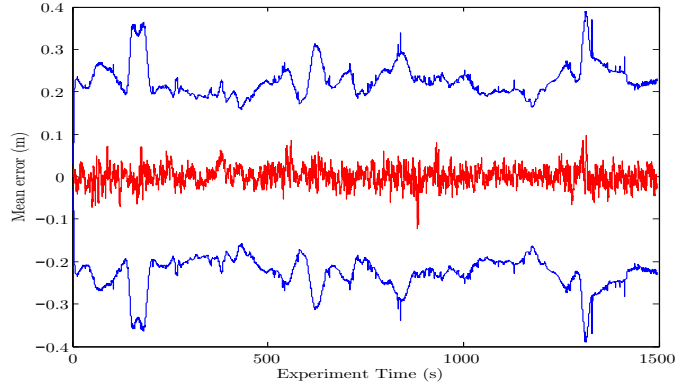
(a) x-position
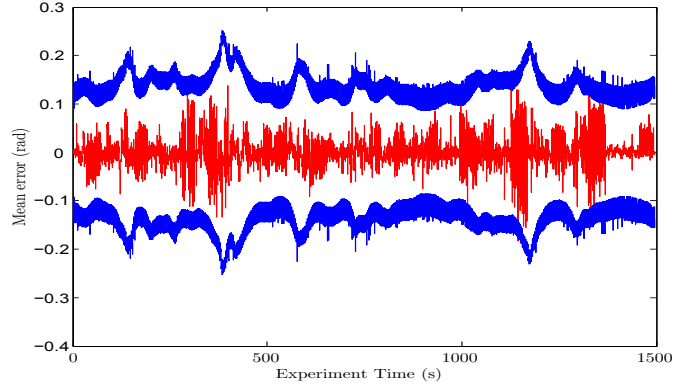
(b) y-position

(c) ϕ-orientation

Figure 6.3: Mean estimation error of $\mathcal{R}_5$ (a robot that does not have absolute position measuring capabilities) for 20 Monte Carlo simulations. In each graph, the solid red line indicates mean estimation error while the solid black lines indicate double-sided 3-σ error boundaries

This method is also known as dead-reckoning. Robots with DGPS measuring capability fuse their DGPS sensor readings with the local estimate in order to improve pose estimation accuracy.

2. *DCL Using Naive Block-diagonal (NB) Method*: In this method, the pose measurements sent by neighbours are treated as independent information and are fused directly with the local estimate. In other words, possible correlations between the local estimate and pose measurements sent by neighbours are neglected at the sensor fusion step.

3. *DCL Using Ellipsoidal Intersection (EI) Algorithm*: The EI algorithm always assumes that there exist unknown correlations between each robot's local pose estimations and uses a set of explicit expressions to calculate these unknown correlations, i.e. mutual-mean and mutual-covariance. When a robot receives a pose measurement(s) from its neighbour(s) the EI algorithm first calculates these unknown correlations. In order to obtain the updated estimation the calculated mutual-mean and mutual-covariance are fused with the robot's local estimates and the pose measurements received from the robot's neighbours [139].

4. *DCL Using Covariance Intersection (CI) Algorithm*: Each robot runs a local estimator to estimate its pose using onboard sensors and the pose measurements from neighbours. When a robot receives pose measurements from its neighbours, the covariance intersection algorithm is used to fuse these pose measurements with the robot's local estimate [59].

5. *Centralized Cooperative Localization (CCL) Approach*: The pose of each robot is augmented into a single state vector. The ego-centric measurements of robots and inter-robot observations are fused using an EKF. This is a centralized approach which can accurately track the correlations between robots' pose estima-

tions. Therefore, the results of this approach will serve as the benchmark for the performance evaluation of the proposed decentralized cooperative localization algorithm.

20 Monte Carlo simulations for each localization algorithm were performed. Then the RMSE of position and orientation estimation for 20 Monte Carlo simulations were computed. Finally, the time averaged RMSE values and associated standard deviations were calculated to compare the different localization schemes.
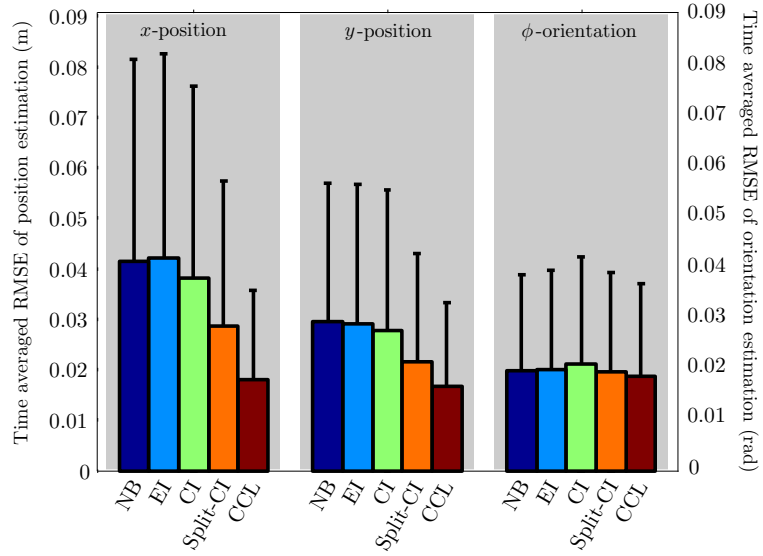
Figure 6.4: Comparison of estimation error of different cooperative localization algorithms. This result is for robot $\mathcal{R}_5$ (one of the robots without the DGPS measuring capabilities)

Consider robots without DGPS measuring capabilities (i.e. $\mathcal{R}_3$, $\mathcal{R}_4$ and $\mathcal{R}_5$). The pose estimation of these robots relies entirely on the odometry readings and the inter-robot observations. Therefore, the time averaged RMSE and the associated standard deviation values of the pose estimation of these robots provide insight into the performance of each localization algorithm. The time averaged RMSE and the associated standard deviation of the localization of $\mathcal{R}_5$ using the single-robot localization scheme was found to be 3.1762 ± 2.3680 m in x-direction, 5.0073 ± 2.3339 m in y-direction,
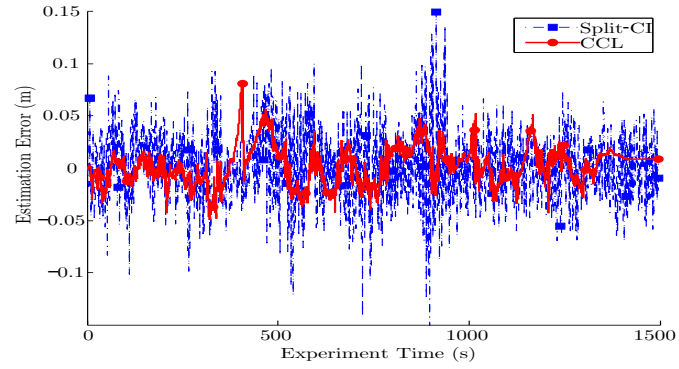
(a) x-position
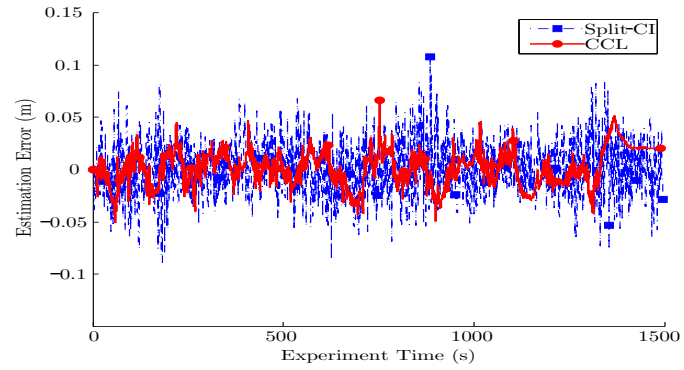
(b) y-position
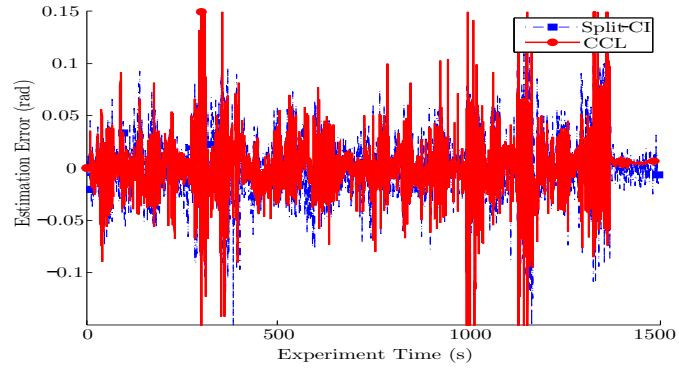
(c) ϕ-orientation

Figure 6.5: Estimation error comparison between the proposed Split-CI based approach and the centralized cooperative localization approach

165

and 1.1776 ± 0.9015 rad in the orientation estimation[2]. The time averaged RMSE of the localization of $\mathcal{R}_5$ using any of the cooperative localization algorithms (NB, EI, CI, Split-CI, and CCL) was less than 10 cm in both x- and y-directions, and less than 0.1 rad in the orientation estimation. These observations imply that the cooperative localization approaches can significantly improve the accuracy of pose estimation of agents in an MRS.

Time averaged RMSE and the associated standard deviation values of x-position, y-position and ϕ-orientation estimates of $\mathcal{R}_5$ using different cooperative localization schemes are compared in Figure 6.4. This comparison shows that the centralized cooperative localization algorithm outperforms all other approaches. This was the expected result, as the centralized estimator maintained the joint-state and the associated dense covariance matrix in order to accurately represent the correlation between teammates' pose estimates. Although the estimated pose using the proposed Split-CI based decentralized cooperative localization algorithm is less accurate than that of the centralized cooperative localization algorithm, it demonstrates better accuracy than all other decentralized cooperative localization approaches that were evaluated in this article.

Figure 6.5 illustrates the estimation error comparison between the proposed Split-CI based decentralized cooperative localization algorithm and the centralized cooperative localization algorithm. It indicates that the centralized approach has better accuracy; however, the estimation accuracy obtained from the proposed decentralized cooperative localization algorithm is comparable with the estimation accuracy obtained from the centralized approach.

---

[2]The format of the listed estimation errors is (mean $\pm$ standard deviation)

6.5 Experimental Results

6.5.1 Setup
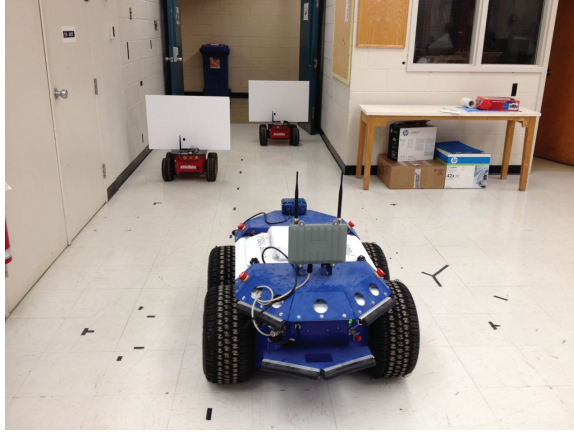
Figure 6.6: Experimental Setup

The proposed decentralized cooperative localization algorithm was experimentally evaluated on a team of three robots (see Figure 6.6): one SeekurJr (designated as platform A) and two Pioneer robots (named platforms B and C). Each robot was equipped with wheel encoders for odometry. Additionally, SICK laser scanners were attached to periodically acquire range and bearing measurements for objects around the robot. Robots were navigated in an indoor environment while maintaining a triangular formation among them.

6.5.2 System Architecture

Figure 6.7 illustrates the system architecture of the experimental setup. Each robot acquires its odometry measurements and laser-scan readings periodically. The acquired measurements are transmitted to a host computer through a TCP/IP interface. Platform A was provided with the map of the navigation space and it performed scan-matching-based localization using this map. The position estimations of this
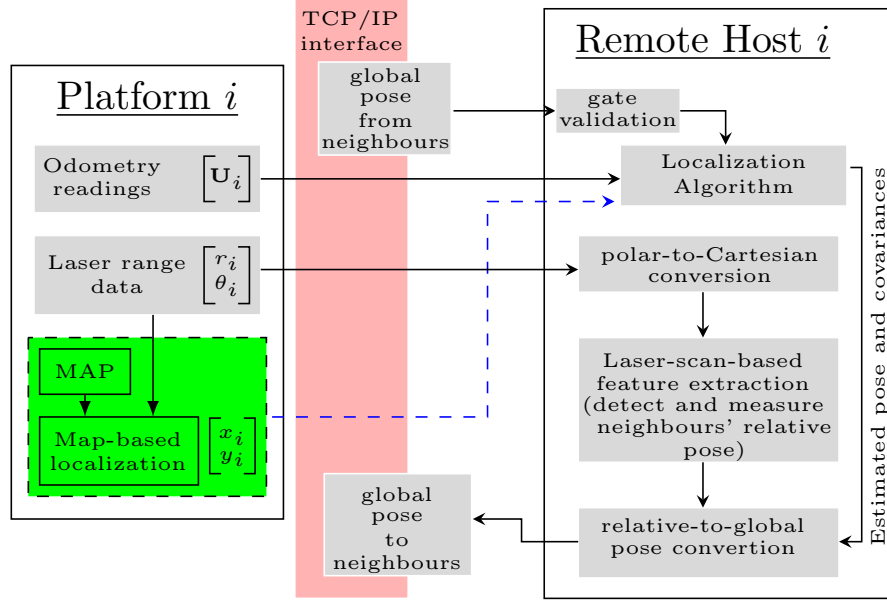
Figure 6.7: System architecture of the experiment setup to validate the proposed decentralized cooperative localization scheme. Note that the map-based (scan-matching-based) localization information is available only for Platform A

scan-matching-based localization for platform A were considered as absolute position measurements for cooperative localization schemes and were transmitted to the host computer that executed the localization for platform A.

In the host computer, odometry readings were used for state propagation and the global pose measurements and the associated noise covariances from the neighbours were used to correct the predicted pose. Note that the pose measurements from neighbours were first evaluated through an ellipsoidal measurement validation gate in order to detect and discard outliers. Only platform A used scan-matching-based position calculation data at the sensor fusion. At each host processing unit, the received laser scan data were first converted to the Cartesian coordinate frame from the polar coordinate system. This gives a set of points that represents the relative positions of objects around the corresponding robot. A laser-scan-based feature extraction algorithm was then employed to detect and measure the relative pose of neighbouring robots. The

data correspondence problem was addressed using the nearest neighbour data association technique. These relative pose measurements were then converted to a global (reference) coordinate frame and next were communicated to the corresponding host.

6.5.3 Results

Figure 6.8 illustrates the comparison of pose estimates for platform B that were obtained from three different sensor fusion approaches: the centralized cooperative localization method, the proposed Split-CI based decentralized cooperative localization algorithm, and the single robot localization (dead-reckoning) method. The estimates obtained from the centralized cooperative localization approach serve as the benchmark for evaluating the proposed decentralized cooperative localization algorithm. On the other hand, the estimates obtained from the single robot localization represent the worst case pose estimates for each time step. These results suggest that the proposed Split-CI based decentralized cooperative localization algorithm and the centralized cooperative localization algorithm generate approximately the same pose estimates for platform B. Although the two estimates are not identical, the difference between the two estimates did not exceed the double-sided 3-σ error boundary, i.e. the gray coloured region of Figure 6.8, of the proposed decentralized cooperative localization algorithm. Pose estimates generated from dead-reckoning diverged from the true state (or the state obtained from the centralized approach) with the increase of the experimental time period.

Figure 6.9 illustrates the comparison of pose uncertainty for three different sensor fusion approaches: the centralized cooperative localization method, the proposed split-CI based decentralized cooperative localization algorithm, and the single robot localization method. These results verify that the cooperative localization approaches have bounded pose estimation uncertainty while the pose estimation uncertainty of the sin-
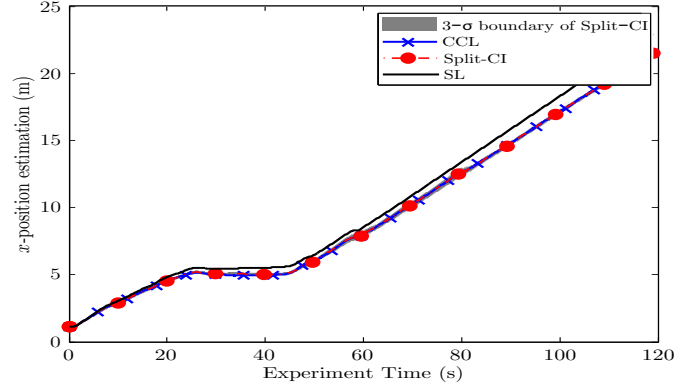
(a) *x*-position
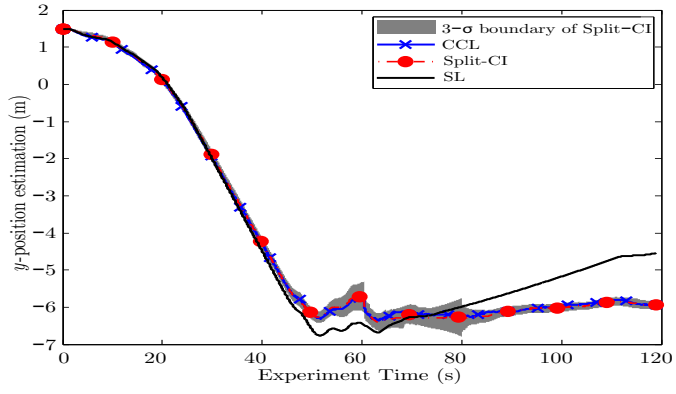
(b) *y*-position
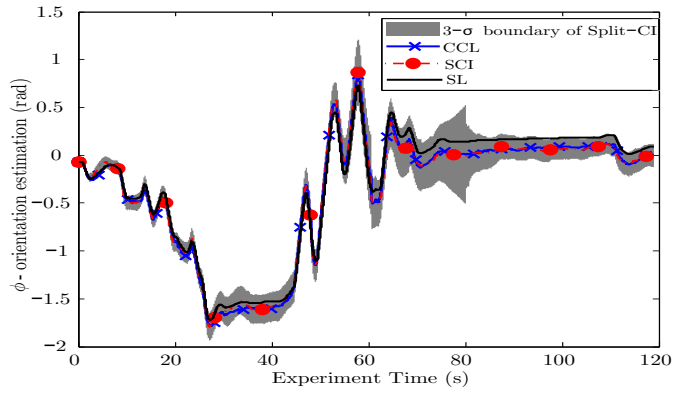
(c) ϕ-orientation

Figure 6.8: Pose estimation comparison of platform B
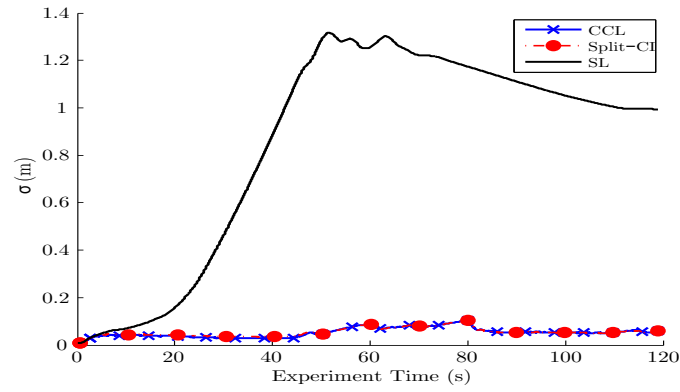
(a) x-position estimation
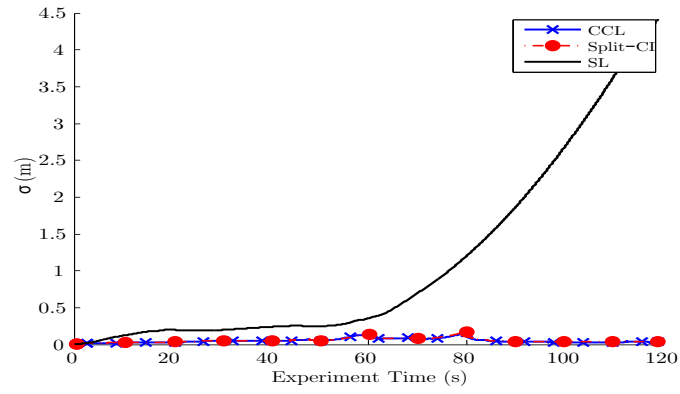
(b) y-position estimation
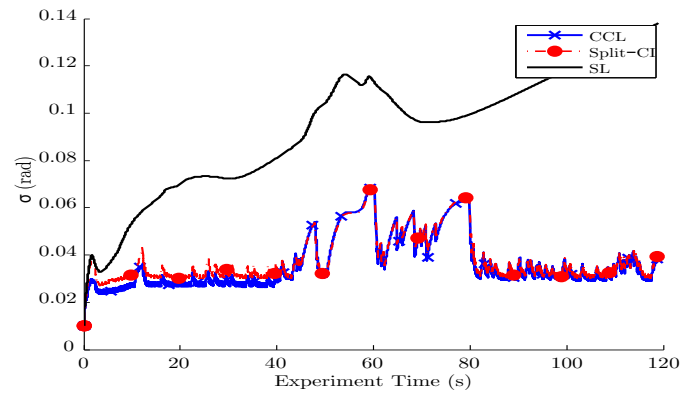
(c) ϕ-orientation estimation

Figure 6.9: Comparison of pose estimation uncertainty (standard deviation) for platform B

171

gle robot localization approach increases unboundedly. The lowest pose uncertainty is recorded in the centralized approach (see Figure 6.9 (c)). The pose uncertainty found in the proposed Split-CI based decentralized cooperative localization algorithm is slightly greater than that of the centralized approach. This is the expected result as the centralized estimator maintained the joint-state and associated dense covariance matrix in order to accurately represent the correlation between teammates' pose estimates.

6.6   Complexity

6.6.1   Computational Complexity

As the pose estimation of the proposed algorithm is decentralized, the computational complexity of the proposed decentralized cooperative localization algorithm increases linearly with the increase of number of neighbouring robots. In other words, the computational complexity of the proposed decentralized cooperative localization algorithm is $\mathcal{O}(|\bar{N}_q|)$, where $|\bar{N}_q|$ is the number of neighbours, per robot per time step. This remains true for all the decentralized cooperative localization algorithms while the computational complexity increases $\mathcal{O}(|N|^4)$ for the centralized cooperative localization where $|N|$ is the number of robots in the MRS.

6.6.2   Communicative Complexity

The proposed decentralized cooperative localization algorithm does not require robots to communicate their high-frequency proprioceptive sensory data to one another or to the central processing unit. Only the inter-robot measurements are required to be exchanged between neighbouring robots. These two properties considerably reduce the bandwidth requirement for the communication network between robots. In general,

communication complexity of the proposed algorithm remains $\mathcal{O}(|\bar{N}_q|)$ per robot, per inter-robot observation event.

6.7 Summary

This chapter presented an innovative decentralized cooperative localization framework addressing the overconfident state generation issue associated with general decentralized cooperative localization schemes. This framework consists of (1) a method to integrate the split-CI-algorithm with the standard CKF, (2) a scalable sensor fusion architecture for multi-robot collaborative localization with a constant per measurement computational and communicative complexity, i.e. $\mathcal{O}(1)$ and (3) a consistent and unbiased approach to convert information between two Cartesian coordinate systems. Although the work presented in [138] showed that the general formulation of the Split-CI algorithm sometimes leads to an inconsistent state update, both the simulation and experimental results of this study verified that the proposed decentralized cooperative localization scheme is consistent. This can be attributed to the modification added at line 19 in **Algorithm 6.4**. Additionally to this improvement, both the simulation and experiment results demonstrate that the estimation accuracy of the proposed method is comparable with centralized cooperative localization.

Chapter 7

Summary and Future Research

7.1 Summary

For heterogeneous MRSs, a sensor sharing technique can be established to enable robots with accurate self-localization capabilities (leader robots) to assist less powerful robots (child robots) in a team for localization. In general, leader-assisted localization frameworks pose a condition that the child robots should be operated within the sensing and communication boundaries of the leader robots. The bonded navigation space therefore require an added algorithm to avoid inter-robot collisions and limit robots' maneuverability and the coverage of the environment. This thesis has developed a innovative leader-assisted localization framework for heterogeneous MRSs that allows child robots to navigate beyond the sensing and communication boundaries of the leader robots while accurately estimating their own poses. The research study is based on four primary objectives:

1. to design a leader-assisted localization framework addressing the finite-range sensing problem;

2. to design a leader-assisted localization framework addressing the finite-range

communication problem;

3. to design a hierarchical sensor fusion architecture to implement the leader-assisted localization scheme using a relative range and bearing measurement system; and

4. to implement a scalable and consistent decentralized cooperative localization scheme.

7.1.1 Research Summary Based on Objective 1

Initially, it was assumed that the MRS had an unbounded communication range. With this assumption, the main focus was to address the finite-range sensing problem. The first modification this study added to the MRS was to equip the child robots with a light-weight and low-power exteroceptive sensory system to measure the relative pose of neighbours. Eventually, exteroceptive sensing capabilities for child robots form a relative pose measurement sensor network. An arbitrary leader robot in the team can then find a relative pose measurement path to an arbitrary child robot as long as both the robots are connected within a single relative pose measurement network. An external observer can see which robots are within one another's sensing range; i.e. the global perspective of the relative pose measurement graph. However, each robot in the team is only aware of its neighbours. Therefore, a bi-directional communication capability was then added to each member of the MRS allowing leader robots to collect all the available relative pose measurements from team members for any inter-robot observation event. The leader robots exploit this collected data to obtain the global pose measurement graph and to compose global pose measurements for child robots. When composing the global pose for child robots, it was important to detect and avoid the possible double counting of the same information, because

double counting information generaly lead to an overconfident state estimation. For the MRS with a single leader robot, the standard breadth first graph search algorithm was exploited to avoid the double counting problem. An innovative graph search algorithm, named the *multi-root breadth first graph search algorithm*, was developed to ensure the independency of each global pose measurement for each child robot in the MRS.

7.1.2 Research Summary Based on Objective 2

The second phase of the research integrated new algorithms and sensor fusion architectures into the first phase of the study so that both the sensing and communication range issues associated with leader-assisted localization were addressed. In the proposed method, only the robots with one another's sensing range are required to exchange information between them. Therefore, despite the fact that the communication range d_{com} is generally greater than the sensing range d_m, it is reasonable to assume $d_{com} = d_m$. When d_{com} is less than d_m, which is more unlikely, to ensure the connectivity of measurement network maximum displacement between pair of robots should set to d_{com}. As robots can communicate only with the robots operate within their communication boundaries, it is sufficient to calculate global pose for these neighbours upon an arrival of information from leader. The thesis considered two types of communication modes: *instantaneous communication mode* and *time-delayed communication mode*. The former assumes that the information which originates from a member of the MRS can communicate with any member of the measurement and communication network within the current sample time step. In contrast, the latter assumes that a single time step is required for information hopping between two robots. In order to reduce the communication overhead, this phase of the study does not entail collecting all available measurements in the leader robots' local processor

and does not execute a centralized multi-root breadth first graph search algorithm. In fact, an innovative distributed graph search algorithm was introduced to avoid double counting of common information, which can be viewed as a distributed multi-root breadth first graph search algorithm. The key challenge of the time-delayed communication mode was that robots cannot exploit the Markov property at each time step as the previous state estimations and measurements are being used for sensor fusion at future time steps. A set of theoretical concepts was introduced to determine the best time step for each robot to apply the Markov property. This theoretical analysis offered an effective way to reduce the onboard memory requirement for maintaining state estimation and measurement history while optimizing the child robots' pose estimation approach.

7.1.3   Research Summary Based on Objective 3

The first two phases of the study assumed the availability of a sensory system for measuring the relative pose of neighbours. However, range and bearing between a pair of robots are widely available inter-robot sensory systems for MRS. Additionally, it is possible to fabricate a light-weight and low-power inter-robot range and bearing measurement system at a low cost [50]. Therefore, it was important to relax the assumption on the exteroceptive sensory system so that the proposed leader-assisted localization scheme can be implemented using inter-robot range and bearing measurements. To this end, the third phase of the research developed a hierarchical sensor fusion architecture. The proposed hierarchical sensor fusion architecture employed a tracking filter to generate the relative pose of neighbours using inter-robot range and bearing measurements. This tracking filter works as a bridge between range/bearing measurements and the proposed leader-assisted localization scheme. The main focus was to develop a fast converging filter approach for relative localization. Therefore,

this research converted general range bearing measurements to a pseudo-linear format prior to performing sensor fusion. The simulation results demonstrated that the pseudo-linear measurement-based relative localization scheme can be initialized with an arbitrary initial pose and that it rapidly converges to the steady state level. This is a significant improvement when compared with traditional EKF-based relative localization schemes. As the conversion of the measurement model from a nonlinear model to a pseudo-linear model potentially affects system observability, this study mathematically evaluated the observability conditions for relative localization using pseudo-linear measurements. The findings of this mathematical analysis are summarized in the following table:

Table 7.1: Summary of observability study

Measurement System	Necessary condition for locally weakly observability
range and bearing	linear velocity of the observed robot should not equal zero
bearing only	observed robot linear velocities and the observing robot angular velocities should not equal zero.
range only	traditional nonlinear measurement-based approaches must be used for sensor fusion, as pseudo-linear measurements cannot be made using only relative range measurements.

7.1.4 Research Summary Based on Objective 4

Finally, the thesis developed a fully decentralized cooperative localization scheme for the MRS. The objective was to develop a scalable and non-overconfident multi-robot collaborative localization scheme for MRS. Decentralized sensor fusion architectures are generally scalable, as the per-measurement computational and communicative complexity of these approaches remain constant regardless of the number of agents

in the team. However, the majority of available decentralized cooperative localization approaches neglect possible interaction between teammates' local pose estimations resulting in an overconfident state estimation for each member of the team. Split-covariance intersection-based sensor fusion architecture was introduced and the required mathematical expressions to calculate and maintain both the independent and dependent information using a cubature Kalman filter (CKF) were derived. The proposed method demonstrated non-overconfident pose estimation with improved accuracy. In the literature, it is reported that a minimum of one agent in a cooperative localization team should possess absolute positioning capability in order to have a bounded estimation error and uncertainty using cooperative localization [12]. Therefore, this approach is suitable for MRSs with long-range sensing and communication capabilities, or for MRSs where the connectivity of the measurement network can always be guaranteed. However, the decentralized cooperative localization scheme that was developed can be exploited to improve the localization accuracy of the leader robots.

7.2   Significant Contributions

To summarize, this thesis made the following key contributions in leader-assisted localization of a heterogeneous MRS, fulfilling all of the outlined research objectives.

1. A centralized equivalent observation framework for MRS:

   Under the first objectives, the thesis developed algorithms to synthesise the missing IRRMs among leader robots and child robots that operate beyond the sensing range boundaries of the leader robots. Additionally to the virtually expanding the sensing range boundaries of leader robots, the localization framework developed in this thesis is capable of avoiding the double counting of common in-

formation. Any multi-robot localization approaches that suffer from finite-range sensing problem, such as relative localization, centralized, multi-centralized, and distributed cooperative localization approaches, can easily adapt the proposed algorithms and virtually enhance any observing robot's sensing range boundaries.

2. A centralized equivalent communication framework for MRS:

Under the second objectives, the thesis developed algorithms to virtually expand communicate boundaries of the leader robots. Additionally to the virtually expanding the communication boundaries of leader robots, the localization framework developed in this thesis is capable of avoiding the double counting of common information, is robust against the time delays associated with the practical communication channels, and is capable of optimizing memory usage. Any multi-robot localization approaches that suffer from finite-range communication problem, such as relative localization, centralized, multi-centralized, and distributed cooperative localization approaches, can easily adapt the proposed algorithms and virtually enhance any observing robot's communication boundaries.

3. Leader-assisted localization scheme using inter-robot range and bearing measurements:

Under the third objective, the thesis enhanced the applicability of the proposed leader-assisted localization scheme, introducing a hierarchical filtering architecture. This runs tracking filters on top of the proposed leader-assisted localization scheme for estimating relative pose of neighbours using range and bearing measurements. The tracking filters were implemented using pseudo-linear measurements in order to obtained the fast convergence than the traditional relative

localization schemes.

4. Scalable and consistent cooperative localization architecture for MRS:
   Under the last objective, a decentralized cooperative localization approach that
   is capable of accurately representing independencies and interdependencies of
   each robot's local pose estimations was designed, implemented, and tested.

7.3   Note to Practitioners

Accurate localization is a critical factor that governs the success of autonomous mo-
bile robots-based missions. In order to improve the accuracy of localization, robots
can be equipped with advanced sensory systems which would increase the cost of the
system. Additionally, robots can execute advanced localization algorithms to generate
an accurate localization which entails extensive processing capability and on-board
memory requirements. Most robotic systems do not possess sufficient resources to
host advanced sensory systems and execute advanced localization algorithms. The
proposed leader-assisted localization scheme is useful for such robotic systems. For
example, consider the application of indoor WiFi heat map generation using an MRS.
If it is possible to acquire more data points the accuracy of the map will be improved.
However, acquiring a dense data set using one robot entails a longer time for comple-
tion of the mission. On the other hand, using a homogeneous MRS for this application
will increase the operational cost. The use of a heterogeneous MRS then becomes the
trade-off between mission completion time and the operational cost when a group of
child robot acts as dynamic sensor nodes for a leader robot. Each child robot acquires
WiFi signal strength measurements and logs these measurements along with the es-
timated pose information. The localization of the child robot can be assisted by the
leader robot. The entire team can then move as a single flock and the formation of

the team can adaptively change in response to the spatial variations of the navigation space. In this application, the proposed leader-assisted localization scheme can be viewed as an observer for the controller. This method is appropriate for various applications such as multi-robot pattern generations, explorations, formation control-based applications, thermal heat map generation of industrial sites, and boundary tracking applications to detect the boundaries of toxic gas leakage and highly radioactive regions. A simulation-based study for multi-robot pattern generation and formation control was performed using the proposed leader-assisted localization scheme as the observer for controllers. The results of these simulation studies can be found in the following two videos:

- multi-robot pattern generation: Link: https://youtu.be/blbhos6yrL0

- multi-robot formation control: Link: https://youtu.be/WJwX0_4bnMI

7.4   Directions for Future Work

There are a number of potential extensions that can be added to the work presented in this thesis. These future developments will be studied for more practical issues to exploit the proposed localization scheme for real-world applications.

The mute robot : The final framework of the proposed leader-assisted localization scheme relies on the ability of teammates to propagate the information from one robot to another, forming a hierarchical inter-robot sensing and communication graph. If one or more robots in the team stop transmitting and/or receiving data, which is referred to as to as *mute robot*, a group of robots may not receive global pose measurements from leader robots. As observed from the experimental and simulation results, child robots' pose estimations tend to

diverge when they do not receive pose measurements from the leaders. Therefore, it is important to identify mute robots in the team and reconfigure the team formation so that the negative effect introduced by the mute robot(s) can be eliminated. Mute robot behaviour may be a temporary effect introduced by various environmental factors or the stochastic nature of the communication channels. These mute robots may reassume an exchange of information with their neighbours after being a mute robot for several time steps. Therefore, it is important to ensure that mute robots do not leave the robot team; in fact, these robots should identify themselves as mute robots and run a local controller so that they will always operate within a sensing and communication range of one or a few other members of the MRS. To this end, future research can be established to effectively identify and handle the mute robots in the MRS.

Connectivity of sensing and communication network : The experimental and simulation results of the proposed leader-assisted localization scheme illustrated that each child robot must be a member of a sensing and communication graph which consists of a minimum of one leader robot. Otherwise, the child robots' localization tends to diverge, as their localization then completely relies on their odometric measurements. Therefore, the connectivity to a sensing and communication network with a minimum of one leader robot is one of the key requirements for the proposed leader-assisted localization scheme. Therefore, a control algorithm such as a rigidity maintenance controller [140–144] can be integrated with the proposed localization scheme so that the network connectivity is always ensured. As the child robots are resource constraint robots, decentralized control architecture is desired to ensure the connectivity of the sensing and measurement network. If there exists more than one sensing and communicating path from the leader robot to a child robot, the proposed algorithms will

become more robust against the single point of failure. For example, assume there exist two sensing and communication paths between a leader robot and a child robot in the MRS. If an intermediate robot in the shortest sensing and communication path suddenly becomes a mute robot, the child robot will not receive pose measurements through this shortest path. However, it is possible for pose measurements to propagate through the second measurement path as no pose measurement is propagated through the first measurement path. This eventually increases the robustness of the proposed localization scheme against the single point of failure. To this end, future studies can be undertaken to integrate a decentralized control architecture to ensure the connectivity of the sensing and communication network, so that more than one sensing and communication path between an arbitrary leader robot and an arbitrary child robot in the MRS exists.

Uneven terrains : The localization framework and theoretical development of this thesis were developed targeting indoor applications. Therefore, a flat navigation surface was assumed for each robot, which is a valid assumption for an indoor environment, and the 3DOF kinematic model was used to represent the robot navigation. This is an overly simplified assumption for outdoor applications, because outdoor navigation terrains are usually uneven. For these applications, the full $SE(3)$ formulation of the proposed localization scheme needs to be considered, which will enable the proposed localization scheme, not only for outdoor applications but also for collaborative missions using both aerial and ground robots. This will be a significant achievement, as the integration of the complementary characteristics of aerial robots and ground robots can enhance the accessibility of cluttered indoor and outdoor environments. For outdoor applications, accurate knowledge about the terrain forces and the parameters are important

factors to generate the command velocities for ground robots. However, this information is generally unavailable and must be estimated. Similar limitations exist with aerial robot systems, wherein wind-disturbance parameters are not generally available and need to be estimated for better control performances. Therefore, the parameter estimation capabilities should be integrated with the full $SE(3)$ formulation when extending the proposed leader-assisted localization scheme to outdoor applications. To this end, a future research study could expand the proposed localization scheme for the $SE(3)$ domain while incorporating the terrain and wind parameter estimation capabilities for each member in the MRS.

Boundedness of Split-CI based decentralized cooperative localization : The proposed decentralized cooperative localization scheme was developed using the Split-CI algorithm. The theoretical analysis and simulation based verification for the consistency of the Split-CI based sensor fusion is reported in [137]. However, the estimation error boundedness of the Split-CI filter based decentralized cooperative localization is yet to be mathematically derived. Future research could perform rigorous mathematical analysis of the stability of Split-CI filter based decentralized cooperative localization.

7.5   List of Publications

All these contributions of this thesis are published in the following technical papers:

Journal Articles

1. Thumeera R. Wanasinghe, G. K. I. Mann, and R. G. Gosine, "Leader-Assistive Localization Framework for Multi-robot Systems with Communication and Sensing Range Constraints," submitted to Journal of Autonomous Robots (Under

review).

2. Thumeera R. Wanasinghe, G. K. I. Mann, and R. G. Gosine, "Decentralized Cooperative Localization Approach for Autonomous Multi-Robot Systems", in Hindawi Journal of Robotics, Feb. 2016

3. Thumeera R. Wanasinghe, G. K. I. Mann, and R. G. Gosine, "Distributed Leader-Assistive Localization Method for a Heterogeneous Multi-Robotic System", in IEEE Transaction of Automation Science and Engineering, July 2015.

4. Thumeera R. Wanasinghe, G. K. I. Mann, and R. G. Gosine, "Relative localization approach for combined aerial and ground robotic system", in Journal of Intelligent and Robotic Systems, January 2015.

Peer-reviewed Conference Articles

5. Thumeera R. Wanasinghe, G. K. I. Mann, and R. G. Gosine, "Stability Analysis of the Discrete-Time Cubature Kalman Filter," in 54th IEEE Conference on Decision and and Control (CDC), Dec. 2015.

6. Thumeera R. Wanasinghe, G. K. I. Mann, and R. G. Gosine, "Decentralized Cooperative Localization for Heterogeneous Multi-robot System Using Split Covariance Intersection Filter", in Canadian Conference on Computer and Robot Vision (CRV), May 2014.

7. Thumeera R. Wanasinghe, G. K. I. Mann, and R. G. Gosine, "A Jacobian free approach for multi-robot relative localization", in 27th IEEE Canadian Conference on Electrical and Computer Engineering (CCECE), May 2014.

8. Thumeera R. Wanasinghe, G. K. I. Mann, and R. G. Gosine, "Distributed collaborative localization for a heterogeneous multi-robot system", in 27th IEEE

Canadian Conference on Electrical and Computer Engineering (CCECE), May 2014.

9. Thumeera R. Wanasinghe, G. K. I. Mann, and R. G. Gosine, "Pseudo-linear measurement approach for heterogeneous multi-robot relative localization", in 16$^{\text{th}}$ International Conference on Advanced Robotics (ICAR), Nov. 2013.

Abstract-reviewed Conference Articles

10. Thumeera R. Wanasinghe, G. K. I. Mann, and R. G. Gosine, "A Consistent, and Debiased Method for Converting Information Between Coordinate Systems," in The 23$^{\text{rd}}$ Annual Newfoundland Electrical and Computer Engineering Conference (NECEC), Nov. 2014.

11. Thumeera R. Wanasinghe, G. K. I. Mann, and R. G. Gosine, "Target tracking aided decentralized multi-robot localization," in The 22$^{\text{nd}}$ Annual Newfoundland Electrical and Computer Engineering Conference (NECEC), Nov. 2013.

12. Thumeera R. Wanasinghe, G. K. I. Mann, and R. G. Gosine, "Vision-based obstacle avoidance and footsteps planner for humanoid robot," in The 21$^{\text{st}}$ Annual Newfoundland Electrical and Computer Engineering Conference (NECEC), Nov. 2012.

Appendix A

Consistent and Debiased Method for Cartesian-to-Cartesian Conversion

Converting a relative pose measurement to a global pose measurement can be defined as the converting of uncertain information from one Cartesian coordinate frame to another Cartesian coordinate frame.

Assume $\mathbf{x}$ is a random variable with mean $\bar{\mathbf{x}}$ and covariance $\mathbf{P}_x$. Additionally, assume there is an another random variable $\mathbf{y}$ which relates to $\mathbf{x}$ as follows:

$$\mathbf{y} = \mathbf{f}(\mathbf{x})$$

where $\mathbf{f}(\cdot)$ represents a nonlinear function. If the objective is to calculate the mean $\bar{\mathbf{y}}$ and covariance $\mathbf{P}_y$ of $\mathbf{y}$, given the $\bar{\mathbf{x}}$, $\mathbf{P}_x$, and $\mathbf{f}(\cdot)$, the transformed statistics are said to be consistent if the inequality

$$\mathbf{P}_y - E\left[\{\mathbf{y} - \bar{\mathbf{y}}\}\{\mathbf{y} - \bar{\mathbf{y}}\}^T\right] \geq \mathbf{0} \tag{A.1}$$

(a) $x - y$ plane

(b) $x - \phi$ plane

(c) $y - \phi$ plane

(d) 3-D $(x - y - \phi)$
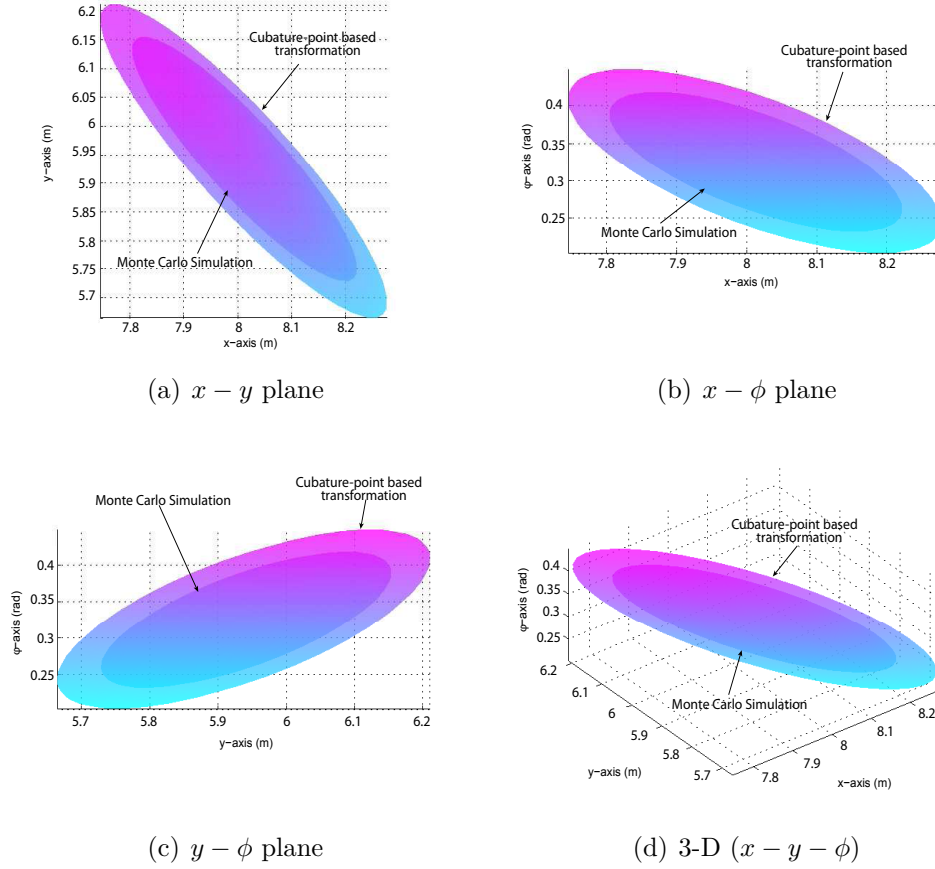
Figure A.1: Comparison of estimated covariance matrixes

holds [145]. Work presented in this study applies a cubature-point based approach to perform Cartesian-to-Cartesian coordinate transformation. Herein, a simulation study is presented to verify that the Cartesian-to-Cartesian conversion algorithm used in **Algorithm 6.2** remains above inequality.

Consider a robot team with two robots, $\mathcal{R}_1$, and $\mathcal{R}_2$. The global poses of $\mathcal{R}_1$ and $\mathcal{R}_2$ are $\begin{bmatrix} 5 & 3 & 0.6981 \end{bmatrix}^T$ and $\begin{bmatrix} 8 & 6 & 0.3491 \end{bmatrix}^T$, respectively[1]. The objective is to find the global pose of $\mathcal{R}_2$ given the global pose of $\mathcal{R}_1$, the relative pose of $\mathcal{R}_2$ with respect to $\mathcal{R}_1$ and their uncertainties. The statistics obtained from **Algorithm 6.2** were compared with

---

[1]The format of the pose vector is $\begin{bmatrix} x & y & \phi \end{bmatrix}^T$ where x and y coordinates are given in m while the orientation ϕ is given in rad.

those calculated by a Monte Carlo simulation which used 10,000 samples. Table A.1 and Figure A.1 illustrate the comparison of the statistics calculated from these two methods. It can be seen that the mean values obtained from the proposed algorithm approximately overlap those calculated by a Monte Carlo simulation which used 10,000 samples. Therefore, the conversion is unbiased. Further, it can be seen that the covariance ellipses of the cubature-point-based approach are always larger than those of the Monte Carlo simulation. This implies that the proposed Cartesian-to-Cartesian transformation holds the inequality given in (A.1). Additionally, principal axes of the covariance ellipse of the proposed approach approximately overlap those of the Monte-Carlo localization. Therefore the proposed coordinate transformation algorithm is consistent.

Table A.1: Comparison of mean global pose

	True pose	Mean from Monte Carlo simulation with 10,000 samples	Mean from cubature-points based transforation
x(m)	8	8.0127	8.0112
y(m)	6	5.9410	5.9375
ϕ(rad)	0.3491	0.3240	0.3250

Appendix B

Observability of the Pseudo-Linear Measurement-based Relative Localization Scheme for Different Relative Observation Models

Case 1: Both the range and bearing measurements are available

The observability analysis for this measurement model is presented in Section 5.2.3.

Case 2: Only the bearing measurements are available

When a system is empowered only with inter-robot relative bearing measurement capabilities, the corresponding pseudo-linear measurement function $\mathbf{h}(\mathbf{x})$ is given in (B.1).

$$\mathbf{h}_2(\mathbf{x}) = \begin{bmatrix} -xs(\theta) + yc(\theta) \\ -xc(\theta)s(\alpha) - ys(\theta)s(\alpha) + zc(\alpha) \end{bmatrix} \tag{B.1}$$

- Zero-order Lie derivatives ($\mathfrak{L}^\circ \mathbf{h}_2$)

$$\mathfrak{L}^\circ \mathbf{h}_2 = \mathbf{h}_2(\mathbf{x}) \tag{B.2}$$

Its gradient is as follows:

$$\nabla \mathfrak{L}^\circ \mathbf{h}_2 = \begin{bmatrix} -s(\theta) & c(\theta) & 0 & 0 \\ -c(\theta)s(\alpha) & -s(\theta)s(\alpha) & c(\alpha) & 0 \end{bmatrix} = \begin{bmatrix} \mathbf{h}^\circ_{pmo_2} & 0_{2\times 1} \end{bmatrix} \tag{B.3}$$

- First-order Lie derivatives ($\mathfrak{L}^1_{\mathbf{f}_2} \mathbf{h}_2$ and $\mathfrak{L}^1_{\mathbf{f}_3} \mathbf{h}_2$)

$$\begin{aligned} \mathfrak{L}^1_{f_2} \mathbf{h}_2 &= \nabla \mathfrak{L}^\circ \mathbf{h}_2 \cdot \mathbf{f}_2 \\ &= \begin{bmatrix} s(\phi - \theta) & c(\phi - \theta) & 0 \\ -c(\phi - \theta)s(\alpha) & s(\phi - \theta)s(\alpha) & c(\alpha) \end{bmatrix} \end{aligned} \tag{B.4}$$

This contains only the relative orientation component. Hence, take the gradient of $\mathfrak{L}^1_{\mathbf{f}_2} \mathbf{h}_2$ with respect to ϕ.

$$\nabla_\phi \mathfrak{L}^1_{\mathbf{f}_2} \mathbf{h}_2 = \begin{bmatrix} c(\phi - \theta) \\ s(\phi - \theta)s(\alpha) \\ -s(\phi - \theta) \\ c(\phi - \theta)s(\alpha) \\ 0 \\ 0 \end{bmatrix} \tag{B.5}$$

192

$$\mathfrak{L}^1_{f_3} \mathbf{h}_2 = \nabla \mathfrak{L}^\circ \mathbf{h}_2 \cdot \mathbf{f}_3$$

$$= \begin{bmatrix} -xc(\theta) - ys(\theta) \\ \\ xs(\alpha)s(\theta) - ys(\alpha)c(\theta) \end{bmatrix} \tag{B.6}$$

Its gradient is as follows:

$$\nabla \mathfrak{L}^1_{f_3} \mathbf{h}_2 = \begin{bmatrix} -c(\theta) & -s(\theta) & 0 & 0 \\ \\ s(\alpha)s(\theta) & -s(\alpha)c(\theta) & 0 & 0 \end{bmatrix} = \begin{bmatrix} \mathbf{h}^1_{pmo_2} & 0_{2\times 1} \end{bmatrix} \tag{B.7}$$

Lemma B.0.1. *Given the 3D bearing measurements, a sufficient condition for the system given in* (5.12) *and* (B.1) *to be locally weakly observable is 1)* $\mathbf{v}_i \neq 0$ *and 2)* $\omega_{z,j} \neq 0$.

Proof. Given the 3D bearing measurements, the observability matrix for the system expressed in (5.12) and (B.1) can be constructed using (B.3), (B.5) and (B.7) and is given as follows:

$$\mathcal{O}_2 = \begin{bmatrix} \nabla \mathfrak{L}^\circ \mathbf{h}_2 \\ \\ \nabla \mathfrak{L}^1_{\mathbf{f}_3} \mathbf{h}_2 \\ \\ \nabla \mathfrak{L}^1_{\mathbf{f}_2} \mathbf{h}_2 \end{bmatrix} = \begin{bmatrix} \mathbf{h}^\circ_{pmo_2} & 0_{2\times 1} \\ \\ \mathbf{h}^1_{pmo_2} & 0_{2\times 1} \\ \\ 0_{6\times 3} & \nabla_\phi \mathfrak{L}^1_{\mathbf{f}_2} \mathbf{h}_2 \end{bmatrix} \tag{B.8}$$

It is sufficient to show that both $\begin{bmatrix} \mathbf{h}^\circ_{pmo_2} \\ \mathbf{h}^1_{pmo_2} \end{bmatrix}$ and $\nabla_\phi \mathfrak{L}^1_{\mathbf{f}_2} \mathbf{h}_2$ are full rank in order to prove that the $\mathcal{O}_2$ retains full column rank condition.

$$\det \left(\begin{bmatrix} \mathbf{h}^\circ_{pmo_2} \\ \mathbf{h}^1_{pmo_2} \end{bmatrix}^T \begin{bmatrix} \mathbf{h}^\circ_{pmo_2} \\ \mathbf{h}^1_{pmo_2} \end{bmatrix} \right) = 1 - s(\alpha)^4 \neq 0 \ \text{ if } \alpha \neq \pi/2 \tag{B.9}$$

$$\det\left((\nabla_\phi\mathfrak{L}^1_{\mathbf{f}_2}\mathbf{h}_2)^T(\nabla_\phi\mathfrak{L}^1_{\mathbf{f}_2}\mathbf{h}_2)\right) = 1 + s(\alpha)^2 \neq 0 \qquad (\text{B.10})$$

According to (B.9) and (B.10), $\begin{bmatrix} \mathbf{h}^\circ_{pmo_2} \\ \mathbf{h}^1_{pmo_2} \end{bmatrix}$ and $\nabla_\phi\mathfrak{L}^1_{\mathbf{f}_2}\mathbf{h}_2$ are full rank. Hence, $\mathcal{O}_2$ has full column rank; thus, the observability rank condition is satisfied. Therefore, from Theorem 1, the system is locally weakly observable when 1) $\mathbf{v}_i \neq 0$ and 2) $\omega_{z,j} \neq 0$. In other words, the pseudo-linear bearing measurement based relative localization scheme that is described in (5.12) and (B.1) is locally weakly observable when the observed robot linear velocities and the observing robot angular velocities are not equal to zero. $\qquad\square$

It is important to note that $\mathbf{v}_i \neq 0$ and $\mathbf{v}_j \neq 0$ are not sufficient conditions, as shown below, to guarantee the observability when bearing measurements are given in pseudo-linear format, although they are sufficient conditions for the system observability when considering the nonlinear bearing measurements in the Cartesian coordinate system [123].

Consider an exteroceptive sensory system which is capable of measuring only the relative bearing for observed robots as given in (B.1). Furthermore, assume zero-order Lie derivatives ((B.2)-(B.3)) and first-order Lie derivatives ((B.4)-(B.5)) are available.

- Compute the first order Lie derivative $\mathfrak{L}^1_{\mathbf{f}_1}\mathbf{h}_2$

$$
\begin{aligned}
\mathfrak{L}^1_{f_1}\mathbf{h}_2 &= \nabla\mathfrak{L}^\circ\mathbf{h}_2 \cdot \mathbf{f}_1 \\
&= \begin{bmatrix} s(\theta) & -c(\theta) & 0 \\ s(\alpha)c(\theta) & s(\alpha)s(\theta) & -c(\alpha) \end{bmatrix}
\end{aligned}
\qquad (\text{B.11})
$$

194

This is independent from the system states; thus, the resulting gradient matrix is as follows:

$$\nabla \mathfrak{L}_{f_1}^1 \mathbf{h}_2 = 0_{6 \times 4} \tag{B.12}$$

The observability matrix then can be defined as (B.13).

$$\mathcal{O}_3 = \begin{bmatrix} \nabla \mathfrak{L}^\circ \mathbf{h}_2 \\ \nabla \mathfrak{L}_{\mathbf{f}_1}^1 \mathbf{h}_2 \\ \nabla \mathfrak{L}_{\mathbf{f}_2}^1 \mathbf{h}_2 \end{bmatrix} = \begin{bmatrix} \mathbf{h}_{pmo_2}^\circ & 0_{2 \times 1} \\ 0_{6 \times 3} & 0_{6 \times 1} \\ 0_{6 \times 3} & \nabla_\phi \mathfrak{L}_{\mathbf{f}_2}^1 \mathbf{h}_2 \end{bmatrix} \tag{B.13}$$

The rank of the observability matrix $\mathcal{O}_3$ is three ($\text{rank}(\mathcal{O}_3) = 3$). This is less than the number of the state variables (DOF) in the state vector given in (5.1). Hence, $\mathbf{v}_c \neq 0$ and $\mathbf{v}_l \neq 0$ are not sufficient conditions to guarantee the observability when the bearing measurements are given in pseudo-linear format.

Case 3: Only the range measurements are available

The bearing measurements are required in order to construct a pseudo-linear measurement model as expressed in (5.3). Hence, no pseudo-linear format exists for a range only exteroceptive sensory system. Thus, the nonlinear range measurement has to be employed with direct linearization for sensor fusion. Then the sufficient condition for the system to be locally weakly observable is 1) $\mathbf{v}_i \neq 0$ and 2) $\mathbf{v}_j \neq 0$ [123].

Bibliography

[1] L. Kuotsan and W. Chulun, "A technical analysis of autonomous floor cleaning robots based on US granted patents," *European International Journal of Science and Technology*, vol. 2, no. 7, pp. 199–216, Sep 2013.

[2] P. S. Schenker, T. L. Huntsberger, P. Pirjanian, E. T. Baumgartner, H. Aghazarian, A. Trebi-Ollennu, P. C. Leger, Y. Cheng, P. G. Backes, E. Tunstel *et al.*, "Robotic automation for space: planetary surface exploration, terrain-adaptive mobility, and multirobot cooperative tasks," in *Intelligent Systems and Advanced Manufacturing*. International Society for Optics and Photonics, 2001, pp. 12–28.

[3] A. Elfes, "Using occupancy grids for mobile robot perception and navigation," *Computer*, vol. 22, no. 6, pp. 46–57, 1989.

[4] P. Chand and D. A. Carnegie, "Mapping and exploration in a hierarchical heterogeneous multi-robot system using limited capability robots," *Robotics and Autonomous Systems*, vol. 61, no. 6, pp. 565–579, 2013.

[5] M. K. Habib, "Humanitarian demining: Reality and the challenge of technology-the state of the arts." *International Journal of Advanced Robotic Systems*, vol. 4, no. 2, 2007.

[6] K. Alex, D. Mellinger, C. Powers, and V. Kumar, "Towards a swarm of agile micro quadrotors," *Autonomous Robots*, vol. 35, no. 4, pp. 287–300, 2013.

[7] T. Balch and R. C. Arkin, "Behavior-based formation control for multirobot teams," *IEEE Transactions on Robotics and Automation*, vol. 14, no. 6, pp. 926–939, Dec 1998.

[8] N. Michael, S. Shen, K. Mohta, Y. Mulgaonkar, V. Kumar, K. Nagatani, Y. Okada, S. Kiribayashi, K. Otake, K. Yoshida, and K. Ohno, "Collaborative mapping of an earthquake-damaged building via ground and aerial robots," *Journal of Field Robotics*, vol. 29, no. 5, pp. 832–841, 2012.

[9] O. De Silva, G. Mann, and R. Gosine, "Development of a relative localization scheme for ground-aerial multi-robot systems," in *IEEE/RSJ International Conference on Intelligent Robots and Systems (IROS)*, Oct 2012, pp. 870–875.

[10] T. R. Wanasinghe, G. K. I. Mann, and R. G. Gosine, "Pseudo-linear measurement approach for heterogeneous multi-robot relative localization," in *16th International Conference on Advanced Robotics (ICAR)*, Nov 2013.

[11] R. Kurazume, S. Nagata, and S. Hirose, "Cooperative positioning with multiple robots," in *IEEE International Conference on Robotics and Automation (ICRA)*, vol. 2, May 1994, pp. 1250–1257.

[12] S. Roumeliotis and G. A. Bekey, "Distributed multirobot localization," *IEEE Transactions on Robotics and Automation*, vol. 18, no. 5, pp. 781–795, Oct. 2002.

[13] T. R. Wanasinghe, G. K. I. Mann, and R. G. Gosine, "Decentralized cooperative localization for heterogeneous multi-robot system using split covariance inter-

section filter," in *Canadian Conference on Computer and Robot Vision (CRV)*, May 2014, pp. 167–174.

[14] I. Rekleitis, G. Dudek, and E. Milios, "Probabilistic cooperative localization and mapping in practice," in *IEEE International Conference on Robotics and Automation (ICRA)*, vol. 2, Sep. 2003, pp. 1907–1912.

[15] ——, "Experiments in free-space triangulation using cooperative localization," in *IEEE/RSJ International Conference on Intelligent Robots and Systems (IROS)*, vol. 2, Oct 2003, pp. 1777–1782.

[16] R. Kurazume, S. Hirose, S. Nagata, and N. Sashida, "Study on cooperative positioning system (basic principle and measurement experiment)," in *IEEE International Conference on Robotics and Automation (ICRA)*, vol. 2, Apr. 1996, pp. 1421–1426.

[17] N. Trawny and T. Barfoot, "Optimized motion strategies for cooperative localization of mobile robots," in *IEEE International Conference on Robotics and Automation (ICRA)*, vol. 1, Apr. 2004, pp. 1027–1032.

[18] S. Tully, G. Kantor, and H. Choset, "Leap-frog path design for multi-robot cooperative localization," in *Field and Service Robotics*, ser. Springer Tracts in Advanced Robotics, A. Howard, K. Iagnemma, and A. Kelly, Eds. Springer Berlin Heidelberg, 2010, vol. 62, pp. 307–317.

[19] E. D. Nerurkar and S. Roumeliotis, "Asynchronous multi-centralized cooperative localization," in *IEEE/RSJ International Conference on Intelligent Robots and Systems (IROS)*, Oct 2010, pp. 4352–4359.

[20] S. Roumeliotis and G. A. Bekey, "Collective localization: a distributed Kalman filter approach to localization of groups of mobile robots," in *IEEE International*

Conference on Robotics and Automation (ICRA), vol. 3, 2000, pp. 2958–2965 vol.3.

[21] D. Fox, W. Burgard, H. Kruppa, and S. Thrun, "A probabilistic approach to collaborative multi-robot localization," *Autonomous robots*, vol. 8, no. 3, pp. 325–344, 2000.

[22] A. Prorok and A. Martinoli, "A reciprocal sampling algorithm for lightweight distributed multi-robot localization," in *IEEE/RSJ International Conference on Intelligent Robots and Systems (IROS)*, Sep. 2011, pp. 3241–3247.

[23] A. Bahr, M. Walter, and J. Leonard, "Consistent cooperative localization," in *IEEE International Conference on Robotics and Automation (ICRA)*, May 2009, pp. 3415–3422.

[24] T. R. Wanasinghe, G. K. I. Mann, and R. G. Gosine, "Decentralized cooperative localization approach for autonomous multirobot systems," *Journal of Robotics*, Feb. 2016.

[25] L. E. Parker and A. Howard, "Experiments with a large heterogeneous mobile robot team: Exploration, mapping, deployment and detection," *International Journal of Robotics Research*, vol. 25, pp. 431–447, 2006.

[26] T. R. Wanasinghe, G. K. I. Mann, and R. G. Gosine, "Distributed leader-assistive localization method for a heterogeneous multirobotic system," *IEEE Transaction on Automation Science and Engineering*, vol. 12, no. 3, pp. 795–809, July 2015.

[27] R. Sharma and C. Taylor, "Cooperative navigation of MAVs in GPS denied areas," in *IEEE International Conference on Multisensor Fusion and Integration for Intelligent Systems (MFI)*, Aug 2008, pp. 481–486.

[28] N. E. Özkucur, B. Kurt, and H. L. Akın, "A collaborative multi-robot localization method without robot identification," in *RoboCup 2008: Robot Soccer World Cup XII.* Springer, 2009, pp. 189–199.

[29] A. Prorok, A. Bahr, and A. Martinoli, "Low-cost collaborative localization for large-scale multi-robot systems," in *IEEE International Conference on Robotics and Automation (ICRA)*, May 2012, pp. 4236–4241.

[30] A. Howard, M. Mataric, and G. Sukhatme, "Cooperative relative localization for mobile robot teams: an ego-centric approach," in *Naval Research Lab. Workshop on Multi-Robot Systems*, 2003, pp. 65—-76.

[31] F. Rivard, J. Bisson, F. Michaud, and D. Letourneau, "Ultrasonic relative positioning for multi-robot systems," in *Robotics and Automation, 2008. ICRA 2008. IEEE International Conference on*, 2008, pp. 323–328.

[32] S. J. Julier and J. K. Uhlmann, "Consistent debiased method for converting between polar and cartesian coordinate systems," in *Proc. AeroSense: 11th Int. Symp. Aerospace/Defense Sensing, Simulation and Controls.* International Society for Optics and Photonics, 1997, pp. 110–121.

[33] J. L. Crassidis, F. L. Markley, and Y. Cheng, "Survey of nonlinear attitude estimation methods," *Journal of Guidance, Control, and Dynamics*, vol. 30, no. 1, pp. 12–28, 2007.

[34] S. J. Julier and J. K. Uhlmann, "A new extension of the Kalman filter to nonlinear systems," in *Proc. AeroSense: 11th Int. Symp. Aerospace/Defense Sensing, Simulation and Controls.* International Society for Optics and Photonics, 1997, pp. 182–193.

[35] ——, "Unscented filtering and nonlinear estimation," *Proceedings of the IEEE*, vol. 92, no. 3, pp. 401–422, 2004.

[36] I. Arasaratnam and S. Haykin, "Cubature Kalman filters," *IEEE Transactions on Automatic Control*, vol. 54, no. 6, pp. 1254–1269, 2009.

[37] S. Julier, J. Uhlmann, and H. Durrant-Whyte, "A new method for the nonlinear transformation of means and covariances in filters and estimators," *IEEE Transactions on Automatic Control*, vol. 45, no. 3, pp. 477–482, 2000.

[38] S. J. Julier, "The scaled unscented transformation," in *Proceedings of the American Control Conference*, vol. 6.   IEEE, 2002, pp. 4555–4559.

[39] K. Xiong, H. Zhang, and C. Chan, "Performance evaluation of UKF-based nonlinear filtering," *Automatica*, vol. 42, no. 2, pp. 261–270, 2006.

[40] K. P. B. Chandra, D.-W. Gu, and I. Postlethwaite, "Cubature Kalman filter based localization and mapping," in *18th International Federantion of Automatic Control (IFAC) World Congress*, Sep 2011, pp. 2121–2125.

[41] Y. Song, Q. Li, Y. Kang, and Y. Song, "CFastSLAM: A new jacobian free solution to slam problem," in *IEEE International Conference on Robotics and Automation (ICRA)*.   IEEE, 2012, pp. 3063–3068.

[42] I. Arasaratnam, S. Haykin, and T. R. Hurd, "Cubature kalman filtering for continuous-discrete systems: theory and simulations," *IEEE Transactions on Signal Processing*, vol. 58, no. 10, pp. 4977–4993, 2010.

[43] J. J. Leonard, H. F. Durrant-Whyte, and I. J. Cox, "Dynamic map building for an autonomous mobile robot," *The International Journal of Robotics Research*, vol. 11, no. 4, pp. 286–298, 1992.

[44] D. Avitzour, "A maximum likelihood approach to data association," *IEEE Transactions on Aerospace and Electronic Systems*, vol. 28, no. 2, pp. 560–566, Apr 1992.

[45] J. Neira, J. Tardos, J. Horn, and G. Schmidt, "Fusing range and intensity images for mobile robot localization," *IEEE Transactions on Robotics and Automation*, vol. 15, no. 1, pp. 76–84, Feb 1999.

[46] H. J. S. Feder, J. J. Leonard, and C. M. Smith, "Adaptive mobile robot navigation and mapping," *The International Journal of Robotics Research*, vol. 18, no. 7, pp. 650–668, 1999.

[47] S. Blackman, "Multiple hypothesis tracking for multiple target tracking," *IEEE Aerospace and Electronic Systems Magazine*, vol. 19, no. 1, pp. 5–18, Jan 2004.

[48] Y. Bar-Shalom, F. Daum, and J. Huang, "The probabilistic data association filter," *IEEE Control Systems*, vol. 29, no. 6, pp. 82–100, Dec 2009.

[49] K. Y. Leung, Y. Halpern, T. D. Barfoot, and H. H. Liu, "The UTIAS multi-robot cooperative localization and mapping dataset," *The International Journal of Robotics Research*, vol. 30, no. 8, pp. 969–974, 2011.

[50] O. de Silva, G. K. I. Mann, and R. G. Gosine, "An ultrasonic and vision-based relative positioning sensor for multirobot localization," *IEEE Sensors Journal*, vol. 15, no. 3, pp. 1716–1726, March 2015.

[51] K. Y. K. Leung, "Cooperative localization and mapping in sparsely-communicating robot networks," PhD thesis, Department of Aerospace Science and Engineering, University of Toronto, 2012.

[52] D. Kurth, G. Kantor, and S. Singh, "Experimental results in range-only localization with radio," in *IEEE/RSJ International Conference on Intelligent Robots and Systems (IROS)*, vol. 1, 2003, pp. 974–979.

[53] E. Olson, J. J. Leonard, and S. Teller, "Robust range-only beacon localization," *IEEE Journal of Oceanic Engineering*, vol. 31, no. 4, pp. 949–958, 2006.

[54] R. Sharma, S. Quebe, R. Beard, and C. Taylor, "Bearing-only cooperative localization," *Journal of Intelligent & Robotic Systems*, vol. 72, no. 3-4, pp. 429–440, 2013.

[55] K. E. Bekris, M. Click, and E. Kavraki, "Evaluation of algorithms for bearing-only slam," in *IEEE International Conference on Robotics and Automation (ICRA)*, 2006, pp. 1937–1943.

[56] A. Farina, "Target tracking with bearings–only measurements," *Signal processing*, vol. 78, no. 1, pp. 61–78, 1999.

[57] L. Montesano, J. Gaspar, J. Santos-Victor, and L. Montano, "Cooperative localization by fusing vision-based bearing measurements and motion," in *IEEE/RSJ International Conference on Intelligent Robots and Systems (IROS)*, Aug. 2005, pp. 2333–2338.

[58] J. Spletzer, A. Das, R. Fierro, C. Taylor, V. Kumar, and J. Ostrowski, "Cooperative localization and control for multi-robot manipulation," in *IEEE/RSJ International Conference on Intelligent Robots and Systems (IROS)*, vol. 2, 2001, pp. 631–636.

[59] L. Carrillo-Arce, E. Nerurkar, J. Gordillo, and S. Roumeliotis, "Decentralized multi-robot cooperative localization using covariance intersection," in

IEEE/RSJ International Conference on Intelligent Robots and Systems (IROS), Nov 2013, pp. 1412–1417.

[60] R. Kurazume and S. Hirose, "An experimental study of a cooperative positioning system," *Autonomous Robots*, vol. 8, no. 1, pp. 43–52, 2000.

[61] ——, "Study on cooperative positioning system: optimum moving strategies for CPS-III," in *IEEE International Conference on Robotics and Automation (ICRA)*, vol. 4, May 1998, pp. 2896–2903.

[62] ——, "Development of a cleaning robot system with cooperative positioning system," *Autonomous Robots*, vol. 9, no. 3, pp. 237–246, 2000.

[63] R. Kurazume, Y. Noda, Y. Tobata, K. Lingemann, Y. Iwashita, and T. Hasegawa, "Laser-based geometric modeling using cooperative multiple mobile robots," in *IEEE International Conference on Robotics and Automation (ICRA)*, May 2009, pp. 3200–3205.

[64] Y. Tobata, R. Kurazume, Y. Noda, K. Lingemann, Y. Iwashita, and T. Hasegawa, "Laser-based geometrical modeling of large-scale architectural structures using co-operative multiple robots," *Autonomous Robots*, vol. 32, no. 1, pp. 49–62, 2012.

[65] C.-H. Chang, S.-C. Wang, and C.-C. Wang, "Vision-based cooperative simultaneous localization and tracking," in *IEEE International Conference on Robotics and Automation (ICRA)*, May 2011, pp. 5191–5197.

[66] K. Leung, T. Barfoot, and H. Liu, "Decentralized localization of sparsely-communicating robot networks: A centralized-equivalent approach," *IEEE Transactions on Robotics*, vol. 26, no. 1, pp. 62–77, Feb. 2010.

[67] A. Martinelli, F. Pont, and R. Siegwart, "Multi-robot localization using relative observations," in *IEEE International Conference on Robotics and Automation (ICRA)*, Apr. 2005, pp. 2797–2802.

[68] E. D. Nerurkar, S. Roumeliotis, and A. Martinelli, "Distributed maximum a posteriori estimation for multi-robot cooperative localization," in *IEEE International Conference on Robotics and Automation (ICRA)*, May 2009, pp. 1402–1409.

[69] T. Bailey, M. Bryson, H. Mu, J. Vial, L. McCalman, and H. Durrant-Whyte, "Decentralised cooperative localisation for heterogeneous teams of mobile robots," in *IEEE International Conference on Robotics and Automation (ICRA)*, May 2011, pp. 2859–2865.

[70] H. Mu, T. Bailey, P. Thompson, and H. Durrant-Whyte, "Decentralised solutions to the cooperative multi-platform navigation problem," *IEEE Transactions on Aerospace and Electronic Systems*, vol. 47, no. 2, pp. 1433–1449, April 2011.

[71] A. Martinelli, "Improving the precision on multi robot localization by using a series of filters hierarchically distributed," in *IEEE/RSJ International Conference on Intelligent Robots and Systems (IROS)*, Oct 2007, pp. 1053–1058.

[72] N. Karam, F. Chausse, R. Aufrere, and R. Chapuis, "Localization of a group of communicating vehicles by state exchange," in *IEEE/RSJ International Conference on Intelligent Robots and Systems (IROS)*, Oct. 2006, pp. 519–524.

[73] ——, "Cooperative multi-vehicle localization," in *IEEE Intelligent Vehicles Symposium*, 2006, pp. 564–570.

[74] S. Panzieri, F. Pascucci, and R. Setola, "Multirobot localisation using interlaced extended Kalman filter," in *IEEE/RSJ International Conference on Intelligent Robots and Systems (IROS)*, Oct. 2006, pp. 2816–2821.

[75] A. Howard, M. J. Mataric, and G. Sukhatme, "Putting the 'i' in 'team': an ego-centric approach to cooperative localization," in *IEEE International Conference on Robotics and Automation (ICRA)*, vol. 1, 2003, pp. 868–874.

[76] H. Durrant-Whyte, M. Stevens, and E. Nettleton, "Data fusion in decentralised sensing networks," in *Proceedings of the 4th International Conference on Information Fusion*, 2001, pp. 302–307.

[77] Y. Bar-Shalom, P. K. Willett, and X. Tian, *Tracking and data fusion: a handbook of algorithms.* YBS publishing, 2011.

[78] J. Curn, D. C. Marinescu, N. O'Hara, and V. Cahill, "Data incest in cooperative localisation with the common past-invariant ensemble kalman filter," in *Proceedings of the 16th International Conference on Information Fusion, (FUSION)*, 2013, pp. 68–76.

[79] G. Hoffmann and C. Tomlin, "Decentralized cooperative collision avoidance for acceleration constrained vehicles," in *47th IEEE Conference on Decision and Control, CDC*, 2008, pp. 4357–4363.

[80] Y. Ikemoto, Y. Hasegawa, F. T, and K. Matsuda, "Graduated spatial pattern formation of robot group," in *Information Science*, vol. 171.

[81] G. Lee and N. Y. Chong, "Decentralized formation control for small-scale robot teams with anonymity," *Mechatronics*, vol. 19, no. 1, pp. 85 – 105, 2009.

[82] B. Shucker, T. Murphey, and J. K. Bennett, "Convergence-preserving switching for topology-dependent decentralized systems," *in IEEE Transactions on Robotics*, vol. 24, no. 6, pp. 1405–1415, 2008.

[83] G. Antonelli, F. Arrichiello, and S. Chiaverini, "Flocking for multi-robot systems via the null-space-based behavioral control," in *IEEE/RSJ International Conference on Intelligent Robots and Systems (IROS)*, 2008, pp. 1409–1414.

[84] T. S. Stirling, S. Wischmann, and D. Floreano, "Energy-efficient indoor search by swarms of simulated flying robots without global information," *Swarm Intelligence*, vol. 4, no. 2, pp. 117–143, 2010.

[85] A. Howard, M. J. Mataric, and G. S. Sukhatme, "Cooperative relative localization for mobile robot teams: An egocentric approach," in *in Proceedings of the Naval Research Laboratory Workshop on Multi-Robot Systems*, 2003, pp. 65–76.

[86] F. Rivard, J. Bisson, F. Michaud, and D. Letourneau, "Ultrasonic relative positioning for multi-robot systems," in *IEEE International Conference on Robotics and Automation (ICRA)*, May 2008, pp. 323–328.

[87] A. Milella, F. Pont, and R. Siegwart, "Model-based relative localization for cooperative robots using stereo vision," in *Twelfth annual Conference on Mechatronics and Machine Vision in Practice*, 2005.

[88] T. R. Wanasinghe, G. K. I. Mann, and R. G. Gosine, "Relative localization approach for combined aerial and ground robotic system," *Journal of Intelligent and Robotic Systems*, vol. 77, no. 1, pp. 113–133, 2015.

[89] O. de Silva, G. K. I. Mann, and R. G. Gosine, "Relative localization with symmetry preserving observers," in *IEEE 27th Canadian Conference on Electrical and Computer Engineering (CCECE)*, May 2014.

[90] T. R. Wanasinghe, G. K. I. Mann, and R. G. Gosine, "A jacobian free approach for multi-robot relative localization," in *IEEE Canadian Conference on Electrical and Computer Engineering (CCECE)*, May 2014.

[91] L. Mao, J. Chen, Z. Li, and D. Zhang, "Relative localization method of multiple micro robots based on simple sensors," *International Journal of Advanced Robotic Systems*, vol. 10, 2013.

[92] A. Franchi, G. Oriolo, and P. Stegagno, "Mutual localization in a multi-robot system with anonymous relative position measures," in *IEEE/RSJ International Conference on Intelligent Robots and Systems*, Oct 2009, pp. 3974–3980.

[93] ——, "On the solvability of the mutual localization problem with anonymous position measures," in *IEEE International Conference on Robotics and Automation (ICRA)*, May 2010, pp. 3193–3199.

[94] M. Cognetti, P. Stegagno, A. Franchi, G. Oriolo, and H. H. Bülthoff, "3-d mutual localization with anonymous bearing measurements," in *IEEE International Conference on Robotics and Automation (ICRA)*. IEEE, 2012, pp. 791–798.

[95] A. Franchi, G. Oriolo, and P. Stegagno, "Mutual localization in multi-robot systems using anonymous relative measurements," *International Journal of Robotics Research*, vol. 32, no. 11, pp. 1302–1322, 2013.

[96] H. Liu, H. Darabi, P. Banerjee, and J. Liu, "Survey of wireless indoor positioning techniques and systems," *IEEE Transactions on Systems, Man, and Cybernetics, Part C (Applications and Reviews)*, vol. 37, no. 6, pp. 1067–1080, Nov 2007.

[97] N. B. Priyantha, A. Chakraborty, and H. Balakrishnan, "The cricket location-support system," in *Proceedings of the 6th annual international conference on Mobile computing and networking.* ACM, 2000, pp. 32–43.

[98] M. Hazas and A. Ward, "A novel broadband ultrasonic location system," in *International Conference on Ubiquitous Computing.* Springer, 2002, pp. 264–280.

[99] A. Mourikis and S. Roumeliotis, "Optimal sensor scheduling for resource-constrained localization of mobile robot formations," *IEEE Transactions on Robotics*, vol. 22, no. 5, pp. 917–931, Oct 2006.

[100] E. D. Nerurkar, K. X. Zhou, and S. Roumeliotis, "A hybrid estimation framework for cooperative localization under communication constraints," in *IEEE/RSJ International Conference on Intelligent Robots and Systems (IROS)*, Sept 2011, pp. 502–509.

[101] E. Nerurkar and S. Roumeliotis, "A communication-bandwidth-aware hybrid estimation framework for multi-robot cooperative localization," in *IEEE/RSJ International Conference on Intelligent Robots and Systems (IROS)*, Nov 2013, pp. 1418–01 425.

[102] I. Rekleitis, G. Dudek, and E. Milios, "Multi-robot cooperative localization: a study of trade-offs between efficiency and accuracy," in *IEEE/RSJ International Conference on Intelligent Robots and Systems (IROS)*, vol. 3, 2002, pp. 2690–2695.

[103] S. I. Roumeliotis and I. M. Rekleitis, "Propagation of uncertainty in cooperative multirobot localization: Analysis and experimental results," *Autonomous Robots*, vol. 17, no. 1, pp. 41–54, 2004.

[104] A. Mourikis and S. Roumeliotis, "Performance analysis of multirobot cooperative localization," *Robotics, IEEE Transactions on*, vol. 22, no. 4, pp. 666–681, Aug. 2006.

[105] Y. Bar-Shalom, "Update with out-of-sequence measurements in tracking: exact solution," *IEEE Transactions on Aerospace and Electronic Systems*, vol. 38, no. 3, pp. 769–777, Jul 2002.

[106] S. Challa, R. J. Evans, X. Wang, and J. Legg, "A fixed-lag smoothing solution to out-of-sequence information fusion problems," *Journal of Communications in Information and Systems*, vol. 2, no. 4, pp. 327–350, Dec 2002.

[107] "A bayesian solution and its approximations to out-of-sequence measurement problems," *Information Fusion*, vol. 4, no. 3, pp. 185–199, 2003.

[108] M. Mallick, S. Schmidt, L. Y. Pao, and K. Chang, "Out-of-sequence track filtering using the decorrelated pseudo-measurement approach," in *Defense and Security*. International Society for Optics and Photonics, 2004, pp. 154–166.

[109] K. Zhang, X. Li, and Y. Zhu, "Optimal update with out-of-sequence measurements," *IEEE Transactions on Signal Processing*, vol. 53, no. 6, pp. 1992–2004, June 2005.

[110] Y. Bar-Shalom, H. Chen, and M. Mallick, "One-step solution for the multi-step out-of-sequence-measurement problem in tracking," *IEEE Transactions on Aerospace and Electronic Systems*, vol. 40, no. 1, pp. 27–37, Jan 2004.

[111] M. Mallick, S. Coraluppi, and C. Carthel, "Advances in asynchronous and decentralized estimation," in *IEEE Proceedings Aerospace Conference*, vol. 4, 2001.

[112] M. Mallick, J. Krant, and Y. Bar-Shalom, "Multi-sensor multi-target tracking using out-of-sequence measurements," in *Proceedings of the Fifth International Conference on Information Fusion*, vol. 1. IEEE, 2002, pp. 135–142.

[113] Z. K. S., X. R. Li, H. Chen, and M. Mallick, "Multi-sensor multi-target tracking with out-of-sequence measurements," in *Proceedings of the Sixth International Conference on Information Fusion*, 2003, pp. 672–679.

[114] F. Lu and E. Milios, "Globally consistent range scan alignment for environment mapping," *Autonomous robots*, vol. 4, no. 4, pp. 333–349, 1997.

[115] T. R. Wanasinghe, G. K. I. Mann, and R. G. Gosine, "Distributed collaborative localization for a heterogeneous multi-robot system," in *IEEE Canadian Conference on Electrical and Computer Engineering (CCECE)*, May 2014.

[116] Y. Kosuge and T. Matsuzaki, "The optimum gate shape and threshold for target tracking," in *SICE Annual Conference*, vol. 2, Aug 2003, pp. 2152–2157.

[117] R. Simpson and J. Revell, "Towards a taxonomy of performance metrics, bounds and tests for tracking and slam algorithms," in *SEAS DTC Technical Conference*, 2009.

[118] H.-J. Von Der Hardt, D. Wolf, and R. Husson, "The dead reckoning localization system of the wheeled mobile robot ROMANE," in *IEEE/SICE/RSJ International Conference on Multisensor Fusion and Integration for Intelligent Systems*, 1996, pp. 603–610.

[119] Y. Bar-Shalom, X. R. Li, and T. Kirubarajan, *Estimation with applications to tracking and navigation: theory algorithms and software.* John Wiley & Sons, 2004.

[120] W. Li, T. Zhang, and K. Kuhnlenz, "A vision-guided autonomous quadrotor in an air-ground multi-robot system," in *IEEE International Conference on Robotics and Automation (ICRA)*, 2011, pp. 2980–2985.

[121] J. Fenwick, P. Newman, and J. Leonard, "Cooperative concurrent mapping and localization," in *IEEE International Conference on Robotics and Automation (ICRA)*, vol. 2, 2002, pp. 1810–1817.

[122] P. Stegagno, M. Cognetti, L. Rosa, P. Peliti, and G. Oriolo, "Relative localization and identification in a heterogeneous multi-robot system," in *IEEE International Conference on Robotics and Automation (ICRA)*, May 2013, pp. 1857–1864.

[123] N. Trawny, X. Zhou, K. Zhou, and S. Roumeliotis, "Interrobot transformations in 3-D," *Robotics, IEEE Transactions on*, vol. 26, no. 2, pp. 226–243, 2010.

[124] C. Pathiranage, K. Watanabe, and K. Izumi, "Simultaneous localization and mapping (slam) based on pseudolinear measurement model with a bias reduction approach," in *Industrial and Information Systems, 2007. ICIIS 2007. International Conference on*, 2007, pp. 73–78.

[125] C. Pathiranage, K. Watanabe, B. Jayasekara, and K. Izumi, "Simultaneous localization and mapping: A pseudolinear Kalman filter (PLKF) approach," in *Information and Automation for Sustainability, 2008. ICIAFS 2008. 4th International Conference on*, 2008, pp. 61–66.

[126] J. L. Speyer and T. L. Song, "A comparison between the pseudomeasurement and extended Kalman observers," in *20th IEEE Conference on Decision and Control including the Symposium on Adaptive Processes*, Dec 1981, pp. 324–329.

[127] T. Song, J. Ahn, and C. Park, "Suboptimal filter design with pseudomeasurements for target tracking," *Aerospace and Electronic Systems, IEEE Transactions on*, vol. 24, no. 1, pp. 28–39, 1988.

[128] P. S. Maybeck, *Stochastic models, estimation and control. Volume I.*, A. Press, Ed., 1979.

[129] W. J. Rugh, *Linear system theory*, 2nd ed. Upper Saddle River, N.J.: Prentice Hall„ 1996.

[130] R. Sharma, R. Beard, C. Taylor, and S. Quebe, "Graph-based observability analysis of bearing-only cooperative localization," *Robotics, IEEE Transactions on*, vol. 28, no. 2, pp. 522–529, 2012.

[131] A. Martinelli and R. Siegwart, "Observability analysis for mobile robot localization," in *Intelligent Robots and Systems, 2005. (IROS 2005). 2005 IEEE/RSJ International Conference on*, 2005, pp. 1471–1476.

[132] Z. M. Kassas and T. E. Humphreys, "Observability analysis of opportunistic navigation with pseudorange measurements," in *In Proceedings of AIAA Guidance, Navigation, and Control Conference (GNC'12)*, Aug. 2012, pp. 4760–4775.

[133] R. Hermann and A. J. Krener, "Nonlinear controllability and observability," *Automatic Control, IEEE Transactions on*, vol. 22, no. 5, pp. 728–740, 1977.

[134] M. Cognetti, P. Stegagno, A. Franchi, G. Oriolo, and H. Bulthoff, "3-d mutual localization with anonymous bearing measurements," in *IEEE International Conference on Robotics and Automation (ICRA)*, May 2012, pp. 791–798.

[135] S. Julier and J. Uhlmann, *General Decentralized Data Fusion With Covariance Intersection (CI)*. CRC Press: Boca Raton FL, USA., 2001, ch. Handbook of Data Fusion.

[136] ——, "A non-divergent estimation algorithm in the presence of unknown correlations," in *Proceedings of the American Control Conference*, vol. 4, Jun 1997, pp. 2369–2373.

[137] H. Li, F. Nashashibi, and M. Yang, "Split covariance intersection filter: Theory and its application to vehicle localization," *IEEE Transactions on Intelligent Transportation Systems*, vol. 14, no. 4, pp. 1860–1871, Dec 2013.

[138] L. Carrillo-Arce, E. Nerurkar, J. Gordillo, and S. Roumeliotis, "Decentralized multi-robot cooperative localization using covariance intersection," in *IEEE/RSJ International Conference on Intelligent Robots and Systems (IROS)*, Nov 2013, pp. 1412–1417.

[139] J. Sijs, M. Lazar, and P. v.d.Bosch, "State fusion with unknown correlation: Ellipsoidal intersection," in *American Control Conference (ACC)*, June 2010, pp. 3992–3997.

[140] D. Zelazo, A. Franchi, F. Allgöwer, H. H. Bülthoff, and P. R. Giordano, "Rigidity maintenance control for multi-robot systems," in *In Robotics, Science and Systems Conference*, July 2012.

[141] D. Zelazo, A. Franchi, H. H. Bülthoff, and P. R. Giordano, "Decentralized rigidity maintenance control with range measurements for multi-robot systems," *The International Journal of Robotics Research*, vol. 34, pp. 105–128, 2014.

[142] D. Zelazo, A. Franchi, and P. R. Giordano, "Rigidity theory in SE(2) for unscaled relative position estimation using only bearing," in *European Control Conference*, June 2014, pp. 2703–2708.

[143] F. Schiano, A. Franchi, D. Zelazo, and P. R. Giordano, "A rigidity-based decentralized bearing formation controller for groups of quadrotor uavs," in *In IEEE/RSJ International Conference on Intelligent Robots and System*, 2016.

[144] G. Michieletto, A. Cenedese, and A. Franchi, "Bearing rigidity theory in SE(3)," in *55th IEEE Conference on Decision and Control*, 2016.

[145] S. J. Julier and J. K. Uhlmann, "Consistent debiased method for converting between polar and cartesian coordinate systems," in *AeroSense'97*. International Society for Optics and Photonics, 1997, pp. 110–121.